GEOLOGICA ULTRAIECTINA

Mededelingen van de Faculteit Geowetenschappen Universiteit Utrecht

No. 304

Quantifying the influences of biogeochemical processes on pH of natural waters

Andreas Felix Hofmann

Doctoral advisors:

Prof. dr. J. J. Middelburg	Netherlands Institute of Ecology, The Netherlands Utrecht University, The Netherlands
Prof. dr. C. H. R. Heip	Netherlands Institute of Ecology, The Netherlands Netherlands Institute of Sea Research, The Netherlands Groningen University, The Netherlands Ghent University, Belgium

Co-advisors:

Prof. dr. K. Soetaert	Netherlands Institute of Ecology, The Netherlands Ghent University, Belgium Vrije Universiteit Brussel, Belgium
Prof. dr. ir. F. J. R. Meysman	Vrije Universiteit Brussel, Belgium Netherlands Institute of Ecology, The Netherlands Ghent University, Belgium

Members of the dissertation committee:

Prof. dr. P. Van Cappellen	Utrecht University, The Netherlands Georgia Institute of Technology, USA
Prof. dr. G. J. de Lange	Utrecht University, The Netherlands
Prof. dr. F. J. Millero	University of Miami, USA
Prof. dr. D. A. Wolf-Gladrow	Alfred Wegener Institute, Germany
Prof. dr. B. P. Boudreau	Dalhousie University, Canada

ISBN 978-90-5744-166-0

NIOO Thesis 71

Quantifying the influences of biogeochemical processes on pH of natural waters

Kwantificatie van de invloed van biogeochemische processen op de pH van natuurlijke wateren

(met een samenvatting in het Nederlands)

Proefschrift

ter verkrijging van de graad van doctor aan de Universiteit Utrecht op gezag van de rector magnificus, prof. dr. J.C. Stoof, ingevolge het besluit van het college voor promoties in het openbaar te verdedigen op dinsdag 12 mei 2009 des ochtends te 10.30 uur

door

Andreas Felix Hofmann

geboren op 14 september 1978 te Würzburg, Duitsland

Promotoren:	Prof. dr. J. J. Middelburg
	Prof. dr. C. H. R. Heip
Co-promotoren:	Dr. K. Soetaert
	Dr. ir. F. J. R. Meysman

This thesis was supported by the EU (Carbo-Ocean, 511176-2) and the Netherlands Organisation for Scientific Research (833.02.2002).

Contents

Part I.

Introduction

1. General introduction

1.1. Anthropogenic ocean acidification

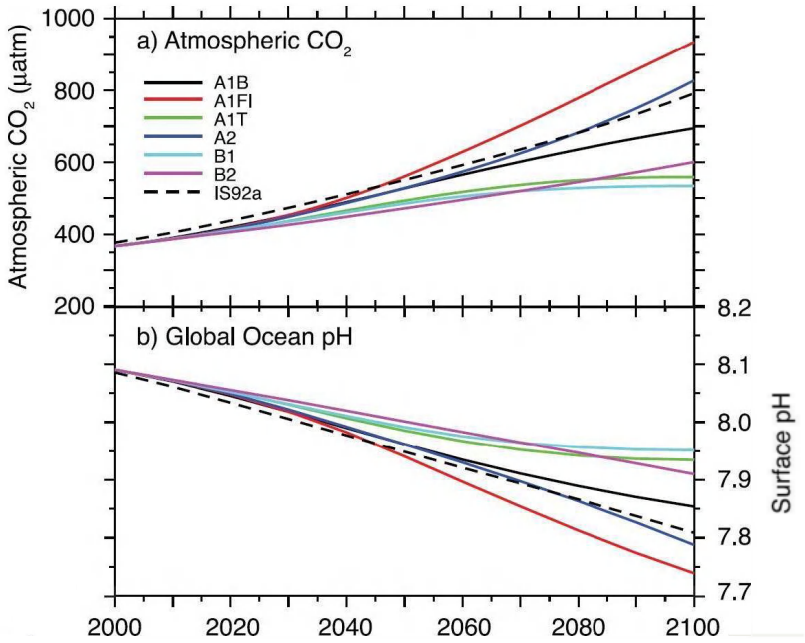

Figure 1.1.: Atmospheric CO_2 partial pressure (a) and average global surface ocean pH (b) under different IPCC emission scenarios. Graph reprinted from Meehl et al. (2007)

Today, during the first decade of the 21st century, there is a strong consensus within the scientific community that humans significantly alter the global carbon cycle, mainly by combustion of fossil fuels, but also by land use and land cover changes such as deforestation (IPCC, 2007). In general, human activities lead to an increased input of the greenhouse gas carbon dioxide (CO_2) into the atmosphere (a process termed "anthropogenic CO_2 emission"), which changes earth's climate significantly and rapidly (Prentice et al., 2001; IPCC, 2007). Due to extensive media coverage, also the general public and policy makers are widely aware of this problem (e.g. Biello, 2007).

One of the key processes mitigating anthropogenic CO_2 release is oceanic CO_2 uptake: over the past 200 years, the oceans have taken up roughly 40 % of anthropogenic CO_2 emissions (Zeebe et al., 2008). Due to this central role of the oceans, intensified scientific effort has been put into the investigation of the marine carbon cycle. However, uptake of CO_2 by the oceans also leads to a decrease of oceanic pH values as the reaction of CO_2 with water and carbonate and subsequent dissociation steps produce protons (e.g. Zeebe and Wolf-Gladrow,

2001), thus "titrating" the ocean. This effect, "anthropogenic ocean acidification", is known for quite some time (e.g. Caldeira and Wickett, 2003, 2005; Royal Society, 2005; Blackford and Gilbert, 2007) and acknowledged by the popular press (e.g. Doney, 2006). However, its mechanisms and causes, as well as its effects on organisms and ecosystems are poorly understood. Due to this lack of understanding, anthropogenic ocean acidification has been termed the "other CO_2 problem" by both the scientific and the popular press (e.g. Henderson, 2006; Davis, 2007; EUR-OCEANS, 2007; Brewer and Barry, 2008; Marshall, 2009; Doney et al., 2009). The authors of a recent Science magazine publication demanded more awareness among the general public and policy-makers and more efforts of the scientific community to better understand ocean acidification, its causes, mechanisms and effects (Zeebe et al., 2008).

Fact is, global oceanic pH declines due to the uptake of antropogenic CO_2: it has already declined since pre-industrial times by 0.1 units (Zeebe et al., 2008) and it is predicted to further decline by a few tenths of a unit towards the end of the century (Caldeira and Wickett (2003): 0.7 units, Caldeira and Wickett (2005): 0.3 - 0.5 units, Royal Society (2005): up to 0.5 units, IPCC (2007); Meehl et al. (2007): 0.15 - 0.35 units). Although a few tenths of a pH unit does not seem a lot, due to the logarithmic nature of pH scales, a pH decline of 0.5 pH units represents a five fold increase in free proton concentration. Figure (1.1) shows atmpospheric CO_2 partial pressure and oceanic pH values as predicted according to different CO_2 emission scenarios by the Intergovernmental Panel on Climate Change (IPCC) in its Fourth Assessment Report in 2007 (IPCC, 2007; Meehl et al., 2007).

A decreasing pH in the global ocean influences marine ecosystems in various ways. The most prominent effect of ocean acidification on ecosystems and biogeochemical functioning is the effect on calcifying organisms. Via a decrease in the carbonate ion concentration ($[CO_3^{2-}]$), decreasing oceanic pH leads to a decrease of the saturation state Ω of oceanic waters with respect to biologically important calcium carbonate forms such as calcite and aragonite (e.g. Zeebe and Wolf-Gladrow, 2001; Guinotte and Fabry, 2008; Salisbury et al., 2008; Doney et al., 2009). A decreasing Ω, especially for the more soluble aragonite, may have negative effects on marine calcifying organisms, even if the waters remain supersaturated (e.g. Orr et al., 2005; Kleypas et al., 2006; Gazeau et al., 2007; Guinotte and Fabry, 2008; Salisbury et al., 2008; Doney et al., 2009). This can impact commercial shellfish production, as well as commercial fisheries, since shelled pteropods contribute to the diet of commercially important fish species (Salisbury et al., 2008). Furthermore, not only the carbonate concentration but also the overall chemistry of natural ocean water will be strongly influenced by a declining oceanic pH (e.g. Zeebe and Wolf-Gladrow, 2001; Doney et al., 2009). As a result, further investigation of the effects of ocean acidification is needed. This is particularly true since there might be unanticipated effects which can have a strong impact on marine ecosystems (e.g., a change in oceanic sound absorption (Hester et al., 2008)).

Because of the possible commercial impact and potential loss of biodiversity, the main research focus today lies on the investigation of the *effects* of ocean acidification on marine ecosystems. However, there is also still work to be done in predicting how global oceanic pH will change in the future and which processes will affect pH the most. The differences between predictions of future pH decrease mainly stem from differences in used CO_2 emission scenarios. However, the oceanic CO_2 uptake rate, and thus also the decline in pH caused by the uptake of CO_2 depend on the current pH value. This adds further uncertainty to predictions,

since pH is not only influenced by CO_2 uptake alone, but by almost any biogeochemical and physical process occurring in natural waters (Stumm and Morgan, 1996). Biogeochemical and physical processes occurring in the oceans might thus have a double impact on pH: (1) a direct influence and (2) an indirect influence by affecting the extent of pH change by CO_2 uptake. For example, there might be a synergistic effect between CO_2 based ocean acidification and atmospheric deposition of HNO_3 and H_2SO_4 (Doney et al., 2007). Even for a given process rate, the effect on pH depends on the current pH of the ocean: it is modulated by the pH dependent buffering capacity of the ocean. As a result, complex feedback mechanisms of processes influencing pH while also being influenced by pH need to be considered for accurate predictions of pH changes (see Figure 1.2). This shows that predicting future oceanic pH changes is far from being straight-forward and is still an open field of research.

While it is obviously important to study the effects of a changing pH on biogeochemical and physical processes, it is also vital to predict future pH changes with a greater accuracy. One needs to be able to unravel the complex feedback mechanisms in predictive calculations and to identify the processes that affect pH the most. That means, one needs to be able to better understand and *quantify the influences of biogeochemical and physical processes on pH of natural waters*. This is the prime goal of this thesis.

1.2. pH modelling

> *"The natural environment, with all the physical, chemical, and biological processes going on, is of an overwhelming complexity. Scientists try to make sense of this complexity, so as to, among other things, have a certain predictive capability. This activity only progresses by the construction of models that make suitable abstractions of reality."*

As summarized excellently by those words from Soetaert and Herman (2009), the essence of science and the key to all understanding is the abstraction of reality via the creation of mechanistic models. This is true for any natural system, including pH of a natural aqueous solution: understanding pH chemistry requires its description via appropriate mechanistic models.

With pH chemistry being treated in classical textbooks like Skoog and West (1982), Morel and Hering (1993), Stumm and Morgan (1996), and Zeebe and Wolf-Gladrow (2001), one might think that pH chemistry and modelling are exhaustively understood and no new insights are to be gained in this field. However, the contrary is true, pH modelling still is an "unfinished symphony" and can be improved in many ways. This might seem a rather bold statement and will be clarified in the following via a closer look on mechanistic model descriptions of pH chemistry.

As commonly known, pH is a measure for the proton concentration, and the proton is a central variable in the biogeochemistry of any aquatic system. It is the "spider in the web" of biogeochemical reactions: almost any process going on in an aquatic system affects pH either directly or indirectly, is affected by pH, or both. This prominent role of the proton makes it difficult to describe changes in the proton concentration explicitly. In a typical aquatic

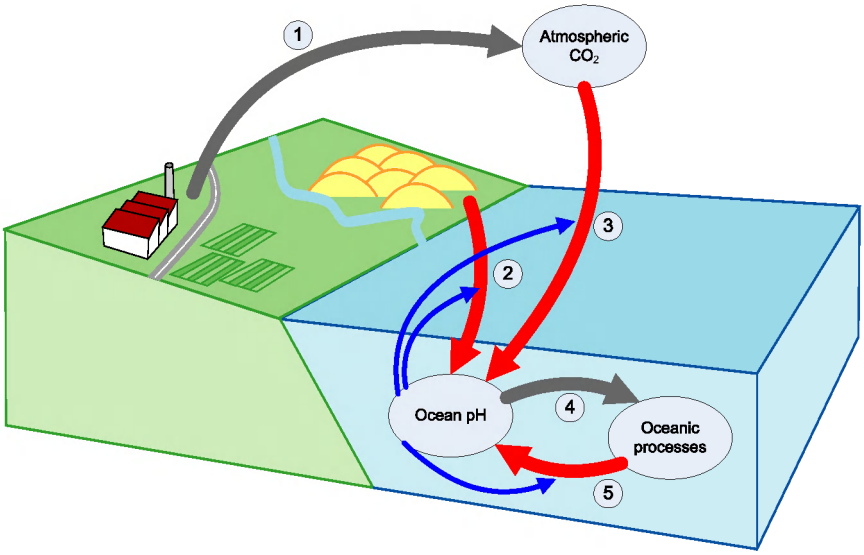

Figure 1.2.: Interactions between oceanic pH and processes. (1) antropogenic CO_2 emissions, (2) land activity based influences on oceanic pH (atmospheric wet and dry deposition, riverine input, etc.), (3) oceanic uptake of antropogenic CO_2, (4) the influence of pH on oceanic processes (e.g., calcification, this arrow represents the prime focus of recent efforts in ocean acidification research), (5) the influence of oceanic processes on pH (quantification of this arrow for different processes (i.e., including arrows (2) and (3)) is the main focus of this thesis), blue arrows: the influences of processes on pH is modulated by pH dependent oceanic buffering (conceptual formulation and quantification of this buffering is also subject of this thesis). (Graphic design in collaboration with S. Donner)

system, there are processes going on on vastly different timescales. One group of comparatively fast acid-base reactions (e.g., the carbonate, borate, silicate, etc. systems) relaxes on timescales of fractions of seconds up to minutes, while another group of rather slow processes relaxes on timescales of hours up to years or even longer. This latter group of processes comprises chemical reactions, such as calcium carbonate precipitation or dissolution, as well as physical transport processes, for example the exchange of CO_2 with the atmosphere. Most biogeochemical models, especially related to ecology and earth system science, seek to investigate changes to systems over days, years, decades, or centuries.

The resulting large gap in average charateristic timescales between the two groups of processes that need to be considered is what makes describing changes to the proton concentration difficult: it is not feasible to describe all processes kinetically in models covering long timescales, as the resulting equation system is a "stiff" system (Boudreau, 1996a). Generally, this problem is overcome by a "mixed-kinetic-equilibrium approach", i.e., by kinetically modelling changes of total quantities, like total carbonate and total alkalinity, that do not depend on the fast equilibrium acid-base reactions, and calculating the concentrations of chemical species that

do depend on those fast acid-base reactions in a second step, using equilibrium mass action equations.

This approach is widely used and seems to be "well known". Differential equations of total quantities like total alkalinity and dissolved inorganic carbon, whose definitions are postulated, are intuitively written down. What is often not realized or neglected is that in doing so, several assumptions (what is to be considered an equilibrium reaction, the precise definition of total alkalinity, etc.) are implicitly made, and chemical as well as mathematical principles are employed unknowingly. However, all those assumptions and principles can only be applied in certain circumstances which might not be true for the respective model at hand. Therein lies a fundamental danger: if concepts and assumptions are used in models without explicitly knowing them and without knowing in what situation they can be applied, the threat of erroneous pH calculations is imminent. Different concepts might even be used in inconsistent or contradictory manner in one single model. Furthermore, there are a variety of "pH modelling approaches" described in literature that appear to be fundamentally different from one another and seem unconnected, but obviously are interrelated as they describe the same property of the system.

In this thesis, we show how pH modelling approaches described in literature are related and how they all can be derived via various reformulations from the initial description of the system, the mass conservation equations of all chemical species. We show that the definitions of total quantities like total alkalinity and dissolved inorganic carbon emerge from the system and do not need to be imposed. Furthermore, we make all assumptions, principles and requirements that are employed in the respective reformulation steps explicit, such that the pH modeller can decide whether the respective reformulation step is appropriate for the model to be built or not.

This shows that in terms of *technicalities of pH model construction*, there is room for improvement by relating existing pH modeling approaches to one another and placing them in a structured and explicit framework of model reformulations.

However, the biggest disadvantage of the "well known" mixed-kinetic-equilibrium pH modelling approaches is that proton concentration changes are described via the detour of total alkalinity changes. The step that connects alkalinity changes and proton concentration changes is obscured by numerical solution techniques employed to solve the nonlinear system of equations derived from the equilibrium mass action equations of the acid-base reactions. This prevents scientists from quantifying the influences of kinetically modelled processes on the proton concentation in models where various kinetic processes are operating concurrently (modelling kinetic processes concurrently, however, is important to describe the system correctly, since there is mutual influence between most processes).

The influences of kinetically modelled processes with rates $\mathbf{R}_i$ on state variables in a model, e.g., total alkalinity (TA), are usually quantified by partitioning the expression for the rate of change of the variable in question into terms that are functions of the respective reaction rates

$$\frac{d[\mathrm{TA}]}{dt} = f(\mathbf{R}_1, \mathbf{R}_2, ...) = \nu^1_{TA}\mathbf{R}_1 + \nu^2_{TA}\mathbf{R}_2, ... \tag{1.1}$$

where $\nu_i R_i$ quantifies the influence of process i on TA and ν_i is a factor depending on the stoichiometric equation of process i. To quantify the effects of kinetic processes on the proton concentration, one needs to step away from the *alkalinity centered* pH modelling approach towards a *proton centered* pH modelling approach, i.e, one needs to derive a similar equation for the proton concentration

$$\frac{d[\mathrm{H}^+]}{dt} = f(\mathbf{R}_1, \mathbf{R}_2, ...) = \nu^1_{\mathrm{H}^+}\mathbf{R}_1 + \nu^2_{\mathrm{H}^+}\mathbf{R}_2, ... \tag{1.2}$$

(See Table 1.1 for a complementary and more intuitive explanation on the quantification of influences of processes on ordinary state variables and on the proton concentration in models, using the example of nitrate concentration.)

In this thesis we provide methods to derive an expression of the form of Eq. 1.2 for the proton concentration, thus providing means of *quantifying the influences of biogeochemical processes on pH of natural waters.*

This shows that also in terms of *providing knowledge about the functioning of dynamic systems*, pH modelling can be improved, i.e., the red arrows in Figure 1.2 can be assigned with associated proton concentration changes for every process in the respective model.

Furthermore, it is obvious that fast acid-base reactions attenuate the effects of kinetic processes on the pH via buffering (indicated by the blue arrows in Figure 1.2), but the exact mechanism of buffering in pH models is obscured by the numerical equilibration step as well. Classical textbooks and previous workers (Morel and Hering, 1993; Frankignoulle, 1994; Stumm and Morgan, 1996) postulate and define "buffer factors" based on pH that describe the buffering capacity of an aqueous solution, but it remains unclear what exactly is expressed by these quantities, and how they are related to the effects of processes with a certain stoichiometry (other than "proton addition" which is equal to only the addition of a strong acid).

In this thesis, we (1) explicitly derive a buffer factor from the model description of the system. This shows that a buffer factor does not need to be postulated as it emerges from consistent model description of any system. Additionally, our buffer factor is related to the proton concentration (i.e., the quantity that is biogeochemically relevant), rather than the negative common logarithm of it. By relating the derived buffer factor to total alkalinity, which is a measure of the dissociation state of the system and can be expressed as function of amongst others acid-base dissociation constants, we make the attenuating role of the acid-base reactions explicit. (2) Furthermore, we provide a direct connection between this buffer factor and the stoichiometry of any process, i.e. we give a recipe of how this buffer factor can be used to describe changes to the pH of the system due to any process that can be expressed by a stoichiometric equation.

This shows that in terms of *conceptual understanding* of pH chemistry a major improvement can be achieved by properly describing buffering and its relation to the stoichiometry of processes and their effects on pH, i.e., by attributing explicit meaning to the blue arrows in Figure 1.2.

A model of a given aquatic system with focus on the nitrate concentration is to be built. It is known that in this system, there are three main processes affecting the nitrate concentration: nitrification (nitrate production), denitrification (nitrate reduction to di-nitrogen gas), and primary production (nitrate assimilation by algae). The graphic below shows a sketch of a suitable abstraction for this system and question. Such a diagram is called a *conceptual model* of the system.

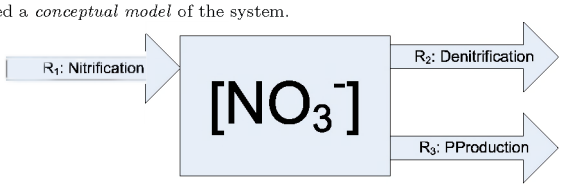

The conceptual model shown above gives a qualitative idea about the system, but it does not allow quantification. For that purpose, the conceptual scheme has to be translated into mathematical expression. In ecological models, this is typically done via mass balances in the form of differential equations. For example, the equation

$$\frac{d[\mathrm{NO_3^-}]}{dt} = \mathbf{R}_1 - \mathbf{R}_2 - \mathbf{R}_3 = f_1(\mathbf{R}_1) + f_2(\mathbf{R}_2) + f_3(\mathbf{R}_3) \tag{1.3}$$

describes changes in the nitrate concentration by the rate of nitrification ($\mathbf{R}_1$) minus the rates of denitrification ($\mathbf{R}_2$) and nitrate consumption by primary production ($\mathbf{R}_3$). This means, the right hand side of Eq. (1.3) can be partitioned into terms that are functions of the rates of the three modelled processes separately, thus quantifying the influences of these processes on $[\mathrm{NO_3^-}]$. Integrating Eq. (1.3) provides the temporal evolution of nitrate in the given system.

Obviously, in the above system, pH will also change due to production and consumption of protons by the modelled processes. To employ a treatment analogous to nitrate, it is sensible to consider the free proton concentration $[\mathrm{H^+}]$ instead of the pH. As already mentioned, the processes nitrification, denitrification, and primary production influence the proton concentration.

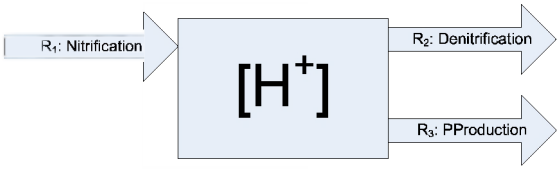

Since the proton concentration depends not only on the processes that are responsible for a change to the system, i.e., nitrification, denitrification, primary production, etc., but also on acid-base reactions occurring in the system (Morel and Hering, 1993; Stumm and Morgan, 1996; Zeebe and Wolf-Gladrow, 2001), the change in the proton concentration cannot simply be described by a differential equation like equation (1.3). Instead, calculating the proton concentration and its temporal evolution in a system involves numerical techniques to solve the system of nonlinear equations comprising kinetic expressions and the equilibrium mass balance equations of the acid-base reactions in the system (e.g. Ben-Yaakov, 1970; Culberson, 1980; Luff et al., 2001).

Using numerical techniques, the resulting temporal evolution of the proton concentration as the combined effect of all modelled processes can be calculated. However, and that may be surprising, since pH chemistry might seem pretty exhaustively "known", a direct and quantitative connection between process rates and effects on the proton concentration is missing. That means a differential equation similar to (1.3) of the form

$$\frac{d[\mathrm{H^+}]}{dt} = f(\mathbf{R}_1, \mathbf{R}_2, \mathbf{R}_3) = f_1(\mathbf{R}_1) + f_2(\mathbf{R}_2) + f_3(\mathbf{R}_3) \tag{1.4}$$

cannot be explicitly written because the connection between process rates and proton concentration change is obscured by the numerical solution of the associated non-linear system of equations.

In this thesis, an explicit expression of the form of Eq. (1.4) will be derived for the proton concentration. This provides a quantification of the influences of modelled processes on the proton concentration, in the same way as Eq. (1.3) provides such a quantification for nitrate.

Table 1.1.: Quantification of influences of biogeochemical processes on state variables in models: $[\mathrm{NO_3^-}]$ and $[\mathrm{H^+}]$

Finally, up to now, there are no flexible, exhaustive, easy to use computational tools to rapidly set up pH models, neither in the classical "alkalinity centered" way, nor in the "proton centered" way introduced here. In this thesis, we provide such a computational tool. This shows that also in terms of *computational tools* for pH modelling, there is still work to be done.

After having shown that pH modelling indeed is an "unfinished symphony" and can be improved in many ways, we have no intention to claim that this thesis completes the "symphony", but we rest assured that we not only sort the existing pages of the script, add some interesting new notes, but also and primarily supply many new, blank sheets and provide pens for pH composers to add all their interesting notes to make the final symphony a real masterpiece.

1.3. Test system: the Scheldt estuary

Figure 1.3.: View on the Scheldt estuary close to Terneuzen in The Netherlands

Estuaries play an important role in the transfer of land derived nutrients and organic matter to the coastal ocean as they act as bio-reactors where both the quantity and the quality of the constituents are altered substantially (Soetaert et al., 2006). Additionally, Borges et al. (2006) and Frankignoulle et al. (1998) report that estuaries are globally important sources of CO_2, by ventilating dissolved inorganic carbon (DIC) to the atmosphere. This DIC can be of different origins, it may be transported into the estuary from upstream or it may be internally produced via the degradation of riverine organic matter. These properties make estuarine ecosystems not only suitable testbeds for methods quantifying the influences of biogeochemical processes on pH but also make them interesting study subjects in their own right, with relevance for the global carbon and nutrient cycles.

Out of these reasons and due to the availability of a large amount of field data for this system as results of a monitoring and research campaigns conducted by the Netherlands Institute of Ecology, we choose the Scheldt estuary (see also picture in figure 1.3) as an example system. Table 1.2 provides details on this ecosystem.

In this thesis, we build an ecosystem model of the Scheldt estuary and constrain the process rates in the model via fitting to data of relevant chemical species concentrations. While doing so, we shed light on the dynamics of key chemical elements like nitrogen, carbon and oxygen in the system. Subsequently, we extend this ecosystem model with an explicit pH modelling

The Scheldt estuary is situated in the southwestern part of the Netherlands and the northern part of Belgium (Fig. 2.1). The roughly 350 km (Soetaert et al., 2006; Van Damme et al., 2005) long Scheldt river drains a basin of around 21 500 km^2 (Soetaert et al., 2006; Vanderborght et al., 2007; Van Damme et al., 2005 and Meire et al., 2005) located in the northwest of France, the west of Belgium and the southwest of the Netherlands (Soetaert et al., 2006). The hydrographical basin of the Scheldt contains one of the most densely populated areas in Europe (Vanderborght et al., 2007) with about 10 million inhabitants (Meire et al., 2005; Soetaert et al., 2006), resulting in an average of 465 inhabitants per km^2. Anthropogenic eutrophication and pollution of the Scheldt estuary therefore were and are of considerable magnitude, especially due to the poor waste water treatment in upstream areas like Brussels[a] (Meire et al., 2005; Van Damme et al., 2005; Soetaert et al., 2006; Vanderborght et al., 2007). The water movement in the Scheldt estuary is dominated by huge tidal displacements with around 200 times more water entering the estuary during a flood than the freshwater discharge during one tidal cycle (Vanderborght et al., 2007). The average freshwater flow is around 100 $m^3 s^{-1}$ (Heip, 1988). The cross sectional area of the estuarine channel shows a regular trumpet-like shape opening up from around 4000 m^2 upstream to around 75 000 m^2 downstream (Soetaert et al., 2006) whilst the mean water depth varies irregularly between values of 6 m and 14 m with the deepest areas towards the downstream boundary (Soetaert and Herman, 1995b). The estuary has a total tidally averaged volume of about 3.619 10^9 m^3 and a total tidally averaged surface area of 338 km^2 (Soetaert et al., 2006; Soetaert and Herman, 1995b), the major parts of which are situated in the downstream area. Peters and Sterling (1976), as cited by Vanderborght et al. (2007), divide the Scheldt river into three zones: The first zone, between the estuarine mouth at Vlissingen and Walsoorden, consists of a complex system of flood and ebb channels and a moderate longitudinal salinity gradient within the polyhaline range. The second zone from Walsoorden to Rupelmonde is characterized by a well defined river channel and a steep salinity gradient with salinities at Rupelmonde between 0 and 5 (Meire et al., 2005). The third zone, upstream from Rupelmonde, consists of the Scheldt freshwater river system and various tributaries, with tidal influence in the Scheldt up to the sluices of Gent (Van Damme et al., 2005).

[a]The city of Brussels, the location of the European Parliament, was one of the last cities in Europe to install an integrated wastwater treatment system.

Table 1.2.: Facts on the Scheldt estuary

approach to *quantify the influences of biogeochemical and physical processes on pH* in the Scheldt estuary.

1.4. Aim and outline of this thesis

In this thesis we (1) develop a one-dimensional biogeochemical model of the Scheldt estuary ecosystem, (2) structure, unify and connect existing pH modelling methods and develop a way to quantify the influence of biogeochemical and physical processes on the pH by establishing an analytical connection between process rates and pH changes, (3) apply this pH modelling approach to the model of the Scheldt estuary, (4) further investigate the analytical connection between process rates and pH changes and explicitly relate this analytical connection to the stoichiometry of the processes, and (5) provide a programming toolbox for the rapid generation of pH models.

As indicated above, pH changes and thus also the absolute values of pH are dependent on the rates of biogeochemical and physical process in an ecosystem. This means that, before one can model the pH of a system, one needs a biogeochemical model which fits the data for key chemical species reasonably well and contains reasonable process rates. **Chapter 2** describes the development of a one-dimensional ecological model of the Scheldt estuary. This model is then used to investigate the nitrogen filtering capacity of the Scheldt estuary, and the change in nitrogen cycling from the seventies to the first decade of the 21^{st} century is assessed. Furthermore, the model is used to estimate CO_2 export from the estuary to the atmosphere.

In **Chapter 3**, a step-by-step method, dealing with the problem of different timescales of the relevant processes, of developing a pH model is given. Every step is related to existing concepts and pH modelling approaches. Along the course of this step-by-step procedure, every assumption made, every mathematical reformulation used, as well as every chemical principle considered is made explicit. This explicit treatment ensures the construction of internally consistent pH models. This analysis merges existing pH modelling approaches into one framework and shows that improvement is possible by further reformulating the model description: the last reformulation step substitutes the differential equation for total alkalinity with an explicit differential equation for the proton concentration. This introduces a direct analytical connection between the process rates and pH changes allowing for a quantification of the influences of biogeochemical and physical processes on pH.

In **Chapter 4**, the method of quantifying the influences of processes on pH introduced in Chapter 3 is applied to the model of the Scheldt estuary developed in Chapter 2. This provides insight on both the factors governing the yearly averaged longitudinal pH profile as well as on the factors governing interannual mean pH changes in the estuary. Furthermore, the analytical connection between process rates and pH changes is given for systems with time variable acid-base dissociation constants, while in Chapter 3 this connection was only given for systems with acid-base dissociation constants which are invariant over time.

In **Chapter 5**, the methodology for quantifying the influences of processes on pH, introduced in Chapter 3, is investigated in greater detail. While the numerical aspects of pH modelling were illuminated in Chapter 3, here, the prime focus lies on concepts and chemical interpretation. It is shown that the influence of a process on the pH can be expressed as the product of the process rate and a *sensitivity* factor. The sensitivity factor in turn is decomposed as the stoichiometric coefficient for the proton in the *introduced fractional reaction equation at ambient pH* over a buffer factor. Thus, the connection between the sensitivity factor and the stoichiometry of the process is made and the approach provides a chemical interpretation of the mechanisms underlying pH changes. Furthermore, the concept of buffer factor and pH sensitivities is applied to an averaged global ocean to investigate the change in buffer factor towards the end of this century. This chapter thus demonstrates best how the concepts and tools presented in this thesis can make a complementary contribution to the existing modelling approaches of global carbon cycling in general and ocean acidification in particular.

Very important for pH modelling and ecological model development in general are flexibility and the ability to readily produce problem specific, running computer code, the results of which can be tested and verified already in early stages of model development. In software engineering, this is called *rapid prototyping*. The statistical programming language R is an interpreted language that allows for a quick execution of scripts without the need of a lengthy compilation step. In **Chapter 6**, the extension package `AquaEnv` for R is introduced which comprises an extensive toolbox for aquatic acid-base modelling that allows for rapid prototyping of pH models of natural aquatic systems. However, `AquaEnv` can also be used as a desktop tool by the experimental scientist to process and visualize measured data. Furthermore, two more elaborate functions are already pre-coded: the conducting of an "in silico" experiment in the form of a titration simulation and the calculation of alkalinity values from measured titration curves via nonlinear curve fitting.

A challenge that remains for the future is to obtain biogeochemical models of ecosystems with realistic process rates. Crucial for this task are good quality data to fit the models to. For pH modelling especially good quality alkalinity data are needed. Obtaining alkalinity data is not straightforward: **Appendix A** gives a short overview of different methods for alkalinity determination from titration data. In the programming toolbox `AquaEnv` described in Chapter 6 one of these methods is implemented.

Part II.

Quantifying the influence of biogeochemical processes on pH

2. Present nitrogen and carbon dynamics in the Scheldt estuary using a novel 1-D model

A. F. Hofmann, K. Soetaert, and J. J. Middelburg
(Biogeosciences, 5, 981-1006, 2008)

Abstract

A 1-D, pelagic, reactive-transport model of a completely mixed, turbid, heterotrophic estuary – the Scheldt estuary – is presented. The model resolves major carbon and nitrogen species and oxygen, as well as pH. The model features two organic matter degradation pathways, oxic mineralisation and denitrification, and includes primary production as well as nitrification. Apart from advective-dispersive transport along the length axis, the model also describes O_2, CO_2, and N_2 air-water exchange. The aim of this study is to present a model which is as simple as possible but still fits the data well enough to determine the fate and turnover of nutrients entering the estuary and their spatial patterns in the years 2000 to 2004. Nitrification is identified as one of the most important processes in the estuary, consuming a comparable amount of oxygen as oxic mineralisation ($1.7\,\mathrm{Gmol\ O_2\,y^{-1}}$ vs. $2.7\,\mathrm{Gmol\ O_2\,y^{-1}}$). About 10% of the 2.5 Gmol of nitrogen entering the estuary per year is lost within the estuary due to denitrification. Nitrogen and carbon budgets are compared to budgets from the seventies and eighties, showing that nitrification activity has peaked in the eighties, while denitrification steadily declined. Our model estimates an average CO_2 emission of $3.3\,\mathrm{Gmol\,y^{-1}}$ in the years 2001 to 2004, which is a comparatively low estimate in the context of previous estimates of CO_2 export from the Scheldt estuary.

2.1. Introduction

Estuaries play an important role in the transfer of land derived nutrients and organic matter to the coastal ocean as they act as bio-reactors where both the quantity and the quality of the constituents are altered (Soetaert et al., 2006). Additionally, Borges et al. (2006) and Frankignoulle et al. (1998) report that estuaries are globally important sources of CO_2, by ventilating riverine dissolved inorganic carbon (DIC) as well as DIC originating from the degradation of riverine organic matter. This estuarine filter function is not a static property and evolves with changing forcings (Cloern, 2001). Thorough assessment of evolving estuarine filter functioning requires not only access to long-term datasets documenting changes in concentrations and loadings, but also biogeochemical models that allow reproducing these trends and deriving transformation intensities.

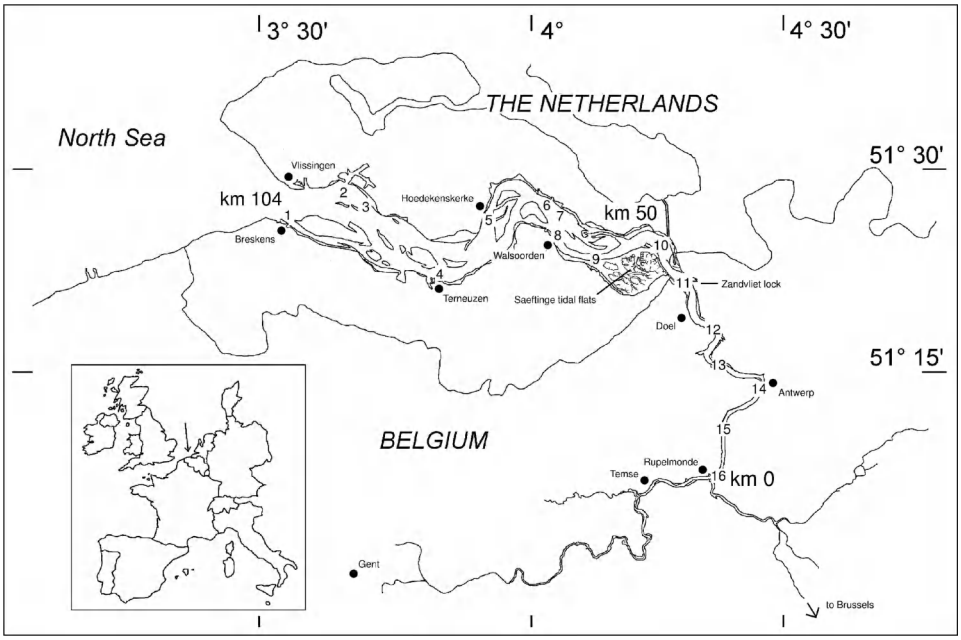

Figure 2.1.: The Scheldt estuary – monitoring stations WS1 to WS16 are indicated with numbers.

Long term changes in estuarine biogeochemical cycling have been well documented for the Scheldt estuary (Soetaert et al., 2006). Billen et al. (1985) predicted that increased oxygen levels due to lowered organic loadings would increase delivery of nitrogen to the North Sea. Soetaert and Herman (1995a) indeed found that an increased percentage of riverine nitrogen was exported to the North Sea in the eighties as compared to the seventies. Recently, Soetaert et al. (2006) report major changes for the Scheldt estuary, not only in nutrient loadings, but also changes in nitrogen and phosphorus retention and regeneration, from the mid sixties to the beginning of the 21st century. Against this background it is of interest to investigate the

interplay of different biogeochemical processes as well as to quantify import from and export to both the North Sea and the atmosphere in the Scheldt estuary during the years 2000 to 2004.

For macrotidal estuaries such as the Scheldt estuary, Vanderborght et al. (2007) identified reactive-transport modelling as a powerful approach to investigate nutrients and carbon budgets and cycling at the estuarine scale. To answer questions about seasonal dynamics, a fully coupled, two-dimensional hydrodynamic and reactive-transport model (e.g. Vanderborght et al., 2007) is the method of choice. However, for the assessment of an average situation for a certain period of time that can be compared to other decades, a simple 1-D model reproducing yearly averaged values is sufficient (cf. also 1-D approaches by Soetaert and Herman, 1994b, 1995a,b,c; Regnier et al., 1997).

The objective of this study was to construct a 1-D, biogeochemical, pelagic, reactive-transport model of the mixed, turbid, heterotrophic Scheldt estuary. The model is deliberately kept as simple as possible (such that the performance is still sufficient) to optimize the ratio between the number of parameters and data available for calibration and validation. Furthermore, the level of complexity of the physical transport processes is kept comparable to the level of complexity of the biogeochemical processes. We use this model to obtain whole estuarine budgets for dissolved inorganic carbon, oxygen and nitrate, and ammonium, determining the fate and turnover of nutrients entering the estuary and describing the spatial patterns of nutrient concentrations and fluxes in the Scheldt estuary in the years 2000 to 2004. We compare our nitrogen budget to budgets from the seventies (Billen et al., 1985) and eighties (Soetaert and Herman, 1995a). The obtained value for an average CO_2 export to the atmosphere in the years 2001 to 2004 will be compared to reported CO_2 water-air flux estimates for the Scheldt estuary (Frankignoulle et al., 1998; Hellings et al., 2001; Vanderborght et al., 2002; Gazeau et al., 2005).

Recently, Vanderborght et al. (2002) and Vanderborght et al. (2007) also published modelling studies for the Scheldt estuary. Both of those models include the physical transport of solutes in the estuary in great detail (Vanderborght et al. (2002) describes a tidally resolved 1-D model and Vanderborght et al. (2007) a tidally resolved 2-D model). This rather complex description of physical processes leads to severe limitations of the models:

1. there is a high demand for high resolution data which makes it difficult to run the model for past decades with scarce data coverage or for predictive future scenarios,

2. the computational demand of the models is rather high, rendering it difficult to run the model for longer model times,

3. and to port these models to other systems, detailed bathymetrical maps are needed which might not always be available.

4. Furthermore, the complex representation of physics together with a rather crude representation of biogeochemistry in the models of Vanderborght et al. (2002) and Vanderborght et al. (2007) implicitly puts emphasis on the role of physics for the estuarine ecosystem functioning, which might not correspond to reality.

Since our model suffers from none of these drawbacks, our model code is public domain (the model codes of Vanderborght et al. (2002) and Vanderborght et al. (2007) cannot be publicly verified), and our model uses more recent data, we feel that this paper provides a complementary contribution to the scientific literature.

2.2. Materials and methods

2.2.1. The Scheldt estuary

The Scheldt estuary is situated in the southwest Netherlands and northern Belgium (Fig. 2.1). The roughly 350 km (Soetaert et al., 2006; Van Damme et al., 2005) long Scheldt river drains a basin of around 21 500 km^2 (average from numbers given in Soetaert et al., 2006; Vanderborght et al., 2007; Van Damme et al., 2005 and Meire et al., 2005) located in the northwest of France, the west of Belgium and the southwest of the Netherlands (Soetaert et al., 2006). The hydrographical basin of the Scheldt contains one of the most densely populated areas in Europe (Vanderborght et al., 2007) with about 10 million inhabitants (Meire et al., 2005; Soetaert et al., 2006), resulting in an average of 465 inhabitants per km^2. Anthropogenic eutrophication and pollution of the Scheldt estuary therefore are of considerable magnitude, especially due to the poor waste water treatment in upstream areas, e.g. in Brussels (Meire et al., 2005; Van Damme et al., 2005; Soetaert et al., 2006; Vanderborght et al., 2007). The water movement in the Scheldt estuary is dominated by huge tidal displacements with around 200 times more water entering the estuary during a flood than the freshwater discharge during one tidal cycle (Vanderborght et al., 2007). The average freshwater flow is around 100 $m^3 s^{-1}$ (Heip, 1988). The cross sectional area of the estuarine channel shows a quite regular trumpet-like shape opening up from around 4000 m^2 upstream to around 75 000 m^2 downstream (Fig. 2.2; Soetaert et al., 2006) whilst the mean water depth varies quite irregularly between values of 6 m and 14 m with the deepest areas towards the downstream boundary (Soetaert and Herman, 1995b). The estuary has a total tidally averaged volume of about 3.619 10^9 m^3 and a total tidally averaged surface area of 338 km^2 (Soetaert et al., 2006; Soetaert and Herman, 1995b), the major parts of which are situated in the downstream area. Peters and Sterling (1976), as cited by Vanderborght et al. (2007), divide the Scheldt river into three zones: The first zone, between the estuarine mouth at Vlissingen and Walsoorden, consists of a complex system of flood and ebb channels and a moderate longitudinal salinity gradient within the polyhaline range. The second zone from Walsoorden to Rupelmonde is characterised by a well defined river channel and a steep salinity gradient with salinities at Rupelmonde between 0 and 5 (Meire et al., 2005). The third zone, upstream from Rupelmonde, consists of the Scheldt freshwater river system and various tributaries, with tidal influence in the Scheldt up to the sluices of Gent (Van Damme et al., 2005). The model presented here comprises the first and the second zone with an upstream boundary at Rupelmonde (river km 0) and a downstream boundary at Vlissingen (river km 104).

2.2.2. Physical-biogeochemical model

2.2.2.1. Biogeochemical processes

The model describes four main biogeochemical processes, oxic mineralisation ($\mathbf{R}_{\mathrm{Ox}}$), denitrification ($\mathbf{R}_{\mathrm{Den}}$), nitrification ($\mathbf{R}_{\mathrm{Nit}}$), and primary production ($\mathbf{R}_{\mathrm{PP}}$) as given in Table 2.1. Although primary production is limited in the Scheldt estuary (much lower than respiration

$\mathbf{R}_{\mathrm{Ox}}$:	$(CH_2O)_\gamma(NH_3)+\gamma O_2$	$\rightarrow NH_3+\gamma CO_2+\gamma H_2O$
$\mathbf{R}_{\mathrm{Den}}$:	$(CH_2O)_\gamma(NH_3)+0.8\gamma NO_3^- + 0.8\gamma H^+$	$\rightarrow NH_3+\gamma CO_2+0.4\gamma N_2 \uparrow +1.4\gamma\ H_2O$
$\mathbf{R}_{\mathrm{Nit}}$:	$NH_3+2\ O_2$	$\rightarrow NO_3^-+H_2O+H^+$
$\mathbf{R}_{\mathrm{PP}}$:	$p^{\mathrm{PP}}_{NH_4^+}\ NH_4^+ + \left(1-p^{\mathrm{PP}}_{NH_4^+}\right) NO_3^-$	$\rightarrow (CH_2O)_\gamma(NH_3) + \left(2+\gamma-2p^{\mathrm{PP}}_{NH_4^+}\right) O_2$
	$+\ \gamma CO_2 + \left(1+\gamma-p^{\mathrm{PP}}_{NH_4^+}\right) H_2O$	$+\left(2p^{\mathrm{PP}}_{NH_4^+}-1\right) H^+$

Table 2.1.: Biogeochemical processes.

in Gazeau et al. (2005) and one order of magnitude lower than respiration in Vanderborght et al., 2002), it is included in the model since it can be of significance in the downstream stretches of our model domain (Soetaert and Herman, 1995c). The primary production description considered in this model lumps the carbon fixing activity of several groups of benthic and pelagic organisms. Oxic mineralisation and denitrification are included as the two pathways of organic matter degradation that are energetically most favourable (Canfield et al., 2005). Nitrification is included in the model since it is one of the most important O_2 consuming processes in the Scheldt estuary (Soetaert and Herman, 1995a; Andersson et al., 2006).

Denitrification is a heterotrophic process and consumes organic matter. The nitrogen of the organic matter mineralised by denitrification can be assumed to be directly oxidised with nitrate to form N_2 (Froelich et al., 1979), which represents an implicit coupling of denitrification and the anammox (anaerobic ammonium oxidation) process. However, denitrification can also be modelled as a source of ammonium if all the organic nitrogen is assumed to be released as ammonium (Froelich et al., 1979; Jorgensen, 1983). To keep the model as simple as possible and because of the absence of data on anammox, we model denitrification as a source of ammonium.

The incorporation of sulfate reduction, sulfide oxidation, biogenic calcification, as well as calcite and aragonite precipitation has been tested, but model performances did not increase significantly. In order to meet the objective of constructing a model as simple as possible we opted against inclusion of these processes in the model.

Reduction of manganese and iron oxyhydroxides is neglected because of their low concentrations. Similarly, due to methane concentrations on the nano molar scale (Middelburg et al., 2002), methanogenesis is also neglected.

Modelling net respiration (respiration – primary production) yields approximately the same model performance as modelling respiration and primary production individually. Following reviewer feedback, we opted for the latter due to the increased amount of information that can be extracted from the model in that way.

Table 2.2 shows kinetic formulations for all processes considered in the model. As in Soetaert and Herman (1995a), organic matter has been split up into two different fractions, one fast decaying fraction FastOM with a low C/N-ratio of γ_{FastOM} and one slow decaying fraction SlowOM with a high C/N-ratio of γ_{SlowOM}, respectively. $\mathbf{R}_{\mathrm{Ox}}$ and $\mathbf{R}_{\mathrm{Den}}$ are modelled as first order processes with respect to organic matter concentration in terms of organic nitro-

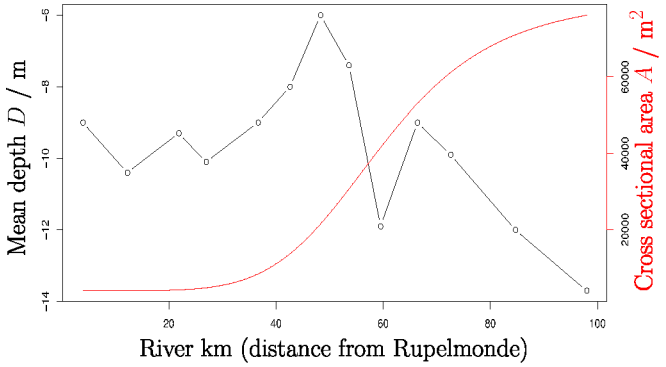

Figure 2.2.: Mean depth D (black broken line) and cross sectional area A (red solid line) of the Scheldt estuary.

gen as done by Soetaert and Herman (1995a). As in Regnier et al. (1997) and Soetaert and Herman (1995a), oxygen concentration inhibits denitrification. Nitrate concentration influences denitrification according to a Monod relationship as given by Regnier et al. (1997). The molecular nitrogen produced by denitrification is assumed to be immediately lost to the atmosphere. Mineralisation processes are thus modelled in the same order of sequence as in diagenetic models, depending on the availability of different oxidants with different free energy yields per mole organic matter oxidised (e.g. Froelich et al., 1979; Soetaert et al., 1996; Canfield et al., 2005).

Total mineralisation rates for fast and slow degrading organic matter are assumed to be only dependent on temperature and not on the mineralisation pathway. To ensure that the total temperature dependent mineralisation rates $rt_{\mathrm{X}}^{\mathrm{Min}}$, for FastOM and SlowOM respectively, are always realised, the independently calculated limitation factors for the two potentially simultaneously occurring mineralisation processes are rescaled as in Soetaert et al. (1996) to partition the total mineralisation rates.

Note that denitrification is an anaerobic process (Canfield et al., 2005) and does not occur in an oxic water column but in the anoxic layers of the sediment. To keep the model as simple as possible, we decided to not include sediment-water exchange of solutes. As a result of that, we model denitrification with parameters allowing a certain extent of denitrification in an oxic watercolumn as a proxy for benthic denitrification (following Regnier et al., 1997). Therefore, the parameters $k_{\mathrm{O_2}}^{\mathrm{Inh}}$ and $k_{\mathrm{NO_3^-}}$ should not be considered true microbiological rate parameters. Since we did not include sediment-water exchange in our model, also other pelagically modelled processes incorporate in part sedimentary processes.

Nitrification is expressed as a first order process with respect to ammonium concentration and with a Monod dependency on oxygen as in Soetaert et al. (1996). The same oxygen half saturation parameter $k_{\mathrm{O_2}}$ as for oxic mineralisation is used for nitrification. The nitrification may depend on the microbial community of nitrifiers. de Bie et al. (2001) documented dra-

Oxic Mineralisation			
$\mathbf{R}_{\mathrm{OxX}}$	=	$rt_{\mathrm{X}}^{\mathrm{Min}}$ OxLim [X]	mmol N m^{-3} d^{-1}
$\mathbf{R}_{\mathrm{Ox}}$	=	$\sum \mathbf{R}_{\mathrm{OxX}}$	mmol N m^{-3} d^{-1}
$\mathbf{R}_{\mathrm{OxCarb}}$	=	$\sum (\mathbf{R}_{\mathrm{OxX}}\ \gamma_{\mathrm{X}})$	mmol C m^{-3} d^{-1}
Denitrification			
$\mathbf{R}_{\mathrm{DenX}}$	=	$rt_{\mathrm{X}}^{\mathrm{Min}}$ DenLim $[X]$	mmol N m^{-3} d^{-1}
$\mathbf{R}_{\mathrm{Den}}$	=	$\sum \mathbf{R}_{\mathrm{DenX}}$	mmol N m^{-3} d^{-1}
$\mathbf{R}_{\mathrm{DenCarb}}$	=	$\sum (\mathbf{R}_{\mathrm{DenX}}\ \gamma_{\mathrm{X}})$	mmol C m^{-3} d^{-1}
Nitrification			
$\mathbf{R}_{\mathrm{Nit}}$	=	$r^{\mathrm{Nit}}\ f_{\mathrm{Q10}}\ f_{\mathrm{O_2}}\ f_S^{\mathrm{Inh}}\ [\sum \mathrm{NH_4^+}]$	mmol N m^{-3} d^{-1}
Primary Production			
$\mathbf{R}_{\mathrm{PP}}$	=	$r_{\mathrm{PP}}\ f_{Q_{10}}\ f_{\mathrm{DIN}}^{\mathrm{Inh}}\ f_D^{\mathrm{Inh}}\ f_{Turb}^{\mathrm{Inh}}$	mmol N m^{-3} d^{-1}
$\mathbf{R}_{\mathrm{PPCarb}}$	=	$\mathbf{R}_{\mathrm{PP}}\ \gamma_{\mathrm{FastOM}}$	mmol C m^{-3} d^{-1}
$p_{\mathrm{NH_4^+}}^{\mathrm{PP}}$	=	$[\sum \mathrm{NH_4^+}]\ (k_{\mathrm{NH_4^+}} + [\sum \mathrm{NH_4^+}])^{-1}$	
$rt_{\mathrm{X}}^{\mathrm{Min}}$	=	$r_{\mathrm{X}}^{\mathrm{Min}}\ f_{\mathrm{Q10}}$	d^{-1}
$f_{Q_{10}}$	=	$q10^{(T-q10_{t0})\ 10^{-1}}$	–
$f_{\mathrm{O_2}}^{\mathrm{Inh}}$	=	$k_{\mathrm{O_2}}^{\mathrm{Inh}}\ \left(k_{\mathrm{O_2}}^{\mathrm{Inh}} + [\mathrm{O_2}]\right)^{-1}$	–
$f_{\mathrm{O_2}}$	=	$[\mathrm{O_2}]\ (k_{\mathrm{O_2}} + [\mathrm{O_2}])^{-1}$	–
$f_{\mathrm{NO_3^-}}$	=	$[\mathrm{NO_3^-}]\ \left(k_{\mathrm{NO_3^-}} + [\mathrm{NO_3^-}]\right)^{-1}$	–
f_S^{Inh}	=	$o^{\mathrm{Nit}} + (k_S^{\mathrm{Inh}})^p\ \left((k_S^{\mathrm{Inh}})^p + (S)^p\right)^{-1}\ (1 - o^{\mathrm{Nit}})$	–
$f_{\mathrm{DIN}}^{\mathrm{Inh}}$	=	$([\sum \mathrm{NH_4^+}] + [\mathrm{NO_3^-}])\ \left(k_{\mathrm{DIN}}^{\mathrm{Inh}} + ([\sum \mathrm{NH_4^+}] + [\mathrm{NO_3^-}])\right)^{-1}$	–
f_D^{Inh}	=	$(k_D^{\mathrm{Inh}})^p\ \left((k_D^{\mathrm{Inh}})^p + (D)^p\right)^{-1}$	–
f_{Turb}^{Inh}	=	$(k_{Turb}^{\mathrm{Inh}})^p\ \left((k_{Turb}^{\mathrm{Inh}})^p + (Turb)^p\right)^{-1}$	–
$\sum$ MinLim	=	$f_{\mathrm{O_2}} + f_{\mathrm{O_2}}^{\mathrm{Inh}}\ f_{\mathrm{NO_3^-}}$	–
OxLim	=	$\sum \mathrm{MinLim}^{-1}\ f_{\mathrm{O_2}}$	–
DenLim	=	$\sum \mathrm{MinLim}^{-1}\ f_{\mathrm{O_2}}^{\mathrm{Inh}}\ f_{\mathrm{NO_3^-}}$	–
parameters			
$q10$	=	2.0	–
$q10_{t0}$	=	15.0	°C
$k_{\mathrm{O_2}}^{\mathrm{Inh}}$	=	22.0	mmol O$_2$ m^{-3}
$k_{\mathrm{O_2}}$	=	30.0	mmol O$_2$ m^{-3}
$k_{\mathrm{NO_3^-}}$	=	45.0	mmol N m^{-3}
$r_{\mathrm{FastOM}}^{\mathrm{Min}}$	=	0.15	d^{-1}
$r_{\mathrm{SlowOM}}^{\mathrm{Min}}$	=	0.002	d^{-1}
r_{PP}	=	3.5	mmol N m^{-3} d^{-1}
r^{Nit}	=	0.27	d^{-1}
o^{Nit}	=	0.05	–
p	=	3.0	–
k_S^{Inh}	=	4.0	–
$k_{\mathrm{NH_4^+}}$	=	1.0	mmol N m^{-3}
$k_{\mathrm{DIN}}^{\mathrm{Inh}}$	=	1.0	mmol N m^{-3}
k_D^{Inh}	=	6.0	m
k_{Turb}^{Inh}	=	0.7	–
γ_{FastOM}	=	4.0	mol C (mol N)$^{-1}$
γ_{SlowOM}	=	12.0	mol C (mol N)$^{-1}$

Table 2.2.: Kinetic process formulation with two organic matter fractions ($X \in$ {FastOM, SlowOM }). D signifies the mean water depth of the estuary, and $Turb$ its relative turbidity ($Turb$=0 downstream; $Turb$=1 at the turbidity maximum for medium dry periods at river km 20 (Meire et al., 2005); $Turb$=0.6 upstream (calibrated)). Note that the notation [Z] signifies the concentration of species Z.

CO_2+H_2O	$\rightleftharpoons$	$H^+ + HCO_3^-$	$K^*_{CO_2}$	=	$\frac{[H^+][HCO_3^-]}{[CO_2]}$
HCO_3^-	$\rightleftharpoons$	$H^+ + CO_3^{2-}$	$K^*_{HCO_3^-}$	=	$\frac{[H^+][CO_3^{2-}]}{[HCO_3^-]}$
H_2O	$\rightleftharpoons$	$H^+ + OH^-$	K^*_W	=	$[H^+][OH^-]$
$B(OH)_3+H_2O$	$\rightleftharpoons$	$H^+ + B(OH)_4^-$	$K^*_{B(OH)_3}$	=	$\frac{[H^+][B(OH)_4^-]}{[B(OH)_3]}$
NH_4^+	$\rightleftharpoons$	$H^+ + NH_3$	$K^*_{NH_4^+}$	=	$\frac{[H^+][NH_3]}{[NH_4^+]}$
HSO_4^-	$\rightleftharpoons$	$H^+ + SO_4^{2-}$	$K^*_{HSO_4^-}$	=	$\frac{[H^+][SO_4^{2-}]}{[HSO_4^-]}$
HF	$\rightleftharpoons$	$H^+ + F^-$	K^*_{HF}	=	$\frac{[H^+][F^-]}{[HF]}$

Table 2.3.: Left: Acid-base equilibria taken into account in the model. Right: Stoichiometric equilibrium constants. Values are calculated from temperature and salinity dependent expressions ($K^*_{HSO_4^-}$: Dickson (1990b); K^*_{HF}: Dickson and Riley (1979a); $K^*_{CO_2}$ and $K^*_{HCO_3^-}$: Roy et al. (1993b); K^*_W: Millero (1995); $K^*_{B(OH)_3}$: Dickson (1990a); $K^*_{NH_4^+}$: Millero (1995)), converted to free proton scale, pressure corrected according to Millero (1995) using the mean estuarine depth for each model box, and converted to volumetric units using the temperature and salinity dependent formulation for seawater density according to Millero and Poisson (1981).

matic shifts in nitrifier populations along the estuary from the freshwater to the marine part. Therefore, we assume that the nitrification activity in the freshwater (upstream) part of the modelled system is performed by freshwater nitrifying organisms that experience increasing stress as salinity increases. As a consequence, their activity collapses in the downstream region due to an insufficient adaptation to marine conditions (see also Helder and Devries, 1983) which is incompletely compensated by activity of marine nitrifying species, so that the overall nitrification activity in the estuary decreases with increasing salinity. This is expressed with an inverse dependency of nitrification on salinity, according to a sigmoid function based on a Holling Type III functional response (Gurney and Nisbet, 1998), modified to have a value of 1 for zero salinity and to asymptotically reach an offset value of o^{Nit} for high salinities.

To simulate light attenuation for primary production, a maximal reaction rate r_{PP} is scaled by a 1 – Holling Type III (Gurney and Nisbet, 1998) dependency term for mean estuarine depth D and for relative turbidity $Turb$ ($Turb$=0 downstream; $Turb$=1 at the turbidity maximum for medium dry periods at river km 20 (Meire et al., 2005); $Turb$=0.6 upstream (calibrated)). Furthermore primary production depends on a Monod term for DIN (Dissolved Inorganic Nitrogen=$[\sum NH_4^+]+[NO_3^-]$). The fraction of ammonium that is used by primary production $p^{\mathrm{PP}}_{NH_4^+}$ is calculated with a Monod term as well. Primary production is assumed to produce reactive organic matter (FastOM) only.

The temperature dependency for all processes is modelled with a Q_{10} formulation using a standard Q_{10} value of 2, all rates are expressed at a standard base temperature of 15°C.

Values for r_{PP}, $k^{\mathrm{Inh}}_{\mathrm{DIN}}$, k^{Inh}_D, k^{Inh}_{Turb}, $k_{NH_4^+}$, and the upstream relative turbidity have been calibrated such that the primary production in our model fits the combined carbon fixation

activity of the groups of organisms given in Soetaert and Herman (1995c). These values have not been calibrated to fit concentration profiles in the model.

Values for k_{O_2} and $k_{NO_3^-}$ are taken from Regnier et al. (1997), values for $k^{Inh}_{O_2}$, r^{Min}_{SlowOM}, γ_{FastOM} and γ_{SlowOM} are taken from Soetaert and Herman (1995a) ($k^{Inh}_{O_2}$, γ_{FastOM} and γ_{SlowOM} have been rounded). The parameters r^{Min}_{FastOM}, r^{Nit}, p, k^{Inh}_{S} and o^{Nit} have been calibrated.

2.2.2.2. Acid-base reactions (equilibria)

In any natural aqueous system, and in saline systems in particular, a certain set of chemical acid-base reactions has to be taken into account if pH is to be modelled. Due to their fast reaction rates compared to all other modelled processes, these reversible acid-base reactions are considered to be in local equilibrium at any time and at any point in the estuary (Stumm and Morgan, 1996), (Hofmann et al., 2008a, i.e., Chapter 3). For the model presented here, the set of acid-base equilibria given in Table 2.3 has been chosen.

2.2.2.3. Physical processes

2.2.2.4. *Air-water exchange*

While N_2 is assumed to be instantaneously lost to the atmosphere, O_2 and CO_2 are exchanged with the atmosphere according to a formulation given in Thomann and Mueller (1987):

$$\begin{aligned} \mathbf{E}_C = \left.\frac{d[C]}{dt}\right|_{Air-Sea} &= K_{L_C}\frac{A}{V}\left([C]_{sat}-[C]\right) \\ &= \frac{K_{L_C}}{D}\left([C]_{sat}-[C]\right) \end{aligned} \tag{2.1}$$

with [C] (mmol m^{-3}) signifying the actual concentration of O_2 or CO_2 respectively, $[C]_{sat}$ (mmol m^{-3}) being the saturation concentration of chemical species C in the water. K_{L_C} (m d^{-1}) is the piston velocity, A (m^2) the horizontal surface area of the model box in question, V (m^3) the volume, and D (m) the mean water depth.

Saturation concentrations are calculated using Henry's law (e.g. Atkins, 1996):

$$[C]_{sat} = fC\ K^{'}_{0_C}\ \rho_{SeaWater} \tag{2.2}$$

with fC (atm) being the fugacity of C, $K^{'}_{0_C}$ (mmol (kg-soln atm)$^{-1}$) being the Henry's constant for C, and $\rho_{SeaWater}$ (kg-soln m^{-3}) being the temperature and salinity dependent density of seawater. Henry's constants are calculated according to Weiss (1974) for CO_2 and based on Weiss (1970) for O_2. Both formulations can be found in Appendix 2.6.1. The atmospheric fugacities of CO_2 and O_2 are assumed to be the same as their atmospheric partial pressures. fCO_2 over the Scheldt waters is assumed to be 383 μatm (averaged from Scheldt area specific values for pCO_2 (partial pressure) given in Borges et al., 2004), fO_2 is assumed[1] to be 0.20946 atm as given by Williams (2004). The temperature and salinity dependent density of seawater is calculated according to Millero and Poisson (1981).

[1] considering an ambient pressure of 1 atm and considering the density of O_2 to be the same as the density of air, and assuming $fO_2 \approx pO_2$

A variety of different empirical relationships between K_{L_C} and wind speed have been proposed in the literature (e.g. Wanninkhof, 1992; Borges et al., 2004; Raymond and Cole, 2001; McGillis et al., 2001; Clark et al., 1995; Liss and Merlivat, 1986; Kuss et al., 2004; Nightingale et al., 2000; Banks and Herrera, 1977; Kremer et al., 2003). All these relationships have been implemented and tested. However, none of these formulations yielded a model fit significantly better than with a constant piston velocity. To keep the model as simple as possible and considering the high degree of uncertainty associated with K_{L_C} – wind speed relations, we used a constant K_{L_C}=2.7 cm h^{-1} (calibrated) in our model.

Inclusion of air sea exchange of NH_3 has been tested but discarded since it did not change the model performance.

2.2.2.5. *Advective-dispersive transport*

Since this model focuses on a period of several years, tidally averaged one-dimensional advective-dispersive transport of substances (all modelled substances/chemical species are assumed to be dissolved) is assumed. This transport approach incorporates longitudinal dispersion coefficients which parametrise a variety of physical mechanisms, including effects of either vertical or horizontal shear in tidal currents (Monismith et al., 2002). Advective-dispersive transport $\mathbf{Tr}_C$ of chemical species C is expressed as given in Thomann and Mueller (1987) and used amongst others by Soetaert and Herman (1995b) and Ouboter et al. (1998) for the Scheldt estuary:

$$\mathbf{Tr}_C = \left.\frac{\partial [C]}{\partial t}\right|_{\text{Adv-Disp}} = \frac{1}{A}\left(\frac{\partial}{\partial x}\left(E\,A\,\frac{\partial [C]}{\partial x}\right) - \frac{\partial}{\partial x}\left(Q\,[C]\right)\right) \tag{2.3}$$

The cross sectional area of the channel A (m^2), the tidal dispersion coefficient E (m^2 s^{-1}) and the advective flow Q (m^3 s^{-1}) are functions of the position x along the estuary. Due to the lack of experimental data for E in the Scheldt estuary, a relationship between local water depth D and E has been developed as part of this work.

The model has been spatially discretised according to a finite differences approach given in Thomann and Mueller (1987). Equation (2.3) can be spatially discretised for concentrations $[C]_i$ in mmol m^{-3} of any modelled species C in spatial model box i, describing the flow of matter across a set of model boxes with homogeneous contents and constant volume over time. This is done by applying a first order centred differencing scheme with a step-width of half a model box to the dispersive term, first to the "outer" derivative, then to the obtained "inner" derivatives. In the discretisation of the advective term, the same centred differencing scheme is used for the flux Q, while a backwards differencing scheme[2] is used for the concentration [C]. This approach leads to a transport formulation of:

$$\mathbf{Tr}_C|_i \approx \left(E'_{i-1,i}\left([C]_{i-1} - [C]_i\right) - E'_{i,i+1}\left([C]_i - [C]_{i+1}\right) + Q_{i-1,i}[C]_{i-1} - Q_{i,i+1}[C]_i \right)\, V_i^{-1} \tag{2.4}$$

with

$$E'_{i-1,i} = E_{i-1,i}\, A_{i-1,i}\, \left(\Delta x_{i-1,i}\right)^{-1} \tag{2.5}$$

[2] Using the same centred differencing scheme for concentrations as well would mean calculating concentrations at the boundary of model boxes. This can lead to a non mass conservative behaviour as the example of a zero concentration in the previous model box and a non-zero one in the current model box shows.

kinetic species:			
[FastOM]	mmol N	m^{-3}	fast decaying particulate organic matter: $[(CH_2O)_{\gamma_{FastOM}}(NH_3)]$
[SlowOM]	mmol N	m^{-3}	slow decaying particulate organic matter: $[(CH_2O)_{\gamma_{SlowOM}}(NH_3)]$
[DOC]	mmol C	m^{-3}	conservative dissolved organic matter: $[(CH_2O)(NH_3)_{(\gamma_{DOM})^{-1}}]$
$[O_2]$	mmol O_2	m^{-3}	
$[NO_3^-]$	mmol N	m^{-3}	$[NO_3^-]$+$[NO_2^-]$
S	–		salinity
equilibrium invariants:			
$[\sum CO_2]$	mmol C	m^{-3}	$[CO_2]$+$[HCO_3^-]$+$[CO_3^{2-}]$
$[\sum NH_4^+]$	mmol N	m^{-3}	$[NH_3]$+$[NH_4^+]$
$[\sum HSO_4^-]$	mmol S	m^{-3}	$[HSO_4^-]$+$[SO_4^{2-}]$
$[\sum B(OH)_3]$	mmol B	m^{-3}	$[B(OH)_3]$+$[B(OH)_4^-]$
$[\sum HF]$	mmol F	m^{-3}	$[HF]$+$[F^-]$
[TA]	mmol	m^{-3}	$[HCO_3^-]$+2$[CO_3^{2-}]$+$[B(OH)_4^-]$+$[OH^-]$ + $[NH_3]$ −$[H^+]$−$[HSO_4^-]$−$[HF]$

Table 2.4.: State variables of the biogeochemical model.

and $Q_{i-1,i}$ ($m^3\,s^{-1}$) being the flow over the interface between box i–1 and i; $E'_{i-1,i}$ ($m^3\,s^{-1}$) the bulk dispersion coefficient at the interface between box i–1 and i; $E_{i-1,i}$ ($m^2\,s^{-1}$) the tidal dispersion coefficient at the interface between box i–1 and i; $A_{i-1,i}$ (m^2) the cross sectional area of the interface between box i–1 and i; Δx_i (m) the length of model box i; and $\Delta x_{i-1,i}$ (m) the length from the centre of box i–1 to the centre of box i.

2.2.2.6. Model state variables and their rates of change

The chemical equilibrium reactions happen on a much faster timescale than the biogeochemical and physical processes (Zeebe and Wolf-Gladrow, 2001). To avoid numerical instabilities while keeping the solution of the model computationally feasible, a set of model state variables that are invariant to the acid-base equilibria has been devised. This was done using the transformation into the canonical form and operator splitting approach (Hofmann et al., 2008a, i.e., Chapter 3). The resulting state variables of the model (kinetic species and equilibrium invariants) are given in Table 2.4 (definitions) and Table 2.5 (rates of change).

Note that N_2 is neglected, salinity (S) and dissolved organic carbon (DOC) are added to the list of state variables, and that organic matter ($(CH_2O)_\gamma(NH_3)$) is split into a reactive (FastOM) and a refractory part (SlowOM).

Note further that "organic matter" ($(CH_2O)_\gamma(NH_3)$, FastOM, SlowOM) refers to particulate organic matter. Dissolved organic matter exhibits quasi conservative mixing in the Scheldt estuary (Soetaert et al., 2006) with a C/N ratio γ_{DOM} of 13.5 (average value for Scheldt estuary dissolved organic matter, T. van Engeland personal communication) and is conservatively

modelled as [DOC]. Note that particulate matter is transported in the same manner as other dissolved state variables.

2.2.2.7. pH

pH, or the free proton concentration $[H^+]$, is modelled since it can be used as a master variable to monitor the chemical state of a natural body of water, as almost any biogeochemical process occurring in such an environment affects $[H^+]$ either directly or indirectly (Stumm and Morgan, 1996; Soetaert et al., 2007). The free pH scale is used here, since all components of the systems in question are considered explicitly, including [HF] and $[HSO_4^-]$ (cf. Dickson, 1984).

Our model contains a pH calculation routine as described by the "solution method 3b" given in Hofmann et al. (2008a, i.e., Chapter 3) which has been inspired by Luff et al. (2001) and Follows et al. (2006). Since pH data for the Scheldt estuary have been measured on the NBS pH scale (Durst, 1975), the modelled free scale pH was converted to the NBS scale using the activity coefficient for H^+, which is calculated by means of the Davies equation (Zeebe and Wolf-Gladrow, 2001). The use of the Davies equation is assumed to be a sufficient approximation, since according to Zeebe and Wolf-Gladrow (2001) it is valid up to ionic strengths of approximately 0.5 and yearly averaged salinity values at the mouth of the Scheldt estuary (the downstream boundary of our model) are about 28 resulting in a ionic strength of approximately 0.57, while in the remaining estuary salinity values, hence ionic strengths, are lower.

2.2.2.8. Data

All data that are referred to as *monitoring data* were obtained by the Netherlands Institute of Ecology (NIOO) for 16 stations in the Scheldt between Breskens/Vlissingen (The Netherlands) and Rupelmonde (Belgium) by monthly cruises of the NIOO RV "Luctor". River kilometres (distance from the start of the model domain at Rupelmonde) and locations of the stations can be found in Table 2.6, a map of the Scheldt estuary indicating the positions of the sampling stations is given in Fig. 2.1.

2.2.2.9. *Calibration and validation data*

Data for the state variables $[\sum NH_4^+]$, $[NO_3^-]$, $[O_2]$, organic matter, pH (on the NBS scale) and salinity are available from the monitoring program. Data for 2003 have been used to calibrate the model and data for 2001, 2002, and 2004 have been used to independently validate it. The model does not distinguish between NO_3^- and NO_2^- and all data referring to the state variable $[NO_3^-]$ are the summed values of $[NO_3^-]$ plus $[NO_2^-]$. Data for organic matter (OM) have been calculated by assuming the measured percentage of nitrogen in the suspended particulate matter concentration to be available as particulate organic nitrogen. Nitrification rates for the year 2003 were obtained from Andersson et al. (2006). They have been measured with the ^{15}N method at salinities 0, 2, 8, 18 and 28 in January, April, July and October 2003. Yearly averaged values of these rate measurements were used to independently validate the model, as these data have not been used in model development and calibration. Total alkalinity [TA] data for the year 2003 have been obtained from Frederic Gazeau (personal communication and

$$
\begin{aligned}
\frac{d[\mathrm{FastOM}]}{dt} &= \mathbf{Tr}_{\mathrm{FastOM}} - \mathbf{R}_{\mathrm{OxFastOM}} - \mathbf{R}_{\mathrm{DenFastOM}} + \mathbf{R}_{\mathrm{PP}} \\
\frac{d[\mathrm{SlowOM}]}{dt} &= \mathbf{Tr}_{\mathrm{SlowOM}} - \mathbf{R}_{\mathrm{OxSlowOM}} - \mathbf{R}_{\mathrm{DenSlowOM}} \\
\frac{d[\mathrm{DOC}]}{dt} &= \mathbf{Tr}_{\mathrm{DOC}} \\
\frac{d[\mathrm{O_2}]}{dt} &= \mathbf{Tr}_{\mathrm{O_2}} + \mathbf{E}_{\mathrm{O_2}} - \mathbf{R}_{\mathrm{OxCarb}} - 2\ \mathbf{R}_{\mathrm{Nit}} + (2 - 2\ p^{\mathrm{PP}}_{\mathrm{NH_4^+}})\ \mathbf{R}_{\mathrm{PP}} + \mathbf{R}_{\mathrm{PPCarb}} \\
\frac{d[\mathrm{NO_3^-}]}{dt} &= \mathbf{Tr}_{\mathrm{NO_3^-}} - 0.8\ \mathbf{R}_{\mathrm{DenCarb}} + \mathbf{R}_{\mathrm{Nit}} - (1 - p^{\mathrm{PP}}_{\mathrm{NH_4^+}})\ \mathbf{R}_{\mathrm{PP}} \\
\frac{d[S]}{dt} &= \mathbf{Tr}_{S} \\
\frac{d[\sum \mathrm{CO_2}]}{dt} &= \mathbf{Tr}_{\sum \mathrm{CO_2}} + \mathbf{E}_{\mathrm{CO_2}} + \mathbf{R}_{\mathrm{OxCarb}} + \mathbf{R}_{\mathrm{DenCarb}} - \mathbf{R}_{\mathrm{PPCarb}} \\
\frac{d[\sum \mathrm{NH_4^+}]}{dt} &= \mathbf{Tr}_{\sum \mathrm{NH_3}} + \mathbf{R}_{\mathrm{Ox}} + \mathbf{R}_{\mathrm{Den}} - \mathbf{R}_{\mathrm{Nit}} - p^{\mathrm{PP}}_{\mathrm{NH_4^+}}\ \ \mathbf{R}_{\mathrm{PP}} \\
\frac{d[\sum \mathrm{HSO_4^-}]}{dt} &= \mathbf{Tr}_{\sum \mathrm{HSO_4^-}} \\
\frac{d[\sum \mathrm{B(OH)_3}]}{dt} &= \mathbf{Tr}_{\sum \mathrm{B(OH)_3}} \\
\frac{d[\sum \mathrm{HF}]}{dt} &= \mathbf{Tr}_{\sum \mathrm{HF}} \\
\frac{d[\mathrm{TA}]}{dt} &= \mathbf{Tr}_{\mathrm{TA}} + \mathbf{R}_{\mathrm{Ox}} + 0.8\ \mathbf{R}_{\mathrm{DenCarb}} + \mathbf{R}_{\mathrm{Den}} - 2\ \ \mathbf{R}_{\mathrm{Nit}} - (2\ p^{\mathrm{PP}}_{\mathrm{NH_4^+}} - 1)\ \mathbf{R}_{\mathrm{PP}}
\end{aligned}
$$

Table 2.5.: Rates of change of model state variables.

Gazeau et al., 2005). These yearly averages are based on four to five measurements along the estuary from January to May 2003 and monthly measurements for all 16 Scheldt monitoring stations from June to December 2003. $[\sum CO_2]$ data for 2003 have been calculated from [TA] data, monitoring pH and salinity, temperature forcing data, and $[\sum B(OH)_3]$, and $[\sum NH_4^+]$ from the model.

2.2.2.10. *Boundary condition forcings*

Values measured at monitoring station WS1 are considered to be downstream boundary conditions and values of station WS16 to be upstream boundary conditions. For $[O_2]$, $[\sum NH_3]$, $[NO_3^-]$, [OM], [DOC] and salinity, monitoring data were used for upstream and downstream boundaries. Organic matter (OM) is partitioned in a reactive (FastOM) and a refractory (SlowOM) fraction. At the downstream boundary a fraction of 0.4 of the organic matter (Soetaert and Herman, 1995a) is considered FastOM, and for the upstream boundary a FastOM fraction of 0.6 has been derived by calibration. Boundary conditions for $[\sum CO_2]$ ($[\sum CO_2]$ upstream: $4700\,\mathrm{mmol\,m^{-3}}$; downstream: $2600\,\mathrm{mmol\,m^{-3}}$; constant for all modelled years) have been calibrated using data from the year 2003. For $[\sum HSO_4^-]$, $[\sum HF]$ and $[\sum B(OH)_3]$ they were calculated from salinity monitoring data using formulae given in Appendix 2.6.2 (DOE, 1994). To ensure consistency, total alkalinity boundary concentrations were calculated from pH, salinity and temperature monitoring data and $[\sum CO_2]$ boundary conditions according to the total alkalinity definition used in our model (Dickson, 1981).

2.2.2.11. *Physical condition forcings*

Table 2.6.: Monitoring stations on the Scheldt estuary (Westerscheldt: "WS"). Coordinates are WGS84 values.

station ID	station name	river km	latitude	longitude
WS1	SSvH Breskens	104	51.41265° N	3.56628° E
WS2	W5 Sloehaven	96.3	51.43517° N	3.66932° E
WS3	Borssele	93.0	51.41720° N	3.69982° E
WS4	W20 Terneuzen	80.0	51.34888° N	3.82437° E
WS5	Boei 10 Hoedekenskerke	68.1	51.41733° N	3.92140° E
WS6	Hansweert	60.5	51.43597° N	4.01965° E
WS7	Waarde	57.7	51.42615° N	4.03527° E
WS8	Perkpolder	56.7	51.40118° N	4.03735° E
WS9	Baalhoek	51.8	51.37145° N	4.08503° E
WS10	Bath	46.1	51.39227° N	4.20527° E
WS11	Zandvliet	35.3	51.35030° N	4.24122° E
WS12	Lillo	29.2	51.29790° N	4.28232° E
WS13	Boei 105 – Punt van Melsele	21.5	51.25148° N	4.32050° E
WS14	Antwerpen	13.2	51.22493° N	4.39357° E
WS15	Hoboken	6.1	51.17525° N	4.32642° E
WS16	Rupelmonde	0.0	51.12912° N	4.31897° E

River flows at the upstream boundary are obtained from the Ministry of the Flemish Community (MVG). Since the advective flow increases from the upstream boundary towards the north sea due to inputs by amongst others the Antwerp harbour and the channel Gent-Terneuzen (van Eck, 1999; Soetaert et al., 2006) and no downstream flow values for the modelled years were available, data from the years 1980 to 1988 obtained from the SAWES model (van Gils et al., 1993; Holland, 1991) have been used to calculate a flow profile along the estuary. This is done by calculating percentages of mean flow increase between SAWES model boxes from the 1980 to 1988 data and scaling the upstream-border data for the years 2001 to 2004 accordingly, implementing a total flow increase of around 45% from Rupelmonde to Vlissingen. This practice implies that the lateral input into a particular part of the estuary has the same concentration as the input from upstream of this area.

The average water depth D (Fig. 2.2) was obtained for 13 MOSES model boxes from Soetaert and Herman (1995b) and interpolated to centres and boundaries of the 100 model boxes used in this work. The cross sectional area A (Fig. 2.2), has been obtained as a continuous function of river kilometres from Soetaert et al. (2006). Temperatures of the water column are monthly monitoring data and range from around freezing in winter to roughly 25°C in summer. Along the estuary there is a small spatial gradient in yearly temperature averages from around 13°C close to Rupelmonde to 12°C at Vlissingen. At 40 km from Rupelmonde, roughly at the position of the entrance to the harbour of Antwerp (Zandvliet lock) the yearly

temperature averages show a pronounced maximum around 1°C higher than values at the upstream boundary. This is probably due to a combined warming effect of the Antwerp harbour and the nuclear power plant at Doel roughly 4 km upstream of the temperature maximum.

2.2.3. Implementation and calibration

The spatial dimension of the model area along the estuary from Rupelmonde to Vlissingen is discretised by means of 100 supposedly homogeneous model boxes of 1.04 km length. These model boxes are assumed to have a tidally averaged volume (constant over time) and are numbered from i=1 (upstream) to i=100 (downstream).

The model has been implemented in FORTRAN using the modelling environment FEMME[3] (Soetaert et al., 2002) and numerically integrated over time with an Euler scheme using a time-step of 0.00781 days. Seasonal dynamics for the four model years were resolved but only yearly averages will be presented. Most post-processing of model output and creation of figures has been done with the R statistical computing environment (R Development Core Team, 2005).

Boundary and physical conditions (weather) are forced onto the model with monthly data from the respective years as described in Sect. 2.2.2.8.

An artificial spin-up year has been created, starting with arbitrary initial conditions for all state variables and containing only the initial values for the year 2001 for each forcing function. After running this spin-up year to create suitable initial conditions, the years 2001 to 2004 were run consecutively using forcing data from the respective year. Since FEMME requires a value for each forcing function at the beginning and at the end of each year, data for the first and the last day of each year were calculated by interpolation. For these calculations also data from 2000 and 2005 were used.

After the fitting of primary production in the year 2003 to values from Soetaert and Herman (1995c) (calibration of 5 biochemical parameters: r_{PP}, $k^{\mathrm{Inh}}_{\mathrm{DIN}}$, k^{Inh}_{D}, k^{Inh}_{Turb}, and $k_{\mathrm{NH}^+_4}$; and 1 boundary condition parameter: the relative turbidity upstream; fit not shown), the model was calibrated against data from the year 2003. During this model-data fitting procedure, 11 parameters were calibrated: 5 biochemical parameters, 3 boundary condition parameters, and 3 transport parameters. The transport formulation (parameters $E_{\max}$ and E_{Min}, see below) has been calibrated by comparing the model output to field data for S. $[\sum \mathrm{CO}_2]$ boundary conditions were calibrated by comparing the model output to [TA] data for 2003, and the parameters $r^{\mathrm{Min}}_{\mathrm{FastOM}}$, r^{Nit}, p, k^{Inh}_{S}, o^{Nit} as well as the fraction of OM that is considered FastOM at the upstream boundary were calibrated by comparing the model output to field data for [OM], $[\sum \mathrm{NH}^+_4]$, $[\mathrm{NO}^-_3]$, $[\mathrm{O}_2]$, and pH from the year 2003.

[3]The model code can be obtained from the corresponding author or from the FEMME website: http://www.nioo.knaw.nl/ceme/femme/

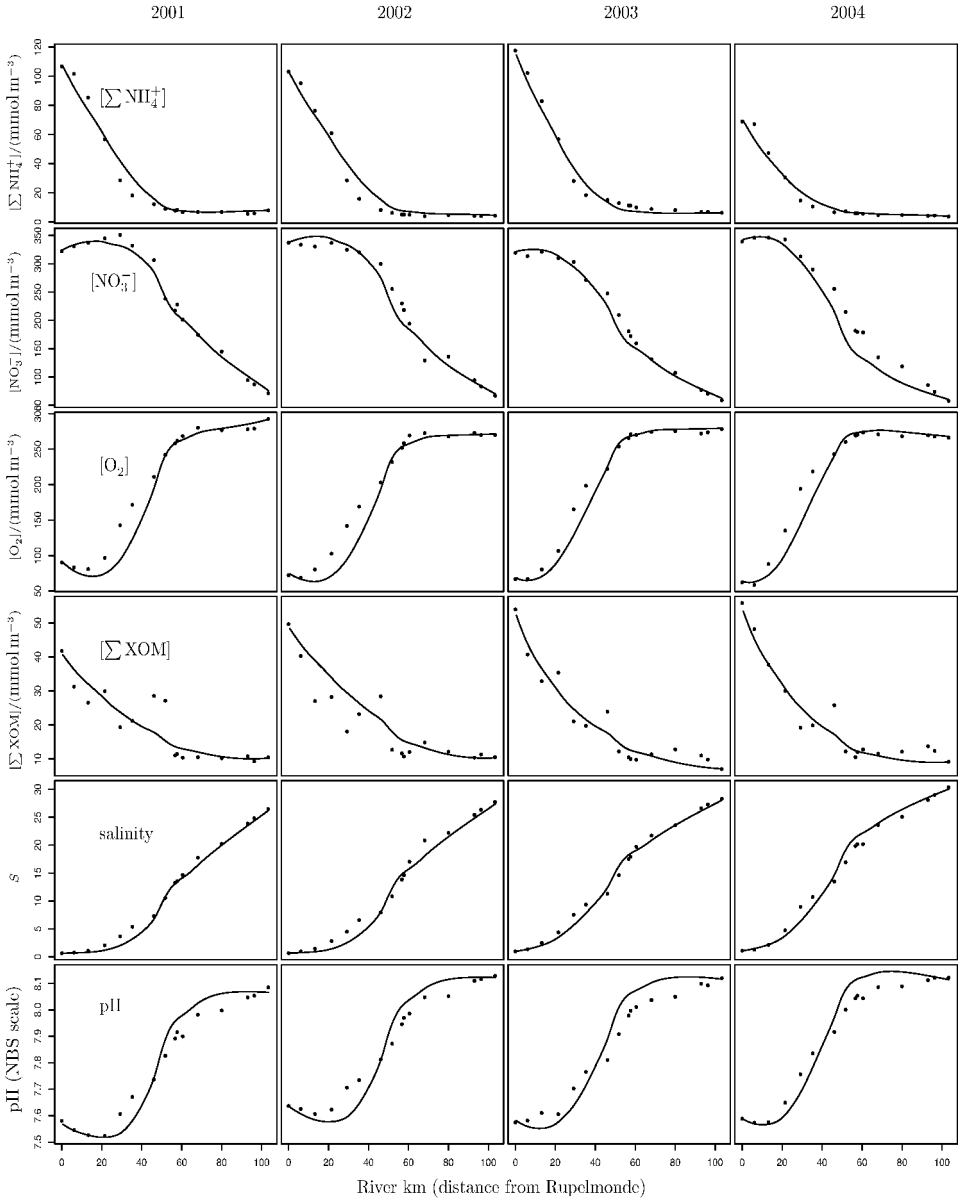

Figure 2.3.: Fit of the biogeochemical model for 4 consecutive years. Calibration was done on data for 2003 only. Data and model output are yearly averages.

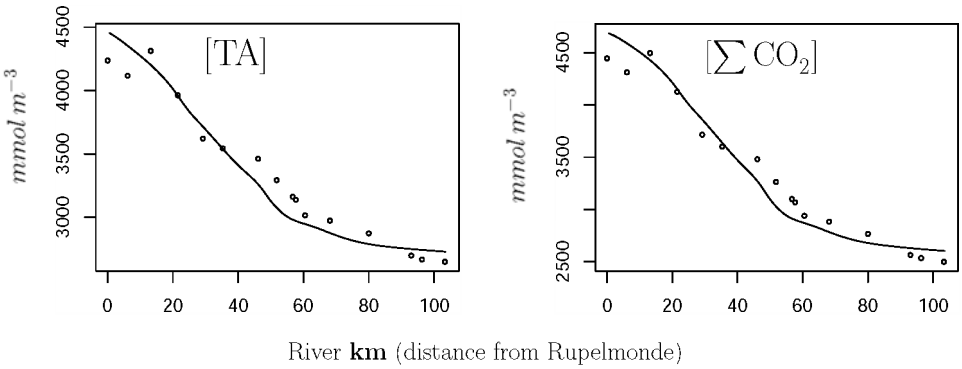

Figure 2.4.: Yearly averaged [TA] and $[\sum CO_2]$ (model output, 2003) vs. field data provided by Frederic Gazeau (personal communication and Gazeau et al., 2005). [TA] data are measurements, $[\sum CO_2]$ data are consistently calculated using conditions of the model.

2.3. Results

2.3.1. A relation between mean water depth D and tidal dispersion coefficients E

Following the idea put forward by Monismith et al. (2002) that there is proportionality between tidal dispersion and water depth and by comparing model output to field data for the conservative tracer salinity (see Fig. 2.3), we devised a linear relationship between tidal dispersion coefficients $E_{i-1,i}$ and mean water depth D_i for model box i:

$$E_{i-1,i} = E_{\mathrm{Max}} + (E_{\mathrm{Max}} - E_{\mathrm{Min}}) \frac{D_i - D_{\mathrm{Max}}}{D_{\mathrm{Max}} - D_{\mathrm{Min}}} \tag{6}$$

with

$$\begin{aligned} E_{\mathrm{Max}} &= 350 && \mathrm{m^2\,s^{-1}} \\ E_{\mathrm{Min}} &= 70 && \mathrm{m^2\,s^{-1}} \\ D_{\mathrm{Max}} &= 13.7 && \mathrm{m} \\ D_{\mathrm{Min}} &= 6.0 && \mathrm{m} \end{aligned}$$

Values for E_{Max} and E_{Min} were calibrated (within the range of E values given in Soetaert and Herman, 1995b), while values for D_{Max} and D_{Min} were obtained for the 13 MOSES model boxes from Soetaert and Herman (1995b).

E values obtained with our formula are comparable to the ones used by Vanderborght et al. (2007) at the respective grid size.

While transport coefficients were calibrated for the year 2003, yearly averaged longitudinal salinity profiles could be reproduced for the years 2001, 2002, and 2004 (see Fig. 2.3) by imposing respective advective flows Q and boundary conditions for salinity.

In all years, salinity more than linearly increases from around 1 upstream to values between 14 and 22 at km 60 and subsequently increases in linear fashion to values between 26 and 30 at the downstream boundary.

2.3.2. Comparison of yearly averaged longitudinal concentration and rate profiles to measured data

Several parameters have been manually calibrated to improve the fit of the biogeochemical model against field data from the year 2003 (Fig. 2.3). Yearly averaged values for data are time weighted averages. While biogeochemical model parameters (and transport coefficients) were fitted for 2003, the model predictions for 2001, 2002, and 2004 did not involve further calibration. Model fits to data from those years can thus be considered as model validation. It can be seen that the model reproduces the data reasonably well; not only for the calibration year 2003 but also for the validation years, with all years showing similar patterns. $[\sum NH_4^+]$ values are between 70 and 115 mmol m^{-3} upstream, falling almost linearly to values around 10 mmol m^{-3} at km 50 and staying below this value in the downstream stretches. Nitrate concentrations initially rise from concentrations approximately between 322 and 343 mmol m^{-3} to concentrations approximately between 325 and 348 mmol m^{-3} at km 16, subsequently fall more than linearly to values of 133 to 202 mmol m^{-3} at km 60, and then further decline quasi-linearly to values between around 60 and 76 mmol m^{-3} in the most downstream model box. Oxygen concentrations start off at values between 64 and 91 mmol m^{-3} upstream, stay constant or even decline between river kilometres 0 and 20, followed by a quasi linear increase to values of ≈265 mmol m^{-3} at river km 60, and staying in this realm until the downstream border. The sum of the concentrations of both fractions of particulate organic matter shows larger discrepancy between model and data. It declines over the stretch of the estuary from values of 41 to 53 mmol m^{-3} upstream down to values of approximately 9 mmol m^{-3} downstream. The NBS pH shows a sigmoidal increase from values around 7.57 to 7.63 upstream to values between 8.07 and 8.12 in the downstream part of the estuary. In all years a slight dip in the order of 0.03 to 0.05 pH values can be observed between km 0 to 30 preceding the sigmoidal increase.

Figure 2.4 shows the fit of predicted [TA] and $[\sum CO_2]$ against observed data for the year 2003 ($[\sum CO_2]$ data calculated from [TA] data). Note that these data (from the year 2003) have been used to calibrate only the $\sum CO_2$ boundary conditions for all four years. Both [TA] and $[\sum CO_2]$ decrease in a sigmoidal fashion from upstream to downstream, [TA] from between 4430 and 4480 mmol m^{-3} to between 2700 and 2740 mmol m^{-3}, and $[\sum CO_2]$ from around 4690 mmol m^{-3} to around 2600 mmol m^{-3}.

Figure 2.5 compares the modelled nitrification rate ($\mathbf{R}_{\mathrm{Nit}}$) for the year 2003 with field data obtained in the same year by Andersson et al. (2006) with the ^{15}N method. This is an independent model validation as these data have not been used in any way for calibration. It shows excellent agreement between measured and modelled nitrification rates, with an initially more than but overall approximately linear decline in nitrification from 13.1 mmol m^{-3} d^{-1} to 0.4 mmol m^{-3} d^{-1} from km 0 to km 60, followed by a gradual decline to 0.12 mmol m^{-3} d^{-1} in the most downstream model box.

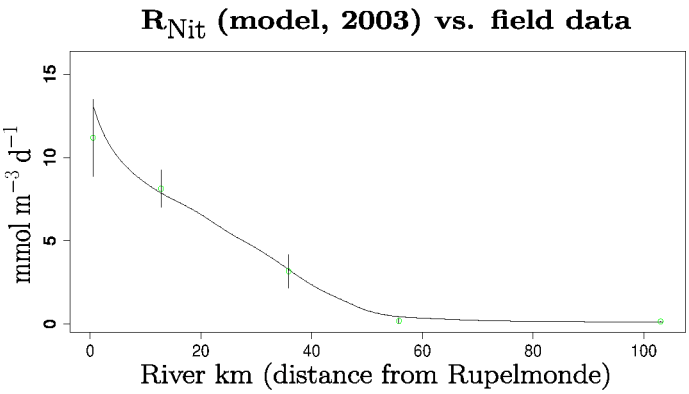

Figure 2.5.: Yearly averaged $\mathbf{R}_{\mathrm{Nit}}$ (model output, 2003) vs. field data (Andersson et al., 2006).

2.3.3. Sources and sinks for $\sum \mathrm{NH}_4^+$, $\sum \mathrm{CO}_2$, O_2 and NO_3^- along the estuary

2.3.3.1. Volumetric budgets

Since the model reproduces the spatial patterns of yearly averaged concentrations of $\sum \mathrm{NH}_4^+$, $\sum \mathrm{CO}_2$, O_2 and NO_3^- well for each of the four years, model rates can be used to compile budgets for these quantities. Figures 2.6 and 2.7 show cumulative plots of volumetric budgets along the estuary averaged over the years 2001 to 2004. A common feature is the pronounced activity in the upper estuary, i.e. between river km 0 and 60. In this stretch of estuary, the absolute values of almost all rates decline in a quasi linear fashion to stay at low levels until the mouth of the estuary.

	km 0	km 60	km 67	km 86	km 104
$\sum$ prod	4727.6	208.2	257.7	150.8	166.8
$\sum$ cons	−4745.7	−213.6	−263.4	−153.3	−168.2
$\mathbf{Tr}_{\sum \mathrm{NH}_4^+}$	3252.5 (69%)	16.2 (8%)	76.1 (30%)	−2.7 (2%)	−60.3 (36%)
$\mathbf{R}_{\mathrm{Ox}}$	913.2 (19%)	180.0 (86%)	170.9 (66%)	143.0 (95%)	159.6 (96%)
$\mathbf{R}_{\mathrm{Den}}$	562.0 (12%)	12.0 (6%)	10.7 (4%)	7.8 (5%)	7.2 (4%)
$\mathbf{R}_{\mathrm{Nit}}$	−4583.0 (97%)	−133.7 (63 %)	−91.8 (35%)	−51.9 (34%)	−39.7 (24%)
$-p^{\mathrm{PP}}_{\mathrm{NH}_4^+}\ \mathbf{R}_{\mathrm{PP}}$	−162.7 (3%)	−79.9 (37%)	−171.6 (65%)	−98.7 (64%)	−68.2 (41%)

Table 2.7.: Budget for $[\sum \mathrm{NH}_4^+]$; values in mmol N $\mathrm{m}^{-3}\,\mathrm{y}^{-1}$; percentages are of total production (positive quantities) or consumption (negative quantities), respectively.

It can be seen that $[\sum \mathrm{NH}_4^+]$ (Fig. 2.6a; Table 2.7) is mainly the result of a balance between nitrification ($\mathbf{R}_{\mathrm{Nit}}$) consuming $\sum \mathrm{NH}_4^+$ and advective-dispersive transport ($\mathbf{Tr}_{\sum \mathrm{NH}_4^+}$) which imports $\sum \mathrm{NH}_4^+$. The remaining gap is filled by $\sum \mathrm{NH}_4^+$ production by oxic mineralisation ($\mathbf{R}_{\mathrm{Ox}}$). Denitrification ($\mathbf{R}_{\mathrm{Den}}$) is responsible for 12% of the $\sum \mathrm{NH}_4^+$ input at the upstream boundary while losing relative importance towards the downstream boundary where it causes 4% of the $\sum \mathrm{NH}_4^+$ input. The situation is reversed for the influence of primary production ($-p^{\mathrm{PP}}_{\mathrm{NH}_4^+}\ \mathbf{R}_{\mathrm{PP}}$)

which causes 3% of the $\sum NH_4^+$ consumption upstream and 41% downstream.

	km 0	km 22	km 48	km 60	km 67	km 104
$\sum$ prod	6796.0	5608.2	3912.9	1047.9	1528.6	694.3
$\sum$ cons	−6796.5	−5632.7	−3988.2	−1094.7	−1559.9	−694.1
$\mathbf{Tr}_{\sum CO_2}$	786.3 (12%)	3299.4 (59%)	2742.4 (70%)	236.3 (23%)	762.9 (50%)	−9.0 (1%)
$\mathbf{R}_{OxCarb}$	3720.0 (55%)	1738.9 (31%)	1078.3 (28%)	760.9 (73%)	720.4 (47%)	664.4 (96%)
$\mathbf{R}_{DenCarb}$	2289.7 (34%)	569.9 (10%)	92.1 (2%)	50.8 (5%)	45.2 (3%)	29.9 (4%)
$-\mathbf{R}_{PPCarb}$	−660.9 (10%)	−279.9 (5%)	−1234.6 (31%)	−376.4 (34%)	−815.4 (52%)	−337.5 (49%)
$\mathbf{E}_{CO_2}$	−6135.6 (90%)	−5352.7 (95%)	−2753.5 (69%)	−718.4 (66%)	−744.4 (48%)	−347.7 (50%)

Table 2.8.: Budget for $[\sum CO_2]$; values in mmol C m^{-3} y^{-1}; percentages are of total production (positive quantities) or consumption (negative quantities), respectively.

The budget for $[\sum CO_2]$ (Fig. 2.6b; Table 2.8) is characterised by CO_2 loss to the atmosphere via air-water exchange ($\mathbf{E}_{CO_2}$), advective-dispersive $\sum CO_2$ input ($\mathbf{Tr}_{\sum CO_2}$), as well as $\sum CO_2$ production by oxic mineralisation ($\mathbf{R}_{OxCarb}$) and denitrification ($\mathbf{R}_{DenCarb}$). Primary production accounts for only 10% of the ≈6800 mmol C m^{-3} y^{-1} $\sum CO_2$ consumption in the upstream region, while its relative importance increases in the downstream area where it accounts for almost 50% of the approximately 700 mmol C m^{-3} y^{-1} of $\sum CO_2$ consumption. $\sum CO_2$ production by oxic mineralisation ($\mathbf{R}_{OxCarb}$) and denitrification ($\mathbf{R}_{DenCarb}$) steadily decrease from values around 3700 and 2300 mmol C m^{-3} y^{-1} to values around 700 and 30 mmol C m^{-3} y^{-1}, where the relative importance of oxic mineralisation increases from 55% to 96% and that of denitrification decreases from 34% to 4%. The net advective-dispersive $\sum CO_2$ input ($\mathbf{Tr}_{\sum CO_2}$) accounts with about 800 mmol C m^{-3} y^{-1} for 12% of the $\sum CO_2$ input at the upstream boundary, has a local maximum at river km 22 with ≈3300 mmol C m^{-3} y^{-1}, and has another one at river km 48 with ≈2700 mmol C m^{-3} y^{-1}, where it accounts for 70% of the total $\sum CO_2$ input. At river km 60, $\mathbf{Tr}_{\sum CO_2}$ exhibits a local minimum with ≈200 mmol C m^{-3} y^{-1}, followed by another local maximum at km 67 with ≈800 mmol C m^{-3} y^{-1} and, finally, a steady decrease reaching negative values at the downstream border.

The budget for $[O_2]$ (Fig. 2.7a; Table 2.9) is clearly dominated by oxygen consumption due to nitrification ($-2\ \mathbf{R}_{Nit}$) and oxic mineralisation ($-\mathbf{R}_{OxCarb}$). O_2 consumption of both of these processes steadily decreases from ≈9200 mmol O_2 m^{-3} y^{-1} and 3700 mmol O_2 m^{-3} y^{-1} to ≈80 mmol O_2 m^{-3} y^{-1} and ≈700 mmol O_2 m^{-3} y^{-1}. Their relative importance profile is approximately mirrored as nitrification accounts for 71% and oxic mineralisation for 29% of O_2 consumption at the upstream boundary while nitrification is responsible for 11% and oxic mineralisation for 89% of O_2 consumption at the downstream boundary. The relative importance of oxygen production by primary production ($(2-2\ p^{PP}_{NH_4^+})\ \mathbf{R}_{PP}+\mathbf{R}_{PPCarb}$) stays below 6% up to river km 29, while reaching values as high as 62% at river km 93. As total oxygen consumption decreases, also oxygen re-areation ($\mathbf{E}_{O_2}$) decreaes from ≈7800 mmol O_2 m^{-3} y^{-1} upstream to ≈150 mmol O_2 m^{-3} y^{-1} downstream. The net effect of advection dispersion on oxygen ($\mathbf{Tr}_{O_2}$) is positive in the upstream region, reaches approximately 0 mmol O_2 m^{-3} y^{-1} at river km 22 and becomes negative from river km 29 on. At river km 48 it shows a local minimum with an O_2 consumption of ≈2500 mmol O_2 m^{-3} y^{-1}, at river km 60 a local maximum can be discerned, but only from river km 93 on $\mathbf{Tr}_{O_2}$ becomes positive again.

	km 0	km 22	km 29	km 48	km 60	km 67	km 93	km 104
$\sum$ prod	12862.8	6374.3	5269.0	4391.7	1185.8	1657.8	683.0	739.4
$\sum$ cons	−12885.9	−6381.7	−5267.4	−4388.7	−1182.1	−1660.6	−687.7	−743.8
$\mathbf{Tr}_{O_2}$	5418.6 (42%)	1.7 (0%)	−105.8 (2%)	−2468.6 (56%)	−153.9 (13%)	−756.5 (46%)	5.6 (1%)	219.9 (30%)
$-\mathbf{R}_{\mathrm{OxCarb}}$	−3720.0 (29%)	−1738.9 (27%)	−1483.7 (28%)	−1078.3 (25%)	−760.9 (64%)	−720.4 (43%)	−594.7 (86%)	−664.4 (89%)
$-2\ \mathbf{R}_{\mathrm{Nit}}$	−9165.9 (71%)	−4642.9 (73%)	−3677.9 (70%)	−841.7 (19%)	−267.3 (23%)	−183.6 (11%)	−93.0 (14%)	−79.4 (11%)
$(2-2\ p^{\mathrm{PP}}_{\mathrm{NH}_4^+})\ \mathbf{R}_{\mathrm{PP}}$								
$+\mathbf{R}_{\mathrm{PPCarb}}$	666.0 (5%)	285.2 (4%)	292.9 (6%)	1317.0 (30%)	404.7 (34%)	879.9 (53%)	424.4 (62%)	369.8 (50%)
$\mathbf{E}_{O_2}$	6778.2 (53%)	6087.5 (95%)	4976.2 (94%)	3074.7 (70%)	781.1 (66%)	777.8 (47%)	253.0 (37%)	149.8 (20%)

Table 2.9.: Budget for $[O_2]$; values in mmol $O_2\,m^{-3}\,y^{-1}$; percentages are of total production (positive quantities) or consumption (negative quantities), respectively.

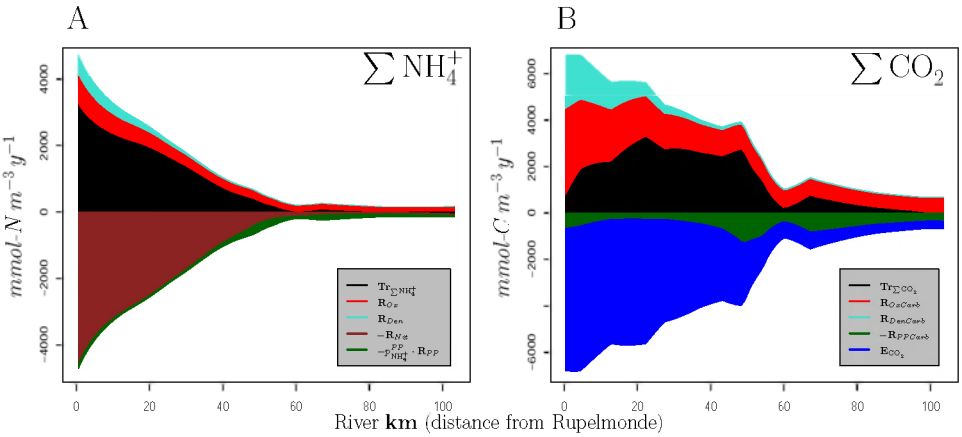

Figure 2.6.: Budgets for $[\sum NH_4^+]$ **(a)** and $[\sum CO_2]$ **(b)** along the estuary, averaged over 2001–2004 (cumulatively plotted); Values are in mmol m^{-3} y^{-1}.

$[NO_3^-]$ along the estuary (Fig. 2.7a; Table 2.10) is governed by nitrate production due to nitrification ($\mathbf{R}_{\mathrm{Nit}}$) and nitrate consumption due to denitrification ($-0.8\ \mathbf{R}_{\mathrm{DenCarb}}$) and advective-dispersive transport ($\mathbf{Tr}_{NO_3^-}$). Nitrate production by nitrification, which is as high as ≈4600 mmol N m^{-3} y^{-1} upstream and ≈40 mmol N m^{-3} y^{-1} downstream, is counteracted upstream for 60% by the net effect of advective dispersive transport ($\mathbf{Tr}_{NO_3^-}$), and for 40% by denitrification ($-0.8\ \mathbf{R}_{\mathrm{DenCarb}}$). Only from km 57 on, NO_3^- consumption by primary production $\left(-(1-p_{NH_4^+})\ \mathbf{R}_{\mathrm{PP}}\right)$ gains relative significance with values as high as 29% of the NO_3^- consumption at river km 104.

2.3.3.2. Volume integrated budgets

As the estuarine cross section area increases from 4000 m^2 upstream to around 76 000 m^2 downstream, there is a much larger estuarine volume in downstream model boxes than in upstream model boxes. Thus, volume integrated production or consumption rates (rates "per river km") are similar in the upstream and the downstream part of the estuary (in accordance with findings of Vanderborght et al., 2002), unlike in the volumetric plots, where the upstream region was clearly dominant. Figures 2.8 and 2.9 show volume integrated budgets along the estuary averaged for the years 2001 to 2004.

While for $\sum NH_4^+$ (Fig. 2.8a) the upstream region can be identified as most important in terms of total turnover, for $\sum CO_2$ (Fig. 2.8b) and O_2 (Fig. 2.9a) a pronounced maximum of total turnover can be distinguished at around km 50 (intertidal flat system of Saeftinge) next to high total turnover values in the downstream region from around river km 70 on. For NO_3^- the upstream area is most important, similar to its volumetric budget.

Figure 2.8a and Table 2.11 in combination with the percentages given in Table 2.7 show that, in contrast to the volumetric budget, volume integrated $\sum NH_4^+$ production due to oxic mineralisation ($\mathbf{R}_{\mathrm{Ox}}$) is maximal at the downstream border with ≈12.2 mmol N km^{-1} y^{-1}. All other processes still contribute most to $[\sum NH_4^+]$ at the upstream boundary, except for ammonium

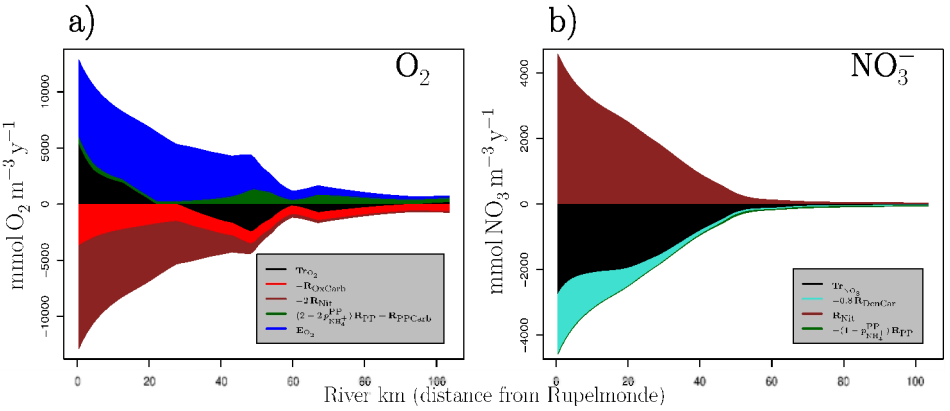

Figure 2.7.: Budgets for $[O_2]$ **(a)** and $[NO_3^-]$ **(b)** along the estuary, averaged over 2001–2004 (cumulatively plotted); Values are in mmol m^{-3} y^{-1}.

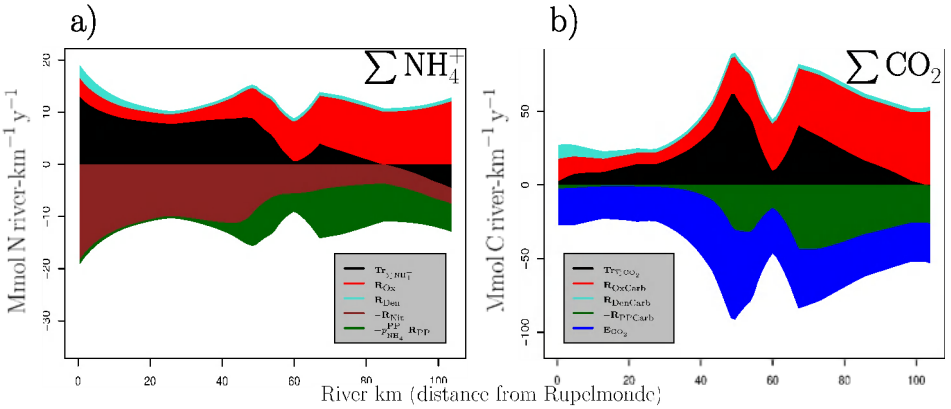

Figure 2.8.: Volume integrated budgets for $\sum NH_4^+$ **(a)** and $\sum CO_2$ **(b)** along the estuary, averaged over 2001–2004; Values are in Mmol (river km)$^{-1}$ y^{-1}.

consumption due to primary production which also has its volumetric maximum in the downstream region. In the volume integrated plot, it can be clearly seen that the net influence of advective dispersive transport on $[\sum NH_4^+]$ ($\mathbf{Tr}_{\sum NH_4^+}$) is negative at the downstream boundary (≈ -4.6 mmol N km^{-1} y^{-1}).

The volume integrated budget for $\sum CO_2$ (Fig. 2.8b; Table 2.11 in combination with Table 2.8) shows a distinct maximum of total $\sum CO_2$ turnover at km 48 with a total $\sum CO_2$ production of 88.5 mmol C km^{-1} y^{-1} and a total $\sum CO_2$ consumption of 90.2 mmol C km^{-1} y^{-1}. This maximum is followed by a slight dip in total turnover at km 60. At river km 86, total $\sum CO_2$ turnover rates reach values slightly lower than at the maximum of km 48 and gradually decline towards the downstream boundary where 60% of the maximal values are reached. Around the downstream boundary, $\sum CO_2$ production by oxic mineralisation has its maximum at $\approx$50.6 mmol C km^{-1} y^{-1} while volume integrated $\sum CO_2$ consuption due to primary produc-

	km 0	km 57	km 104
$\sum$ prod	4583.0	157.4	39.7
$\sum$ cons	−4581.2	−200.7	−55.2
$\mathbf{Tr}_{NO_3^-}$	−2746.9 (60%)	−132.9 (66%)	−15.1 (27%)
$-0.8\ \mathbf{R}_{DenCarb}$	−1831.8 (40%)	−44.3 (22%)	−23.9 (43%)
$\mathbf{R}_{Nit}$	4583.0 (100%)	157.4 (100%)	39.7 (100%)
$-(1-p_{NH_4^+})\ \mathbf{R}_{PP}$	−2.5 (0%)	−23.5 (12%)	−16.1 (29%)

Table 2.10.: Budget for $[NO_3^-]$; values in mmol N m^{-3} y^{-1}; percentages are of total production (positive quantities) or consumption (negative quantities), respectively.

		km 0	km 22	km 29	km 48	km 57	km 60	km 67	km 86	km 93	km 104
$\sum NH_4^+$	$\sum$ prod	18.9	10.5	10.4	15.2	10.4	8.8	13.8	10.7	11.0	12.7
	$\sum$ cons	−19.0	−10.5	−10.5	−15.6	−10.7	−9.0	−14.1	−10.9	−11.2	−12.8
$\sum CO_2$	$\sum$ prod	27.2	24.7	25.3	88.5	57.7	44.2	81.9	61.5	55.8	52.9
	$\sum$ cons	−27.2	−24.8	−25.5	−90.2	−59.6	−46.1	−83.5	−61.6	−55.8	−52.9
O_2	$\sum$ prod	51.5	28.1	28.9	99.4	64.6	50.0	88.8	60.2	50.6	56.3
	$\sum$ cons	−51.5	−28.2	−28.9	−99.3	−64.5	−49.8	−88.9	−60.6	−51.0	−56.7
NO_3^-	$\sum$ prod	18.3	10.2	10.1	9.5	5.8	5.6	4.9	3.7	3.4	3.0
	$\sum$ cons	−18.3	−10.3	−10.1	−10.3	−7.4	−7.5	−7.1	−5.7	−5.2	−4.2

Table 2.11.: Volume integrated budgets for $\sum NH_4^+$, $\sum CO_2$, O_2, and NO_3^-; values in Mmol (river km)$^{-1}$ y^{-1}.

tion has its maximum at km 67 with ≈43.4 mmol C km^{-1} y^{-1}. Especially at kilometres 48 to 67 it can be seen that the volume integrated total loss of $\sum CO_2$ is higher than the total $\sum CO_2$ production.

The volume integrated budget for O_2 (Fig. 2.9a; Table 2.11 in combination with Table 2.9) shows similar process patterns and basic shape as the volume integrated budget for $\sum CO_2$, with a maximum of absolute values of total O_2 turnover at km 48 followed by a dip in absolute values of total O_2 turnover at km 60, with the exception of $\mathbf{Tr}_{O_2}$ changing sign twice.

Unlike for the other chemical species, the volume integrated budget for NO_3^- (Fig. 2.9b; Table 2.11 in combination with Table 2.10) shows distinct maxima in total turnover at the upstream boundary and decreases towards the downstream boundary. However, the resulting trumpet-like shape is not as pronounced as for the volumetric budget for $[NO_3^-]$.

2.3.3.3. Whole estuarine budgets

Figures 2.10 and 2.11 show budgets of $\sum NH_4^+$, $\sum CO_2$, O_2, and NO_3^- production and consumption, integrated over the whole model area and one year (averaged over the four modelled years).

Figure 2.10a shows a budget of $\sum NH_4^+$. It becomes clear that nitrification is the most important process affecting $\sum NH_4^+$ in the estuary with a total loss of ≈0.8 Gmol in the whole model region. This $\sum NH_4^+$ consumption together with the $\sum NH_4^+$ consumption of primary production of ≈0.4 Gmol is counteracted by $\sum NH_4^+$ production/import due to mainly oxic

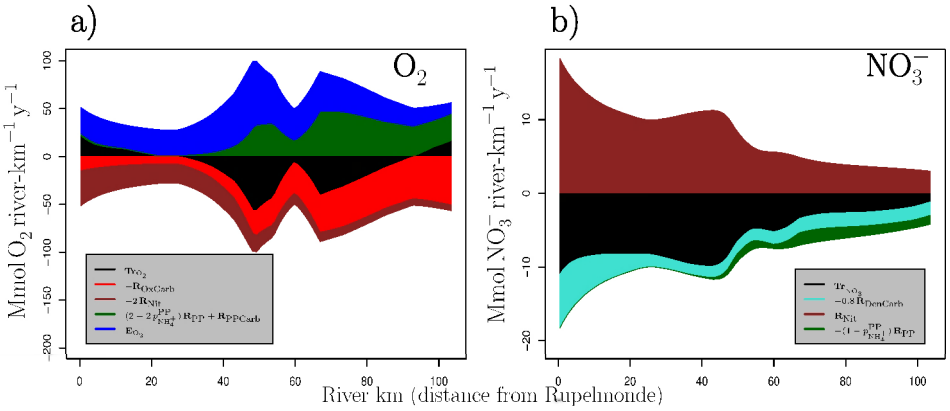

Figure 2.9.: Volume integrated budgets for O_2 **(a)** and NH_3^- **(b)** along the estuary, averaged over 2001–2004; Values are in Mmol (river km)$^{-1}$ y^{-1}.

mineralisation (≈0.7 Gmol) and advective-dispersive transport (≈0.5 Gmol). Denitrification plays a minor role producing less than 0.1 Gmol of $\sum NH_4^+$ per year.

Total estuarine $\sum CO_2$ (Fig. 2.10b) is prominently influenced by out-gassing of CO_2 to the atmosphere, which consumes ≈3.3 Gmol, while primary production consumes only ≈2.0 Gmol. Advective-dispersive input and oxic mineralisation supply $\sum CO_2$ at values of ≈2.2 Gmol and ≈2.7 Gmol respectively. Again, denitrification has a minor influence, producing less than 0.3 Gmol of inorganic carbon per year.

In our model, oxygen (Fig. 2.11a) is net supplied to the estuary via re-aeration (≈3.4 Gmol) and primary production (≈2.1 Gmol). All other modelled processes consume oxygen, advective-dispersive transport net exports ≈1.2 Gmol to the sea, oxic mineralisation consumes ≈2.7 Gmol, and nitrification ≈1.7 Gmol.

Nitrate (Fig. 2.11b) is produced by nitrification (≈0.8 Gmol), exported by advective-dispersive transport (≈0.6 Gmol), consumed by denitrification (≈0.2 Gmol), and by primary production (less than 0.1 Gmol).

2.3.4. Interannual differences

Although the freshwater discharge Q of the Scheldt shows no consistent trend during the years 1990 to 2004, it peaked in 2001 and fell rapidly until 2004 (Meire et al., 2005; Van Damme et al., 2005; van Eck, 1999), resulting in a downwards trend during our model time period. The plots in Fig. 2.12 show trends of freshwater discharge Q, volume averaged S and $[CO_2]$, and CO_2 degassing $\mathbf{E}_{CO_2}$ in the estuary from the year 2001 to 2004.

This decrease in Q is most likely the reason for several observed trends in our model. E.g. salinity S increases from 2001 to 2004 which is clearly a result of lowered freshwater discharge, as more saline seawater can enter the estuary (Meire et al., 2005; Van Damme et al., 2005).

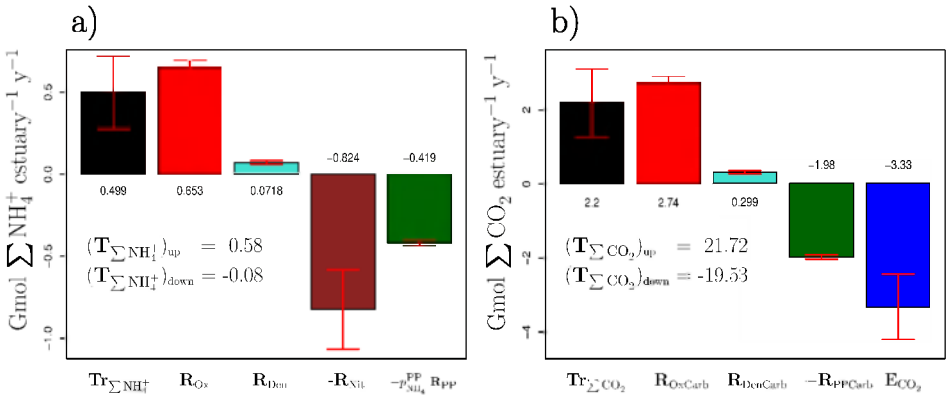

Figure 2.10.: Total annual budgets for $\sum NH_4^+$ **(a)** and $\sum CO_2$ **(b)** for the whole estuary, averaged over 2001–2004. $(\mathbf{Tr}_X)_{up}$ and $(\mathbf{Tr}_X)_{down}$ signify advective-dispersive import or export at the upstream and downstream boundary. The error bars give the standard deviation σ, obtained from averaging over the four model years.

Similarly, the observed decrease in $[\sum CO_2]$ can be explained by less $\sum CO_2$ being imported into the estuary from the river at lower freshwater discharge ($[\sum CO_2]$ not shown). A decrease in $[\sum CO_2]$ also means a decrease in $[CO_2]$. However, via its influence on the dissociation constants K^*, salinity also influences $[CO_2]$, higher salinity meaning lower $[CO_2]$, reinforcing its downward trend from 2001 to 2004. Decreasing levels of $[CO_2]$ lower the CO_2 saturation state of the water and eventually lead to less CO_2 export to the atmosphere (The total amount of CO_2 export to the atmosphere and the volume averaged saturation states for the four modelled years and the whole estuary are given in Table 2.12). Model runs with scaled freshwater flow (results not shown) confirm the inverse correlation between freshwater flow Q and $\mathbf{E}_{CO_2}$.

	2001	2002	2003	2004
CO_2 export	4.50	3.43	2.96	2.41
$[CO_2]$	69.00	56.05	51.37	45.21
$[CO_2]_{sat}$	17.97	17.62	17.60	17.33
% CO_2 saturation	384.09	318.07	291.95	260.88

Table 2.12.: CO_2 export to the atmosphere ($-\mathbf{E}_{CO_2}$) in $Gmol\,y^{-1}$ per modelled area, $[CO_2]$ and $[CO_2]_{sat}$ are volume and yearly averaged values for the whole estuary in $mmol\,m^{-3}$.

Furthermore, pH influences $[CO_2]$, higher pH implying lower $[CO_2]$. There was an upward trend in pH during our model years, which reinforces the downward trend in CO_2 export to the atmosphere. We believe that there is a relation between the decrease in freshwater flow and the upward trend in pH from 2001 to 2004, however, the exact mechanism for this relationship is not straight-forward. A mechanistic model able to quantify the influence of

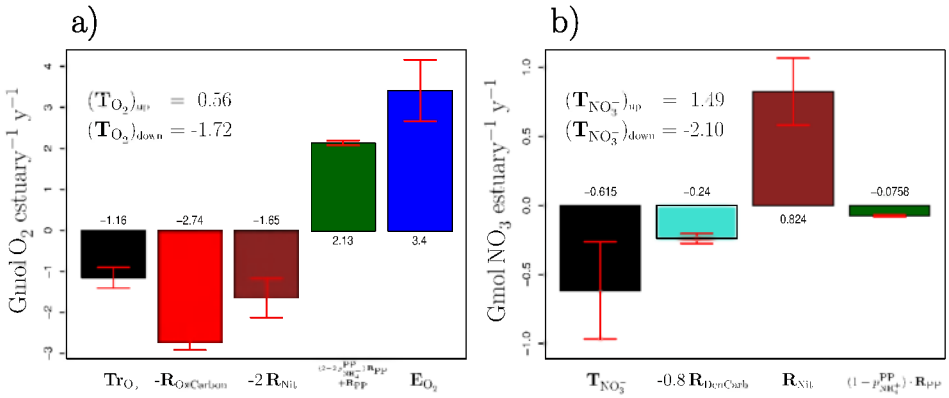

Figure 2.11.: Total annual budgets for O_2 **(a)** and NH_3^- **(b)** for the whole estuary, averaged over 2001–2004. $(\mathbf{Tr_X})_{up}$ and $(\mathbf{Tr_X})_{down}$ signify advective-dispersive import or export at the upstream and downstream boundary. The error bars give the standard deviation, σ, obtained from averaging over the four model years.

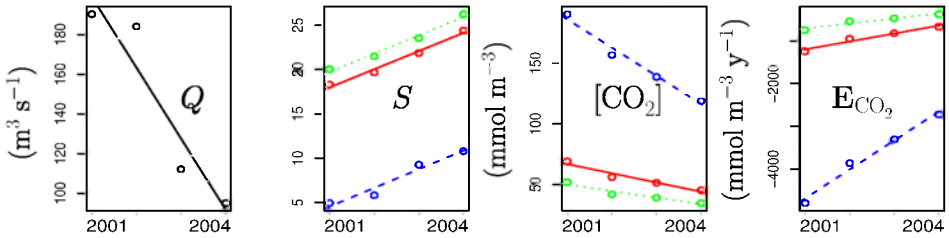

Figure 2.12.: Trends in key quantities from 2001 to 2004 (Q signifies the freshwater flow at the upstream boundary; S, $[CO_2]$, $\mathbf{E}_{CO_2}$: volume averaged, solid red line: total estuary, dashed blue line: upper part (to box 50), dotted green line: lower part).

different modelled kinetic processes on the pH (Hofmann et al., 2008a, i.e., Chapter 3) will shed some further light on this issue.

2.4. Discussion

2.4.1. Model performance: data-model validation

Our objective was to construct a simple model reproducing observed data and interannual differences, allowing the establishment of annual budgets. Advective-dispersive transport is accurately reproduced (confer the fit of yearly averaged logitudinal profiles of the conservative tracer salinity, Fig. 2.3).

The model also reproduces $[\sum NH_4^+]$, $[NO_3^-]$, $[O_2]$, and pH versus river kilometres very well.

This level of performance has been achieved by using 7 biochemical parameters from literature

and calibrating the other 5 using data for the year 2003 (plus the calibration of 5 biochemical parameters to fit primary production to values from Soetaert and Herman, 1995c). To run the model for the years 2001, 2002, and 2004, the upstream advective forcing, the temperature forcing, and the boundary concentrations have been adapted, but no further calibration was involved, making the fits for those years a model validation. Furthermore the model has been independently validated by comparing nitrification rates to field data from the year 2003 (Andersson et al., 2006) realising the objective of creating a tool to examine interannual differences and annual budgets of key chemical species in the Scheldt estuary.

The very good overall performance of our rather simple model confirms the notion of Arndt et al. (2007) that for estuaries biogeochemical model complexity can be kept low as long as physical processes (i.e. transport) perform sufficiently well. (Note that a good model performance in terms of physics does not imply a complex representation of physical processes.)

This argument is strengthened by the fact that the fits of a model including NH_3 air-sea exchange, sulfate reduction, sulfide oxidation, biogenic calcification as well as calcite and aragonite precipitation did not significantly differ from the fits of the model presented here.

However, some features of the fits of state variables given in Fig. 2.3 suggest that the inclusion of further processes might make the model even more accurate. Modelled $[\sum NH_4^+]$ for example is slightly too high between river km 30 and km 50, which could be explained by microbial ammonium uptake (cf. Middelburg and Nieuwenhuize, 2000). Furthermore, a reason for an underestimated organic matter concentration around the intertidal flat area of Saeftinge (≈river km 35 to 50) might be the fact that the model does not include any explicit organic matter input from this ecosystem consisting mainly of vascular plants. Although these and other arguments can be made about details, we consider the fit of our model adequate for our aims and for the simplified conceptual model.

2.4.1.1. Denitrification

Denitrification is not strongly constrained in our model because of the lack of direct measurements.

Figure 2.13 shows the model fit for $[NO_3^-]$ with three different parametrisations for denitrification: our parametrisation based on literature values (solid black line), no denitrification (dashed red line) and denitrification maximised (dotted blue line) by using a very small $k_{NO_3^-}$ (10^{-8} mmol N m^{-3}) and a very large $k_{O_2}^{Inh}$ (10^8 mmol N m^{-3}), resulting in ≈1.3 Gmol NO_3^- consumption due to denitrification per year (compared to 0.2 Gmol y^{-1} with our parametrisation). Although the effect of denitrification on $[NO_3^-]$ along the estuary is small, this plot shows that our parametrisation based on literature values gives the best model performance.

Andersson (2007) reports 16 mmol m^{-2} d^{-1} of NO_3^- consumption due to denitrification for sediment from one lower estuary location in the Scheldt. Considering 338 km^2 of estuarine surface area, our model result of 0.2 Gmol NO_3^- consumption due to denitrification per year implies an average denitrification of 1.6 mmol NO_3^- m^{-2} d^{-1}, i.e. only one tenth of this number. Even with maximal denitrification and the associated worse model performance (Fig. 2.13),

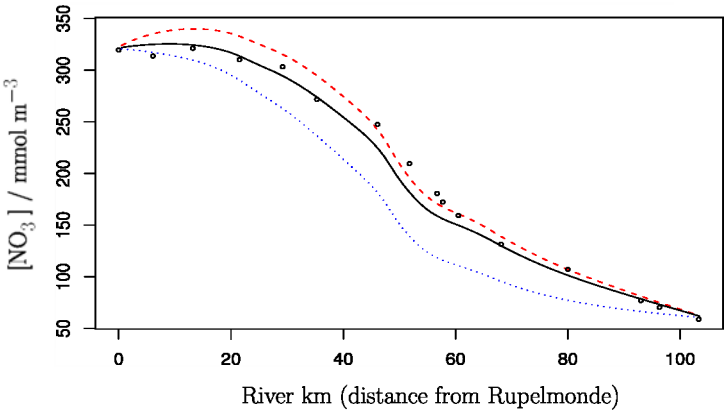

Figure 2.13.: $[NO_3^-]$ fit with different denitrification parametrisations: our parametrisation based on literature values (solid black line), no denitrification (dashed red line) and denitrification maximised (dotted blue line)

only a denitrification of $10.5\,\mathrm{mmol\,NO_3^-\,m^{-2}\,d^{-1}}$ can be achieved. This difference between our top-down whole estuarine estimate and the estimate of Andersson (2007) clearly shows the difficulties one encounters when upscaling sedimentary biogeochemical process rates over large areas and long timescales.

Furthermore we model denitrification pelagically as a proxy for a sedimentary process. As a result of this practice the effect of denitrification on the concentrations in the water column is not geographically fixed but moves up and down the river. This would have a large effect on a tidally resolved model as parts of the sediment may fall dry and loose contact with the water column. However, for a tidally averaged model as ours and for yearly averaged values in particular, this effect is rather small. Nevertheless, we are aware that modelling pelagic denitrification as a proxy for benthic processes introduces an error in our volumetric and volume integrated logitudinal estuarine budget. But since the region of main denitrification activity always stays within our model domain, our total stock budgets are not significantly affected by this error.

2.4.2. Volumetric budgets for $[\sum NH_4^+]$, $[\sum CO_2]$, $[O_2]$ and $[NO_3^-]$

According to the volumetric budgets for $[\sum NH_4^+]$, $[\sum CO_2]$, $[O_2]$ and $[NO_3^-]$, the estuary can be divided into two parts, an upstream region (river km 0 until roughly km 55 at Walsoorden) and a downstream area, with process rates being up to an order of magnitude higher in the upstream part. This division, which is in accordance to findings of Vanderborght et al. (2007), Regnier et al. (1997), and Soetaert and Herman (1995a,c), is more pronounced for $[NO_3^-]$ and $[\sum NH_4^+]$ than for $[O_2]$ and $[\sum CO_2]$, because the latter two quantities also depend on gas exchange with the atmosphere which in turn only depends on the concentration of the species to be exchanged and not on the concentrations of other species. Biogeochemical rates, in contrast, usually depend on the concentrations of several substances. Therefore the rates

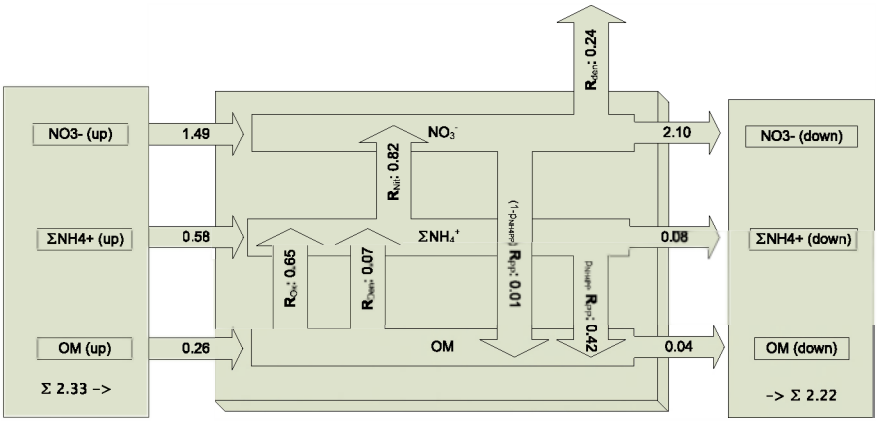

Figure 2.14.: Tentative nitrogen budget per year over the whole model area, averaged over 2001 to 2004. Values are given in Gmol y^{-1}. Note that the budget is not fully closed, there is an overall loss term of 0.13 Gmol N y^{-1}. This is consistent with the temporal downward trend in $[\sum NH_4^+]$ and $[NO_3^-]$. Note also that organic nitrogen (Org-N) refers to particulate organic matter (OM). Dissolved organic nitrogen (DON) is not shown in this budget. Using γ_{DOM} and conservatively modelled [DOC], one can estimate that around 0.16 Gmol of DON enters and leaves the estuary on average per year.

of gas exchange processes decrease less than biogeochemical rates as nutrient levels decrease when going from upstream to downstream in the Scheldt estuary. However, $\mathbf{E}_{CO_2}$ is also strongly influenced by the pH in the estuary, which rises from ≈7.6 in the upstream regions to ≈8.1 downstream. This is because $\mathbf{E}_{CO_2}$ depends linearly on $[CO_2]$ which in turn depends on pH. A rising pH induces a declining $[CO_2]$. Considering the estuarine averages of $[\sum CO_2]$ ≈3400 mmol m^{-3}, T≈13°C, and S≈10, $[CO_2]$ declines by a factor of about 3.25 from around 130 mmol m^{-3} to around 40 mmol m^{-3} for pH increasing from around 7.6 to 8.1. This means, that the increase in pH along the estuary contributes to the decline in the absolute values of $\mathbf{E}_{CO_2}$ from upstream to downstream.

While the volumetric budgets for $[\sum NH_4^+]$ (Fig. 2.6a) and $[NO_3^-]$ (Fig. 2.7b) show relatively smooth features, the volumetric budget for $[\sum CO_2]$ (Fig. 2.6b) exhibits a more spiked pattern. Its shape is a result of the dependency of $[\sum CO_2]$ on CO_2 air-water exchange ($\mathbf{E}_{CO_2}$) which in turn is influenced by the estuarine depth D. This fact makes estuarine depth patterns visible in the budget for $[\sum CO_2]$. To a lesser extent the same can be seen in the volumetric budget for $[O_2]$ (Fig. 2.7a), which in the upper reaches of the estuary, between river km 0 and about 22, smoothly follows the $[\sum NH_4^+]$ budget (dominated by nitrification), but in the downstream part of the estuary also shows estuarine depth patterns, attributable to its dependency on O_2 air-water exchange ($\mathbf{E}_{O_2}$).

2.4.3. Oxygen budget

It is clear that oxygen consumption by nitrification and oxic mineralisation, and export by advective-dispersive transport processes are balanced not only by oxygen production due to primary production but mainly by oxygen import from the atmosphere. Similarly to Ouboter et al. (1998), in our model about one third of the total oxygen consumption in the estuary is due to nitrification; oxygen consumption by oxic mineralisation is comparable to oxygen consumption by nitrification, similar to conditions reported by Regnier et al. (1997). To be noted, however, is that integrated over the whole estuary, oxic mineralisation consumes more oxygen per year than nitrification which is in accordance with experimental findings of Gazeau et al. (2005). In accordance with its heterotrophic nature (Gazeau et al., 2005), the estuary is a net consumer of oxygen, only about 43% of the oxygen entering the estuary by advection-dispersion and re-aeration leaves the estuary at the mouth. 86% of the total O_2 input into the estuary is due to re-aeration.

2.4.4. Synopsis of single species budgets: elemental budgets and comparisons with earlier decades

Nitrogen and carbon budgets have been constructed for the entire estuary (Figs. 2.14 and 2.15).

2.4.4.1. Nitrogen

The Scheldt estuary is a net consumer of ammonium. The total advective-dispersive input at the upstream boundary per year ($(\mathbf{Tr}_{\sum NH_4^+})_{up}$), averaged over the years 2001 to 2004, of 0.58 Gmol $\sum NH_4^+$ is lower than the 0.82 Gmol $\sum NH_4^+$ consumed by nitrification per year in the same period. The sum of $\sum NH_4^+$ imports and production processes is 1.3 Gmol, 63% of which is consumed by nitrification within the estuary and roughly 6% of which leaves the estuary at the mouth. This number is less than half of the export of about 16% of the total input (including mineralisation processes) of $\sum NH_4^+$ in the years 1980 to 1986 as reported by Soetaert and Herman (1995a). However, the absolute values of process rates affecting $[\sum NH_4^+]$ in the years 2001 to 2004 are at about 25% of the values during the years 1980 to 1986. This is most likely due to reduced riverine nutrient and organic loadings and resulting lower $[\sum NH_4^+]$ in the years 2001 to 2004 as compared to the years 1980 to 1986 (Soetaert et al., 2006). Due to lower $[\sum NH_4^+]$ in 2001 to 2004, volumetric nitrification rates in the upstream region were 77%, at km 60 roughly 11%, and in the downstream region roughly 5% of the values in the early eighties as reported by Soetaert and Herman (1995a). Due to the large estuarine volume in the downstream region, the drop in nitrification in this area is mostly responsible for the drop in total ammonium consumption by nitrification in the whole estuary from the early eighties to our model time period (2001 to 2004).

This downward trend in total nitrification shows that the initial intensification of nitrification in the Scheldt due to increasing oxygen levels since the second half of the seventies (Van Damme et al., 2005; Soetaert and Herman, 1995c) has peaked and subsequently decreased again, most likely due to reduced ammonium concentrations in the estuary (Soetaert et al., 2006), suggesting a shift from initial oxygen limitation of nitrification towards ammonium limitation now. A similar shift as has happened in time can be observed longitudinally during our model time period, as nitrification is oxygen limited upstream and ammonium

decade	'70	'80	'00
Gmol N y^{-1} imported into the Scheldt	3.7	4.7	2.5
% of total N lost to the atmosphere	40	23	10
Gmol N y^{-1} exported to the North Sea	1.9	3.6	2.4

Table 2.13.: Trends in denitrification from the seventies to our model time period. Note that DON is included in the values.

limited downstream. However, as in the seventies (Billen et al., 1985), eighties (Van Damme et al., 2005; Soetaert and Herman, 1995c; Regnier et al., 1997), and nineties (Vanderborght et al., 2007), nitrification remains the major process governing N cycling in this estuary.

reference	value
Frankignoulle et al. (1998)	14.5
Gazeau et al. (2005)	11.3
Hellings et al. (2001)	8.2
Vanderborght et al. (2002)	6.8
this study	3.3

Table 2.14.: Export of CO_2 to the atmosphere (-$\mathbf{E}_{CO_2}$) in Gmol y^{-1}, integrated over our model area.

Furthermore, the estuary is a net producer of nitrate in the year 2001 to 2004. Roughly 1.4 times as much nitrate leaves the estuary by advection-dispersion at the mouth of the estuary, as is advectively imported (confer Fig. 2.11b). Yet, the nitrate producing character of the Scheldt estuary diminished due to reduced nitrification rates relative to the early eighties, as Soetaert and Herman (1995a) reported that three times as much nitrate was exported to the sea as entered the estuary in the eighties.

Only 10% of the total N input in the system (nitrate, ammonium and particulate and dissolved organic nitrogen together) is lost to the atmosphere as N_2 due to denitrification (Fig. 2.14), while the rest is exported to the Southern Bight of the North Sea. This shows a clear downwards trend in the percentage of N_2 production, as in the eighties 21–25% of the total nitrogen imported into the Scheldt (Soetaert and Herman, 1995a; Ouboter et al., 1998), and in the seventies around 40% (Soetaert and Herman, 1995a; Billen et al., 1985) of the total nitrogen import into the estuary was removed within the estuary, mainly due to denitrification. This phenomenon is likely due to improved oxygen conditions in the Scheldt from the seventies until now (Soetaert and Herman, 1995a; Soetaert et al., 2006), moving the zone of denitrification more into the narrow upstream regions and generally allowing for less denitrification because of the limited area of sediments, the prime location of denitrification, in the upstream regions. A downward trend in the percentage of N_2 generated and escaping means an upward trend in the percentage of N export to the sea. In absolute values, however, this resulted initially in an increasing N export to the North Sea from the seventies to the eighties from 1.9 Gmol y^{-1} to 3.6 Gmol y^{-1} (Soetaert and Herman, 1995a), before it decreased to 2.5 Gmol y^{-1} in our model period (value incl. DON export). This decrease in N export is due to approximately halved

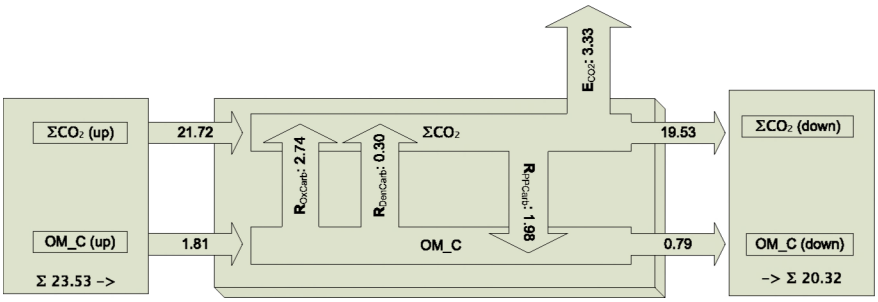

Figure 2.15.: Tentative carbon budget per year over the whole model area, averaged over 2001 to 2004. Values are given in Gmol y^{-1}. Note that the budget is not fully closed. There is an overall loss term of 0.12 Gmol C y^{-1}. This is consistent with the temporal downwards trend in $[\sum CO_2]$. Note also that organic carbon (Org-C) refers to particulate organic matter (OM). Dissolved organic carbon (DOC) is not shown in this budget. Around 2.2 Gmol of conservatively modelled DOC enters and leaves the estuary on average per year.

input loads (4.7 Gmol y^{-1} in the eighties (Soetaert and Herman, 1995a), 2.3 Gmol y^{-1} in our model). Yet the N export to the sea in 2001 to 2004 is still higher than in the seventies, in spite of the fact that the input into the system was much higher then (3.7 Gmol y^{-1}, Billen et al., 1985). Table 2.13 summarises these numbers. Note that these results should be considered tentative, since denitrification is poorly constrained by data and in our model (Sect. 2.4.1.1).

2.4.4.2. Carbon

Estuaries are a significant source of CO_2 to the atmosphere and are even important on a global scale (Borges et al., 2006). Our model suggests an averaged CO_2 export to the atmosphere of 3.3 Gmol y^{-1}, which is about 13% of the total carbon input (including DOC) into the system (Fig. 2.15).

This value is much lower than values reported by others (Table 2.14). These differences represent both a true trend in time as well as uncertainties in the estimations. Frankignoulle et al. (1998), Hellings et al. (2001), and Vanderborght et al. (2002) use data from the early to mid nineties of the 20th century. pCO_2 levels in the Scheldt estuary considerably dropped from the nineties to our model time period (Borges and Middelburg, unpublished data), entailing a true downwards trend in CO_2 degassing. One reason for this might be decreasing nitrification rates resulting in a higher pH and thus lower pCO_2.

However, there are several sources of uncertainties associated with estimating CO_2 degassing which could contribute in part to the differences shown in Table 2.14:

1. differences in the riverine discharge between the estimation periods and resulting carbon import into the system (confer a factor 2 difference in $\mathbf{E}_{CO_2}$ from 2001 and 2004 with an approximately halving freshwater discharge),

2. differences in estimates of the estuarine surface area which contributes to CO_2 air-sea exchange (see also Borges et al., 2006),

3. former overestimations of the piston velocity parametrisation mostly due to overestimated gas exchange flux measurements with the floating chamber method (Raymond and Cole, 2001), and

4. the use of budgeting approaches without the employment of mechanistic models with rigorous mass conservation (e.g. upscaling of discrete flux measurements).

Frankignoulle et al. (1998) reported that in the Scheldt estuary two thirds of the CO_2 flux to the atmosphere results from heterotrophy and only one third from ventilation of riverine DIC and Abril et al. (2000) estimate that riverine DIC contributes only 10% to the total CO_2 degassing of the Scheldt estuary. In contrast, our model suggests that, averaged over the four modelled years, 67% of the CO_2 export to the atmosphere can be attributed to ventilation of riverine DIC (based on results of model runs with and without biogeochemical processes).

2.5. Summary

The Scheldt estuary is an active biogeochemical reactor where, all along its path, the transformations occur at a similar magnitude. This is due to the combined effects of very high volumetric process rates and a small estuarine volume upstream, giving way to gradually decreasing volumetric rates and an increasing estuarine volume downstream.

With respect to the nitrogen cycle, the estuary has evolved towards a more and more neutral passage way of total nitrogen, with only 10% of the total imported nitrogen being lost from the estuary. This is in sharp contrast to the situation in the eighties and seventies where this loss amounted to more than 20% and 40%, respectively. Coinciding with a reduced total nitrogen import in the estuary, this has led to a current total nitrogen export to the North Sea which is smaller than the export in the eighties but still larger than what was observed in the seventies. However, the estuary has a large effect on the nitrogen speciation, especially by transforming ammonium and, indirectly, the imported organic nitrogen to nitrate. Similarly to previous budget estimates, nitrification remains one of the most important oxygen consuming processes in the estuary.

The loss of imported carbon in the estuary amounts to about 13%, and occurs through physical ventilation of CO_2 to the atmosphere. Two thirds of this lost C is riverine-borne DIC, one third of the ventilated CO_2 originates from heterotrophic production in the estuary itself. Whilst the estuary remains a significant source of CO_2 to the atmosphere, our results suggest that there is a downward trend in CO_2 degassing from the nineties to our model time period. This result should be considered tentative due to the high degree of uncertainty associated with CO_2 degassing estimations.

Finally, in the four-year period (2001–2004) during which our model was applied, clear trends in the chemical concentrations and budgets were observed. These trends were clearly linked to the decreased freshwater discharge, that was halved in that period.

2.6. Appendix

2.6.1. Gas exchange constants ($f(T,S)$)

Empirical formulations for the temperature and salinity dependency of the gas exchange constants used here, can be brought into the generic form:

$$\ln \frac{K_X}{k_0^\circ} = A + \frac{B}{\frac{T}{K}} + C \ln\left(\frac{T}{K}\right) + D\frac{T}{K} + E\left(\frac{T}{K}\right)^2$$

$\frac{T}{K}$	=	temperature stripped of unit
A, B, C, D, E	=	$f(S)$
S	=	salinity
k_0°	=	unit of the constant

The coefficients for gas exchange constants (Henry's constants) for CO_2 and O_2:

$K_{0_{CO_2}}$ (Weiss, 1974)	$K_{0_{O_2}}$ derived from Weiss (1970)
$A = 0.023517S - 167.81077$	$A = -846.9975 - 0.037362\ S$
$B = 9345.17$	$B = 25559.07$
$C = 23.3585$	$C = 146.4813$
$D = -2.3656\ 10^{-4} S$	$D = -0.22204 + 0.00016504 \times S$
$E = 4.7036\ 10^{-7} S$	$E = -2.0564 \times 10^{-7} \times S$
$k_0^\circ = [\text{mol(kg-soln atm)}^{-1}]$	$k_0^\circ = [\mu\text{mol (kg-soln atm)}^{-1}]$

The formulation for $K_{0_{O_2}}$ has been derived using the formulation for a gravimetric $[O_2]_{sat}$ given in Weiss (1970). It has been converted from ml O_2 $(\text{kg-soln})^{-1}$ to μmol O_2 $(\text{kg-soln})^{-1}$ using the molar volume of O_2 calculated with the virial equation using a first virial coefficient for oxygen at 273.0 K of $-22\,\text{cm}^3\,\text{mol}^{-1}$ (Atkins, 1996), a value of $8.314\,\text{Nm}\,(\text{K mol})^{-1}$ for the gas constant R and an ambient pressure of $101\,300\,\text{N}\,\text{m}^{-2}$. The expression for the Henry's constant has then been created by dividing the expression for the saturation concentration by an atmospheric oxygen fugacity of fO_2=0.20946 atm (Williams, 2004).

2.6.2. Total concentrations of seawater components ($f(S)$)

In DOE (1994) a table of concentrations of seawater components relative to chlorinity is given that allows to infer formulations for total concentrations of all seawater components.

The formulae for the concentrations needed here, rewritten as functions of salinity with S=1.80655×Cl (DOE, 1994), are:

total sulfate	$[\sum \text{HSO}_4^-]$	$S_T = \frac{0.1400}{96.062} \frac{S}{1.80655}$
total fluoride	$[\sum \text{HF}]$	$F_T = \frac{0.000067}{18.9984} \frac{S}{1.80655}$
total borate	$[\sum \text{BOH}_3]$	$B_T = \frac{0.000232}{10.811} \frac{S}{1.80655}$

3. A step-by-step procedure for pH model construction in aquatic systems

A. F. Hofmann, F. J. R. Meysman, K. Soetaert, and J. J. Middelburg
(Biogeosciences, 5, 227-251, 2008)

Abstract

We present, by means of a simple example, a comprehensive step-by-step procedure to consistently derive a pH model of aquatic systems. As pH modelling is inherently complex, we make every step of the model generation process explicit, thus ensuring conceptual, mathematical, and chemical correctness. Summed quantities, such as total inorganic carbon and total alkalinity, and the influences of modeled processes on them are consistently derived. The different time scales of processes involved in the pH problem (biological and physical reactions: days; aquatic chemical reactions: fractions of seconds) give rise to a stiff equation system. Subsequent reformulations of the system reduce its stiffness, accepting higher non-linear algebraic complexity. The model is reformulated until numerically and computationally simple dynamical solutions, like a variation of the operator splitting approach (OSA) and the direct substitution approach (DSA), are obtained. As several solution methods are pointed out, connections between previous pH modelling approaches are established. The final reformulation of the system according to the DSA allows for quantification of the influences of kinetic processes on the rate of change of proton concentration in models containing multiple biogeochemical processes. These influences are calculated including the effect of re-equilibration of the system due to a set of acid-base reactions in local equilibrium. This possibility of quantifying influences of modeled processes on the pH makes the end-product of the described model generation procedure a powerful tool for understanding the internal pH dynamics of aquatic systems.

3.1. Introduction

Human activities have increased atmospheric CO_2 levels by 36% since pre-industrial times, and further increases are expected over the next decades (Prentice et al., 2001; Alley et al., 2007). Rising atmospheric CO_2 levels lead to an input of CO_2 into the oceans and to subsequent acidification of surface waters (e.g. Orr et al., 2005).

Against this background, it is of high importance to analyze the impact of different biogeochemical processes onto alkalinity and the pH of natural waters (Sarmiento and Gruber, 2006; Stumm and Morgan, 1996). In recent years, various pH modeling approaches have been developed. These range from simple empirical correlations (Bjerknes and Tjomsland, 2001), over neural network approaches (Moatar et al., 1999), to mechanistic biogeochemical models that include reactive transport descriptions of varying complexity (e.g. Luff et al., 2001; Jourabchi et al., 2005). Mechanistic models have the advantage that they not only reproduce pH but also allow the prediction of future changes, and enable quantitative analysis of the processes that govern pH. As a result, they are a powerful tool to understand the pH dynamics of aquatic systems.

However, there are still two pending problems with mechanistic pH models. The first issue relates to the apparent diversity of approaches. Most modeling approaches have been presented without cross linking to other methods. As a result, it is difficult to assess whether approaches are mutually consistent, i.e., whether they would predict the same pH dynamics for exactly the same underlying biogeochemical model. Moreover, it is not clear what the respective advantages of the different solution techniques are, and whether they yield the same amount of information with respect to pH dynamics. Only some approaches are able to quantify the individual contribution of modelled processes on the pH.

The second issue relates to the complexity of the present approaches. The construction of pH models is inherently complex, involving many sequential steps and assumptions. Furthermore, the different time scales of processes involved in the pH problem (biological and physical reactions: days; aquatic chemical reactions: fractions of seconds) give rise to a stiff equation system. It is important to deal with this complexity by making every assumption explicit and justifying every step. Even for a relatively simple biogeochemical system, the model generation procedure becomes quite lengthy and intricate. A disadvantage of recent pH modeling approaches is that they have been typically applied to complex reaction sets, generating lengthy expressions. The illustration of a complex solution procedure with a complex model is not always optimal. Accordingly, there is a clear need to illustrate the various approaches to model pH with a simple biogeochemical application.

The objective of the present study is to provide a generic step-by-step procedure to construct and solve a pH model for an aquatic system. We will illustrate this step-by-step approach using an example, i.e., by constructing an example pH model for a simple estuarine system. This example is simple enough to facilitate understanding, yet complex enough to illustrate all features of the pH modeling approach. Accordingly, the focus lies on concepts and principles rather than on mimicking the biogeochemical complexity of real aquatic systems. Models of more realistic and complex systems can be built by suitably changing the transport formulation or extending the reaction set. The feature of our analysis is that we carry out a number

of sequential reformulations of the pH problem until elegant and efficient numerical solutions are possible. Along the way, we outline the implicit and explicit assumptions that are needed in every step of the procedure. This enables us to identify the weaknesses and strengths of past modeling procedures and solution methods. Our work therefore does not introduce a novel approach to pH modelling, but gives a systematic framework which encompasses existing approaches.

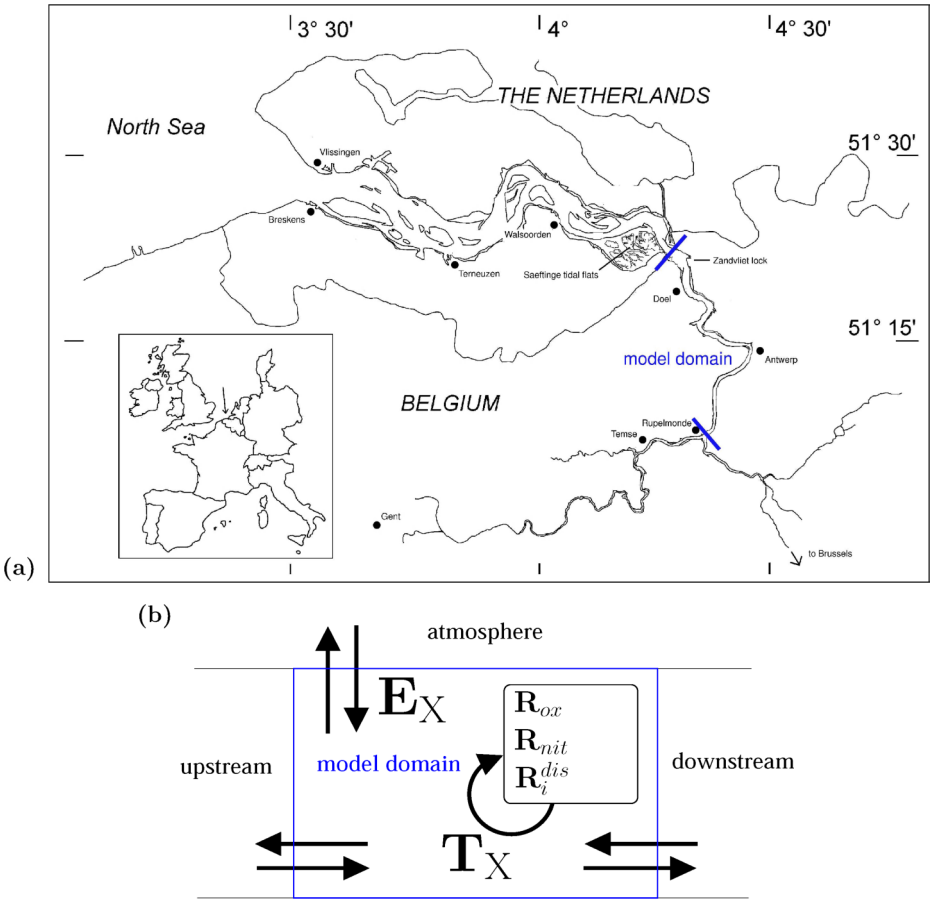

Figure 3.1.: **(a)**: the example estuarine system: the model domain (the stretch of river between the blue lines) encompasses around 40 river kilometres; **(b)**: The model domain is represented by a conceptual model scheme with biogeochemical processes; For explanations of symbols, see text.

3.2. pH model construction: a step-by-step procedure

3.2.1. Step 1: Formulation of the model questions

Our example system is the upper Schelde estuary in northern Belgium (Fig. 3.1a). The model domain includes 40 km of river ranging from the inflow of the Rupel tributary to the Belgian-Dutch border. A set of characteristic parameters is given in the Results section. Our principal goal is to examine the pH changes associated with some (drastic) perturbations in the biogeochemistry of this estuary. Two types of changes to the system are examined:

1) The estuary receives municipal water from the city of Brussels, which is one of the last major European cities to implement a coordinated waste water treatment policy. In 2007, a new sewage treatment plant for 1.1 million inhabitants has started operating, and it is estimated that this will reduce the organic matter input to the estuary by 50%. How will the pH of the estuary react to this abrupt change? Which biogeochemical processes govern the pH steady state before and after the reduction?

2) Alongside the estuary lies the port of Antwerp, which concentrates one of the largest chemical industries in the world. The port harbours a large fertilizer industry with associated ship traffic of resources and products. Potential hazard scenarios include ship accidents with tankers carrying ammonia or ammonium-nitrate. What are the effects of such pulse-inputs on the estuarine pH and the influences of processes on it? Ammonia input and ammonium-nitrate input are examined as two separate perturbation scenarios.

3.2.2. Step 2: Formulation of the conceptual model

In general, the concentration of a chemical species [X] in an aquatic system is influenced by a set of physical (transport) processes $\mathbf{P}^j$, and a set of biogeochemical reactions $\mathbf{R}^i$. The resulting mass conservation equation (MCE) (Morel and Hering, 1993) reads

$$\frac{d[\mathrm{X}]}{dt} = \sum_j \mathbf{P}^j_{\mathrm{X}} + \sum_i \nu^i_{\mathrm{X}} \mathbf{R}^i \tag{1}$$

where ν^i_{X} is the stoichiometric coefficient of species X in the i-th reaction. Throughout this paper, all species concentrations [X] are expressed as per kg of *solution* (gravimetric units per mass of solution). A crucial step in the model development is the decision which physical and biogeochemical processes to include in the model. This decision should be based on prior knowledge about the physics and biogeochemistry of the system. For our problem, two physical processes are of major relevance: advective-dispersive transport $\mathbf{T}_{\mathrm{X}}$ along the length axis of the river, and the exchange of volatile compounds with the atmosphere $\mathbf{E}_{\mathrm{X}}$. Although it would be possible here, no benthic exchange is taken into account to keep the mathematical expressions tractable. For the same reason, the estuary is modelled as a single box (Fig. 3.1b). Note that the implementation of a spatially explicit description would be entirely analogous in terms of pH modeling: the $\mathbf{T}_{\mathrm{X}}$ terms would simply give rise to partial rather than ordinary differential equations.

pelagic primary production	$\mathbf{R}_{\text{pri}}$	$\approx$	0.1	(a)
pelagic nitrification	$\mathbf{R}_{\text{nit}}$	$\approx$	7.5	(b)
pelagic denitrification	$\mathbf{R}_{\text{den}}$	$\approx$	6.1	(c)
pelagic oxic respiration	$\mathbf{R}_{\text{ox}}$	$\approx$	2.9	(c)
benthic denitrification	$\mathbf{R}_{\text{bden}}$	$\approx$	0.7	(c)
benthic oxic respiration	$\mathbf{R}_{\text{box}}$	$\approx$	0.3	(d)

Table 3.1.: Estimated rates (μmol-N $(\text{kg}\cdot\text{d})^{-1}$) of biogeochemical processes in the example system ((a): Soetaert and Herman, 1995c; (b): Andersson et al., 2006; (c): Soetaert and Herman, 1995a; (d): Middelburg et al., 1996).

To assist in the selection of the biogeochemical reactions, Table 3.1 provides an overview of the relative importance of the various processes in the Schelde estuary. From the six biogeochemical reactions listed, we only retain pelagic oxic respiration $\mathbf{R}_{\text{ox}}$ and pelagic nitrification $\mathbf{R}_{\text{nit}}$. These are described according to reaction stoichiometries:

$$(CH_2O)_\gamma(NH_3) + \gamma\, O_2 \rightarrow NH_3 + \gamma\, CO_2 + \gamma\, H_2O \quad (2)$$

$$NH_4^+ + 2O_2 \rightarrow NO_3^- + H_2O + 2H^+ \quad (3)$$

With γ being the C/N ratio of organic matter (see Table 3.14).

Pelagic primary production, benthic denitrification and benthic respiration can be justifiably neglected compared to pelagic nitrification and pelagic oxic mineralization (Table 3.1). Pelagic denitrification was important in the 1970's, but, due to improved water quality, is now of minor significance (Soetaert et al., 2006). For this reason and for didactical purposes, we did not include it in the model (to avoid lengthy expressions in the mathematical derivations). However, we will include it a posteriori to check on the importance of denitrification in pH regulation of the model domain.

Since our aim is to model the pH, a number of acid-base reactions have to be accounted for. To select these reactions, we first have to constrain the set of chemical species that are modelled. For simplicity, we consider the estuary as an aqueous solution of the three most abundant seawater ions Cl^-, Na^+, and SO_4^{2-} (DOE, 1994). For a realistic model application other quantities like borate might be important, but we neglect these to keep the model as simple as possible. Furthermore, we also incorporate organic matter, nitrate, oxygen and the ammonium and carbonate systems, as these species feature in the retained reactions ($\mathbf{R}_{\text{ox}}$ and $\mathbf{R}_{\text{nit}}$, Eq. 2). Table 3.2 lists the set of acid-base dissociation reactions $\mathbf{R}_i^{\text{dis}}$ that involve all the mentioned chemical species. This finalizes the conceptual model formulation – see scheme in Fig. 3.1b.

3.2.3. Step 3: Constraining the model pH range – selection of acid-base reactions

Currently there are different definitions for pH in use, which all express the "protonating capability" of a solution. The difference between these so-called pH scales relates to the calibration buffers that are used in pH measurements, which then determine the type of equilibrium constants (K^* values) that should be used in calculations. A detailed description

reaction (HA $\rightleftharpoons$ H^+ + A^-)		pK_{HA}	$\frac{\sum A}{\mu mol\,kg^{-1}}$	$\frac{\epsilon}{\%}$
(1) HCl	$\rightleftharpoons H^+ + Cl^-$	−3	$2.8\ 10^4$	$5.6\ 10^{-7}$
(2) $Na^+ + H_2O$	$\rightleftharpoons H^+ + NaOH$	14	$2.4\ 10^4$	$4.8\ 10^{-3}$
(3) H_2SO_4	$\rightleftharpoons H^+ + HSO_4^-$	−3	$1.5\ 10^3$	$2.9\ 10^{-8}$
(4) HSO_4^-	$\rightleftharpoons H^+ + SO_4^{2-}$	2	$1.5\ 10^3$	$2.9\ 10^{-3}$
(5) HNO_3	$\rightleftharpoons H^+ + NO_3^-$	−1	$3.2\ 10^2$	$6.4\ 10^{-7}$
(6) NH_4^+	$\rightleftharpoons H^+ + NH_3$	9	$2.9\ 10^1$	*0.58*
(7) $CO_2 + H_2O$	$\rightleftharpoons H^+ + HCO_3^-$	6	$6.0\ 10^3$	*120*
(8) HCO_3^-	$\rightleftharpoons H^+ + CO_3^{2-}$	10	$6.0\ 10^3$	*12*
(9) H_2O	$\rightleftharpoons H^+ + OH^-$	16	$5.5\ 10^7$	0.11

Table 3.2.: Acid-base reactions in the example system, thermodynamical pK_{HA}'s are infinite dilution values at 25°C as given in Stumm and Morgan (1996). According to the exclusion criterion given in Appendix 3.6.1, reactions with an ϵ below 0.5 % are neglected. ϵ has been calculated for a desired pH range of 6 to 9, with pK^*_{HA} ≈pK_{HA}, and with [TA]=5000 $\mu mol\,kg^{-1}$ (estimated from upstream and downstream boundary conditions given in Table 3.14), and with total concentrations for the given system as listed (total nitrate and ammonium are measured values for the example model system, total carbon dioxide has been estimated and all other total quantities have been calculated from salinity S=5 according to DOE, 1994).

of these pH scales can be found, for example, in Dickson (1984) or Zeebe and Wolf-Gladrow (2001). Here, we model the free gravimetric proton concentration $[H^+]$=$[H_3O^+]$, and the associated pH scale is the *free hydrogen ion concentration scale* (Dickson, 1984), which is defined as

$$pH = -\log_{10}\left(\frac{[H^+]}{[H^+]_{ref}}\right) \tag{4}$$

The reference proton concentration $[H^+]_{ref}$=1 $mol\,kg^{-1}$ makes the argument of the logarithm dimensionless.

After the selection of the pH scale, we can proceed to a formal delineation of the pH range of the model. This setting of the pH range determines which dissociation reactions should be incorporated. Note that most pH modeling approaches do not explicitly mention this step. In these, the set of acid-base reactions is simply imposed without further consideration. However, models are simplified representations of reality, and they should be kept as simple as possible. This is particularly true for pH models, which are computationally demanding. Accordingly, one should avoid incorporating dissociation reactions that have no chance of affecting the pH dynamics.

Therefore, we propose a formal procedure for the selection of acid-base reactions which is based on prior knowledge about the buffering capacity and the possible pH range of the specific system. In our case, we know that the part of the Schelde estuary which we model is strongly buffered, as are most estuarine and marine systems, with a total alkalinity [TA] of ≈5000 $\mu mol\,kg^{-1}$ (estimated from upstrean and downstream boundary conditions given in

Table 3.14). We furthermore know that the pH only fluctuates over a range from 7.5 to 8. Nonetheless, we anticipate stronger excursions because of the quite drastic perturbation scenarios outlined above. Allowing a suitable margin, we require that the model should represent the pH dynamics properly within a pH range of 6 to 9. This constraint enables us to reduce the reaction set in Table 3.2 considerably.

Whether or not a certain acid-base system has to be taken into account depends on a combination of

1) its pK value(s) which tell us whether the speciation of the acid-base species will change within the pH range under consideration,

2) the total concentration of the acid $[\sum \mathrm{A}]$ which tells us how large theoretical changes in $[\mathrm{H^+}]$ due to the speciation of the respective acid-base system would be in a completely unbuffered system, and

3) the mean [TA] of the system which tells us if these theoretical changes in $[\mathrm{H^+}]$ will be appreciable or negligible in a buffered aquatic system.

Appendix 3.6.1 details a formal selection procedure which integrates these three criteria into a single quantity ϵ for each acid-base system. ϵ represents the amount of protons ignored (theoretical unbuffered proton concentration offset) by neglecting the reaction in question, in percent of the average [TA] of the modeled system.

Finally, we exclude all reactions whose ϵ value is smaller than 0.5%. This means the total amount of protons which could be taken up or released in the model, if the reaction in question would be included and the pH reaches the border of the pH range, is less than half a percent of typical alkalinity levels of the system.

Note that polyprotic acids are treated as a set of monoprotic acids considering each dissociation step independently.

Applying this rule (ϵ values are given in Table 3.2), we do not need to incorporate the dissociation reactions of HCl, NaOH, $\mathrm{H_2SO_4}$, $\mathrm{HSO_4^-}$, $\mathrm{HNO_3}$ and $\mathrm{H_2O}$. Table 3.3 shows the reduced set of acid-base reactions considered in the model. Technically, it would not be "wrong" to include the other reactions. However, there is no reason to do so, provided that the simulated pH stays within the range [6–9] (this should be checked a posteriori).

$\mathbf{R}^{\mathbf{dis}}_{\mathrm{NH_4^+}}$	$\mathrm{NH_4^+}$	$\rightleftharpoons$	$\mathrm{H^+ + NH_3}$
$\mathbf{R}^{\mathbf{dis}}_{\mathrm{CO_2}}$	$\mathrm{CO_2 + H_2O}$	$\rightleftharpoons$	$\mathrm{H^+ + HCO_3^-}$
$\mathbf{R}^{\mathbf{dis}}_{\mathrm{HCO_3^-}}$	$\mathrm{HCO_3^-}$	$\rightleftharpoons$	$\mathrm{H^+ + CO_3^{2-}}$

Table 3.3.: pH range adjusted set of acid-base reactions.

Note that the auto-dissociation reaction of water is not included in Table 3.3. Effectively, this reaction has been treated in a rather arbitrary fashion in past models. The auto-dissociation of water is included in some models (e.g. Jourabchi et al., 2005), while excluded from others (e.g. Luff et al., 2001). Usually, the reasons for inclusion or exclusion are not mentioned. Here

(1)	$\frac{d[\mathrm{OM}]}{dt}$	=	$\mathbf{Tr}_{\mathrm{OM}} - \mathbf{R}_{\mathrm{ox}}$
(2)	$\frac{d[\mathrm{O_2}]}{dt}$	=	$\mathbf{Tr}_{\mathrm{O_2}} + \mathbf{E}_{\mathrm{O_2}}\text{-}\gamma\ \mathbf{R}_{\mathrm{ox}} - 2\ \mathbf{R}_{\mathrm{nit}}$
(3)	$\frac{d[\mathrm{NO_3^-}]}{dt}$	=	$\mathbf{Tr}_{\mathrm{NO_3^-}} + \mathbf{R}_{\mathrm{nit}}$
(4)	$\frac{d[\mathrm{CO_2}]}{dt}$	=	$\mathbf{Tr}_{\mathrm{CO_2}} + \mathbf{E}_{\mathrm{CO_2}} + \gamma\ \mathbf{R}_{\mathrm{ox}} - \mathbf{R}^{\mathrm{dis}}_{\mathrm{CO_2}}$
(5)	$\frac{d[\mathrm{HCO_3^-}]}{dt}$	=	$\mathbf{Tr}_{\mathrm{HCO_3^-}} + \mathbf{R}^{\mathrm{dis}}_{\mathrm{CO_2}} - \mathbf{R}^{\mathrm{dis}}_{\mathrm{HCO_3^-}}$
(6)	$\frac{d[\mathrm{CO_3^{2-}}]}{dt}$	=	$\mathbf{Tr}_{\mathrm{CO_3^{2-}}} + \mathbf{R}^{\mathrm{dis}}_{\mathrm{HCO_3^-}}$
(7)	$\frac{d[\mathrm{NH_4^+}]}{dt}$	=	$\mathbf{Tr}_{\mathrm{NH_4^+}}\text{-}\ \mathbf{R}^{\mathrm{dis}}_{\mathrm{NH_4^+}} - \mathbf{R}_{\mathrm{nit}}$
(8)	$\frac{d[\mathrm{NH_3}]}{dt}$	=	$\mathbf{Tr}_{\mathrm{NH_3}} + \mathbf{E}_{\mathrm{NH_3}} + \mathbf{R}_{\mathrm{ox}} + \mathbf{R}^{\mathrm{dis}}_{\mathrm{NH_4^+}}$
(9)	$\frac{d[\mathrm{H^+}]}{dt}$	=	$\mathbf{Tr}_{\mathrm{H^+}} + 2\ \mathbf{R}_{\mathrm{nit}} + \mathbf{R}^{\mathrm{dis}}_{\mathrm{CO_2}} + \mathbf{R}^{\mathrm{dis}}_{\mathrm{HCO_3^-}} + \mathbf{R}^{\mathrm{dis}}_{\mathrm{NH_4^+}}$

Table 3.4.: Mass conservation equations (MCEs) for each chemical species.

however, our formal selection procedure predicts that it is unimportant (we will check this a posteriori).

3.2.4. Step 4: A mass conservation equation (MCE) for each species

Overall, our model set includes a set of n_p=7 processes encompassing 5 reactions ($\mathbf{R}_{\mathrm{ox}}$, $\mathbf{R}_{\mathrm{nit}}$, $\mathbf{R}^{\mathrm{dis}}_{\mathrm{NH_4^+}}$, $\mathbf{R}^{\mathrm{dis}}_{\mathrm{CO_2}}$, $\mathbf{R}^{\mathrm{dis}}_{\mathrm{HCO_3^-}}$) and 2 transport processes ($\mathbf{Tr}_{\mathrm{X}}$, $\mathbf{E}_{\mathrm{X}}$) that feature a set of n_s=9 chemical species:

$$\mathrm{OM}, \mathrm{O_2}, \mathrm{NO_3^+}, \mathrm{CO_2}, \mathrm{HCO_3^+}, \mathrm{CO_3^{2+}}, \mathrm{NH_4^+}, \mathrm{NH_3}, \text{ and } \mathrm{H^+}$$

Note that organic matter $(\mathrm{CH_2O})_\gamma(\mathrm{NH_3})$ has been abbreviated by OM and that the concentrations of $\mathrm{Cl^-}$, $\mathrm{Na^+}$, $\mathrm{HSO_4^-}$, $\mathrm{SO_4^{2-}}$, NaOH and $\mathrm{OH^-}$ are not simulated, since they are not affected by the modeled processes[1].

Although $\mathrm{H_2O}$ does feature in the biogeochemical reactions retained in the model ($\mathbf{R}_{\mathrm{ox}}$ and $\mathbf{R}_{\mathrm{nit}}$; Eqs. (2) and (3)) and in the set of acid-base reactions (Table 3.3), its concentration is nevertheless considered constant (Morel and Hering, 1993). The resulting mass conservation equations for all 9 chemical species are given in Table 3.4, where again $\mathbf{T}_{\mathrm{X}}$ denotes advective-dispersive transport of chemical species X and $\mathbf{E}_{\mathrm{X}}$ denotes the exchange of chemical species X with the atmosphere.

At this point, a first attempt to solve the system can be made.

[1] All species are of course affected by advective-dispersive transport $\mathbf{Tr}_{\mathrm{X}}$. It would be correct to include the transport of conservative ions (conservative with respect to all other processes except transport) in the model by a variable salinity which is advective-dispersively transported. However, we consider a constant salinity for the sake of didactical simplicity.

Solution method [1a]: Together with suitable initial conditions, the equation set in Table 3.4 represents an initial-value problem of ordinary differential equations (ODEs) (Fabian et al., 2001). Using suitable kinetic expressions for all modeled process rates (i.e. for the forward and backward rates for acid-base reactions), this system is fully determined. In principle, it can be directly solved by common numerical integration techniques, such as Euler or Runge-Kutta integration (Press et al., 1992) or more complex integration schemes. This solution procedure is referred to as the *Full Kinetic Approach (FKA)* (Steefel and MacQuarrie, 1996; Meysman, 2001).

For the reaction $\mathbf{R}^{\mathrm{dis}}_{\mathrm{NH_4^+}}$, for example, suitable kinetic expressions for the forward and backward reaction would be

$$\left(\mathbf{R}^{\mathrm{dis}}_{\mathrm{NH_4^+}}\right)_{\mathrm{forward}} = k_f\,[\mathrm{NH_4^+}] \tag{5}$$

$$\left(\mathbf{R}^{\mathrm{dis}}_{\mathrm{NH_4^+}}\right)_{\mathrm{backward}} = k_b\,[\mathrm{NH_3}][\mathrm{H^+}] \tag{6}$$

with $\mathbf{R}^{\mathrm{dis}}_{\mathrm{NH_4^+}} = \left(\mathbf{R}^{\mathrm{dis}}_{\mathrm{NH_4^+}}\right)_{\mathrm{forward}} - \left(\mathbf{R}^{\mathrm{dis}}_{\mathrm{NH_4^+}}\right)_{\mathrm{backward}}$ and k_f and k_b being the forward and backward rate constants. Zeebe and Wolf-Gladrow (2001) give formulations for forward and backward rate constants of some acid-base systems relevant in seawater. However, problems arise when the values of the rate constants are not available.

Solution method [1b]: One way to avoid this problem is to adopt the principle of microscopic reversibility or detailed balancing (Morel and Hering, 1993), which requires the quotient of the kinetic forward and backward rate constants k_f and k_b to be equal to the equilibrium constant of the reaction ($\frac{k_f}{k_b} = K^*$).

Based on this principle, e.g., $\mathbf{R}^{\mathrm{dis}}_{\mathrm{NH_4^+}}$ can be written as

$$\mathbf{R}^{\mathrm{dis}}_{\mathrm{NH_4^+}} = k_f\left([\mathrm{NH_4^+}] - \frac{[\mathrm{NH_3}][\mathrm{H^+}]}{K^*_{\mathrm{NH_4^+}}}\right) \tag{7}$$

which only features the forward rate constant k_f. Assuming a sufficiently high value for k_f this is an approximation of the local equilibrium assumption (Steefel and MacQuarrie, 1996) which will be discussed later.

Although it overcomes the problem of undetermined kinetic rate constants, solution method 1b does not resolve a serious limitation of the FKA: it is bound to lead to very long computation times and numerical problems. The reason for this problem is that the transport and reaction processes that are included in the model occur on widely different time scales. Table 3.5 gives approximative values for the characteristic time scale τ for each process.

These characteristic time scales span several orders of magnitude, ranging from microseconds to days. This phenomenon is called numerical *stiffness* (Boudreau, 1996a). Problems that are numerically stiff basically require special integration methods or rather small time steps in order to ensure accuracy. Effectively, the process with the smallest characteristic time scale

(1)	$\mathbf{R}_{\mathrm{ox}}$	10	d
(2)	$\mathbf{R}_{\mathrm{nit}}$	4	d
(3)	$\mathbf{T}_{\mathrm{X}}$	13	d
(4)	$\mathbf{E}_{\mathrm{X}}$	4	d
(5)	$\mathbf{R}^{\mathrm{dis}}_{\mathrm{NH}_4^+}$	10	s
(6)	$\mathbf{R}^{\mathrm{dis}}_{\mathrm{CO}_2}$	10^{-7}	s
(7)	$\mathbf{R}^{\mathrm{dis}}_{\mathrm{HCO}_3^-}$	10^{-2}	s

Table 3.5.: Characteristic time τ of processes to be modeled. Values for $\mathbf{R}^{\mathrm{dis}}_{\mathrm{NH}_4^+}$ and $\mathbf{R}^{\mathrm{dis}}_{\mathrm{CO}_2}$ are obtained from Zeebe and Wolf-Gladrow (2001), and $\mathbf{R}^{\mathrm{dis}}_{\mathrm{HCO}_3^-}$ from Morel and Hering (1993). Values for the remaining processes are estimated from Tables 3.1 and 3.14. For the exchange with the atmosphere, piston velocities K_L as given by Raymond and Cole (2001) were used.

will set the pace of how the integration procedure progresses with time. Given the small time scales of the acid base reactions, pH models are very impractical or virtually impossible to solve with the FKA, even with integration methods that are specifically geared towards stiff problems (Chilakapati et al., 1998). A runtime comparison of all our presented approaches, including the FKA (solution method 1b), is given at the end of the paper.

In conclusion, the FKA does not form a good choice for pH problems. As shown below, more refined alternatives to the FKA exist which do not depend on well constrained acid-base forward and backward rate constants[2] and which drastically reduce the computation time by reducing the stiffness of the system.

3.2.5. Step 5: Kinetic and equilibrium processes and species

Table 3.5 shows that the characteristic time scales cluster in two groups. There is a group of comparatively slow processes happening on a timescale of days (Processes 1 to 4) and a group of comparatively fast processes happening on timescales of fractions of a second to seconds (Processes 5 to 7). If the rate of one process is "sufficiently fast" compared to that of another process, this process can be assumed in local equilibrium on the timescale of the "slower" process (e.g. Olander, 1960; Aris and Mah, 1963; Otto and Quinn, 1971; DiToro, 1976; Saaltink et al., 1998). This allows to group the processes into slow *kinetic processes*, whose kinetics enter the model via suitable expressions, and fast *equilibrium processes*, whose kinetics are neglected, i.e., local equilibrium is assumed to be reached instantaneously at any time.

The designation of processes as "kinetic" or "equilibrium" also entails a corresponding classification of the species. *Kinetic species* are those species whose concentrations are exclusively influenced by kinetic processes, while *equilibrium species* are species that take part in at least one equilibrium reaction.

[2] Still, rough estimates of the kinetic rate constants for all reactions are necessary to estimate the corresponding time scales for step 5.

species	kinetic	OM, O_2, NO_3^-	$n_{ks} = 3$
(n_s=9)	equilibrium	CO_2, HCO_3^-, CO_3^{2-}, NH_4^+, NH_3, H^+	$n_{es} = 6$
processes	kinetic	$\mathbf{R}_{ox}$, $\mathbf{R}_{nit}$, $\mathbf{T}_X$, $\mathbf{E}_X$	$n_{kp} = 4$
(n_p=7)	equilibrium	$\mathbf{R}^{dis}_{NH_4^+}$, $\mathbf{R}^{dis}_{CO_2}$, $\mathbf{R}^{dis}_{HCO_3^-}$	$n_{ep} = 3$

Table 3.6.: Kinetic and equilibrium processes and species. n_x denotes the number of respective species or processes.

The grouping in kinetic and equilibrium processes depends on the minimal time resolution of the model simulations (cf. Saaltink et al., 1998) That means, the reference time to which to compare processes as "fast" and "slow" is the integration timestep of the model. In our model simulations, the goal is to examine the pH changes over a period of days to weeks, resulting in an integration timestep of about one minute.

Accordingly, we assume the kinetics of reactions whose characteristic time scales are less than one minute to be negligible. Table 3.6 provides the resulting grouping of processes and species.

Note that local equilibrium is an assumption that is commonly used for systems to which our pH modelling approach is geared: macroscopic aquatic systems that contain reactions on the timescale of several days as well as fast acid-base reactions. For models on this temporal and spatial scale, assuming local equilibrium does not change the model results.

However, the assignment of a process to the kinetic or equilibrium group is not absolute: it depends on the model time-scale, and hence, on the questions addressed by the model. In our case, the exchange with the atmosphere is catalogued as a kinetic process. However, in a model that describes the pH evolution in the ocean over a million year time-scale, exchange with the atmosphere can be considered an equilibrium process. Similarly, the dissociation Reactions (5) to (7) are classified as equilibrium processes in our model. Yet, in a model that focuses on the fast relaxation of intracellular pH (model time-scale of fractions of seconds), these same Reactions (5) to (7) would be considered kinetic reactions[3].

The Processes (1) to (4) from Table 3.5 are modeled kinetically, and hence, we need to provide suitable constitutive expressions for their process rates . We describe oxic respiration and nitrification as first order processes with respect to [OM] and $[NH_4^+]$ respectively, and with a Monod dependency on $[O_2]$. The advective-dispersive transport is simply modeled as an exchange across the upstream and downstream system boundaries. The exchange with the atmosphere is described by the classical reaeration mechanism (Thomann and Mueller, 1987). Table 3.7 lists the resulting kinetic expressions, parameters are given and explained in Table 3.14.

3.2.6. Step 6: Mathematical closure of the system – the mass action laws

Although the kinetics of the processes considered to be in local equilibrium are neglected, these reactions are still part of the model. If the concentrations of species on either side of

[3]However, then the rates of reactions on the time scale of our slow kinetic reactions can be assumed to be zero.

$\mathbf{R}_{\text{ox}}$	=	$r_{\text{ox}} \cdot [\text{OM}] \cdot ([\text{O}_2]/([\text{O}_2] + ks_{\text{O}_2}))$
$\mathbf{R}_{\text{nit}}$	=	$r_{\text{nit}} \cdot [\text{NH}_4{}^+] \cdot ([\text{O}_2]/([\text{O}_2] + ks_{\text{O}_2}))$
$\mathbf{T}_{\text{X}}$	=	$(Q/V) \cdot ([\text{X}]_{\text{up}} - [\text{X}]) + (E'/V) \cdot ([\text{X}]_{\text{up}} + [\text{X}]_{\text{down}} - 2 \cdot [\text{X}])$
$\mathbf{E}_{\text{X}}$	=	$(K_L/d_w) \cdot ([\text{X}]_{\text{sat}} - [\text{X}])$

Table 3.7.: Kinetic process formulations. $[\text{X}]_{\text{up}}$ represents the upstream concentration of species X, $[\text{X}]_{\text{down}}$ its downstream concentration, and $[\text{X}]_{\text{sat}}$ its saturation concentration.

the reaction equation changes, the equilibrium shifts according to Le Chatelier's principle. However, the rate of this shift is not governed by the kinetics of the equilibrium reaction themselves since they are assumed to be infinitely fast (local equilibrium is reached instantaneously). The net equilibrium reaction rates $\mathbf{R}^{\text{dis}}$ are non-zero quantities and only depend on the supply rates of reactants and products of the equilibrium reaction in question due to slow kinetic processes in the model. In solution method 1b we approximated the local equilibrium assumption by calculating, e.g., $\mathbf{R}^{\text{dis}}_{\text{NH}_4^+}$ by equation 7 using a very high value for k_f. However, under the true local equilibrium assumption the equilibrium is reached "instantaneously" which means

$$k_f \to \infty \tag{8}$$

and

$$\left([\text{NH}_4^+] - \frac{[\text{NH}_3][\text{H}^+]}{K^*_{\text{NH}_4^+}}\right) \to 0 \tag{9}$$

The latter expression is the equilibrium mass action law (Morel and Hering, 1993). This multiplication of an infinite quantity with 0 renders the net equilibrium reaction rates $\mathbf{R}^{\text{dis}}$ into mathematical unknowns. Chemical reasoning tells us that they are finite quantities.

As a result, the system in Table 3.4 becomes an underdetermined system with 9 equations (the MCE's) and 12 unknowns (9 species concentrations and the 3 equilibrium reaction rates). To solve this system, it has to be mathematically closed by adding the equilibrium mass-action laws of the equilibrium reactions as additional algebraic constraints.

Including the mass action laws results in a fully determined initial-value differential algebraic equation (DAE) system (Fabian et al., 2001) (Table 3.8). The structure of this DAE system can be generalized as:

$$\frac{dy}{dt} = f(t, y, z) \tag{10}$$

$$0 = g(y) \tag{11}$$

where t is time. The DAE system is split into two parts: a differential part containing differential equations (Eq. 10), and an algebraic part containing equations with no differentials (Eq. 11). It also contains two types of variables: the variables y whose differentials $\frac{dy}{dt}$ are present (*differential variables* – the species concentrations) and the variables z whose differentials are absent (*algebraic variables* – the unknown equilibrium reaction rates $\mathbf{R}_{\text{NH}_4^+}$, $\mathbf{R}_{\text{CO}_2}$, and $\mathbf{R}_{\text{HCO}_3^-}$). The algebraic part of the DAE system (Eq. 11) only contains the differential variables y, and not the algebraic variables z (the equilibrium reaction rates). As

$\frac{d[\mathrm{OM}]}{dt}$	=	$\mathbf{Tr}_{\mathrm{OM}} - \mathbf{R}^{\mathrm{dis}}_{\mathrm{ox}}$
$\frac{d[\mathrm{O_2}]}{dt}$	=	$\mathbf{Tr}_{\mathrm{O_2}} + \mathbf{E}_{\mathrm{O_2}} - \gamma\ \mathbf{R}^{\mathrm{dis}}_{\mathrm{ox}} - 2\ \mathbf{R}^{\mathrm{dis}}_{\mathrm{nit}}$
$\frac{d[\mathrm{NO_3^-}]}{dt}$	=	$\mathbf{Tr}_{\mathrm{NO_3^-}} + \mathbf{R}^{\mathrm{dis}}_{\mathrm{nit}}$
$\frac{d[\mathrm{CO_2}]}{dt}$	=	$\mathbf{Tr}_{\mathrm{CO_2}} + \mathbf{E}_{\mathrm{CO_2}} + \gamma\ \mathbf{R}^{\mathrm{dis}}_{\mathrm{ox}} - \mathbf{R}^{\mathrm{dis}}_{\mathrm{CO_2}}$
$\frac{d[\mathrm{HCO_3^-}]}{dt}$	=	$\mathbf{Tr}_{\mathrm{HCO_3^-}} + \mathbf{R}^{\mathrm{dis}}_{\mathrm{CO_2}} - \mathbf{R}^{\mathrm{dis}}_{\mathrm{HCO_3^-}}$
$\frac{d[\mathrm{CO_3^{2-}}]}{dt}$	=	$\mathbf{Tr}_{\mathrm{CO_3^{2-}}} + \mathbf{R}^{\mathrm{dis}}_{\mathrm{HCO_3^-}}$
$\frac{d[\mathrm{NH_4^+}]}{dt}$	=	$\mathbf{Tr}_{\mathrm{NH_4^+}} - \mathbf{R}^{\mathrm{dis}}_{\mathrm{nit}} - \mathbf{R}^{\mathrm{dis}}_{\mathrm{NH_4^+}}$
$\frac{d[\mathrm{NH_3}]}{dt}$	=	$\mathbf{Tr}_{\mathrm{NH_3}} + \mathbf{E}_{\mathrm{NH_3}} + \mathbf{R}^{\mathrm{dis}}_{\mathrm{ox}} + \mathbf{R}^{\mathrm{dis}}_{\mathrm{NH_4^+}}$
$\frac{d[\mathrm{H^+}]}{dt}$	=	$\mathbf{Tr}_{\mathrm{H^+}} + 2\ \mathbf{R}^{\mathrm{dis}}_{\mathrm{nit}} + \mathbf{R}^{\mathrm{dis}}_{\mathrm{CO_2}} + \mathbf{R}^{\mathrm{dis}}_{\mathrm{HCO_3^-}} + \mathbf{R}^{\mathrm{dis}}_{\mathrm{NH_4^+}}$
0	=	$[\mathrm{H^+}][\mathrm{HCO_3^-}] - K^*_{\mathrm{CO_2}}[\mathrm{CO_2}]$
0	=	$[\mathrm{H^+}][\mathrm{CO_3^{2-}}] - K^*_{\mathrm{HCO_3^-}}[\mathrm{HCO_3^-}]$
0	=	$[\mathrm{H^+}][\mathrm{NH_3}] - K^*_{\mathrm{NH_4^+}}[\mathrm{NH_4^+}]$

Table 3.8.: Fully determined explicit DAE system. Note that the dissociation constants used are stoichiometric constants (denoted by the star as superscript; in contrast to thermodynamic constants; see Zeebe and Wolf-Gladrow (2001) for a description of different dissociation constants).

can be seen from Table 8, the DAE system is fully determined (12 equations for 12 unknowns).

To our knowledge, this DAE system cannot be numerically integrated in the above form, despite being fully determined. To this end, the DAE system has to be reformulated first. For example, the DASSL routine (Differential Algebraic System Solver; Petzold, 1982) can solve implicit DAE systems (with suitable initial conditions given) of the form:

$$F\left(t, y, \frac{dy}{dt}\right) = 0 \tag{12}$$

This means that, if one wants to use the DASSL solver, the DAE equations may contain differentials of more than one variable (i.e., implicit differential equations), but the whole equation system can no longer contain the algebraic variables z. In the next step, we will discuss a suitable transformation that brings the DAE system in Table 3.8 in a form that can be solved by DASSL.

3.2.7. Step 7: Reformulation 1: Transformation into the canonical form

The system can be brought into a DASSL-solvable form by means of a *transformation into the canonical form* as discussed in, e.g., DiToro (1976), Steefel and MacQuarrie (1996), Lichtner (1996), Saaltink et al. (1998), Chilakapati et al. (1998) and Meysman (2001), based on an idea put forward by Aris and Mah (1963). During this transformation, the unknown equilibrium reaction rates are eliminated from the system. In a system with n_{es} equilibrium species and n_{ep} equilibrium reactions, the n_{es} differential MCEs of the equilibrium species are then replaced by n_{ei}=n_{es}–n_{ep} combined MCEs which do no longer contain the unknown equilibrium

differential MCEs of kinetic species	
(1) $\frac{d[\mathrm{OM}]}{dt}$	$= -\mathbf{Tr}_{\mathrm{OM}} - \mathbf{R}_{\mathrm{ox}}$
(2) $\frac{d[\mathrm{O_2}]}{dt}$	$= \mathbf{Tr}_{\mathrm{O_2}} + \mathbf{E}_{\mathrm{O_2}} - \gamma\,\mathbf{R}_{\mathrm{ox}} - 2\,\mathbf{R}_{\mathrm{nit}}$
(3) $\frac{d[\mathrm{NO_3^-}]}{dt}$	$= \mathbf{Tr}_{\mathrm{NO_3^-}} + \mathbf{R}_{\mathrm{nit}}$
combined differential MCEs of equilibrium species	
(4) $\frac{d[\mathrm{CO_2}]}{dt} + \frac{d[\mathrm{HCO_3^-}]}{dt} + \frac{d[\mathrm{CO_3^{2-}}]}{dt}$	$= \mathbf{Tr}_{\mathrm{CO_2}} + \mathbf{Tr}_{\mathrm{HCO_3^-}} + \mathbf{Tr}_{\mathrm{CO_3^{2-}}} + \mathbf{E}_{\mathrm{CO_2}} + \gamma\,\mathbf{R}_{\mathrm{ox}}$
(5) $\frac{d[\mathrm{NH_3}]}{dt} + \frac{d[\mathrm{NH_4^+}]}{dt}$	$= \mathbf{Tr}_{\mathrm{NH_3}} + \mathbf{Tr}_{\mathrm{NH_4^+}} + \mathbf{E}_{\mathrm{NH_3}} + \mathbf{R}_{\mathrm{ox}} - \mathbf{R}_{\mathrm{nit}}$
(6) $\frac{d[\mathrm{HCO_3^-}]}{dt} + 2\frac{d[\mathrm{CO_3^{2-}}]}{dt} + \frac{d[\mathrm{NH_3}]}{dt} - \frac{d[\mathrm{H^+}]}{dt}$	$= \mathbf{Tr}_{\mathrm{HCO_3^-}} + 2\,\mathbf{Tr}_{\mathrm{CO_3^{2-}}} + \mathbf{Tr}_{\mathrm{NH_3}} - \mathbf{Tr}_{\mathrm{H^+}} + \mathbf{E}_{\mathrm{NH_3}} + \mathbf{R}_{\mathrm{ox}} - 2\,\mathbf{R}_{\mathrm{nit}}$
algebraic constraints (AEs): mass-action laws	
(7) 0	$= [\mathrm{H^+}][\mathrm{HCO_3^-}] - K^*_{\mathrm{CO_2}}[\mathrm{CO_2}]$
(8) 0	$= [\mathrm{H^+}][\mathrm{CO_3^{2-}}] - K^*_{\mathrm{HCO_3^-}}[\mathrm{HCO_3^-}]$
(9) 0	$= [\mathrm{H^+}][\mathrm{NH_3}] - K^*_{\mathrm{NH_4^+}}[\mathrm{NH_4^+}]$

Table 3.9.: Model transformed into the canonical form: a fully determined implicit initial-value DAE system. The combined mass conservation equations obtained by this transformation are equivalent to the result of a series of linear combinations of the MCEs from Table 3.4: (4)+(5)+(6); (7)+(8); and (5)+2·(6)+(8)−(9).

reaction rates. Appendix 3.6.2 details this procedure for our problem. In our case the transformation of the system into the canonical form results in the reformulated DAE system as given in Table 3.9, which contains 9 variables and 9 equations. Note that the transformation procedure also provides explicit expressions for the unknown net equilibrium reaction terms $\mathbf{R}^{\mathrm{dis}}_{\mathrm{CO_2}}$, $\mathbf{R}^{\mathrm{dis}}_{\mathrm{HCO_3^-}}$, and $\mathbf{R}^{\mathrm{dis}}_{\mathrm{NH_4^+}}$ (see Appendix 3.6.2). These can be used as output variables in the model and are sometimes of interest.

Solution method [2]: The model in Table 3.9 can be directly solved with the differential algebraic system solver DASSL (Petzold, 1982). This approach is referred to as the *Full Numerical Approach (FNA)*.

Still, this full numerical approach is not the most elegant way to approach the pH calculation. The equation set is supplied "as it is" to an external numerical solver routine, which then performs the number crunching. A further reformulation explicitly takes advantage of the chemical structure of the pH problem, thus allowing for less demanding numerical methods.

3.2.8. Step 8: Introduction of equilibrium invariants

The Eqs. (4) to (6) of Table 3.9 contain differentials of more than one species on their left-hand sides. This means the differential part of the DAE system is not explicit and cannot be solved by common integration methods such as Euler integration. To obtain a single differential on the left-hand side, one can introduce composite variables – as done in Table 3.10 for our model. These composite concentration variables are referred to as *equilibrium invariants*.

A	:=	$[CO_2]+[HCO_3^-]+[CO_3^{2-}]$	$\triangleq$	$[\sum CO_2]$
B	:=	$[NH_3]+[NH_4^+]$	$\triangleq$	$[\sum NH_4^+]$
C	:=	$[HCO_3^-]+2[CO_3^{2-}]+[NH_3]-[H^+]$	$\triangleq$	$[TA]$

Table 3.10.: Composite variables to create explicit ODEs in Table 3.9.

The reason for this nomenclature is straightforward. The right hand sides of Eqs. (4) to (6) do no longer contain the equilibrium reaction rates, and as a consequence, the rate of change of the equilibrium invariants is not influenced by the equilibrium reactions. Chemically, these equilibrium invariants thus can be seen as quantities that are conservative or invariant with respect to the equilibrium reactions. Note that the definition of the equilibrium invariants introduces n_{ei}=3 new variables. To keep the DAE system determined, the definitions of the equilibrium invariants have to be added.

The equilibrium invariants are in fact familiar quantities. We immediately recognize A and B as the dissolved inorganic carbon (DIC) and total ammonium concentrations, which are denoted $[\sum CO_2]$ and $[\sum NH_4^+]$. The third equilibrium invariant is termed total alkalinity [TA]. Again it has a familiar form: it is a subset of the total alkalinity [TA] as defined by Dickson (1981). Still a number of subtleties should be stressed:

1) In our approach, the definition of total alkalinity follows naturally from the transformation into the canonical form and the elimination of the equilibrium process rates. It is not postulated a priori like in many previous pH modeling procedures (e.g. Regnier et al., 1997; Luff et al., 2001; Jourabchi et al., 2005).

2) The alkalinity definition is linked to a particular choice of kinetic and equilibrium reactions. Accordingly, when the reaction set is modified, the alkalinity definition might change as well. Also, even when keeping the same reaction set but choosing a different model time-scale, one could arrive at a different alkalinity definition.

3) In our transformation procedure into canonical form we deliberately select suitable row operations during the Gauss-Jordan elimination (Appendix 3.6.2) such that we obtain a subset of Dickson's total alkalinity as an equilibrium invariant. Sticking to this practice, modifications in the reaction set and in the model time-scale, as mentioned above, might result in different subsets of Dickson's total alkalinity. However, if this practice is abandoned, also different related quantities like, for example, the "sum of excess negative charge" as used by Soetaert et al. (2007) can be obtained.

4) The right-hand side of the [TA] equation (Eq. (6) in Table 3.9) does not contain the rate of any equilibrium reaction. This immediately shows that the alkalinity is a true equilibrium invariant, i.e., [TA] is not influenced by equilibrium reactions, even though all its constituents are affected by these reactions[4].

5) The influence of kinetic processes on [TA] can be directly inferred from the right-hand side of the [TA] equation (Eq. (6) in Table 3.9). This implies that one does not need

[4]Similarly the temperature invariance of [TA] can be inferred, since on the timescale of an integration timestep, temperature only influences the acid-base equilibrium reactions (via the K^{**}'s), and these do not influence [TA].

to invoke the electroneutrality of the solution or the notion of "explicit conservative total alkalinity" as advocated by Wolf-Gladrow et al. (2007) to obtain the influences of kinetic processes on [TA].

Note that the concept of equilibrium invariants is based on ideas put forward by amongst others DiToro (1976), Boudreau (1987), Boudreau and Canfield (1988), Boudreau (1991), Boudreau and Canfield (1993), and Morel and Hering (1993). Furthermore, as illustrated in Table 3.11, transforming the system into the canonical form and introducing equilibrium invariants is a formal mathematical way of finding suitable *components* in the *tableau* notation of Morel and Hering (1993) including the corresponding mole balance equations.

Note also that the sum of the transport terms on the right-hand side of the MCE's for the equilibrium invariants (Eqs. (4–6) in Table 3.9) can be directly calculated from the concentrations of the equilibrium invariants if the transport formulation for all species is the same, i.e., there is no differential transport in the model. Mathematically that means that the transport formulation needs to be distributive over the sum. In our model, for example, this is realized by assuming the same bulk dispersion coefficient E' for all chemical species.

species	components		
	CO_2	NH_4^+	H^+
CO_2	1		
HCO_3^-	1		−1
CO_3^{2-}	1		−2
NH_4^+		1	
NH_3		1	−1
H^+			1

$$
\begin{aligned}
\mathrm{TOTCO_2} &= [CO_2] + [HCO_3^-] + [CO_3^{2-}] && \triangleq [\textstyle\sum CO_2] \\
\mathrm{TOTNH_4} &= [NH_4^+] + [NH_3] && \triangleq [\textstyle\sum NH_4^+] \\
\mathrm{TOTH} &= -[HCO_3^-] - 2[CO_3^{2-}] - [NH_3^+] + [H^+] && \triangleq -[TA]
\end{aligned}
$$

Table 3.11.: The model system written in tableau notation (Morel and Hering, 1993) with corresponding mole balance equations including their equivalence to our equilibrium invariants.

3.2.9. Step 9: Reformulation 2: Operator splitting

The algebraic part of our DAE system now consists of the mass action relations (Eqs. (7–9) in Table 3.9) and the definitions of the equilibrium invariants (Table 3.10). These equations feature the equilibrium species. However, each of the equilibrium species concentrations ($[CO_2]$, $[HCO_3^-]$, $[CO_3^{2-}]$, $[NH_3]$ and $[NH_4^+]$) can be readily expressed in terms of the proton concentration $[H^+]$ and the associated equilibrium invariants ($[\sum CO_2]$ and $[\sum NH_4^+]$). Appendix 3.6.3 describes this reformulation of the algebraic part of the DAE system. As a result, we obtain a novel DAE system (Table 3.12) where both the DE part and the AE part are reformulated

MCEs of kinetic species	
(1)	$\frac{d[\mathrm{OM}]}{dt} = \mathbf{Tr}_{\mathrm{OM}} - \mathbf{R}_{\mathrm{ox}}$
(2)	$\frac{d[\mathrm{O_2}]}{dt} = \mathbf{Tr}_{\mathrm{O_2}} + \mathbf{E}_{\mathrm{O_2}} - \gamma\,\mathbf{R}_{\mathrm{ox}} - 2\;\mathbf{R}_{\mathrm{nit}}$
(3)	$\frac{d[\mathrm{NO_3^-}]}{dt} = \mathbf{Tr}_{\mathrm{NO_3^-}} + \mathbf{R}_{\mathrm{nit}}$
MCEs of equilibrium invariants	
(4)	$\frac{d[\sum \mathrm{CO_2}]}{dt} = \mathbf{Tr}_{\mathrm{CO_2}} + \mathbf{Tr}_{\mathrm{HCO_3^-}} + \mathbf{Tr}_{\mathrm{CO_3^{2-}}} + \mathbf{E}_{\mathrm{CO_2}} + \gamma\,\mathbf{R}_{\mathrm{ox}}$
(5)	$\frac{d[\sum \mathrm{NH_4^+}]}{dt} = \mathbf{Tr}_{\mathrm{NH_3}} + \mathbf{Tr}_{\mathrm{NH_4^+}} + \mathbf{E}_{\mathrm{NH_3}} + \mathbf{R}_{\mathrm{ox}} - \mathbf{R}_{\mathrm{nit}}$
(6)	$\frac{d[\mathrm{TA}]}{dt} = \mathbf{Tr}_{\mathrm{HCO_3^-}} + 2\,\mathbf{Tr}_{\mathrm{CO_3^{2-}}} + \mathbf{Tr}_{\mathrm{NH_3}} - \mathbf{Tr}_{\mathrm{H^+}} + \mathbf{E}_{\mathrm{NH_3}} + \mathbf{R}_{\mathrm{ox}} - 2\,\mathbf{R}_{\mathrm{nit}}$
algebraic constraints (AEs)	
(7)	$[\mathrm{CO_2}] = \frac{[\mathrm{H^+}]^2}{[\mathrm{H^+}]^2 + K^*_{\mathrm{CO_2}}[\mathrm{H^+}] + K^*_{\mathrm{CO_2}}K^*_{\mathrm{HCO_3^-}}}[\sum \mathrm{CO_2}] \triangleq f_1^c([\mathrm{H^+}]) \cdot [\sum \mathrm{CO_2}]$
(8)	$[\mathrm{HCO_3^-}] = \frac{K^*_{\mathrm{CO_2}}[\mathrm{H^+}]}{[\mathrm{H^+}]^2 + K^*_{\mathrm{CO_2}}[\mathrm{H^+}] + K^*_{\mathrm{CO_2}}K^*_{\mathrm{HCO_3^-}}}[\sum \mathrm{CO_2}] \triangleq f_2^c([\mathrm{H^+}]) \cdot [\sum \mathrm{CO_2}]$
(9)	$[\mathrm{CO_3^{2-}}] = \frac{K^*_{\mathrm{CO_2}}K^*_{\mathrm{HCO_3^-}}}{[\mathrm{H^+}]^2 + K^*_{\mathrm{CO_2}}[\mathrm{H^+}] + K^*_{\mathrm{CO_2}}K^*_{\mathrm{HCO_3^-}}}[\sum \mathrm{CO_2}] \triangleq f_3^c([\mathrm{H^+}]) \cdot [\sum \mathrm{CO_2}]$
(10)	$[\mathrm{NH_4^+}] = \frac{[\mathrm{H^+}]}{[\mathrm{H^+}] + K^*_{\mathrm{NH_4^+}}}[\sum \mathrm{NH_4^+}] \triangleq f_1^n([\mathrm{H^+}]) \cdot [\sum \mathrm{NH_4^+}]$
(11)	$[\mathrm{NH_3}] = \frac{K^*_{\mathrm{NH_4^+}}}{[\mathrm{H^+}] + K^*_{\mathrm{NH_4^+}}}[\sum \mathrm{NH_4^+}] \triangleq f_2^n([\mathrm{H^+}]) \cdot [\sum \mathrm{NH_4^+}]$
(12)	$[\mathrm{TA}] = [\mathrm{HCO_3^-}] + 2\,[\mathrm{CO_3^{2-}}] + [\mathrm{NH_3}] - [\mathrm{H^+}]$

Table 3.12.: System refomulated in terms of equilibrium invariants: explicit ODEs and equilibrium species as functions of $[\mathrm{H^+}]$ and equilibrium invariants.

in terms of the equilibrium invariants.

Solution method [3a]: Although it still can be directly solved with DASSL, the system given in Table 3.12 can be solved with less numerical effort using the *Operator Splitting Approach (OSA)*. This two step approach decouples the DAE system into an ordinary differential equation (ODE) system describing the kinetic reactions and an algebraic equation (AE) system that governs the equilibrium part (Luff et al., 2001; Meysman, 2001).

At each time step, the differential equation system is numerically integrated, e.g., with an Euler integration routine (Press et al., 1992), which provides values for the differential variables (kinetic species and equilibrium invariants) at the next time step. Subsequently, the algebraic equation system is solved at each timestep using the values for the differential variables provided by the numerical integration of the ODE system. Due to its nonlinearity in $[\mathrm{H^+}]$, the algebraic equation system must be solved numerically (e.g. using the van Wijngaarden-Dekker-Brent or Newton-Raphson methods given by Press et al., 1992) to find the chemically meaningful root ($f([\mathrm{H^+}])$=0) of the function:

$$\begin{aligned} f([\mathrm{H^+}]) &= [\mathrm{TA}] - \left([\mathrm{HCO_3^-}] + 2\,[\mathrm{CO_3^{2-}}] + [\mathrm{NH_3}] - [\mathrm{H^+}]\right) \\ &= [\mathrm{TA}] - \left(\left(f_2^c([\mathrm{H^+}]) + 2 \cdot f_3^c([\mathrm{H^+}])\right) \cdot [\sum \mathrm{CO_2}] + f_1^n([\mathrm{H^+}]) \cdot [\sum \mathrm{NH_4^+}] - [\mathrm{H^+}]\right) \end{aligned} \tag{13}$$

The classical OSA (solution method 3a) takes advantage of the specific structure of the model to solve it in a more elegant fashion than the FNA using DASSL. Still it requires at each time step the iteration between a numerical integration solver and a numerical root-finding technique, which might be computationally demanding.

Solution method [3b]: Recently, a modified OSA has been proposed (Follows et al., 2006), which is computationally faster. Rather than solving Eq. (13) directly, it acknowledges that carbonate alkalinity ($[CA]=[HCO_3^-]+2[CO_3^{2-}]$) contributes most to total alkalinity.

In our case, using the proton concentration of the previous timestep $[H^+]_{prev}$ and modelled equilibrium invariants (here $[TA]$ and $[\sum NH_4^+]$), the modelled carbonate alkalinity can be estimated by:

$$[CA] \approx [TA] - f_1^n\left([H^+]_{prev}\right) \cdot [\sum NH_4^+] - [H^+]_{prev} \tag{14}$$

which allows a first guess for the $[H^+]$ at the current time step by analytically solving the quadratic equation:

$$0 = [CA][H^+]^2 + K^*_{CO_2}\left([CA] - [\sum CO_2]\right)[H^+] + K^*_{CO_2}K^*_{HCO_3^-}\left([CA] - 2[\sum CO_2]\right) \tag{15}$$

This first guess for $[H^+]$ is then used to evaluate Eq. (13) and test if its root has been found (with sufficient accuracy). If not, the first guess for $[H^+]$ is used to calculate a better estimate for $[CA]$ and the procedure is iteratively repeated. Iteration is mostly not necessary for buffered systems.

Note that this method also works if there are more minor contribution terms to $[TA]$ than in our simple example. Note further that this method is inspired by the classical pH calculation methods of Culberson (1980), who analytically solved a cubic equation for systems with total alkalinity consisting of carbonate and borate alkalinity only, and Ben-Yaakov (1970), who iteratively solved an equation for $[H^+]$ by starting with an initial guess and by subsequent uniform increment of $[H^+]$.

Although this improved OSA approach (solution method 3b) is advantageous, it does not allow assessing the influences of modelled kinetic processes on the pH. A further reformulation of the system is possible, which avoids numerical root-finding as well as the iterative procedure according to Follows et al. (2006). This method allows for the assessment of the influences of modelled kinetic processes (including subsequent re-equilibration of the system) on the pH.

3.2.10. Step 10: Reformulation 3: Direct substitution

The classical OSA needs a numerical root-finding procedure because the algebraic equation (AE) part is non-linear with respect to the unknown proton concentration $[H^+]$. Therefore, if one could make $[H^+]$ a differential variable, its value would be known before the solution of the algebraic equation system. This way, the algebraic equation system could be solved analytically and the numerical root-finding procedure would not be necessary. To achieve this goal, the differential equation for $[TA]$ in Table 3.12 should be substituted by a differential equation in $[H^+]$. Partially following the ideas developed by Jourabchi et al. (2005) and Soetaert et al.

(2007), this can be done by starting with the total derivative of the equilibrium invariant [TA].

Equation (12) in Table 3.12 tells us, that if all the dissociation constants (K*'s) are constant, the equilibrium invariant [TA] can be written as a function of exclusively the proton concentration and the equilibrium invariants

$$[\mathrm{TA}] = f\left([\mathrm{H^+}], [\textstyle\sum \mathrm{CO_2}], [\textstyle\sum \mathrm{NH_4^+}]\right) \tag{16}$$

These variables are functions of time t. Consequently, the total derivative of [TA] can be written as

$$\frac{d[\mathrm{TA}]}{dt} = \frac{d[\mathrm{H^+}]}{dt}\frac{\partial[\mathrm{TA}]}{\partial[\mathrm{H^+}]}\bigg|_{c,n} + \frac{d[\textstyle\sum \mathrm{CO_2}]}{dt}\frac{\partial[\mathrm{TA}]}{\partial[\textstyle\sum \mathrm{CO_2}]}\bigg|_{h,n} + \frac{d[\textstyle\sum \mathrm{NH_4^+}]}{dt}\frac{\partial[\mathrm{TA}]}{\partial[\textstyle\sum \mathrm{NH_4^+}]}\bigg|_{h,c} \tag{17}$$

The subscripts indicate which quantities are held constant upon differentiation, and the shorthand notation c=[$\sum \mathrm{CO_2}$], n=[$\sum \mathrm{NH_4^+}$] and h=[$\mathrm{H^+}$] has been used. Eq. (17) can be readily solved for $\frac{d[\mathrm{H^+}]}{dt}$, resulting in

$$\frac{d[\mathrm{H^+}]}{dt} = \left(\frac{d[\mathrm{TA}]}{dt} - \left(\frac{d[\textstyle\sum \mathrm{CO_2}]}{dt}\frac{\partial[\mathrm{TA}]}{\partial[\textstyle\sum \mathrm{CO_2}]}\bigg|_{h,n} + \frac{d[\textstyle\sum \mathrm{NH_4^+}]}{dt}\frac{\partial[\mathrm{TA}]}{\partial[\textstyle\sum \mathrm{NH_4^+}]}\bigg|_{h,c}\right)\right) \Big/ \frac{\partial[\mathrm{TA}]}{\partial[\mathrm{H^+}]}\bigg|_{c,n} \tag{18}$$

Equation (18) can replace the differential equation for [TA] in Table 3.12. Each of the quantities on the right hand-side of Eq. (18) is explicitly known. The time derivatives of the equilibrium invariants are given by expressions (4)–(6) in Table 3.12. Furthermore, Appendix 3.6.4.1 shows how the partial derivatives of total alkalinity can be analytically calculated. Table 3.13 shows the reformulated DE's/MCE's of the DAE system. The AE part is the same as given in Table 3.12 (except for the equation for [TA] which is obsolete) and is not repeated.

The quantity $\frac{\partial[\mathrm{TA}]}{\partial[\mathrm{H^+}]}$ is a central and important quantity for pH modelling, as it modulates the effect of changes in state variables on [$\mathrm{H^+}$]. Soetaert et al. (2007) call a similar quantity the *buffering capacity* of the solution, and Frankignoulle (1994) refers to the inverse of a related quantity as the *chemical buffer factor* of the solution.

Solution method [4]: The explicit ODE system in Table 3.13 can be numerically integrated. Subsequently, the AE system is used to analytically calculate the equilibrium concentrations for every timestep of the numerical integration. The resulting approach is referred to as the *Direct Substitution Approach (DSA)* (Saaltink et al., 1998; Meysman, 2001).

The DSA is the end result of three sequential reformulations of the pH problem. The DSA has two advantages. The first advantage is that it makes maximal use of the chemical structure of the pH problem, to gain understanding and insight and to reduce the numerical effort. However, depending on the application, the OSA improved according to Follows et al. (2006) might have about the same computational requirements. The second and major advantage is that Eq. (18) directly quantifies the influence of the various kinetic processes on [$\mathrm{H^+}$] and hence on pH. To show this, one can rearrange Eq. (18) (or rather the last equation in

kinetic species
$\frac{d[\mathrm{OM}]}{dt} = \mathbf{Tr}_{\mathrm{OM}} - \mathbf{R}_{\mathrm{ox}}$
$\frac{d[\mathrm{O_2}]}{dt} = \mathbf{Tr}_{\mathrm{O_2}} + \mathbf{E}_{\mathrm{O_2}} - \gamma\,\mathbf{R}_{\mathrm{ox}} - 2\;\mathbf{R}_{\mathrm{nit}}$
$\frac{d[\mathrm{NO_3^-}]}{dt} = \mathbf{Tr}_{\mathrm{NO_3^-}} + \mathbf{R}_{\mathrm{nit}}$
equilibrium invariants
$\frac{d[\sum \mathrm{CO_2}]}{dt} = \mathbf{Tr}_{\mathrm{CO_2}} + \mathbf{Tr}_{\mathrm{HCO_3^-}} + \mathbf{Tr}_{\mathrm{CO_3^{2-}}} + \mathbf{E}_{\mathrm{CO_2}} + \gamma\,\mathbf{R}_{\mathrm{ox}}$
$\frac{d[\sum \mathrm{NH_4^+}]}{dt} = \mathbf{Tr}_{\mathrm{NH_3}} + \mathbf{Tr}_{\mathrm{NH_4^+}} + \mathbf{E}_{\mathrm{NH_3}} + \mathbf{R}_{\mathrm{ox}} - \mathbf{R}_{\mathrm{nit}}$
equilibrium species
$\frac{d[\mathrm{H^+}]}{dt} = \Big(\mathbf{Tr}_{\mathrm{HCO_3^-}} + 2\;\mathbf{Tr}_{\mathrm{CO_3^{2-}}} + \mathbf{Tr}_{\mathrm{OH^-}} + \mathbf{Tr}_{\mathrm{NH_3}} - \mathbf{Tr}_{\mathrm{H^+}} + \mathbf{E}_{\mathrm{NH_3}} + \mathbf{R}_{\mathrm{ox}} - 2\mathbf{R}_{\mathrm{nit}}\Big) \Big/ \frac{\partial[\mathrm{TA}]}{\partial[\mathrm{H^+}]}\Big\vert_{c,n}$ $-\Big(\mathbf{Tr}_{\mathrm{CO_2}} + \mathbf{Tr}_{\mathrm{HCO_3^-}} + \mathbf{Tr}_{\mathrm{CO_3^{2-}}} + \mathbf{E}_{\mathrm{CO_2}} + \gamma\mathbf{R}_{\mathrm{ox}}\Big)\frac{\partial[\mathrm{TA}]}{\partial[\sum \mathrm{CO_2}]}\Big\vert_{h,n} \Big/ \frac{\partial[\mathrm{TA}]}{\partial[\mathrm{H^+}]}\Big\vert_{c,n}$ $-\Big(\mathbf{Tr}_{\mathrm{NH_3}} + \mathbf{Tr}_{\mathrm{NH_4^+}} + \mathbf{E}_{\mathrm{NH_3}} + \mathbf{R}_{\mathrm{ox}} - \mathbf{R}_{\mathrm{nit}}\Big)\frac{\partial[\mathrm{TA}]}{\partial[\sum \mathrm{NH_4^+}]}\Big\vert_{h,c} \Big/ \frac{\partial[\mathrm{TA}]}{\partial[\mathrm{H^+}]}\Big\vert_{c,n}$

Table 3.13.: ODE part of the DAE system with direct substitution of $\frac{d[\mathrm{TA}]}{dt}$ by $\frac{d[\mathrm{H^+}]}{dt}$

Table 3.13) to the form

$$\frac{d[\mathrm{H^+}]}{dt} = \alpha_{\mathbf{R}_{\mathrm{ox}}}\mathbf{R}_{\mathrm{ox}} + \alpha_{\mathbf{R}_{\mathrm{nit}}}\mathbf{R}_{\mathrm{nit}} + \alpha_{\mathbf{E}_{\mathrm{CO_2}}}\mathbf{E}_{\mathrm{CO_2}} + \alpha_{\mathbf{E}_{\mathrm{NH_3}}}\mathbf{E}_{\mathrm{NH_3}} + \sum \mathbf{T} \tag{19}$$

where the α coefficients and $\sum \mathbf{T}$ can be calculated at each time step using the expressions given in Appendix 3.6.4.2. The α-coefficients are modulating factors that express the influence on pH for each of the four kinetic reactions/processes. Similarly, the term $\sum \mathbf{T}$ lumps the influence of advective-dispersive transport processes on pH.

Splitting up α coefficients into process specific modulation factors and the buffering capacity of the solution, the influences of kinetic processes (except transport) on the rate of change of the proton concentration can be formalized as:

$$\alpha_{\mathbf{R}_X}\mathbf{R}_X = \left(\beta_{\mathbf{R}_X} \Big/ \frac{\partial[\mathrm{TA}]}{\partial[\mathrm{H^+}]}\right)\mathbf{R}_X \tag{20}$$

where the β coefficients represent the process specific modulation factors, which can also be found in Table 3.20 in Appendix 3.6.4.2.

The influence of transport on the rate of change of the proton concentration can be written as

$$\sum \mathbf{T} = \left(\mathbf{T}_{\mathrm{TA}} - \mathbf{T}_{\sum \mathrm{CO_2}}\frac{\partial[\mathrm{TA}]}{\partial[\sum \mathrm{CO_2}]}\Big|_{h,n} - \mathbf{T}_{\sum \mathrm{NH_4^+}}\frac{\partial[\mathrm{TA}]}{\partial[\sum \mathrm{NH_4^+}]}\Big|_{h,c}\right) \Big/ \frac{\partial[\mathrm{TA}]}{\partial[\mathrm{H^+}]} \tag{21}$$

with

$$\mathbf{T}_{TA} = \mathbf{Tr}_{HCO_3^-} + 2\,\mathbf{Tr}_{CO_3^{2-}} + \mathbf{Tr}_{NH_3} - \mathbf{Tr}_{H^+} \quad (22)$$

$$\mathbf{T}_{\sum CO_2} = \mathbf{Tr}_{CO_2} + \mathbf{Tr}_{HCO_3^-} + \mathbf{Tr}_{CO_3^{2-}} \quad (23)$$

$$\mathbf{T}_{\sum NH_4^+} = \mathbf{Tr}_{NH_3} + \mathbf{Tr}_{NH_4^+} \quad (24)$$

This means that the influence of a modelled kinetic process (except transport) on the $\frac{d[H^+]}{dt}$ can be calculated by multiplying the kinetic rate of the process in question by a modulating factor β divided by the buffering capacity of the solution $\frac{\partial[TA]}{\partial[H^+]}$. The influence of transport on $\frac{d[H^+]}{dt}$, however, is an expression of the transport terms for the equilibrium invariants divided by, again, the buffering capacity of the solution.

3.3. Results

3.3.1. Baseline simulation

In a first step, we performed a baseline steady state calculation for our model estuary with boundary conditions for the year 2004, which serves as a reference situation for the two perturbations scenarios outlined in the introduction. Table 3.14 provides an overview of the parameters and boundary conditions that were used in this baseline simulation.

Using the set of parameter values in Table 3.14, the DSA approach (solution method 4) was implemented within the modeling environment FEMME (Soetaert et al., 2002). The FORTRAN model code can be obtained from the author or downloaded from the FEMME website: http://www.nioo.knaw.nl/ceme/femme/.

The upstream concentrations were used as initial conditions, and a time-dependent simulation was performed until steady-state was reached. Table 3.15 compares the concentrations in the baseline simulation with values averaged over the year 2004. There is a good agreement between measured and modeled values. Also, the steady state rates for oxic mineralisation ($\mathbf{R}_{ox}$=2.8 μmol-N kg^{-1} d^{-1}) and nitrification ($\mathbf{R}_{nit}$=8.2 μmol-N kg^{-1} d^{-1}) are in good agreement with values from Table 3.1. This correspondence between model and measurements was obtained without tuning of model parameters. This provides confidence that the baseline simulation captures the essential features of the carbon and nitrogen dynamics, and thus provides a good starting point for the dynamic perturbation simulations.

Mass balance closure was verified for carbon, nitrogen and oxygen. The CO_2 export to the atmosphere ($\mathbf{E}_{CO_2}$=−40.8 μmol-C kg^{-1} d^{-1}) is larger than the internal CO_2 release from mineralization ($\gamma \cdot \mathbf{R}_{ox}$=22.7 μmol-C kg^{-1} d^{-1}), and this difference is balanced by the advective-dispersive $\sum CO_2$ input ($\mathbf{Tr}_{\sum CO_2}$=18.1 μmol-C kg^{-1} d^{-1}; positive $\mathbf{Tr}_{\sum CO_2}$ means larger $\sum CO_2$ inflow than outflow). Accordingly, the upper Schelde estuary emits carbon dioxide from upstream resources. The water is reaerated with oxygen at a rate of $\mathbf{E}_{O_2}$ = 46.8 μmol-O_2 kg^{-1} d^{-1}. Oxygen is mostly consumed in oxic mineralization (22.7 μmol-C kg^{-1} d^{-1}: 49%) and nitrification (16.4 μmol-O_2 kg^{-1} d^{-1}: 35 %). The budget for oxygen is again closed by advective-dispersive transport, which exports O_2 downstream at a rate of $\mathbf{Tr}_{O_2}$=7.7 μmol-O_2 kg^{-1} d^{-1} (16%).

Parameters				
Volume	V	108 798 000	m^3	(Soetaert and Herman, 1994a)
Freshwater flow	Q	100	$m^3\,s^{-1}$	(Heip, 1988)
Bulk dispersion coefficient	E'	160	$m^3\,s^{-1}$	(Soetaert and Herman, 1994a)
Mean water depth	d_w	10	m	(Soetaert and Herman, 1994a)
Residence time	t_r	14	d	(Soetaert and Herman, 1994a)
Piston velocity	K_L	2.8	$m\,d^{-1}$	(Borges et al., 2004; Wanninkhof, 1992)
First order oxic mineralisation rate	r_{ox}	0.1	d^{-1}	(Soetaert and Herman, 1995a), NM 2004
First order nitrification rate	r_{nit}	0.26	d^{-1}	(Andersson et al., 2006), NM 2004
Oxygen inhibition half saturation constant	ks_{O_2}	20.0	$\mu mol\text{-}O_2\,kg^{-1}$	(Soetaert and Herman, 1995a)
Carbon to nitrogen ratio of organic matter	γ	8	mol-C mol-N^{-1}	(Soetaert and Herman, 1995a)
Mean water temperature	T	12	C	NM 2004
Mean salinity	S	5		NM 2004
CO_2 saturation concentration	$[CO_2]_{sat}$	19	$\mu mol\,kg^{-1}$	(Weiss, 1974; Borges et al., 2004)
O_2 saturation concentration	$[O_2]_{sat}$	325	$\mu mol\,kg^{-1}$	(Garcia and Gordon, 1992)
NH_3 saturation concentration	$[NH_3]_{sat}$	0.0001	$\mu mol\,kg^{-1}$	estimated
Dissociation constant of CO_2	$K^*_{CO_2}$	$6.93\,10^{-1}$	$\mu mol\,kg^{-1}$	(Roy et al., 1993a)
Dissociation constant of HCO_3^-	$K^*_{HCO_3^-}$	$2.59\,10^{-4}$	$\mu mol\,kg^{-1}$	(Roy et al., 1993a)
Dissociation constant of NH_4^+	$K^*_{NH_4^+}$	$2.23\,10^{-4}$	$\mu mol\,kg^{-1}$	(Millero, 1995)
Ion product of H_2O	$K^*_{H_2O}$	$7.30\,10^{-3}$	$(\mu mol\,kg^{-1})^2$	(Millero, 1995)
Boundary conditions				
		upstream	*downstream*	
organic matter concentration	$[OM]$	50	25	$\mu mol\text{-}N\,kg^{-1}$ NM 2004
nitrate	$[NO_3^-]$	350	260	$\mu mol\,kg^{-1}$ NM 2004
oxygen	$[O_2]$	70	240	$\mu mol\,kg^{-1}$ NM 2004
total ammonium	$[\sum NH_4^+]$	80	7	$\mu mol\,kg^{-1}$ NM 2004
total carbon dioxide	$[\sum CO_2]$	7100	4400	$\mu mol\,kg^{-1}$ (Hellings et al., 2001)
free protons	$[H]$	0.025	0.0121	$\mu mol\,kg^{-1}$ NM 2004
total alkalinity	$[TA]$	6926	4416	$\mu mol\,kg^{-1}$ calculated

Table 3.14.: *Characteristic parameters of the model domain*: K_L has been calculated by using a k_{600} value (piston velocity), normalized to a Schmidt number of 600 (the value for carbon dioxide in freshwater at 20°C), for the Schelde at Antwerp from Borges et al. (2004), and a Schmidt number for carbon dioxide at a temperature of 12 C and a salinity of 5 from Wanninkhof (1992). r_{ox} has been obtained by dividing pelagic oxic mineralisation rates from Soetaert and Herman (1995a) by measured $[OM]$ values for 2004. r_{nit} has been calculated in similar fashion using nitrification rates obtained from Andersson et al. (2006). $[CO_2]_{sat}$ has been calculated according to a formula given in Weiss (1974) and atmospheric carbon dioxide levels from Borges et al. (2004). All dissociation constants are on the free hydrogen ion scale and for a temperature of T=12 C and salinity S=5. *Boundary conditions of the model domain*: Values for $[\sum CO_2]$ have been obtained from Hellings et al. (2001). All other values are NIOO monitoring values for 2004, except for the values for [TA] which have been consistently calculated. "NM 2004" refers to measured data from 2004 obtained by the NIOO monitoring program.

quantity	baseline	baseline $+\mathbf{R}_{H_2O}$	baseline $+\mathbf{R}_{H_2O}$ $+\mathbf{R}_{den}$	measured
[OM]	32	32	30	29
$[NO_3^-]$	340	340	328	322
$[O_2]$	158	158	159	154
pH	7.70	7.70	7.71	7.70
$[\sum NH_4^+]$	36	36	37	29
$[\sum CO_2]$	6017	6017	6030	
[TA]	5929	5929	5942	

Table 3.15.: Steady state baseline values compared with measured values from 2004 (NIOO monitoring data). All quantities except for pH have the unit μ mol kg^{-1}.

As noted above, one of the major advantages of the DSA approach is that one can partition $\frac{d[H^+]}{dt}$ (= total change in proton concentration) into contributions by different kinetic processes (Eq. 19). At steady state, overall consumption of protons should match overall production. Figure 3.2 shows that in our baseline simulation, the pH steady state is dominated by the interplay between oxic mineralisation, nitrification and CO_2 air-water exchange. Oxic mineralisation and nitrification respectively produce about 49% and 40% of the protons consumed by CO_2 outgassing. The remaining 11% are the result of advective-dispersive transport ($\sum \mathbf{T}$). The NH_3 exchange with the atmosphere plays a negligible role, as it produces only 0.3% of the protons consumed by CO_2 air-water exchange.

3.3.2. The influence of H_2O auto-dissociation and denitrification

In the formulation of the model, we deliberately neglected the auto-dissociation of water ($\mathbf{R}_{H_2O}$) and denitrification ($\mathbf{R}_{den}$) to keep the model analysis as simple as possible. A model including H_2O auto-dissociation does not show any differences in steady state results (Table 3.15, Fig. 3.2). Accordingly, $\mathbf{R}_{H_2O}$ can be safely omitted.

To check the importance of denitrification, we included the reaction

$$(CH_2O)_\gamma(NH_3)+0.8\,\gamma\,NO_3^-+0.8\,\gamma\,H^+ \rightarrow NH_3+\gamma\,CO_2+0.4\,\gamma\,N^2\uparrow+1.4\,\gamma\,H_2O \qquad (25)$$

with the kinetic formulation

$$\mathbf{R}_{den} = r_{den}\cdot[OM]\cdot(ks_{O_2}^{inhib}/([O_2]+ks_{O_2}^{inhib}))\cdot([NO_3^-]/([NO_3^-]+ks_{NO_3^-})) \qquad (26)$$

with rate constant r_{den}=0.2 d^{-1} (Soetaert and Herman, 1995a), an inhibition constant $ks_{O_2}^{inhib}$ = 45 μ mol kg^{-1} (Soetaert and Herman, 1995a), and a saturation constant $ks_{NO_3^-}$=22 μ mol kg^{-1} (Regnier et al., 1997). The inclusion of denitrification results in marginal differences in concentrations (Table 3.15) and does not affect the steady state pH (Fig. 3.2).

3.3.3. Three perturbation scenarios

In the perturbation scenarios, the baseline steady state values were imposed as initial conditions.

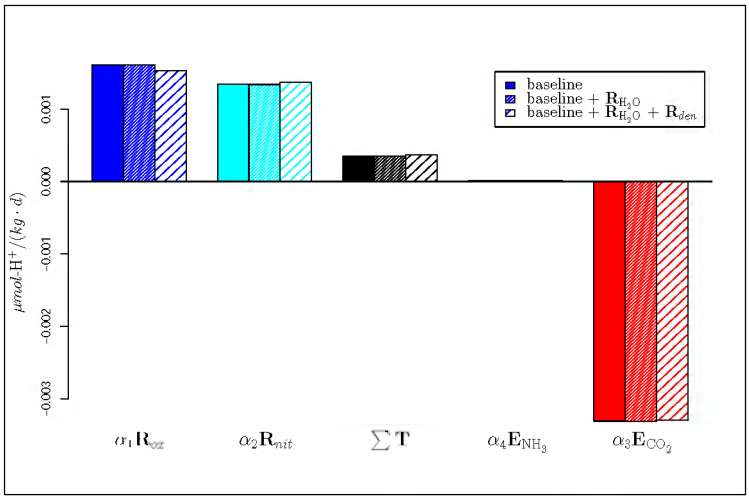

Figure 3.2.: Partitioning of $\frac{d[H^+]}{dt}$ according to Table 3.20.

3.3.3.1. *Scenario A:* Decrease in the upstream organic matter loading

It is estimated that the organic matter loading in the river Schelde will be halved by a new sewage-treatment plant for the city of Brussels, which became operational in 2007. To simulate the impact of this change, we started off from the baseline simulation (values for the year 2004), and decreased the upstream organic matter concentration $[OM]_{up}$ from 50 μmol N kg^{-1} to 25 μmol N kg^{-1} on the fifth day of a 40-day model run. Figure 3.3 shows the evolution of pH, [TA], $[\sum CO_2]$ and $[O_2]$ for this scenario. After about 35 days a new steady state is reached, in line with the 10 day response time-scale of the dominant transport and reaction processes (Table 5). The decrease in OM loading reduces the steady state concentration of organic matter [OM] by 38% (not shown), while oxygen levels increase by 10% and $[\sum CO_2]$ levels remain virtually unchanged (slight decrease by 0.3%). Note that the changes occur monotonically. This is different for the total alkalinity, which shows a slight "overshoot" response. TA decreases from 5928.9 μmol kg^{-1} to a minimum value of 5927.9 μmol kg^{-1} after 6 days, but then stabilizes at a higher level of 5928.1 μmol kg^{-1}. This dip in [TA] is explained by a different temporal response of the mineralization, nitrification and transport terms (Fig. 4a). The change in the upstream OM concentration leads to a sharp decline in [OM] in the system, causing $\mathbf{R}_{ox}$ (which produces alkalinity) to drop sharply as well. The nitrification rate $\mathbf{R}_{nit}$ (which consumes alkalinity) however drops less sharply. As a result, temporarily "too much" alkalinity TA is consumed, which results in the observed dip in [TA]. Note that this discussion is only interesting in terms of model internals but is not relevant to the real system, since the changes in [TA] are near or below the measurement accuracy.

Also note that the decrease in [TA] (0.8 μmol kg^{-1}) is much smaller than the corresponding decrease in the DIC concentration (16 μmol kg^{-1}). This difference is due to the rising pH and the associated re-equilibration within the carbonate system. Although $[\sum CO_2]$ decreases, the

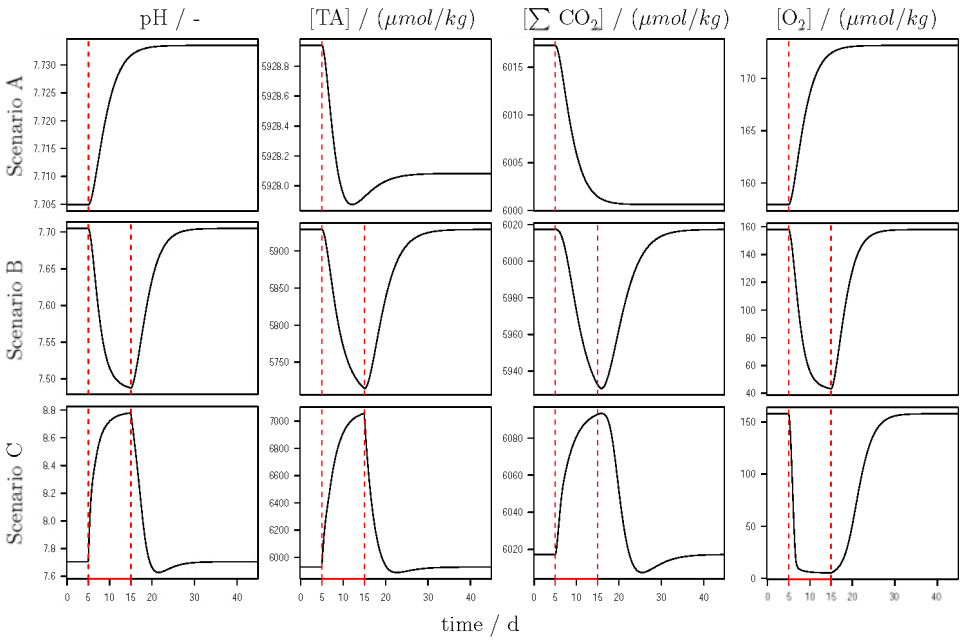

Figure 3.3.: The pH, [TA], $[\sum CO_2]$ and $[O_2]$ development for the three model scenarios.

CO_2 system dissociates more, due to the pH increase, increasing $[CO_3^{2-}]$. Hence, alkalinity does not follow the decrease in $[\sum CO_2]$ to similar extent (see Table 3.16).

species	before	after	Δ
$[CO_2]$	164.57	153.8	−10.77
$[HCO_3^-]$	5776.88	5766.0	−10.88
$[CO_3^{2-}]$	75.84	80.85	+5.01

Table 3.16.: The carbonate system before and after the change in upstream organic matter loading (all values in $\mu\,\mathrm{mol\,kg^{-1}}$).

The new steady state pH of 7.734 is only 0.4% higher than the baseline pH of 7.705. Figure 3.5 shows that the abrupt decrease in organic matter loading has only a small influence on the pH steady state. The individual contributions of all processes decline, except for the small contribution of advective-diffusive transport. That means the model results are in agreement with intuitive expectations: In a system with less organic matter input, the influence of physical processes on pH increases relative to that of biological processes.

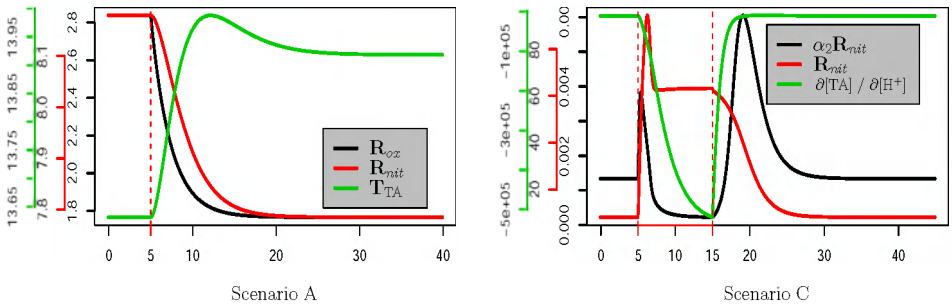

Figure 3.4.: Key quantities of scenario A and C, all scaled to the plot area.

3.3.3.2. *Scenario B:* Spill of ammonium nitrate

Due to the presence of the harbour of Antwerp and the surrounding chemical industry, there is potential danger of ship accidents and spills of chemicals into the Schelde estuary. As an example, we consider a spill of ten thousand tons of ammonium-nitrate fertilizer (NH_4^+ NO_3^-; in the molar ratio 1:1). Furthermore, we consider a slowly leaking ship, where the chemicals are released within a period of 10 days (between day 5 and 15 of the simulation). To model this release, we need to include an extra source term for ammonium and nitrate in the MCE's (cf. Table 3.4).

$$\mathbf{A}_{NH_4^+} = \mathbf{A}_{NO_3^-} = 115\,\mu\text{mol kg}^{-1}\,d^{-1} \tag{27}$$

In a similar manner as for the other kinetic processes, one can derive the influence of the addition of substance X to the system $\mathbf{A}_X$ on the proton change $\frac{d[H^+]}{dt}$, by including $\mathbf{A}_X$ in the MCE's from Table 3.4. Whereas the addition of nitrate has no effect on the pH, the contribution of $\mathbf{A}_{NH_4^+}$ to $\frac{d[H^+]}{dt}$ has the form as given in Eq. (20), and results in

$$-\left(\frac{\partial[TA]}{\partial[\sum NH_4^+]} \Big/ \frac{\partial[TA]}{\partial[H^+]}\right) \cdot \mathbf{A}_{NH_4^+} := \alpha_5 \cdot \mathbf{A}_{NH_4^+} \tag{28}$$

The second row in Fig. 3.3 shows the profiles for pH, [TA], $[\sum CO_2]$ and $[O_2]$ for this scenario. Drastic perturbations in the geochemistry of the estuary are simulated during the 10 days of leakage, and during a small period of about 15 days afterwards. The leakage results in a distinct peak in $[\sum NH_4^+]$ (not shown), with values rising by roughly 620% from 36 μmol kg^{-1} to 260 μmol kg^{-1}. This is accompanied by a peak in $[NO_3^-]$, rising by 130% from 340 μmol kg^{-1} to 778 μmol kg^{-1}, which is due to both the leakage $\mathbf{A}_{NO_3}$ and increased nitrification. Total alkalinity and $[\sum CO_2]$ temporarily drop by 4% and 1% respectively. Oxygen conditions drastically drop from 158 μmol kg^{-1} to hypoxic conditions at 43 μmol kg^{-1}, due to a short period of intense nitrification.

pH levels drop by approximately two tenths of a unit from 7.71 to 7.49. Figure 3.5 shows that this is mainly due to an increase of nitrification, and that the contribution of $\mathbf{A}_{NH_4^+}$ itself is negligible. After 10 days of leakage, dynamic pH equilibrium is almost re-installed, and the proton production of nitrification is compensated by the proton release due to outgassing of CO_2 and from transport. The influence of oxic mineralisation on $\frac{d[H^+]}{dt}$ does not significantly

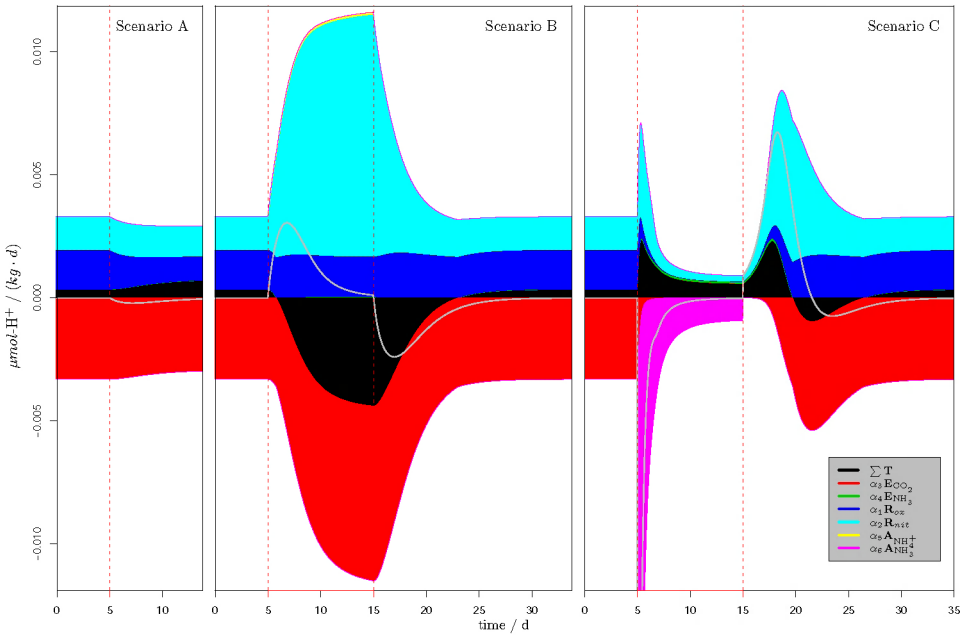

Figure 3.5.: Budget of $\frac{d[H^+]}{dt}$ for the three model scenarios. The gray line indicates the net $\frac{d[H^+]}{dt}$.

change during the spill, compared to the dominant components. After 10 days, the end of the leakage imposes a new perturbation on the system.

3.3.3.3. *Scenario C:* Spill of ammonia

In this sceneario, we investigate a similar ship accident, but now with a spill of ten thousand tons of ammonia (NH_3). The leakage period is identical to the previous case, and the input term for ten thousand tons of ammonia within 10 days becomes

$$\mathbf{A}_{NH_3} = 541\ \mu\text{mol kg}^{-1}\ d^{-1} \tag{29}$$

The contribution of $\mathbf{A}_{NH_3}$ to $\frac{d[H^+]}{dt}$ is

$$\left(\left(1 - \frac{\partial[TA]}{\partial[\sum NH_4^+]}\right) / \frac{\partial[TA]}{\partial[H^+]}\right) \cdot \mathbf{A}_{NH_3} := \alpha_6 \cdot \mathbf{A}_{NH_3} \tag{30}$$

Figure 3.3 shows the profiles for pH, [TA], $[\sum CO_2]$ and $[O_2]$ for this scenario. Again a distinct peak in $[\sum NH_4^+]$ is observed (not shown), with the baseline concentration rising by a factor of 37. This is again accompanied by a 50% increase in $[NO_3^-]$, which is now solely the result of increased nitrification. Total alkalinity and $[\sum CO_2]$ temporarily rise by 20% and 1% respectively. Oxygen concentrations are again greatly reduced (by roughly 97%), now almost

reaching full anoxia with a minimum of 5 μ mol kg^{-1}. The oxic mineralisation rate is much lower than in the baseline-simulation due to low oxygen concentrations.

The pH level increases by more than one pH unit from 7.71 to 8.78. Figure 3.5 shows that this is mainly due to the input of NH_3 into the estuary by the leak. Nitrification initially counters the proton consumption of NH_3 input (via conversion to ammonia), but this effect decreases drastically due to decreasing oxygen levels (cf. the initial steep spike in $\mathbf{R}_{\text{nit}}$ shown in the right panel of Fig. 3.4). The effect of outgassing of ammonia $\mathbf{E}_{NH_3}$ on $\frac{d[H^+]}{dt}$ only becomes important towards the end of the 10 day spill period, when almost steady state conditions are reached. At this point, NH_3 outgassing and subsequent dissociation of ammonium (as the equilibrium state changes due to Le Chatelier's principle) balance, together with the effects of nitrification and advective-dispersive transport, the proton consumption of $\mathbf{A}_{NH_3}$ and subsequent association of ammonium. When the leakage is stopped, the system returns to the pre-leakage state within a matter of 15 days. There is however a dip in pH and alkalinity before baseline values are attained again. Immediately after the leakage stops, there is still a lot of $\sum NH_4^+$ in the system, which is further nitrified. The effects of CO_2 outgassing and advective-dispersive transport (which changes sign again) compensate for the proton production associated with nitrification. However, this compensation occurs with a certain time lag, creating the dip in pH after the initial spike.

The net absolute values of proton consumption or production of all processes decreases during the 10 day spill period due to an increase in the absolute value of the buffering capacity $\frac{\partial[TA]}{\partial[H^+]}$, which changes from $-0.165\ 10^5$ to $-5.15\ 10^5$ (Fig. 3.4). It can be noted that in our modelled pH range the absolute value of $\frac{\partial[TA]}{\partial[H^+]}$ increases with increasing pH. This leads to the conclusion that the higher the pH of the system, the closer to zero the influences of processes on $\frac{d[H^+]}{dt}$.

3.4. Discussion

3.4.1. A consistent framework for pH model generation

The overall result of our work is a general recipe for pH model formulation, consisting of 10 separate steps (Table 3.17), which we clarified by means of an example. We have identified four main solution techniques (FKA, FNA, OSA, DSA), which all enable the solution of the non-steady-state pH problem. These four solution techniques are connected by three consecutive mathematical transformations of the pH problem. Although it requires an initial investment, such a reformulation effort has multiple advantages, both practically, in terms of more efficient simulations, as well as theoretically, in terms of improved physical and chemical insight into the problem.

Along the course of the mathematical reformulations two approximations have been made.

1) To make the transition from the FKA to the FNA (the transformation into the canonical form) the local equilibrium assumption has been applied. As mentioned earlier, this approximation generally has no influence on the results of models of macroscopic systems.

2) To reformulate the system into a form solvable by the DSA, the K^*'s of the system are

assumed constant. This has been done for didactical reasons to keep the mathematical expressions simple. This, however, is no limitation: variable K^*'s can be integrated into the DSA as well.

pH modeling in 10 steps
1 Formulation of the model question.
2 Formulation of the conceptual model.
3 Constraining the model pH range - selection of acid-base reactions.
4 Writing down a MCE for all species whose concentrations are influenced by modeled processes. The system is now solvable with the **full kinetic approach (FKA)**.
5 Partitioning the modeled process into kinetic and equilibrium processes according to their timescales and defining kinetic expressions for kinetic processes.
6 Mathematically closing the system by formulating the mass action laws of the equilibrium processes.
7 Transforming the system into the canonical form: reformulating it into an implicit DAE system without any purely algebraic variables. The system is now solvable with the **full numerical approach (FNA)**.
8 Introducing the equilibrium invariants to convert the differential equations of the DAE into explicit ODEs.
9 Reformulating the algebraic part of the DAE to explicitly express all equilibrium species as functions of $[H^+]$ and equilibrium invariants. The system is now solvable with the **operator splitting approach (OSA)**.
10 Reformulating the system according to the **direct substitution approach (DSA)**: substitute the expression for $\frac{d[TA]}{dt}$ by an expression for $\frac{d[H^+]}{dt}$ to get rid of the AE systems non-linearity in an unknown variable. The expression for $\frac{d[H^+]}{dt}$ can be partitioned such that the influences of modeled kinetic processes onto $\frac{d[H^+]}{dt}$ can be quantified.

Table 3.17.: Summary of our pH modeling approach.

Although these approximations have been made, our four main solution methods are still different mathematical formulations of the same model yielding the same results: both approximations can also be made from the very beginning. The local equilibrium assumption can be included into the FKA (solution method 1b) and the K^*'s can be assumed constant for all approaches. What remains is a chain of mathematical transformations, with no further approximations involved.

scenario	FKA(1b)	FNA	OSA (3a)	OSA (3b)	DSA
baseline simulation	70	63	48	43	43
A	74	69	53	48	48
B	77	72	58	50	50
C	80	74	59	51	52

Table 3.18.: CPU time in miliseconds for one model run of all mentioned solution approaches and scenarios. Values are averages of 1000 runs each. All approaches are integrated with DASSL to be comparable. The model output generated with the five approaches is identical. The FKA is implemented according to solution method 1b. The OSA (3a) has been implemented using the Newton-Raphson root finding procedure. Constant K^*'s are assumed for all approaches. The benchmarking has been done on an Intel Pentium 4 CPU with 3 GHz and 1 GB RAM, running Microsoft Windows XP Professional, Version 2002, SP2. The compiling has been done with Compaq Visual Fortran Professional Edition 6.6.0. Please note that the computational advantage of OSA (3b) and DSA over FKA, FNA and OSA (3b) is expected to me more prominent for more complex systems. However, a detailed theoretical runtime analysis of all methods is beyond the scope of this paper.

As shown in Table 3.18 and in Fig. 3.6, even if the local equilibrium assumption and constant K^*'s are applied to all approaches, there is a clear trade-off between reformulation effort and the numerical resources required. The more the pH problem is initially reformulated, the less computation time is spent on actual pH simulations afterwards. The reformulations transform the pH problem into a more elegant mathematical form, and only require a one-time investment during the model generation process. Accordingly, when doing multiple simulations as in a sensitivity analysis, the initial time investment in reformulation is likely to pay off very rapidly. Although, in terms of computational performance, the improved OSA and the DSA are comparable, the DSA additionally allows for the quantification of the influences of kinetically modelled processes on the pH. These influences are calculated against the background of re-equilibration of the system due to a set of acid-base equilibria.

The DSA approach thus comes out as the most powerful procedure to tackle pH models. However, in a system where the dissociation constants (K^*'s) cannot be assumed constant, the influence of temperature, salinity and pressure on the dissociation constants has to be incorporated into the DSA. This has been deliberately omitted from this paper for didactical reasons.

3.4.2. Comparison with previous approaches

Past pH modeling approaches can be equated to one of the four solution methods in Fig. 3.6. The most basic approach, the Full Kinetic Approach (FKA) has only been implemented sporadically (Steefel and MacQuarrie, 1996; Zeebe, 2007), because of the numerical stiffness of the obtained equation systems (solution method 1a and 1b), and the need to obtain parameters that are not very well constrained (forward and backward rates of acid-base reactions in solution method 1a). After one reformulation step termed the transformation into canon-

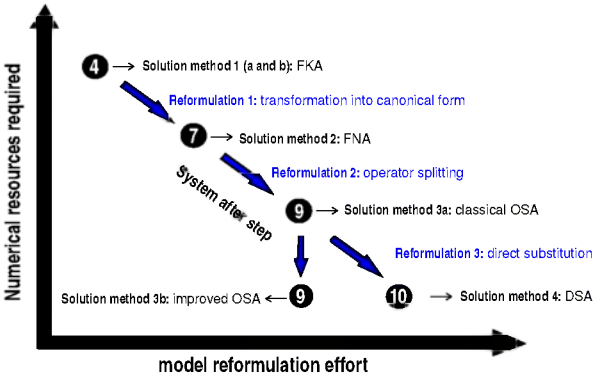

Figure 3.6.: The trade-off between numerical resource requirement and model reformulation effort.

ical form (DiToro, 1976; Lichtner, 1996; Steefel and MacQuarrie, 1996; Chilakapati et al., 1998; Saaltink et al., 1998; Meysman, 2001) based on an idea first put forward by Aris and Mah (1963), one can implement the Full Numerical Approach (FNA), which involves a direct numerical solution of the resulting differential algebraic equation system. Steefel and MacQuarrie (1996) list a number of packages, including DASSL (Petzold, 1982), capable of solving a system according to the FNA. Gehlen et al. (1999) applied this solution technique in a relatively simple pH problem (4 acid-base reactions) to study the distribution of stable carbon isotopes in the pore water of deep sea sediments. We are not aware of FNA applications with realistic "field-type" reaction sets (including 10 or more acid-base reactions). In these situations, FNA simulations are expected to require significant computational resources.

The demanding computations of the FNA can be avoided by means of a second reformulation, via the introduction of equilibrium invariants. This reformulation allows uncoupling the differential and algebraic part of the DAE system and solving them independently. The resulting approach is termed operator splitting (OSA, steps 8 and 9). Regnier et al. (1997) used the OSA to model pH along an estuarine gradient, Marinelli and Boudreau (1996) used it to study the pH in irrigated anoxic coastal sediments, and Follows et al. (1996) used the OSA to investigate the carbonate system in the water column of the North Atlantic. Besides pointing out different varieties of the FNA, Chilakapati et al. (1998) also applied the OSA to simple groundwater problems. While not explicitly reformulating the system, Boudreau (1987), Boudreau and Canfield (1988), Boudreau (1991), Boudreau and Canfield (1993), and Boudreau (1996b) (the CANDI model) used the notion of dividing the reaction set into kinetic reactions and equilibrium reactions. Imposed equilibrium invariants were then used to simulate steady state pH profiles of aquatic sediments. Therefore, these approaches can be viewed as predecessors of the OSA. Although equilibrium invariants were not explicitly defined, Wang and VanCappellen (1996) (the STEADYSED1 model) uncoupled the DE and the AE part of the DAE system and solved them separately, making their approach a quasi OSA. In a detailed methodological study on pH modeling, Luff et al. (2001) examined different variations of the OSA: three different possibilities for the algebraic equation part of the DAE system were introduced.

As noted above, there are two major disadvantages associated with the classical OSA approach (1) the equilibration step requires a numerical solution, which makes the OSA computationally intense, and (2) the OSA does not allow quantifying the influence of different processes on $\frac{d[H^+]}{dt}$. The numerical solution step can be eliminated using the improved OSA put forward by Follows et al. (2006), but it still lacks the possibility of assessing influences of kinetically modelled processes on the pH.

The two problems of the OSA vanish after a third reformulation, which leads to the Direct Substitution Approach (DSA). Therefore, we consider the DSA approach to be the most elegant and promising pH modeling procedure, especially if knowledge of the influences of modelled processes on the pH is desired. If this knowledge is not desired, the improved OSA according to Follows et al. (2006) might be the method of choice, since the third reformulation of the system (step 10) is not necessary. In the DSA, the differential equation for total alkalinity is replaced by a differential equation for the proton concentration, which enables a direct analytical solution of the equilibration step. The most important advantage is that the change in $[H^+]$ can be partitioned into contributions by different processes, and hence, the influence of processes on pH can be directly assessed (as discussed further below).

Although applying the DSA, Meysman et al. (2003) (the MEDIA modelling environment) did not make use of its capability of assessing influences of processes on the pH.

In recent years two other studies have employed DSA-like approaches to assess influences of processes on the pH. Yet the way these methods were derived is not fully clear as the presentations are prone to internal inconsistencies.

The approach of Jourabchi et al. (2005) is situated somewhere between the DSA and the FNA. As a by-product in calculating stoichiometric coefficients for equilibrium species, Jourabchi et al. (2005) calculated a rate of change of protons over time for a given modelled process, starting from the total derivative of total alkalinity. However, these rates do not add up to a total rate of change since the effect of transport is not made explicit. Direct proton transport is even omitted as they remove the mass conservation equation for protons to cope with an overdetermined equation system, which introduces an error. Their equation system was subsequently solved with a numerical solver that depended on steady state conditions of the system. This means dynamic pH simulations are not possible. Total quantities like total alkalinity were imposed and not consistently derived. Subsequently, [TA] was used in a way that in some points contradicted Dickson's (Dickson, 1981) notion of [TA].

Soetaert et al. (2007) also made a step towards a DSA, but fell short of deriving a total rate of change of protons. They needed to invoke several ad-hoc assumptions and concepts like the mean and total charge of postulated total quantities to arrive at formulae for the influence of modeled processes on the pH. These formulae did not add up to a total rate of change of protons over time, because no transport terms were included. This means that modeling the pH of a real system containing several processes at the same time was not possible.

3.4.3. Implicit assumptions

The subsequent reformulations of the system (Fig. 3.6) yield more insight into the physical, chemical, and mathematical structure of the pH problem. By delineating all steps of the model generation process explicitly, one achieves a high level of model transparency. Typically, past treatments do not explicitly list all assumptions and decisions made during the model generation process. This practice has led to the introduction of unnecessary assumptions and constraints, as well as inconsistently employed concepts.

A first difference between our approach and past treatments is that we do not need an a priori definition of alkalinity. In other words, in our treatment, the way alkalinity is defined in terms of the other chemical species follows directly from the model reformulation. As shown above, alkalinity is one of the equilibrium invariants (like total inorganic carbon and total ammonium). These equilibrium invariants emerge after the transformation of the pH problem into the canonical form and are equivalent to the mole balance equations of Morel's *components* (Morel and Hering, 1993) as well as to DiToro's *reaction invariants* (DiToro, 1976) of the system. Similar quantities appear in Boudreau (1987), Boudreau and Canfield (1988), Boudreau (1991), and Boudreau and Canfield (1993). Equilibrium invariants, and hence alkalinity, are quantities that are conservative with respect to equilibrium reactions. The exact form of alkalinity depends on the chosen set of equilibrium reactions, and hence, it is dependent on the chosen pH range of the model and the chosen time scale of the model. This practice ensures (1) consistency between the definition of total alkalinity and the model, and (2) the correct stoichiometric coefficients in the MCE for total alkalinity (cf. Eq. (6) in Table 3.12).

A second difference is that we do not need the assumption of electroneutrality. Approaches like e.g. Luff's (Luff et al., 2001) charge balance approach, or the CANDI model (Boudreau, 1996b) implicitly assume electroneutrality of the solution. They use a measure of total charge (including conservative ions like Na^+), which is assumed to be zero, to close their equation systems[5]. Although sometimes wrongly termed so (e.g. Boudreau, 1991; Follows et al., 1996, 2006), total alkalinity is not a charge balance, but a proton balance. It expresses the excess of proton equivalents (protons and proton donors) to proton acceptors (Dickson, 1981; Wolf-Gladrow et al., 2007). This means that if, for example, NO_3^- is assumed not to react with H^+ in the pH range that is modelled, the concentration of nitrate does not have any influence on total alkalinity, although it is an integral part of the total charge balance of the solution. By consistently using total alkalinity instead of a charge balance, concentrations of conservative ions do not enter the pH calculation.

Furthermore, as mentioned above, our approach directly provides the stoichiometric coefficients for total alkalinity for all kinetic processes. Although these coefficients are not obvious from the definition of [TA], as all component concentrations are influenced by equilibrium reactions, our model generation procedure unambiguously provides them. To this end, a reformulation of the expression of [TA] into the "explicit conservative total alkalinity", which

[5] Similar to our approach, the approach put forward by Soetaert et al. (2007) does not depend on the electroneutrality of the solution, although the names of the quantities they use suggest so. They sometimes require "electroneutrality" of both sides of a reaction equation, but this is not the same as electroneutrality of the solution and should be better termed "reactional charge conservation".

requires electroneutrality of the solution, as put forward by Wolf-Gladrow et al. (2007), is not needed.

3.4.4. Assessing the influence of processes on pH

In a system that contains slow kinetic processes (slow kinetic biogeochemical reactions, but also transport) and fast equilibrium processes, the independent drivers of the system, that means the factors that determine the temporal evolution of the state of the system, are only the slow kinetic processes. When adopting local equilibrium, the net rates of the equilibrium processes become dependent on the rates of the kinetic processes.

Therefore it is of interest to assess the influences of the slow kinetic processes on the pH. To do so, one needs an explicit formulation for $\frac{d[\mathrm{H}^+]}{dt}$ which can be partitioned into explicit contributions by each of these different slow kinetic processes.

Two of our main solution approaches provide an explicit formulation for $\frac{d[\mathrm{H}^+]}{dt}$: the FKA and the DSA. However, the formulation for $\frac{d[\mathrm{H}^+]}{dt}$ as obtained by the FKA contains terms contributed by equilibrium reactions. These equilibrium terms implicitly contain the influences of all slow kinetic processes that influence the reactants and products of the equilibrium reaction in question. Therefore, the formulation for $\frac{d[\mathrm{H}^+]}{dt}$ as obtained by the FKA cannot be partitioned into explicit separate terms for the influences of all slow kinetic processes on the pH.

Exactly there lies the most important advantage of the DSA method as it provides an explicit partitioning of the formulation for $\frac{d[\mathrm{H}^+]}{dt}$ into the influences of all slow kinetic processes on the pH against the background of buffering by an equilibrium reaction system.

Unlike Soetaert et al. (2007) and Jourabchi et al. (2005), in our DSA we obtain an explicit formulation for the contribution of all kinetic processes to $\frac{d[\mathrm{H}^+]}{dt}$, including transport. This enables a deeper understanding of how pH steady state is attained, and what processes exactly are responsible for a pH change upon disturbance of the system. This is clearly illustrated in our disturbance scenarios for a simple estuarine system.

Furthermore, the buffering capacity of the solution $\frac{\partial[\mathrm{TA}]}{\partial[\mathrm{H}^+]}$ is identified as an important and central quantity, as it modulates the influence of all processes on the pH. A process with the same rate, can have a different influence on the pH depending on the state of the system, as represented by $\frac{\partial[\mathrm{TA}]}{\partial[\mathrm{H}^+]}$. Our disturbance scenario C shows that it is possible that in certain circumstances, although process rates increase, the absolute values of influences of processes on $\frac{d[\mathrm{H}^+]}{dt}$ can decrease, since the absolute value of $\frac{\partial[\mathrm{TA}]}{\partial[\mathrm{H}^+]}$ increases due to an increased pH. Figuratively this can be explained by the fact that a higher pH means less free protons in solution. Therefore, the amount of protons affected by a certain process is decreased. $\frac{\partial[\mathrm{TA}]}{\partial[\mathrm{H}^+]}$ is a measure for this condition.

3.5. Conclusions

In the present paper, we systematically and consistently derived a succession of methods to model pH, making every step of the model generation process explicit. The chemical structure of the model was used for sucessive reformulations until fast and elegant numerical solutions were possible. Existing pH modelling approaches were identified within this framework and advantages and drawbacks were pointed out. Definitions for summed quantities and the influence of all modelled processes on them where derived from the model. With the DSA the influence of modelled kinetic processes on the pH can be quantified.

3.6. Appendix

3.6.1. Criterion for exclusion of acid-base reactions

To decide whether or not a certain acid-base reaction will be included in the model, we calculate a quantity ϵ for every acid-base dissociation step. Polyprotic acids are treated as a set of monoprotic acids, considering each dissociation step independently. The total concentration $[\sum \mathrm{A}]$ considered for each dissociation step is assumed equal to the total concentration of the polyprotic acid (For example, for both dissociation steps of CO_2 in seawater, the total concentration is assumed to be $[\sum \mathrm{CO_2}]$). Since this overestimates the error, it is a conservative practice. The quantity ϵ represents the amount of protons δ (concentration offset) ignored by neglecting the reaction in question, in percent of the average [TA] of the modeled system.

$$\epsilon = (\delta/[\mathrm{TA}]) \cdot 100 \tag{31}$$

Reactions with an ϵ value below the desired error threshold percentage ν can be neglected.

Consider the acid in question to be HA with pK^*_A and a total concentation of $[\sum \mathrm{A}]$. Consider further a designated pH range of $\mathrm{pH_{low}} \leq \mathrm{pH} \leq \mathrm{pH_{up}}$. To calculate δ, we distinguish three cases (Fig. 3.7)

1) $\mathrm{pH}_{low} < \mathrm{pK}^*_\mathrm{A} < \mathrm{pH_{up}}$: Neglecting the dissociation reaction in this case means not including any species of the respective acid-base system in the model. δ can be as high as the total concentration of the acid:

$$\delta = [\sum \mathrm{A}] \tag{32}$$

2) $\mathrm{pK}^*_\mathrm{A} \leq \mathrm{pH_{low}}$: Neglecting the dissociation reaction in this case means that the acid is assumed to be fully dissociated. δ can be as high as the concentration of the undissociated form of the acid at the lower boundary of the pH range $[\mathrm{HA}]_\mathrm{low}$. One can estimate an upper limit for $[\mathrm{HA}]_\mathrm{low}$:

$$\delta = 10^{(\mathrm{pK}^*_\mathrm{A} - \mathrm{pH_{low}})} \cdot [\sum \mathrm{A}] \geq [\mathrm{HA}]_\mathrm{low} \tag{33}$$

3) $\mathrm{pH_{up}} \leq \mathrm{pK}^*_\mathrm{A}$: Neglecting the dissociation reaction in this case means that the acid is assumed to be fully undissociated. δ can be as high as the concentration of the corresponding base at the upper boundary of the pH range $[\mathrm{A}^-]_\mathrm{up}$. One can estimate an upper limit for $[\mathrm{A}^-]_\mathrm{up}$:

$$\delta = 10^{(\mathrm{pH_{up}} - \mathrm{pK}^*_\mathrm{A})} \cdot [\sum \mathrm{A}] \geq [\mathrm{A}^-]_\mathrm{up} \tag{34}$$

ϵ values for our reactions, model pH range and [TA] are given in Table 3.2.

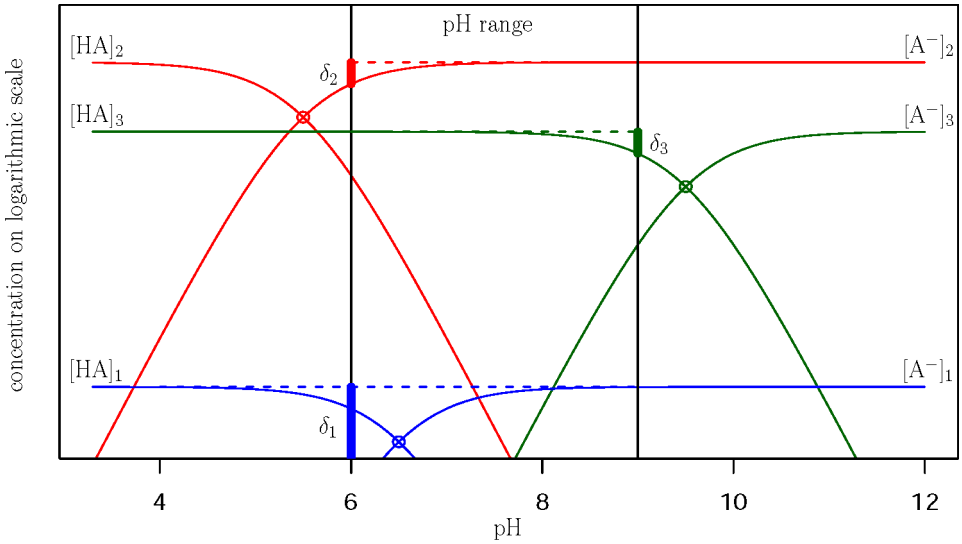

Figure 3.7.: Bjerrum plot for three different cases to calculate δ for acid-base dissociation reactions. Locations of pK^*_A are indicated with circles.

3.6.2. Transformation into canonical form

Having partitioned the processes into n_{kp} kinetic and n_{ep} equilibrium processes, the mass-balance Eq. (1), can be written in matrix notation for all n_{es} equilibrium species

$$\mathbf{I} \times \frac{d[C]}{dt} = \vec{\nu}_{\text{kin}} \times \vec{R}_{\text{kin}} + \vec{\nu}_{\text{eq}} \times \vec{R}_{\text{eq}} \tag{35}$$

where $\mathbf{I}$ is the $n_{es} \times n_{es}$ identity matrix, $\frac{d[C]}{dt}$ is a vector with time derivatives of all n_{es} species, $\vec{\nu}_{\text{eq}}$ is the $n_{ep} \times n_{es}$ stoichiometric matrix for the equilibrium reactions, $\vec{\nu}_{\text{kin}}$ is the $n_{kp} \times n_{es}$ stoichiometric matrix for the influence of the kinetic reactions on the equilibrium species, $\vec{R}_{\text{kin}}$ is the vector of the kinetic reactions, and $\vec{R}_{\text{eq}}$ is the vector of the equilibrium reactions.

The goal is to find a linear transformation $\mathbf{P}$ such that

$$\mathbf{P} \times \frac{d[C]}{dt} = \mathbf{P} \times \vec{\nu}_{\text{kin}} \times \vec{R}_{\text{kin}} + \mathbf{P} \times \vec{\nu}_{\text{eq}} \times \vec{R}_{\text{eq}} \tag{36}$$

$\mathbf{P}$ can be constructed by performing a Gauss-Jordan elimination applied to the matrix $\vec{\nu}_{\text{eq}}$ (By adequate selection of the row operations during the Gauss-Jordan elimination, a subset of Dickson's total alkalinity (Dickson, 1981) as well as a subset of any other desired similar quantity like Soetaert's "sum of excess negative charges" (Soetaert et al., 2007) can be obtained as an equilibrium invariant).

The result of this operation is the *reduced row-echelon* form of $\vec{\nu}_{\text{eq}}$, which is also known as the *row canonical form*. Equation (37) gives $\mathbf{P}$, $\vec{\nu}_{\text{eq}}$ and the reduced row-echelon form of $\vec{\nu}_{\text{eq}}$ of our system.

$$\mathbf{P} \times \vec{\nu}_{\text{eq}} = \begin{pmatrix} 0 & 1 & 1 & 0 & 0 & 0 \\ 0 & 0 & 1 & 0 & 0 & 0 \\ 0 & 0 & 0 & 0 & 1 & 0 \\ 1 & 1 & 1 & 0 & 0 & 0 \\ 0 & 0 & 0 & 1 & 1 & 0 \\ 0 & 1 & 2 & 0 & 1 & -1 \end{pmatrix} \times \begin{pmatrix} -1 & 0 & 0 \\ 1 & -1 & 0 \\ 0 & 1 & 0 \\ 0 & 0 & -1 \\ 0 & 0 & 1 \\ 1 & 1 & 1 \end{pmatrix} = \begin{pmatrix} 1 & 0 & 0 \\ 0 & 1 & 0 \\ 0 & 0 & 1 \\ 0 & 0 & 0 \\ 0 & 0 & 0 \\ 0 & 0 & 0 \end{pmatrix} \tag{37}$$

Expanding Eq. (36) and plugging in P leads to:

$$\begin{pmatrix} 0 & 1 & 1 & 0 & 0 & 0 \\ 0 & 0 & 1 & 0 & 0 & 0 \\ 0 & 0 & 0 & 0 & 1 & 0 \\ 1 & 1 & 1 & 0 & 0 & 0 \\ 0 & 0 & 0 & 1 & 1 & 0 \\ 0 & 1 & 2 & 0 & 1 & -1 \end{pmatrix} \times \begin{pmatrix} \frac{d[\mathrm{CO_2}]}{dt} \\ \frac{d[\mathrm{HCO_3^-}]}{dt} \\ \frac{d[\mathrm{CO_3^{2-}}]}{dt} \\ \frac{d[\mathrm{NH_4^+}]}{dt} \\ \frac{d[\mathrm{NH_3}]}{dt} \\ \frac{d[\mathrm{H^+}]}{dt} \end{pmatrix} = \tag{38}$$

$$\begin{pmatrix} 0 & 1 & 1 & 0 & 0 & 0 \\ 0 & 0 & 1 & 0 & 0 & 0 \\ 0 & 0 & 0 & 0 & 1 & 0 \\ 1 & 1 & 1 & 0 & 0 & 0 \\ 0 & 0 & 0 & 1 & 1 & 0 \\ 0 & 1 & 2 & 0 & 1 & -1 \end{pmatrix} \times \begin{pmatrix} 1 & 0 & 0 & 0 & 0 & 0 & \gamma & 0 & 1 & 0 \\ 0 & 1 & 0 & 0 & 0 & 0 & 0 & 0 & 0 & 0 \\ 0 & 0 & 1 & 0 & 0 & 0 & 0 & 0 & 0 & 0 \\ 0 & 0 & 0 & 1 & 0 & 0 & 0 & 0 & 0 & 0 \\ 0 & 0 & 0 & 0 & 1 & 0 & 1 & -1 & 0 & 1 \\ 0 & 0 & 0 & 0 & 0 & 1 & 0 & 1 & 0 & 0 \end{pmatrix} \times \begin{pmatrix} \mathbf{T}_{\mathrm{CO_2}} \\ \mathbf{T}_{\mathrm{HCO_3^-}} \\ \mathbf{T}_{\mathrm{CO_3^{2-}}} \\ \mathbf{T}_{\mathrm{NH_4^+}} \\ \mathbf{T}_{\mathrm{NH_3}} \\ \mathbf{T}_{\mathrm{H^+}} \\ \mathbf{R}_{\mathrm{ox}} \\ \mathbf{R}_{\mathrm{nit}} \\ \mathbf{E}_{\mathrm{CO_2}} \\ \mathbf{E}_{\mathrm{NH_3}} \end{pmatrix} + \begin{pmatrix} 1 & 0 & 0 \\ 0 & 1 & 0 \\ 0 & 0 & 1 \\ 0 & 0 & 0 \\ 0 & 0 & 0 \\ 0 & 0 & 0 \end{pmatrix} \times \begin{pmatrix} \mathbf{R}^{\mathrm{dis}}_{\mathrm{CO_2}} \\ \mathbf{R}^{\mathrm{dis}}_{\mathrm{HCO_3^-}} \\ \mathbf{R}^{\mathrm{dis}}_{\mathrm{NH_4^+}} \end{pmatrix}$$

$$= \begin{pmatrix} 0 & 1 & 1 & 0 & 0 & 0 & 0 & 0 & 0 & 0 \\ 0 & 0 & 1 & 0 & 0 & 0 & 0 & 0 & 0 & 0 \\ 0 & 0 & 0 & 0 & 1 & 0 & 1 & -1 & 0 & 1 \\ 1 & 1 & 1 & 0 & 0 & 0 & \gamma & 0 & 1 & 0 \\ 0 & 0 & 0 & 1 & 1 & 0 & 1 & -1 & 0 & 1 \\ 0 & 1 & 2 & 0 & 1 & -1 & 1 & -2 & 0 & 1 \end{pmatrix} \times \begin{pmatrix} \mathbf{T}_{\mathrm{CO_2}} \\ \mathbf{T}_{\mathrm{HCO_3^-}} \\ \mathbf{T}_{\mathrm{CO_3^{2-}}} \\ \mathbf{T}_{\mathrm{NH_4^+}} \\ \mathbf{T}_{\mathrm{NH_3}} \\ \mathbf{T}_{\mathrm{H^+}} \\ \mathbf{R}_{\mathrm{ox}} \\ \mathbf{R}_{\mathrm{nit}} \\ \mathbf{E}_{\mathrm{CO_2}} \\ \mathbf{E}_{\mathrm{NH_3}} \end{pmatrix} + \begin{pmatrix} 1 & 0 & 0 \\ 0 & 1 & 0 \\ 0 & 0 & 1 \\ 0 & 0 & 0 \\ 0 & 0 & 0 \\ 0 & 0 & 0 \end{pmatrix} \times \begin{pmatrix} \mathbf{R}^{\mathrm{dis}}_{\mathrm{CO_2}} \\ \mathbf{R}^{\mathrm{dis}}_{\mathrm{HCO_3^-}} \\ \mathbf{R}^{\mathrm{dis}}_{\mathrm{NH_4^+}} \end{pmatrix}$$

Expanding further and solving the first three equations for the equilibrium reaction rates results in the equation system:

$$\begin{aligned} \mathbf{R}^{\mathrm{dis}}_{\mathrm{CO_2}} &= \frac{d[\mathrm{HCO_3^-}]}{dt} + \frac{d[\mathrm{CO_3^{2-}}]}{dt} - \mathbf{T}_{\mathrm{HCO_3^-}} - \mathbf{T}_{\mathrm{CO_3^{2-}}} \\ \mathbf{R}^{\mathrm{dis}}_{\mathrm{HCO_3^-}} &= \frac{d[\mathrm{CO_3^{2-}}]}{dt} - \mathbf{T}_{\mathrm{CO_3^{2-}}} \\ \mathbf{R}^{\mathrm{dis}}_{\mathrm{NH_4^+}} &= \frac{d[\mathrm{NH_3}]}{dt} - \mathbf{T}_{\mathrm{NH_3}} - \mathbf{R}_{\mathrm{ox}} + \mathbf{R}_{\mathrm{nit}} - \mathbf{E}_{\mathrm{NH_3}} \\ \frac{d[\mathrm{CO_2}]}{dt} + \frac{d[\mathrm{CO_3^{2-}}]}{dt} + \frac{d[\mathrm{HCO_3^-}]}{dt} &= \mathbf{T}_{\mathrm{CO_2}} + \mathbf{T}_{\mathrm{HCO_3^-}} + \mathbf{T}_{\mathrm{CO_3^{2-}}} + \gamma\mathbf{R}_{\mathrm{ox}} + \mathbf{E}_{\mathrm{CO_2}} \\ \frac{d[\mathrm{NH_4^+}]}{dt} + \frac{d[\mathrm{NH_3}]}{dt} &= \mathbf{R}_{\mathrm{ox}} - \mathbf{R}_{\mathrm{nit}} + \mathbf{E}_{\mathrm{NH_3}} \\ \frac{d[\mathrm{HCO_3^-}]}{dt} + 2\,\frac{d[\mathrm{CO_3^{2-}}]}{dt} + \frac{d[\mathrm{NH_3}]}{dt} - \frac{d[\mathrm{H^+}]}{dt} &= \mathbf{T}_{\mathrm{HCO_3^-}} + 2\mathbf{T}_{\mathrm{CO_3^{2-}}} + \mathbf{T}_{\mathrm{NH_3}} - \mathbf{T}_{\mathrm{H^+}} + \mathbf{R}_{\mathrm{ox}} \\ &\quad - 2\mathbf{R}^{\mathrm{nit}} + \mathbf{E}_{\mathrm{NH_3}} \end{aligned}$$

This system is a replacement for the e_s differential MCE's of the equilibrium species as given in Table 3.4. The first three equations can be removed reducing both the number of unknowns and the number of equations. The removed equations can be used to calculate the unknown net equilibrium reaction rates $\mathbf{R}^{\text{dis}}_{CO_2}$, $\mathbf{R}^{\text{dis}}_{HCO_3^-}$, and $\mathbf{R}^{\text{dis}}_{NH_4^+}$ as output variables of the model.

3.6.3. Reformulation of the AE system

The algebraic equations of the DAE system including the substituted equilibrium invariants reads:

$$
\begin{aligned}
0 &= [H^+][HCO_3^-] - K^*_{CO_2}[CO_2] && (39)\\
0 &= [H^+][CO_3^{2-}] - K^*_{HCO_3^-}[HCO_3^-] && (40)\\
0 &= [H^+][NH_3] - K^*_{NH_4^+}[NH_4^+] && (41)\\
[\textstyle\sum CO_2] &= [CO_2] + [HCO_3^-] + [CO_3^{2-}] && (42)\\
[\textstyle\sum NH_4^+]f &= [NH_3] + [NH_4^+] && (43)\\
[TA] &= [HCO_3^-] + 2[CO_3^{2-}] + [NH_3] - [H^+] && (44)
\end{aligned}
$$

We can solve Eqs. (39) to (41) for concentrations of equilibrium species to obtain:

$$
\begin{aligned}
[HCO_3^-] &= \frac{K^*_{CO_2}[CO_2]}{[H^+]} && (45)\\
[CO_2] &= \frac{[H^+][HCO_3^-]}{K^*_{HCO_3^-}} && (46)\\
[CO_3^{2-}] &= \frac{K^*_{HCO_3^-}[HCO_3^-]}{[H^+]} && (47)\\
[HCO_3^-] &= \frac{[H^+][CO_3^{2-}]}{K^*_{HCO_3^-}} && (48)\\
[NH_3] &= \frac{K^*_{NH_4^+}[NH_4^+]}{[H^+]} && (49)\\
[NH_4^+] &= \frac{[H^+][NH_3]}{K^*_{NH_4^+}} && (50)
\end{aligned}
$$

Adding up Eqs. (45), (46) and (47), as well as (49) and (50) yields:

$$
\begin{aligned}
[\textstyle\sum CO_2] &= \frac{K^*_{CO_2}[CO_2]}{[H^+]} + \frac{[H^+][HCO_3^-]}{K^*_{HCO_3^-}} + \frac{K^*_{HCO_3^-}[HCO_3^-]}{[H^+]} && (51)\\
[\textstyle\sum NH_4^+] &= \frac{K^*_{NH_4^+}[NH_4^+]}{[H^+]} + \frac{[H^+][NH_3]}{K^*_{NH_4^+}} && (52)
\end{aligned}
$$

Plugging Eq. (45) into (52) and solving for $[CO_2]$, plugging Eq. (46) into (52) and solving for $[HCO_3^-]$, plugging first (46) and then (48) into (52) and solving for $[CO_3^{2-}]$, plugging (49) into (52) and solving for $[NH_4^+]$, plugging (50) into (52) and solving for $[NH_3]$ results in the reformulated form of the algebraic equation system as given in Table 3.12.

3.6.4. Additional formulae

3.6.4.1. Analytical partial derivatives in Eq. (18)

Analytically deriving the equations in Table 3.12, the equations in Table 3.19 can be obtained.

$$\left.\frac{\partial[\mathrm{TA}]}{\partial[\sum \mathrm{CO_2}]}\right|_{h,n} = \frac{K^*_{\mathrm{CO_2}}[\mathrm{H^+}]}{[\mathrm{H^+}]^2 + K^*_{\mathrm{CO_2}}[\mathrm{H^+}] + K^*_{\mathrm{CO_2}}K^*_{\mathrm{HCO_3^-}}} + 2\left(\frac{K^*_{\mathrm{CO_2}}K^*_{\mathrm{HCO_3^-}}}{[\mathrm{H^+}]^2 + K^*_{\mathrm{CO_2}}[\mathrm{H^+}] + K^*_{\mathrm{CO_2}}K^*_{\mathrm{HCO_3^-}}}\right)$$

$$\left.\frac{\partial[\mathrm{TA}]}{\partial[\sum \mathrm{NH_4^+}]}\right|_{h,c} = \frac{K^*_{\mathrm{NH_4^+}}}{[\mathrm{H^+}] + K^*_{\mathrm{NH_4^+}}}$$

$$\left.\frac{\partial[\mathrm{TA}]}{\partial[\mathrm{H^+}]}\right|_{c,n} = \frac{\partial[\mathrm{HCO_3^-}]}{\partial[\mathrm{H^+}]} + 2\frac{\partial[\mathrm{CO_3^{2-}}]}{\partial[\mathrm{H^+}]} + \frac{\partial[\mathrm{NH_3}]}{\partial[\mathrm{H^+}]} - \frac{\partial[\mathrm{H^+}]}{\partial[\mathrm{H^+}]}$$

$$\frac{\partial[\mathrm{HCO_3^-}]}{\partial[\mathrm{H^+}]} = \left(\frac{K^*_{\mathrm{CO_2}}}{[\mathrm{H^+}]\mathrm{K}^*_{\mathrm{CO_2}} + \mathrm{K}^*_{\mathrm{CO_2}}\mathrm{K}^*_{\mathrm{HCO_3^-}} + [\mathrm{H^+}]^2} - \frac{[\mathrm{H^+}]\mathrm{K}^*_{\mathrm{CO_2}}\left(2[\mathrm{H^+}] + \mathrm{K}^*_{\mathrm{CO_2}}\right)}{\left([\mathrm{H^+}]\mathrm{K}^*_{\mathrm{CO_2}} + \mathrm{K}^*_{\mathrm{CO_2}}\mathrm{K}^*_{\mathrm{HCO_3^-}} + [\mathrm{H^+}]^2\right)^2}\right)[\textstyle\sum \mathrm{CO_2}]$$

$$\frac{\partial[\mathrm{CO_3^{2-}}]}{\partial[\mathrm{H^+}]} = -\frac{K^*_{\mathrm{CO_2}}K^*_{\mathrm{HCO_3^-}}\left(2[\mathrm{H^+}] + \mathrm{K}^*_{\mathrm{CO_2}}\right)}{\left([\mathrm{H^+}]\mathrm{K}^*_{\mathrm{CO_2}} + \mathrm{K}^*_{\mathrm{CO_2}}\mathrm{K}^*_{\mathrm{HCO_3^-}} + [\mathrm{H^+}]^2\right)^2}[\textstyle\sum \mathrm{CO_2}]$$

$$\frac{\partial[\mathrm{NH_3}]}{\partial[\mathrm{H^+}]} = -\frac{K^*_{\mathrm{NH_4^+}}}{[\mathrm{H^+}]^2 + 2[\mathrm{H^+}]K^*_{\mathrm{NH_4^+}} + (K^*_{\mathrm{NH_4^+}})^2}[\textstyle\sum \mathrm{NH_4^+}]$$

$$\frac{\partial[\mathrm{H^+}]}{\partial[\mathrm{H^+}]} = 1$$

Table 3.19.: Analytical partial derivatives in Eq. (18).

3.6.4.2. Coefficients for the rearrangement of the equation for $\frac{d[\mathrm{H^+}]}{dt}$ (Eq. 19)

$$\alpha_{\mathbf{R}_{\mathrm{ox}}}\left.\frac{\partial[\mathrm{TA}]}{\partial[\mathrm{H^+}]}\right|_{c,n} = \beta_{\mathbf{R}_{\mathrm{ox}}} = 1 - \left(\gamma\left.\frac{\partial[\mathrm{TA}]}{\partial[\sum \mathrm{CO_2}]}\right|_{h,n} + \left.\frac{\partial[\mathrm{TA}]}{\partial[\sum \mathrm{NH_4^+}]}\right|_{h,c}\right)$$

$$\alpha_{\mathbf{R}_{\mathrm{nit}}}\left.\frac{\partial[\mathrm{TA}]}{\partial[\mathrm{H^+}]}\right|_{c,n} = \beta_{\mathbf{R}_{\mathrm{nit}}} = -2 + \left.\frac{\partial[\mathrm{TA}]}{\partial[\sum \mathrm{NH_4^+}]}\right|_{h,c}$$

$$\alpha_{\mathbf{E}_{\mathrm{CO_2}}}\left.\frac{\partial[\mathrm{TA}]}{\partial[\mathrm{H^+}]}\right|_{c,n} = \beta_{\mathbf{E}_{\mathrm{CO_2}}} = -\left.\frac{\partial[\mathrm{TA}]}{\partial[\sum \mathrm{CO_2}]}\right|_{h,n}$$

$$\alpha_{\mathbf{E}_{\mathrm{NH_3}}}\left.\frac{\partial[\mathrm{TA}]}{\partial[\mathrm{H^+}]}\right|_{c,n} = \beta_{\mathbf{E}_{\mathrm{NH_3}}} = 1 - \left.\frac{\partial[\mathrm{TA}]}{\partial[\sum \mathrm{NH_4^+}]}\right|_{h,c}$$

$$\sum \mathbf{T}\left.\frac{\partial[\mathrm{TA}]}{\partial[\mathrm{H^+}]}\right|_{c,n} = +\left(\mathbf{Tr}_{\mathrm{HCO_3^-}} + 2\,\mathbf{Tr}_{\mathrm{CO_3^{2-}}} + \mathbf{Tr}_{\mathrm{NH_3}} - \mathbf{Tr}_{\mathrm{H^+}}\right) - \left(\mathbf{Tr}_{\mathrm{CO_2}} + \mathbf{Tr}_{\mathrm{HCO_3^-}} + \mathbf{Tr}_{\mathrm{CO_3^{2-}}}\right)\left.\frac{\partial[\mathrm{TA}]}{\partial[\sum \mathrm{CO_2}]}\right|_{h,n} - \left(\mathbf{Tr}_{\mathrm{NH_3}} + \mathbf{Tr}_{\mathrm{NH_4^+}}\right)\left.\frac{\partial[\mathrm{TA}]}{\partial[\sum \mathrm{NH_4^+}]}\right|_{h,c}$$

Table 3.20.: Coefficients for the partitioning of $\frac{d[H^+]}{dt}$ into contributions by modeled kinetic processes.

Table 3.20 gives the coefficients for the partitioning of Eq. (19) into contributions by different kinetically modelled processes.

4. Factors governing the pH in a heterotrophic, turbid, tidal estuary

A. F. Hofmann, F. J. R. Meysman, K. Soetaert, and J. J. Middelburg
(Biogeosciences Discussion, 6, 197-240, 2009)

Abstract

A method to quantify the influence of kinetically modelled biogeochemical processes on the pH of an ecosystem with time variable acid-base dissociation constants is presented and applied to the heterotrophic, turbid Scheldt estuary (SW Netherlands, N Belgium). Nitrification is identified as the main process governing the pH profile of this estuary, while CO_2 degassing and advective-dispersive transport "buffer" the effect of nitrification. CO_2 degassing accounts for the largest proton turnover per year in the whole estuary. There is a clear inverse correlation between oxygen turnover and proton turnover. The main driver of long-term changes in the mean estuarine pH from 2001 to 2004 is a changing freshwater flow which influences the pH "directly" via $[\sum CO_2]$ and [TA] and to a significant amount also "indirectly" via $[\sum NH_4^+]$ and the nitrification rates in the estuary.

4.1. Introduction

The pH is often considered a master variable to monitor the chemical state of a natural body of water, since almost any process affects the pH either directly or indirectly (e.g. Stumm and Morgan, 1996; Morel and Hering, 1993). This textbook knowledge has rarely been applied in studies of natural ecosystems due to limited understanding of the complex interplay of factors controlling the pH of natural waters. While current approaches do allow for modelling the pH of complex ecosystems (e.g. Boudreau and Canfield, 1988; Regnier et al., 1997; Vanderborght et al., 2002), (Hofmann et al., 2008c, , i.e., Chapter 2), the influences and relative importances of the different physical and biological processes on the pH in those systems remain unquantified.

Especially considering the acidification of the ocean (e.g. Orr et al., 2005) and coastal seas (e.g. Blackford and Gilbert, 2007) and potential impacts of pH changes on biogeochemical processes and organisms (e.g. Gazeau et al., 2007; Guinotte and Fabry, 2008), it is desirable to obtain a better quantitative understanding of factors controlling the pH in natural aquatic systems.

Estuarine ecosystems are suitable testbeds for methods quantifying the influences of especially biological processes on the pH due to their role as bio-reactors (Soetaert et al., 2006) and associated large biological influences on the pH. Mook and Koene (1975) suggested that the characteristic pH profile observed in estuaries simply results from chemical equilibration following the mixing of freshwater and seawater. They stated that, due to the rapid increase of the dissociation constants of the carbonate system with salinity, estuaries like the Scheldt estuary (SW Netherlands and N Belgium), with high river inorganic carbon loadings and associated low riverine pH, exhibit a distinct pH minimum at low salinities. However, Mook and Koene (1975) assumed a closed system and conservative mixing of total dissolved inorganic carbon ($[\sum CO_2]$) and total alkalinity ($[TA]$), i.e. they were neither considering carbon dioxide exchange with the atmosphere nor processes changing total alkalinity. Although Wong (1979) obtained reasonable agreement applying this approach to measurements in the Chesapeake Bay and it is still used to predict estuarine pH profiles (Spiteri et al., 2008), it is a rather crude approximation of reality. Whitfield and Turner (1986) showed that assuming an open system, i.e. allowing for CO_2 exchange with the atmosphere, results in significantly different pH profiles with differences up to 0.7 pH units at low salinities for systems that are fully equilibrated with the atmosphere. Furthermore, biogeochemical processes can play a significant role in influencing the pH of aquatic ecosystems (e.g. Ben-Yaakov, 1973; Regnier et al., 1997; Soetaert et al., 2007). As can be seen in Fig. 4.1, the importance of both considering an open system with air-water exchange and including biogeochemical processes is obvious: the distinct pH minimum at low salinities found for a closed system by Mook and Koene (1975), but doubted for an open system by Whitfield and Turner (1986), can be clearly confirmed with a full biogeochemical model. However, the relative importance of single biogeochemical processes, CO_2 air-water exchange, and transport for the pH of the system still remains unknown.

Regnier et al. (1997), Vanderborght et al. (2002), and Hofmann et al. (2008c, , i.e., Chapter 2) show that reaction transport models with gas exchange, including the effects of biogeochemical processes consuming or producing protons, can reproduce the longitudinal pH profile of the Scheldt estuary fairly well. However, in none of these studies the influences of transport,

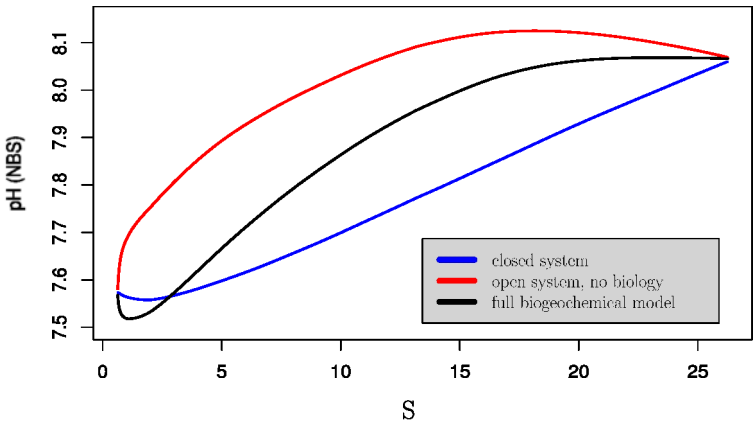

Figure 4.1.: pH profiles along the Scheldt estuary salinity gradient. The blue line represents the pH calculated with a closed system model (comparable to Mook and Koene, 1975); the red line represents the pH calculated with an open system model (comparable to Whitfield and Turner (1986) but with realistic kinetic CO_2 air-water exchange instead of a fully equilibrated system); the black line represents the pH calculated with the full biogeochemical model as presented in Hofmann et al. (2008c, , i.e., Chapter 2).

CO_2 air-water exchange, and biogeochemical processes on the pH are quantified independently, because in those studies the pH was calculated using an implicit numerical approach[1] which did not allow for such a quantification.

While Jourabchi et al. (2005) and Soetaert et al. (2007) took steps in that direction, Hofmann et al. (2008a, , i.e., Chapter 3) present a comprehensive step by step method to set up a biogeochemical model that allows for the quantification of the influences of kinetically modelled processes (e.g. transport, CO_2 air-water exchange, biogeochemical processes) on the pH. Their direct substitution approach describes the pH evolution explicitly using an expression for the rate of change of the proton concentration over time. Hofmann et al. (2008a, , i.e., Chapter 3) introduce their explicit approach to pH modelling for systems where the dissociation constants[2] of the involved acid-base reactions are considered constant over time. However, in studies of the Scheldt estuary (e.g. Vanderborght et al., 2002), (Hofmann et al., 2008c, , i.e., Chapter 2) the dissociation constants are calculated dynamically as functions of salinity and temperature to obtain reasonable pH values. While the explicit approach presented in Hofmann et al. (2008a, , i.e., Chapter 3) can be applied to a system with a spatial gradient in the dissociation constants which remains constant over time, the approach needs to be extended for application to a system where the dissociation constants vary over time, e.g. due to changes in temperature and salinity.

[1] Hofmann et al. (2008a, , i.e., Chapter 3) call this approach the operator splitting approach

[2] Throughout the paper "dissociation constant" means the stoichiometric equilibrium constant K^*_{HA} of the reaction $HA \rightleftharpoons A^- + H^+$ with $K^*_{HA} = \frac{[H^+][A^-]}{[HA]}$

Hence, this study has four objectives: 1) the extension of the explicit pH modelling approach presented by Hofmann et al. (2008a, , i.e., Chapter 3) such that it can be applied to systems where the dissociation constants are variable over time, 2) the validation of this explicit approach by comparing predicted pH values to those obtained with an implicit approach (Hofmann et al., 2008c, , i.e., Chapter 2), 3) the quantification of proton production and consumption along the Scheldt estuary by transport, CO_2 air-water exchange, and biogeochemical processes independently, given a certain freshwater flow and boundary conditions, and 4) an exploration of factors governing the mean estuarine pH in changing estuarine systems such as the Scheldt over the years 2001 to 2004.

4.2. Materials and methods

4.2.1. The Scheldt estuary

The turbid tidal Scheldt estuary is situated in the southwest Netherlands and northern Belgium (Fig. 4.2). The roughly 350 km (Soetaert et al., 2006) long Scheldt river drains a basin of around 21 500 km^2 (Soetaert et al., 2006) located in the northwest of France, the west of Belgium and the southwest of the Netherlands. The water movement in the Scheldt estuary is dominated by huge tidal displacements with around 200 times more water entering the estuary during a flood than freshwater discharge during one tidal cycle (Vanderborght et al., 2007). The average freshwater flow is around 100 $m^3 s^{-1}$ (Heip, 1988). The cross sectional area of the estuarine channel shows a quite regular trumpet-like shape opening up from around 4000 m^2 upstream to around 75 000 m^2 downstream (Soetaert et al., 2006) whilst the mean water depth varies quite irregularly between values of 6 m and 14 m with the deepest areas towards the downstream boundary (Soetaert and Herman, 1995b). The estuary has a total tidally averaged volume of about 3.619×10^9 m^3 and a total tidally averaged surface area of 338 km^2 (Soetaert et al., 2006; Soetaert and Herman, 1995b), the major parts of which are situated in the downstream area. The model presented here comprises the stretch of river between the upstream boundary at Rupelmonde (river km 0) and the downstream boundary at Vlissingen (river km 104).

4.2.2. The one dimensional model of the Scheldt estuary

Hofmann et al. (2008c, , i.e., Chapter 2) present a 100 box one dimensional model of the Scheldt estuary (henceforth referred to as "the model"). This model contains the kinetically modelled processes oxic mineralisation, denitrification, nitrification, and primary production (for details see Hofmann et al., 2008c, , i.e., Chapter 2). Furthermore air-water exchange of carbon dioxide and oxygen as well as advective-dispersive transport of all chemical species are included. Acid-base equilibria as given in Table 4.1 have been considered for the pH calculation. Note that the dissociation constants (K^*) of the acid-base reactions are calculated dynamically as functions of salinity, temperature and hydrostatic pressure, where salinity and temperature vary over time while the mean estuarine depth and thus the hydrostatic pressure remains constant over time. Furthermore all dissociation constants are converted to the free pH scale (Dickson, 1984).

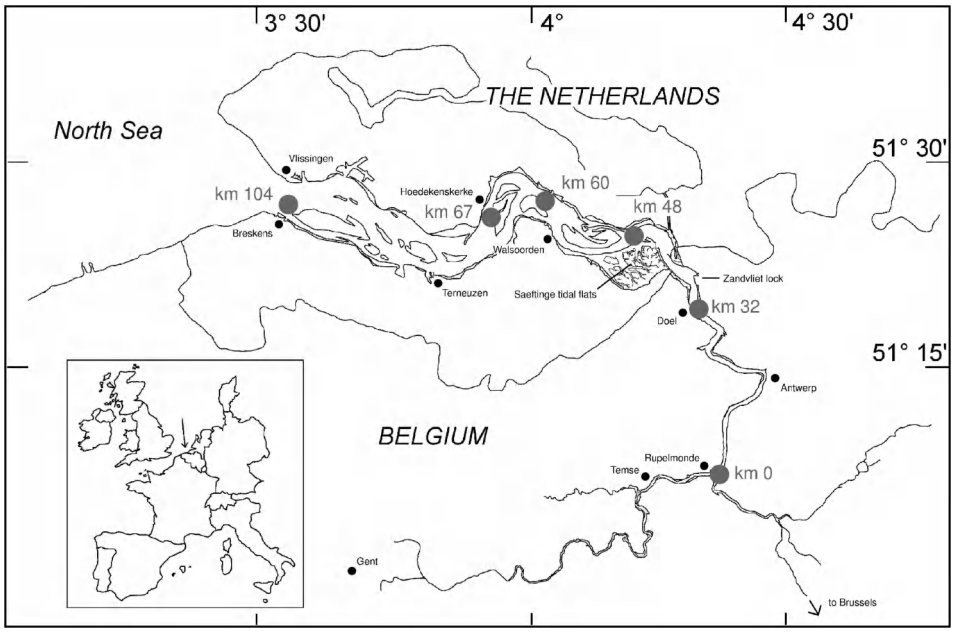

Figure 4.2.: The Scheldt estuary. Gray dots represent positions in the river where the logitudinal profiles of influences of processes on the pH, presented in the Results section, show interesting features.

Organic matter has been split into a reactive (FastOM) and a refractory (SlowOM) fraction, entailing two different rates for the two fractions for oxic mineralisation and denitrification. The resulting mass balances for the state variables of the model are given in Table 4.2. Note that X signifies the set of all total quantities except for total alkalinity in the model (total quantities are called equilibrium invariants in Hofmann et al., 2008a,c, , i.e., Chapters 3, 2).

4.2.3. The implicit pH modelling approach

In Hofmann et al. (2008c, , i.e., Chapter 2) the pH is modelled implicitly by numerically solving a system of equations constructed from the equilibrium mass action laws of the acid-base reactions given in Table 4.1 and the concentrations of the total quantities in X at every time step of the numerical integration of the equations given in Table 4.2. This implicit pH modelling approach (operator splitting approach, Hofmann et al., 2008a, , i.e., Chapter 3), is equivalent to the approach presented by Follows et al. (2006) and similar to the approaches presented by Luff et al. (2001). Furthermore, it is inspired by classical pH calculation methods as given by Ben-Yaakov (1970) and Culberson (1980) and variations of it are used by Regnier et al. (1997) and Vanderborght et al. (2002). Due to its implicit nature, this approach does not allow for quantifying the individual influences of the kinetically modelled processes.

$CO_2 + H_2O$	$\rightleftharpoons$	$H^+ + HCO_3^-$	$K^*_{CO_2}$	$=$	$\frac{[H^+][HCO_3^-]}{[CO_2]}$
HCO_3^+	$\rightleftharpoons$	$H^+ + CO_3^{2-}$	$K^*_{HCO_3^-}$	$=$	$\frac{[H^+][CO_3^{2-}]}{[HCO_3^-]}$
H_2O	$\rightleftharpoons$	$H^+ + OH^-$	K^*_W	$=$	$[H^+][OH^-]$
$B(OH)_3 + H_2O$	$\rightleftharpoons$	$H^+ + B(OH)_4^-$	$K^*_{B(OH)_3}$	$=$	$\frac{[H^+][B(OH)_4^-]}{[B(OH)_3]}$
NH_4^+	$\rightleftharpoons$	$H^+ + NH_3$	$K^*_{NH_4^+}$	$=$	$\frac{[H^+][NH_3]}{[NH_4^+]}$
HSO_4^+	$\rightleftharpoons$	$H^+ + SO_4^{2-}$	$K^*_{HSO_4^-}$	$=$	$\frac{[H^+][SO_4^{2-}]}{[HSO_4^-]}$
HF	$\rightleftharpoons$	$H^+ + F^-$	K^*_{HF}	$=$	$\frac{[H^+][F^-]}{[HF]}$

$$K^* = \left\{K^*_{CO2}, K^*_{HCO_3^-}, K^*_{B(OH)_3}, K^*_W, K^*_{NH_4^+}, K^*_{HSO_4^-}, K^*_{HF}\right\}$$

Table 4.1.: Left: acid-base equilibria taken into account in the model. Right: definition of stoichiometric equilibrium constants.

4.2.4. The explicit pH modelling approach

With their direct substitution approach, Hofmann et al. (2008a, i.e., Chapter 3) present a new methodology for pH modelling that describes the pH evolution over time with an explicit expression for the rate of change of the proton concentration. Since all the kinetically modelled processes are independent from one another, they separately contribute to the rate of change of the proton concentration

$$\frac{d[H^+]}{dt} = \sum_i \frac{d[H^+]}{dt}_i \tag{1}$$

where $\frac{d[H^+]}{dt}_i$ expresses the contribution of process i to the rate of change of the proton concentration $\frac{d[H^+]}{dt}$. This partitioning of $\frac{d[H^+]}{dt}$ into terms due to the kinetically modelled processes provides a quantitification of their influences on the pH.

In Hofmann et al. (2008c, i.e., Chapter 2) a subset of Dickson's total alkalinity [TA] (Dickson, 1981) is used[3]

$$[TA] = [HCO_3^-] + 2[CO_3^{2-}] + [B(OH)_4^-] + [OH^-] + [NH_3] - [H^+] - [HSO_4^-] - [HF] \tag{2}$$

Assuming constant acid-base dissociation constants entails

$$[TA] = f([H^+], X) \tag{3}$$

which allows formulating a total derivative of total alkalinity

$$\frac{d[TA]}{dt} = \frac{\partial[TA]}{\partial[H^+]}\frac{d[H^+]}{dt} + \sum_j \frac{\partial[TA]}{\partial[X_j]}\frac{d[X_j]}{dt} \tag{4}$$

[3]Note that [X] signifies the concentration of chemical species X. Since the total alkalinity values are equivalent to concentrations, also total alkalinity is denoted by [TA].

$$
\begin{aligned}
\frac{d[\mathrm{FastOM}]}{dt} &= \mathbf{Tr}_{\mathrm{FastOM}} - \mathbf{R}_{\mathrm{OxFastOM}} - \mathbf{R}_{\mathrm{DenFastOM}} + \mathbf{R}_{\mathrm{PP}} \\
\frac{d[\mathrm{SlowOM}]}{dt} &= \mathbf{Tr}_{\mathrm{SlowOM}} - \mathbf{R}_{OxSlowOM} - \mathbf{R}_{DenSlowOM} \\
\frac{d[\mathrm{DOC}]}{dt} &= \mathbf{Tr}_{\mathrm{DOC}} \\
\frac{d[\mathrm{O_2}]}{dt} &= \mathbf{Tr}_{\mathrm{O_2}} + \mathbf{E}_{\mathrm{O_2}} - \mathbf{R}_{OxCarb} - 2 \cdot \mathbf{R}_{Nit} + (2 - 2 \cdot p^{PP}_{\mathrm{NH_4^+}}) \cdot \mathbf{R}_{PP} + \mathbf{R}_{PPCarb} \\
\frac{d[\mathrm{NO_3^-}]}{dt} &= \mathbf{Tr}_{\mathrm{NO_3^-}} - 0.8 \cdot \mathbf{R}_{DenCarb} + \mathbf{R}_{Nit} - (1 - p^{PP}_{\mathrm{NH_4^+}}) \cdot \mathbf{R}_{PP} \\
\frac{d[\mathrm{S}]}{dt} &= \mathbf{Tr}_{\mathrm{S}} \\
\frac{d[\sum \mathrm{CO_2}]}{dt} &= \mathbf{Tr}_{\sum \mathrm{CO_2}} + \mathbf{E}_{\mathrm{CO_2}} + \mathbf{R}_{OxCarb} + \mathbf{R}_{DenCarb} - \mathbf{R}_{PPCarb} \\
\frac{d[\sum \mathrm{NH_4^+}]}{dt} &= \mathbf{Tr}_{\sum \mathrm{NH_4^+}} + \mathbf{R}_{Ox} + \mathbf{R}_{Den} - \mathbf{R}_{Nit} - p^{PP}_{\mathrm{NH_4^+}} \cdot \mathbf{R}_{PP} \\
\frac{d[\sum \mathrm{HSO_4^-}]}{dt} &= \mathbf{Tr}_{\sum \mathrm{HSO_4^-}} \\
\frac{d[\sum \mathrm{B(OH)_3}]}{dt} &= \mathbf{Tr}_{\sum \mathrm{B(OH)_3}} \\
\frac{d[\sum \mathrm{HF}]}{dt} &= \mathbf{Tr}_{\sum \mathrm{HF}} \\
\frac{d[\mathrm{TA}]}{dt} &= \mathbf{Tr}_{\mathrm{TA}} + \mathbf{R}_{Ox} + 0.8 \cdot \mathbf{R}_{DenCarb} + \mathbf{R}_{Den} - 2 \cdot \mathbf{R}_{Nit} - (2 \cdot p^{PP}_{\mathrm{NH_4^+}} - 1) \cdot \mathbf{R}_{PP} \\
\multicolumn{3}{c}{\mathrm{X} = \{[\textstyle\sum \mathrm{CO_2}], [\sum \mathrm{NH_4^+}], [\sum \mathrm{HSO_4^-}], [\sum \mathrm{B(OH)_3}], [\sum \mathrm{HF}]\}}
\end{aligned}
$$

Table 4.2.: Rates of change of model state variables. $\mathbf{R}_{\mathrm{OxFastOM}}$ and $\mathbf{R}_{\mathrm{OxSlowOM}}$ are the reaction rates of oxic mineralisation for the reactive and refractory organic matter fraction respectively. Similarly, $\mathbf{R}_{\mathrm{DenFastOM}}$, $\mathbf{R}_{\mathrm{DenSlowtOM}}$, $\mathbf{R}_{\mathrm{Nit}}$, and $\mathbf{R}_{\mathrm{PP}}$ are the rates of denitrification, nitrification and primary production. $\mathbf{E}_C$ and $\mathbf{Tr}_C$ express the air-water exchange and advective-dispersive transport rates of the respective chemical species. $p^{PP}_{\mathrm{NH_4^+}}$ is the fraction of $\mathrm{NH_4^+}$ usage of primary production as explained in Hofmann et al. (2008c, i.e., Chapter 2).

From Eq. (4), Hofmann et al. (2008a, i.e., Chapter 3) algebraically derive $\frac{d[\mathrm{H^+}]}{dt}$ as

$$
\frac{d[\mathrm{H^+}]}{dt} = \left(\frac{d[\mathrm{TA}]}{dt} - \sum_j \frac{\partial[\mathrm{TA}]}{\partial[\mathrm{X}_j]} \frac{d[\mathrm{X}_j]}{dt} \right) \Bigg/ \frac{\partial[\mathrm{TA}]}{\partial[\mathrm{H^+}]} \tag{5}
$$

By plugging the expressions for $\frac{d[\mathrm{TA}]}{dt}$ and $\frac{d[\mathrm{X}_j]}{dt}$ given in Table (4.2) into Eq. (5) and rearranging the terms, we arrive at an equivalent to Eq. (1) for the given model. This allows us to individually quantify the influence of oxic mineralisation, denitrification, nitrification, primary production, air-water exchange and advective-dispersive transport on the pH if the acid-base dissociation constants are assumed to be constant over time. (Note again that a spatial gradient in the dissociation constants which is constant over time does not pose a

problem.)

In the following we describe how to apply the explicit pH modelling approach to a system with time variable acid-base dissociation constants.

4.2.5. The explicit pH modelling approach with time variable dissociation constants

Letting the dissociation constants vary over time entails

$$[\mathrm{TA}] = f([\mathrm{H^+}], \mathrm{X}, \mathrm{K^*}) \tag{6}$$

which means that [TA] is a function of the proton concentration $[\mathrm{H^+}]$, the total quantities in X and the dissociation constants in K^*. Obviously, the dissociation constants are functions of temperature T, salinity S and pressure P

$$K_i^* = f_i(T, S, P) \tag{7}$$

Since the mean depth in the model does not vary over time, we consider constant pressure P. However, the functions for temperature and salinity dependence of some dissociation constants are expressed on the seawater pH scale ($K^{*,\mathrm{SWS}}$) or the total pH scale ($K^{*,\mathrm{tot}}$) (Dickson, 1984) and not on the free pH scale ($K^{*,\mathrm{free}}$) which is consistently used in the model presented here. These dissociation constants were converted to the free pH scale, without loss of generality from the seawater scale by (Dickson, 1984; Zeebe and Wolf-Gladrow, 2001)

$$K_i^{*,\mathrm{free}} = K_i^{*,\mathrm{SWS}} \Bigg/ \left(1 + \frac{[\sum \mathrm{HSO_4^-}]}{K_{\mathrm{HSO_4^-}}^{*,\mathrm{free}}} + \frac{[\sum \mathrm{HF}]}{K_{\mathrm{HF}}^{*,\mathrm{free}}}\right) \tag{8}$$

This shows that, in general, the dissociation constants are also functions of $[\sum \mathrm{HSO_4^-}]$ and $[\sum \mathrm{HF}]$, two quantities needed for pH scale conversions. Thus

$$K_i^* = f_i(T, S, [\sum \mathrm{HSO_4^-}], [\sum \mathrm{HF}]) \tag{9}$$

This means the total derivative of [TA] considering dissociation constants variable over time can be written as

$$\begin{aligned}\frac{d[\mathrm{TA}]}{dt} = &\frac{\partial[\mathrm{TA}]}{\partial[\mathrm{H^+}]}\frac{d[\mathrm{H^+}]}{dt} + \sum_j \left(\frac{\partial[\mathrm{TA}]}{\partial[\mathrm{X}_j]}\frac{d[\mathrm{X}_j]}{dt}\right) + \sum_i \left(\frac{\partial \mathrm{TA}}{\partial K_i^*}\frac{\partial K_i^*}{\partial T}\right)\frac{dT}{dt} + \sum_i \left(\frac{\partial \mathrm{TA}}{\partial K_i^*}\frac{\partial K_i^*}{\partial S}\right)\frac{dS}{dt} \\ &+ \sum_i \left(\frac{\partial[\mathrm{TA}]}{\partial[K_i^*]}\frac{\partial K_i^*}{\partial[\sum \mathrm{HSO_4^-}]}\right)\frac{d[\sum \mathrm{HSO_4^-}]}{dt} + \sum_i \left(\frac{\partial[\mathrm{TA}]}{\partial[K_i^*]}\frac{\partial K_i^*}{\partial[\sum \mathrm{HF}]}\right)\frac{d[\sum \mathrm{HF}]}{dt}\end{aligned} \tag{10}$$

Appendix 4.6.1 details how the partial derivatives of [TA] and of the dissociation constants can be calculated[4].

[4] Note that Eq. (10) contains partial derivatives of [TA] and K_i^* with respect to one of their variables. This entails that all other variables of these quantities, as defined by Eqs. (6) and (9) are kept constant. That means, e.g. in the term $\frac{\partial[\mathrm{TA}]}{\partial[\sum \mathrm{HSO_4^-}]}$ the dissociation constants are considered constants, although they are also functions of $[\sum \mathrm{HSO_4^-}]$. Likewise, in $\frac{\partial \mathrm{TA}}{\partial K_i^*}$, $[\sum \mathrm{HSO_4^-}]$ is considered constant, while for $\frac{\partial K_i^*}{\partial[\sum \mathrm{HSO_4^-}]}$ it is the variable. Note further that we model $[\sum \mathrm{B(OH)_3}]$ independently from the salinity S (although borate species contribute to S). Therefore, for $\frac{\partial[\mathrm{TA}]}{\partial[\sum \mathrm{B(OH)_3}]}$, S is considered a constant, although, strictly speaking, changes in $[\sum \mathrm{B(OH)_3}]$ would also change S. This is done to mathematically separate influences of changes in S via the dissociation constants on [TA] and changes in the equilibrium invariant $[\sum \mathrm{B(OH)_3}]$ on [TA] directly.

In the same way as done in Hofmann et al. (2008a, i.e., Chapter 3), we can derive a rate of change of the proton concentration from Eq. (10)

$$\frac{d[\mathrm{H}^+]}{dt} = \left(\frac{d[\mathrm{TA}]}{dt} - \left(\sum_j \frac{\partial[\mathrm{TA}]}{\partial[\mathrm{X}_j]} \frac{d[\mathrm{X}_j]}{dt} + \sum_i \left(\frac{\partial \mathrm{TA}}{\partial K_i^*} \frac{\partial K_i^*}{\partial T} \right) \frac{dT}{dt} + \sum_i \left(\frac{\partial \mathrm{TA}}{\partial K_i^*} \frac{\partial K_i^*}{\partial S} \right) \frac{dS}{dt} + \sum_i \left(\frac{\partial[\mathrm{TA}]}{\partial[K_i^*]} \frac{\partial[K_i^*]}{\partial[\sum \mathrm{HSO}_4^-]} \right) \frac{d[\sum \mathrm{HSO}_4^-]}{dt} + \sum_i \left(\frac{\partial[\mathrm{TA}]}{\partial[K_i^*]} \frac{\partial[K_i^*]}{\partial[\sum \mathrm{HF}]} \right) \frac{d[\sum \mathrm{HF}]}{dt} \right) \right) \Big/ \frac{\partial[\mathrm{TA}]}{\partial[\mathrm{H}^+]} \tag{11}$$

which can be partitioned into contributions by the different kinetically modelled processes and by the influences of changes in the dissociation constants due to changes in their four variables T, S, $[\sum \mathrm{HSO}_4^-]$, and $[\sum \mathrm{HF}]$. This can be done by plugging in expressions for $\frac{d[\mathrm{TA}]}{dt}$, and $\frac{d[\mathrm{X}_j]}{dt}$ as given in Table 4.2 and rearranging the terms. The result is an equivalent to Eq. (1) for the given model that takes into account the respective contributions of transport, air-water exchange of CO_2, oxic mineralisation, denitrification, nitrification, primary production, the temperature and the salinity effect on the dissociation constants, as well as two terms for pH scale conversions

$$\begin{aligned} \frac{d[\mathrm{H}^+]}{dt} = & \frac{d[\mathrm{H}^+]}{dt}_{\mathbf{T}} + \frac{d[\mathrm{H}^+]}{dt}_{\mathbf{E}_{CO_2}} + \frac{d[\mathrm{H}^+]}{dt}_{\mathbf{R}_{\mathrm{Ox}}} + \frac{d[\mathrm{H}^+]}{dt}_{\mathbf{R}_{\mathrm{Den}}} + \frac{d[\mathrm{H}^+]}{dt}_{\mathbf{R}_{\mathrm{Nit}}} + \frac{d[\mathrm{H}^+]}{dt}_{\mathbf{R}_{\mathrm{PP}}} \\ & + \frac{d[\mathrm{H}^+]}{dt}_{K^*(T)} + \frac{d[\mathrm{H}^+]}{dt}_{K^*(S)} + \frac{d[\mathrm{H}^+]}{dt}_{K^*([\sum \mathrm{HSO}_4^-])} + \frac{d[\mathrm{H}^+]}{dt}_{K^*([\sum \mathrm{HF}])} \end{aligned} \tag{12}$$

with

$$\frac{d[\mathrm{H}^+]}{dt}_{\mathbf{T}} = \left(\mathbf{T}_{\mathrm{TA}} - \left(\sum_i \left(\mathbf{T}_{\mathrm{X}_i} \frac{\partial[\mathrm{TA}]}{\partial[\mathrm{X}_i]} \right) \right) \right) \Big/ \frac{\partial[\mathrm{TA}]}{\partial[\mathrm{H}^+]} \tag{13}$$

$$\frac{d[\mathrm{H}^+]}{dt}_{\mathbf{E}_{CO_2}} = \left(- \left(\mathbf{E}_{CO_2} \frac{\partial[\mathrm{TA}]}{\partial[\sum \mathrm{CO}_2]} \right) \right) \Big/ \frac{\partial[\mathrm{TA}]}{\partial[\mathrm{H}^+]} \tag{14}$$

$$\frac{d[\mathrm{H}^+]}{dt}_{\mathbf{R}_{\mathrm{Ox}}} = \left(\mathbf{R}_{\mathrm{Ox}} - \left(\mathbf{R}_{\mathrm{OxCarb}} \frac{\partial[\mathrm{TA}]}{\partial[\sum \mathrm{CO}_2]} + \mathbf{R}_{\mathrm{Ox}} \frac{\partial[\mathrm{TA}]}{\partial[\sum \mathrm{NH}_4^+]} \right) \right) \Big/ \frac{\partial[\mathrm{TA}]}{\partial[\mathrm{H}^+]} \tag{15}$$

$$\frac{d[\mathrm{H}^+]}{dt}_{\mathbf{R}_{\mathrm{Den}}} = \left(0.8\mathbf{R}_{\mathrm{DenCarb}} + \mathbf{R}_{\mathrm{Den}} - \left(\mathbf{R}_{\mathrm{DenCarb}} \frac{\partial[\mathrm{TA}]}{\partial[\sum \mathrm{CO}_2]} + \mathbf{R}_{\mathrm{Den}} \frac{\partial[\mathrm{TA}]}{\partial[\sum \mathrm{NH}_4^+]} \right) \right) \Big/ \frac{\partial[\mathrm{TA}]}{\partial[\mathrm{H}^+]} \tag{16}$$

$$\frac{d[\mathrm{H}^+]}{dt}_{\mathbf{R}_{\mathrm{Nit}}} = \left(-2\mathbf{R}_{\mathrm{Nit}} - \left(-\mathbf{R}_{\mathrm{Nit}} \frac{\partial[\mathrm{TA}]}{\partial[\sum \mathrm{NH}_4^+]} \right) \right) \Big/ \frac{\partial[\mathrm{TA}]}{\partial[\mathrm{H}^+]} \tag{17}$$

$$\frac{d[\mathrm{H}^+]}{dt}_{\mathbf{R}_{\mathrm{PP}}} = \left(\left(-2p_{\mathrm{NH}_4^+}^{PP} - 1 \right) \mathbf{R}_{\mathrm{PP}} - \left(-\mathbf{R}_{\mathrm{PP}} \mathrm{Carb} \frac{\partial[\mathrm{TA}]}{\partial[\sum \mathrm{CO}_2]} - p_{\mathrm{NH}_4^+}^{PP} \mathbf{R}_{\mathrm{PP}} \frac{\partial[\mathrm{TA}]}{\partial[\sum \mathrm{NH}_4^+]} \right) \right) \Big/ \frac{\partial[\mathrm{TA}]}{\partial[\mathrm{H}^+]} \tag{18}$$

$$\frac{d[\mathrm{H}^+]}{dt}_{K^*(T)} = \left(- \left(\frac{dT}{dt} \sum_i \left(\frac{\partial K_i^*}{\partial T} \frac{\partial[\mathrm{TA}]}{\partial K_i^*} \right) \right) \right) \Big/ \frac{\partial[\mathrm{TA}]}{\partial[\mathrm{H}^+]} \tag{19}$$

$$\frac{d[\mathrm{H}^+]}{dt}_{K^*(S)} = \left(- \left(\frac{dS}{dt} \sum_i \left(\frac{\partial K_i^*}{\partial S} \frac{\partial[\mathrm{TA}]}{\partial K_i^*} \right) \right) \right) \Big/ \frac{\partial[\mathrm{TA}]}{\partial[\mathrm{H}^+]} \tag{20}$$

$$\frac{d[\mathrm{H}^+]}{dt}_{K^*([\sum \mathrm{HSO}_4^-])} = \left(- \left(\frac{d[\sum \mathrm{HSO}_4^-]}{dt} \sum_i \left(\frac{\partial K_i^*}{\partial[\sum \mathrm{HSO}_4^-]} \frac{\partial[\mathrm{TA}]}{\partial K_i^*} \right) \right) \right) \Big/ \frac{\partial[\mathrm{TA}]}{\partial[\mathrm{H}^+]} \tag{21}$$

$$\frac{d[\mathrm{H}^+]}{dt}_{K^*([\sum \mathrm{HF}])} = \left(- \left(\frac{d[\sum \mathrm{HF}]}{dt} \sum_i \left(\frac{\partial K_i^*}{\partial[\sum \mathrm{HF}]} \frac{\partial[\mathrm{TA}]}{\partial K_i^*} \right) \right) \right) \Big/ \frac{\partial[\mathrm{TA}]}{\partial[\mathrm{H}^+]} \tag{22}$$

4.2.6. Implementation

The model including the implicit and explicit pH modelling methods (Sect. 4.2.5) has been coded in FORTRAN within the ecological modelling framework FEMME (Soetaert et al.,

2002). The model code can be obtained from the corresponding author or from the FEMME website: http://www.nioo.knaw.nl/projects/femme/. Post processing of model results and the generation of graphs has been done using the statistical programming language R (R Development Core Team, 2005).

4.2.7. Model runs

4.2.7.1. Quantification of proton production and consumption along the estuary

A seasonality resolving, time dependent, continuous simulation over the years 2001 to 2004 has been performed. The boundary conditions for [TA], S, $[\sum \mathrm{NH_4^+}]$, [OM], $[\mathrm{O_2}]$, $[\mathrm{NO_3^-}]$, $[\sum \mathrm{HSO_4^-}]$, $[\sum \mathrm{B(OH)_3}]$, and $[\sum \mathrm{HF}]$, the temperature forcing and the freshwater flow were varied over the four modelled years based on measured values (for details see Hofmann et al., 2008c, i.e., Chapter 2). Results of a steady state model run with all forcings set to their first 2001 values serve as initial conditions for the time dependent simulation. The initial condition for the state variable $[\mathrm{H^+}]$ has been calculated from the initial conditions of all other state variables using the implicit pH calculation approach. Model output has been generated as yearly averaged longitudinal profiles for the four modelled years. The influences of kinetically modelled processes as well as those of changes in the dissociation constants on the pH have been calculated according to Eqs. (13) to (22).

4.2.7.2. Factors governing changes in the mean estuarine pH from 2001 to 2004

	2001	2002	2003	2004
freshwater flow (Q)	190	184	112	95
$[\mathrm{TA}]_{\mathrm{up}}$	4441	4493	4470	4473
$[\mathrm{TA}]_{\mathrm{down}}$	2702	2728	2726	2733
S_{up}	0.6	0.6	0.9	1.0
S_{down}	26.5	27.7	28.3	30.2
$[\sum \mathrm{NH_4^+}]_{\mathrm{up}}$	110	105	118	72
$[\sum \mathrm{NH_4^+}]_{\mathrm{down}}$	8	4	6	4
$(\sum_{x\in\{\mathrm{fast,slow}\}}[\mathrm{xOM}])_{\mathrm{up}}$	41	49	54	55
$(\sum_{x\in\{\mathrm{fast,slow}\}}[\mathrm{xOM}])_{\mathrm{down}}$	10	10	7	9
$[\mathrm{O_2}]_{\mathrm{up}}$	94	76	71	65
$[\mathrm{O_2}]_{\mathrm{down}}$	293	272	280	268
pH (NBS)	8.010	8.053	8.069	8.095

Table 4.3.: Changes in important mean model forcing values and the pH from 2001 to 2004. The subscript "up" denotes upstream boundary condition forcings, the subscript "down" denotes downstream boundary condition forcings. Concentrations are given in mmol $\mathrm{m^{-3}}$, Q is given in $\mathrm{m^3\,s^{-1}}$. Note that Q refers to the flow at the upstream boundary.

Hofmann et al. (2008c, i.e., Chapter 2) report an upward trend in the annual whole estuarine mean pH over the years 2001 to 2004. As mentioned above, the changes in the boundary

conditions, the temperature forcing and the freshwater discharge (Table 4.3) are responsible for trends in the model results. Due to the minimal change in the mean estuarine temperature, the effect of changes in the temperature forcing has been neglected. In our simulation runs (as described above), boundary conditions and freshwater discharge vary simultaneously, obscuring the effect of boundary conditions and the effect of freshwater flow change for single chemical compounds. Therefore, we executed a number of explorative runs in which freshwater discharge or boundary values (upstream and downstream) for individual state variables or groups of them were allowed to vary while freshwater discharge and boundary conditions for all other state variables remained at 2001 values (Table 4.4). This has been done to investigate their individual effect on the annual whole estuarine mean pH. End of the year 2001 conditions were used as initial conditions for these explorative runs and as a result the mean pH value for 2001 slightly differed from the one obtained from the simulation runs described above.

sc.	freshwater flow change	sc.	boundary condition change
a)	all state variables	h)	all state variables
b)	$[\sum CO_2]$, [TA]	i)	[TA] (pH)
c)	S	j)	S
d)	$[\sum NH_4^+]$	k)	$[\sum NH_4^+]$
e)	[FastOM], [SlowOM]	l)	[FastOM], [SlowOM]
f)	$[O_2]$	m)	$[O_2]$
g)	$[NO_3^-]$, $[\sum HSO_4^-]$, $[\sum B(OH)_3]$, $[\sum HF]$	n)	$[NO_3^-]$, $[\sum HSO_4^-]$, $[\sum B(OH)_3]$, $[\sum HF]$

Table 4.4.: Model scenarios to investigate the pH trend from 2001 to 2004. The entries in the list indicate for which state variables either the freshwater flow or the boundary conditions have been changed to values for 2001 to 2004 while all other forcings have been kept at 2001 values. Note that in all these scenarios, [TA] boundary conditions are calculated consistently from pH boundary forcing values.

4.3. Results

4.3.1. Comparison of the implicit and the explicit pH modelling approach – verification of consistency

Figure 4.3 shows the model fit for the NBS scale pH for the years 2001 to 2004 (yearly averaged longitudinal profiles). The black and blue lines represent the fit of the pH calculated with the implicit and explicit approach, respectively: in the upper row assuming time constant dissociation constants; in the middle row considering the terms describing the variations in the dissociation constants due to changes in S and T but without the pH scale conversion related terms; in the lower row considering all terms as described in Sect. 4.2.5. It can be seen that assuming constant dissociation constants yields pH values that are substantially different from the implicitly calculated ones, i.e. pH values that are inconsistent with the modelled concentrations of the total quantities like total alkalinity and total inorganic carbon assuming time variable dissociation constants. Including the terms describing variations in the dissociation constants due to variations in temperature and salinity yields much better pH values, yet they are not identical. One can see that especially in the year 2004 the small

errors in $\frac{d[H^+]}{dt}$ resulted in a drifting apart of the two pH values. Finally, including also the pH scale conversion related terms as described in Sect. 4.2.5 yields explicitly calculated pH values that are identical to those calculated implicitly, confirming the consistent implementation of the explicit pH calculation approach.

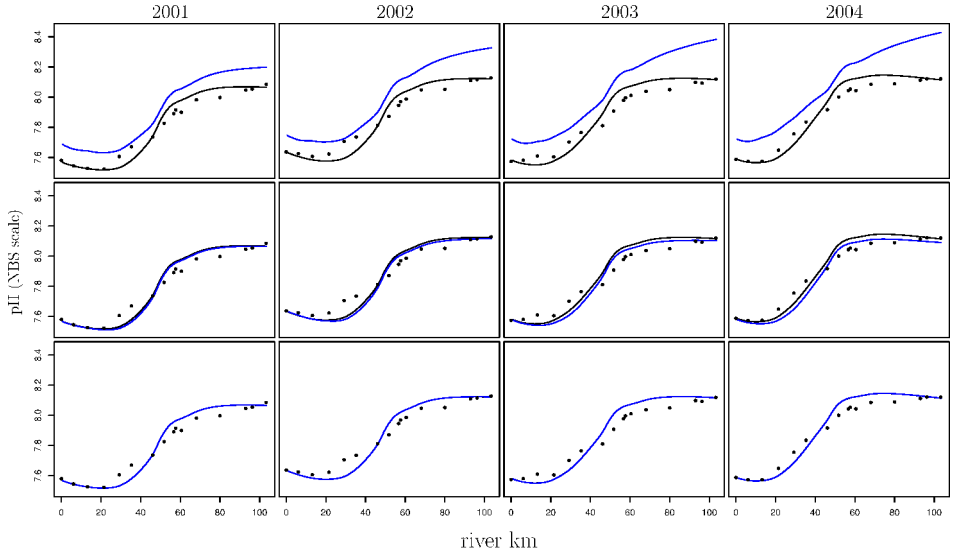

Figure 4.3.: The model fit for pH for the modelled years 2001 through 2004. The black dots represent NIOO monitoring data (see Hofmann et al., 2008c, i.e., Chapter 2), the black lines represent the fit of the pH calculated with the implicit approach and the blue lines represents the fit of the pH calculated with the explicit approach: in the upper row assuming time constant dissociation constants; in the middle row considering the terms describing the variations in the dissociation constants due to changes in S and T but without the pH scale conversion related terms; in the lower row considering all terms as described in Sect. (4.2.5).

4.3.2. Quantification of proton production and consumption along the estuary

Figure 4.4a shows longitudinal profiles of volumetric influences of kinetically modelled processes on the proton concentration as calculated with Eqs. (13) to (22), averaged over the four modelled years. Table 4.5 shows selected influences on the proton concentration (including the influences of changes in the dissociation constants): at positions in the river where the profiles shown in Fig. 4.4 exhibit interesting features (see also Fig. 4.2).

Influences of changes in the dissociation constants are about three orders of magnitude smaller than the influences of kinetically modelled processes. Furthermore their patterns along the estuary (not shown) depend on the respective implementation of the model (e.g. on which pH scale the dissociation constants are calculated and to which pH scale they are converted) and

are rather erratic and of limited scientific value: they are therefore not presented in Figs. 4.4 and 4.5. Yet, incorporation of these influences is necessary to obtain the excellent agreement between the explicitly calculated pH and the implicitly calculated pH as shown in Fig. 4.3.

Figure 4.4a exhibits a trumpet-like shape due to pronounced activity in the upper estuary, i.e. between river km 0 and 60. In this stretch of the estuary, the absolute influences of most kinetically modelled processes decline to stay at low levels until the mouth of the estuary. The most important proton producer at the upstream boundary is nitrification and its relative importance drops from 77% upstream to 11% downstream. The proton production of oxic mineralisation also decreases from upstream to downstream. However, its relative importance as a proton producer increases from 23% at the upstream boundary to 64% at the downstream boundary. The most important proton consuming process is CO_2 degassing and its relative importance first increases from 50% at the upstream boundary to 92% at km 32 and then decreases again to 65% at the downstream boundary. Compared to CO_2 degassing, the proton consumption by primary production is rather small. It shows a steady downstream decrease with local maxima in the zone of maximal volumetric primary production in the estuary around km 48 and around km 67. The relative importance of primary production as a proton consumer increases from 4% at the upstream boundary to 38% at km 67 and decreases again to 33% at the downstream boundary. Denitrification is a proton consuming process with relatively low importance in the Scheldt estuary. Its relative importance is 2% at the upstream boundary, 1% at river km 32 and 0% along the rest of the estuary. Advective-dispersive transport counteracts the dominant proton consuming or producing processes, exporting protons from the model boxes between the upstream boundary and around km 32 and importing protons from km 32 on until the downstream boundary. It shows a maximum of proton import around river km 48 and a secondary maximum around river km 67. At the upstream boundary advective-dispersive transport accounts for 44% of proton consumption while at river kilometres 48 and 67 it delivers about 50% of the protons.

Figure 4.4b shows longitudinal profiles of volume integrated ("per river kilometre") influences on the proton concentration as calculated with Eqs. (13) to (22), averaged over the four modelled years. Table 4.6 shows selected values of those volume integrated influences on the proton concentration.

As the estuarine cross section area increases from around 4000 m^2 upstream to around 76 000 m^2 downstream, while the mean estuarine depth remains at around 10 m, there is a much larger estuarine volume in downstream model boxes than there is in upstream model boxes. As a consequence, volume integrated proton production or consumption rates in Fig. 4.4b are similar in the upstream and downstream region of the estuary. This is in contrast to volumetric rates which are much larger upstream than they are downstream for all processes. The mid-region of the estuary (between kms 30 and 60) can be identified as the most important region for volume integrated proton turnover. The volume integrated proton turnover of oxic mineralisation, primary production and CO_2 degassing, is clearly larger downstream than it is upstream, while the volume integrated proton turnover of nitrification is still larger upstream than downstream.

Figure 4.5 shows a budget of proton production and consumption over the whole model area and one year, averaged over the four modelled years. It can be seen that CO_2 degassing

and primary production are (except for the minor contribution of denitrification) the only processes that net consume protons in the estuary. Advective-dispersive transport, oxic mineralisation, and nitrification all net produce protons. CO_2 degassing has the largest influence on the pH by causing the largest proton consumption, while nitrification is the main proton producer, closely followed by oxic mineralisation.

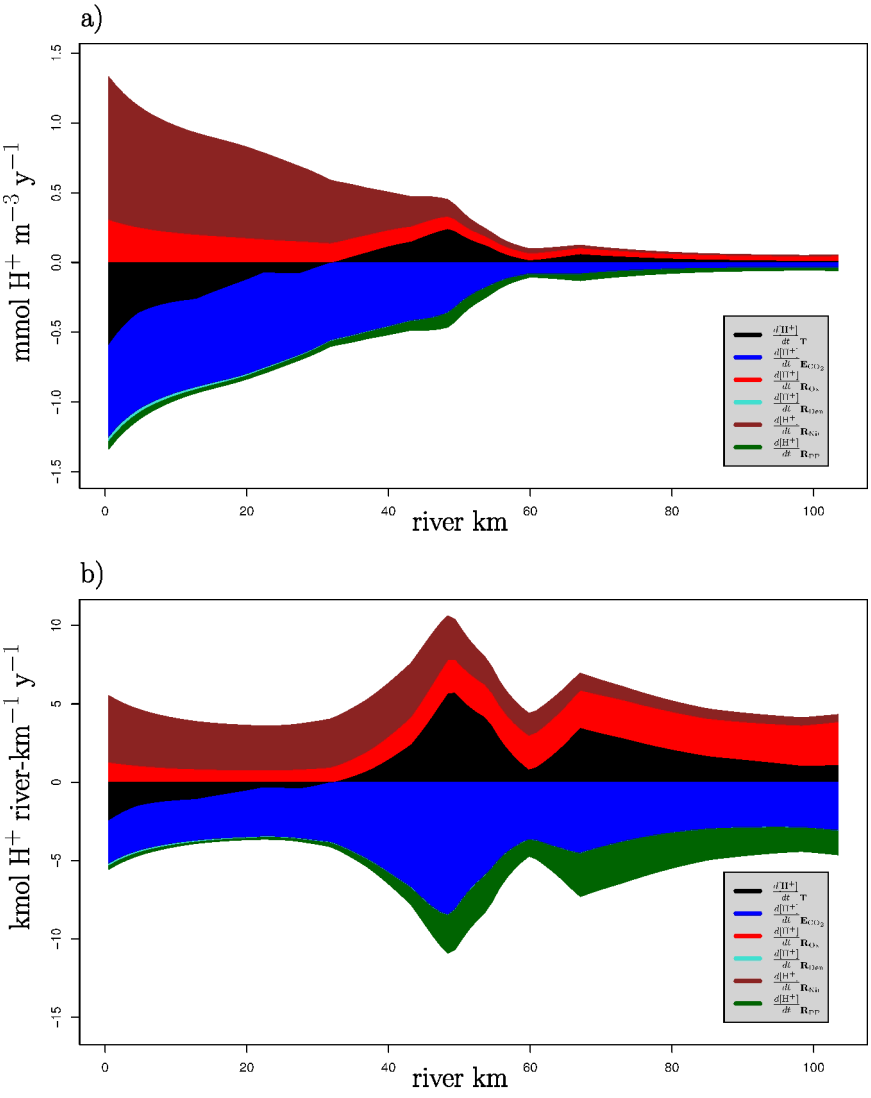

Figure 4.4.: The influences of kinetically modelled processes on the pH – volumetrically and volume integrated.

	km 0		km 32		km 48		km 60		km 67		km 104	
$\sum$prod	$1.33\,10^{-0}$		$5.99\,10^{-1}$		$4.56\,10^{-1}$		$1.03\,10^{-1}$		$1.27\,10^{-1}$		$5.47\,10^{-2}$	
$\sum$cons	$-1.34\,10^{-0}$		$-6.05\,10^{-1}$		$-4.64\,10^{-1}$		$-1.08\,10^{-1}$		$-1.31\,10^{-1}$		$-5.99\,10^{-2}$	
$\frac{d[H^+]}{dt}_{\mathbf{T}}$	$-5.93\,10^{-1}$	(44%)	$-4.37\,10^{-3}$	(1%)	$2.42\,10^{-1}$	(53%)	$1.91\,10^{-2}$	(19%)	$6.27\,10^{-2}$	(49%)	$1.39\,10^{-2}$	(25%)
$\frac{d[H^+]}{dt}_{\mathbf{E}_{CO_2}}$	$-6.64\,10^{-1}$	(50%)	$-5.59\,10^{-1}$	(92%)	$-3.60\,10^{-1}$	(78%)	$-8.34\,10^{-2}$	(77%)	$-8.16\,10^{-2}$	(62%)	$-3.90\,10^{-2}$	(65%)
$\frac{d[H^+]}{dt}_{\mathbf{R}_{Ox}}$	$3.09\,10^{-1}$	(23%)	$1.40\,10^{-1}$	(23%)	$8.98\,10^{-2}$	(20%)	$4.93\,10^{-2}$	(48%)	$4.28\,10^{-2}$	(34%)	$3.48\,10^{-2}$	(64%)
$\frac{d[H^+]}{dt}_{\mathbf{R}_{Den}}$	$-2.45\,10^{-2}$	(2%)	$-3.26\,10^{-3}$	(1%)	$-5.56\,10^{-4}$	(0%)	$-1.20\,10^{-4}$	(0%)	$-7.14\,10^{-5}$	(0%)	$-3.17\,10^{-5}$	(0%)
$\frac{d[H^+]}{dt}_{\mathbf{R}_{Nit}}$	$1.02\,10^{-0}$	(77%)	$4.53\,10^{-1}$	(76%)	$1.20\,10^{-1}$	(26%)	$3.19\,10^{-2}$	(31%)	$1.96\,10^{-2}$	(15%)	$5.88\,10^{-3}$	(11%)
$\frac{d[H^+]}{dt}_{\mathbf{R}_{PP}}$	$-5.65\,10^{-2}$	(4%)	$-3.73\,10^{-2}$	(6%)	$-1.03\,10^{-1}$	(22%)	$-2.43\,10^{-2}$	(22%)	$-4.94\,10^{-2}$	(38%)	$-1.96\,10^{-2}$	(33%)
$\frac{d[H^+]}{dt}_{K^*\langle T\rangle}$	$1.70\,10^{-4}$	(0%)	$2.95\,10^{-3}$	(0%)	$2.27\,10^{-3}$	(0%)	$1.38\,10^{-3}$	(1%)	$9.71\,10^{-4}$	(1%)	$-7.27\,10^{-4}$	(1%)
$\frac{d[H^+]}{dt}_{K^*\langle S\rangle}$	$6.22\,10^{-4}$	(0%)	$3.67\,10^{-3}$	(1%)	$2.16\,10^{-3}$	(0%)	$1.35\,10^{-3}$	(1%)	$1.07\,10^{-3}$	(1%)	$-5.24\,10^{-4}$	(1%)
$\frac{d[H^+]}{dt}_{K^*\langle[\sum HSO_4^-]\rangle}$	$-1.84\,10^{-4}$	(0%)	$-1.02\,10^{-3}$	(0%)	$-6.80\,10^{-4}$	(0%)	$-3.66\,10^{-4}$	(0%)	$-2.87\,10^{-4}$	(0%)	$8.62\,10^{-5}$	(0%)
$\frac{d[H^+]}{dt}_{K^*\langle[\sum HF]\rangle}$	$-5.78\,10^{-8}$	(0%)	$-2.79\,10^{-8}$	(0%)	$4.52\,10^{-9}$	(0%)	$-9.92\,10^{-9}$	(0%)	$-1.31\,10^{-8}$	(0%)	$-7.25\,10^{-9}$	(0%)

Table 4.5.: Volumetric budget of influences on $[H^+]$; values in mmol H^+ m^{-3} y^{-1}; percentages are of total production (positive quantities) or consumption (negative quantities), respectively.

	km 0		km 32		km 48		km 60		km 67		km 104	
$\sum$prod	$5.54\,10^{-0}$		$4.08\,10^{-0}$		$10.70\,10^{-0}$		$4.52\,10^{-0}$		$7.08\,10^{-0}$		$4.34\,10^{-0}$	
$\sum$cons	$-5.57\,10^{-0}$		$-4.12\,10^{-0}$		$-10.90\,10^{-0}$		$-4.74\,10^{-0}$		$-7.32\,10^{-0}$		$-4.74\,10^{-0}$	
$\frac{d[H^+]}{dt}_{\mathbf{T}}$	$-2.47\,10^{-0}$	(44%)	$-2.97\,10^{-2}$	(1%)	$5.70\,10^{-0}$	(53%)	$8.36\,10^{-1}$	(19%)	$3.50\,10^{-0}$	(49%)	$1.10\,10^{-0}$	(25%)
$\frac{d[H^+]}{dt}_{\mathbf{E}_{CO_2}}$	$-2.76\,10^{-0}$	(50%)	$-3.81\,10^{-0}$	(92%)	$-8.48\,10^{-0}$	(78%)	$-3.66\,10^{-0}$	(77%)	$-4.55\,10^{-0}$	(62%)	$-3.09\,10^{-0}$	(65%)
$\frac{d[H^+]}{dt}_{\mathbf{R}_{Ox}}$	$1.29\,10^{-0}$	(23%)	$9.51\,10^{-1}$	(23%)	$2.11\,10^{-0}$	(20%)	$2.16\,10^{-0}$	(48%)	$2.39\,10^{-0}$	(34%)	$2.76\,10^{-0}$	(64%)
$\frac{d[H^+]}{dt}_{\mathbf{R}_{Den}}$	$-1.02\,10^{-1}$	(2%)	$-2.22\,10^{-2}$	(1%)	$-1.31\,10^{-2}$	(0%)	$-5.24\,10^{-3}$	(0%)	$-3.98\,10^{-3}$	(0%)	$-2.51\,10^{-3}$	(0%)
$\frac{d[H^+]}{dt}_{\mathbf{R}_{Nit}}$	$4.25\,10^{-0}$	(77%)	$3.08\,10^{-0}$	(76%)	$2.81\,10^{-0}$	(26%)	$1.40\,10^{-0}$	(31%)	$1.09\,10^{-0}$	(15%)	$4.66\,10^{-1}$	(11%)
$\frac{d[H^+]}{dt}_{\mathbf{R}_{PP}}$	$-2.35\,10^{-1}$	(4%)	$-2.54\,10^{-1}$	(6%)	$-2.42\,10^{-0}$	(22%)	$-1.07\,10^{-0}$	(22%)	$-2.75\,10^{-0}$	(38%)	$-1.55\,10^{-0}$	(33%)
$\frac{d[H^+]}{dt}_{K^*(T)}$	$7.09\,10^{-4}$	(0%)	$2.01\,10^{-2}$	(0%)	$5.34\,10^{-2}$	(0%)	$6.03\,10^{-2}$	(1%)	$5.41\,10^{-2}$	(1%)	$-5.76\,10^{-2}$	(1%)
$\frac{d[H^+]}{dt}_{K^*(S)}$	$2.59\,10^{-3}$	(0%)	$2.50\,10^{-2}$	(1%)	$5.09\,10^{-2}$	(0%)	$5.93\,10^{-2}$	(1%)	$5.97\,10^{-2}$	(1%)	$-4.15\,10^{-2}$	(1%)
$\frac{d[H^+]}{dt}_{K^*([\sum HSO_4^-])}$	$-7.65\,10^{-4}$	(0%)	$-6.94\,10^{-3}$	(0%)	$-1.60\,10^{-2}$	(0%)	$-1.61\,10^{-2}$	(0%)	$-1.60\,10^{-2}$	(0%)	$6.83\,10^{-3}$	(0%)
$\frac{d[H^+]}{dt}_{K^*([\sum HF])}$	$-2.41\,10^{-7}$	(0%)	$-1.90\,10^{-7}$	(0%)	$1.06\,10^{-7}$	(0%)	$-4.35\,10^{-7}$	(0%)	$-7.30\,10^{-7}$	(0%)	$-5.75\,10^{-7}$	(0%)

Table 4.6.: Volume integrated budget of influences on $[H^+]$; values in kmol H^+ river-km^{-1} y^{-1}; percentages are of total production (positive quantities) or consumption (negative quantities), respectively.

4.3.3. Factors responsible for the change in the mean estuarine pH from 2001 to 2004

Figure 4.6 shows the trend in the overal volume averaged pH in the estuary and the associated influences of the major kinetically modelled processes on the proton concentration over the years 2001 to 2004. It can be seen that, on the NBS scale, the pH changed by ≈0.085 units from 8.010 to 8.095, absolute values of the influences of CO_2 degassing and nitrification on the proton concentration steadily declined from 2001 to 2004 (with the decline being more pronounced for CO_2 degassing), while the influence of oxic mineralisation showed no clear trend and the influence of transport declined from 2001 to 2003 and slightly increased again from 2003 to 2004. These changes are caused only by differences in the boundary conditions and the freshwater flow (and temperature forcing but changes therein are negligible) from 2003 to 2004.

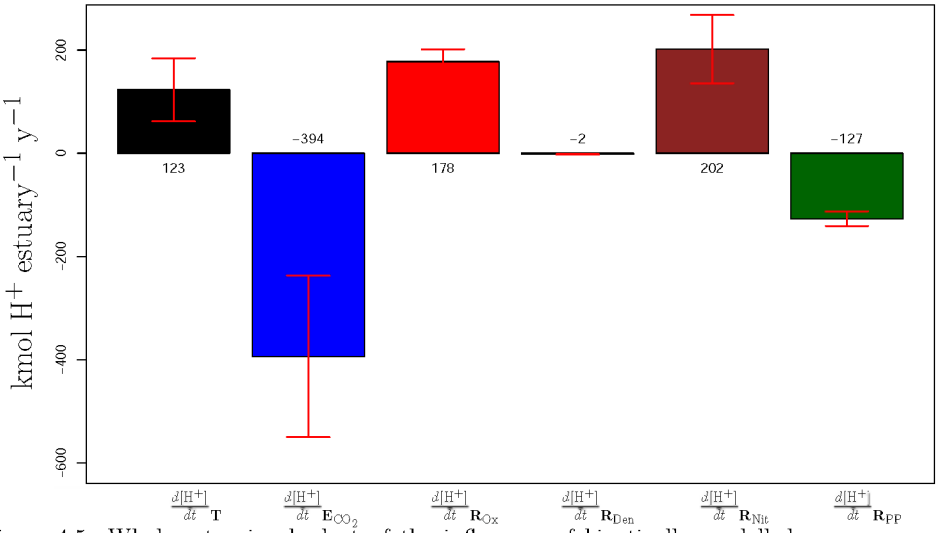

Figure 4.5.: Whole estuarine budget of the influences of kinetically modelled processes on the pH. The errorbars represent the standard deviations resulting from averaging over the four years.

We use model scenarios to investigate the sensitivity of the estuarine pH to changes in freshwater flow and boundary conditions. Fig. 4.7 shows the results of the different model scenarios summarised in Table 4.4.

Around 59% of the pH change in the system from 2001 to 2004 can be attributed to the change in the freshwater discharge (Fig. 4.7a) which also reproduces the general trend of decreasing absolute influences on the proton concentration. Especially the decline in the influence of nitrification can be clearly seen. However, the steep decrease in the influence of transport from 2001 to 2002 and its slight increase from 2003 to 2004 is not reproduced. As shown in Fig. 4.7h, about 44% of the pH change in the system from 2001 to 2004 can be attributed to the change in boundary conditions (Note that in this complex non-linear model the pH changes due to separate freshwater discharge and boundary condition changes are not

necessarily additive). In the more erratic pattern of influences displayed in Fig. 4.7h, one can identify the steep decrease in the influence of transport from 2001 to 2002, as well as its increase between the two following years.

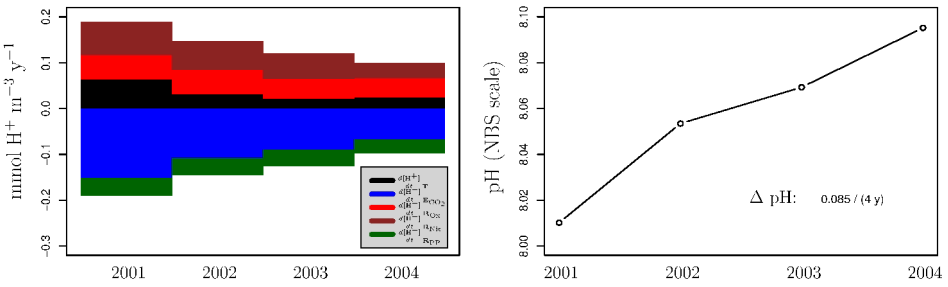

Figure 4.6.: Trends in pH and the influences of major kinetically modelled processes on $[H^+]$ from 2001 to 2004.

Influences via $[\sum CO_2]$ and [TA] are most important for changes in the pH, as changes in freshwater flow for these quantities account for 49% (Fig. 4.7b) and changes in boundary conditions account for 28% (Fig. 4.7i) of the total pH change to the system. However, the pattern of influences in Fig. 4.6 cannot fully be explained by just influences via $[\sum CO_2]$ and [TA]. Especially the decrease in the influence of nitrification and the distinct pattern of the influence of advective-dispersive transport is missing.

Influences via $[\sum NH_4^+]$ are also substantial: the change of freshwater flow accounts for 22% (Fig. 4.7d) and the change of the boundary conditions accounts for 19% (Fig. 4.7k) of the total pH change to the system. It can be seen that the influence is indirect as the influence of nitrification is decreased. Influences via $[\sum NH_4^+]$ allow for a further explanation of the pattern of the influences in Fig. 4.6: in Fig. 4.7k the decrease in the influence of nitrification between 2003 and 2004 is reproduced which most likely entails the counteracting increase in the influence of transport between those years.

Freshwater flow changes for S do not lead to a pH increase but a decrease of 22% primarily via changes in the influence of transport (Fig. 4.7c).

As shown in Fig. 4.7e, f, g, j, l, m, and n the influences of freshwater flow changes for the two organic matter fractions ([FastOM] and [SlowOM]), $[O_2]$ and the rest of the state variables ($[NO_3^-]$, $[\sum HSO_4^-]$, $[\sum B(OH)_3]$, and $[\sum HF]$), as well as the boundary condition changes for S, [FastOM], [SlowOM], $[O_2]$ and the rest of the state variables are minor.

4.4. Discussion

4.4.1. Quantification of proton production and consumption along the estuary

To our knowledge, we are the first to quantify the influences of kinetic processes on the pH for an entire estuarine ecosystem like the Scheldt estuary. Although pH profiles have been sim-

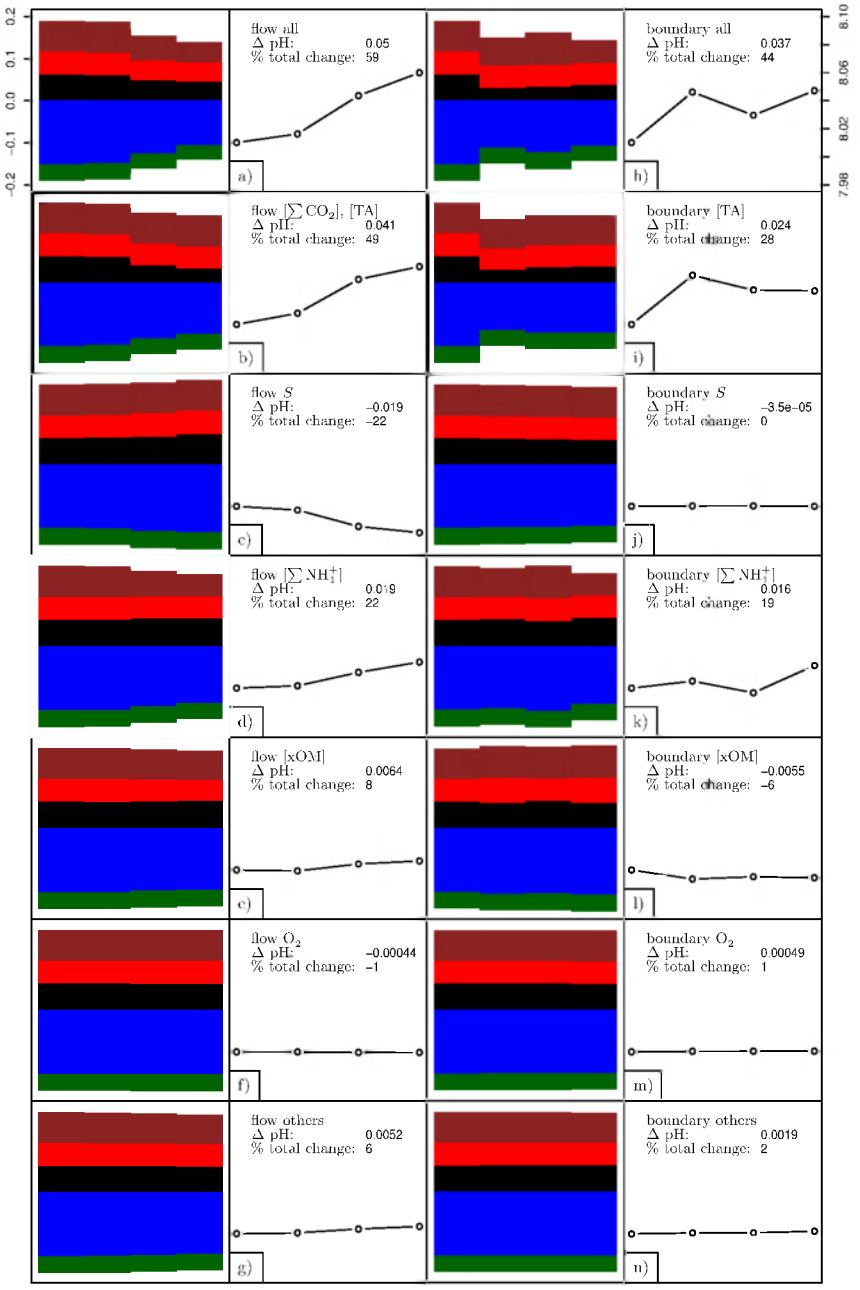

Figure 4.7.: Results of the model scenarios given in Table 4.4 investigating the factors governing the change in the mean estuarine pH from 2001 to 2004. See Fig. 4.6 left side for a legend.

ulated quite accurately (e.g. Regnier et al., 1997; Vanderborght et al., 2002, 2007; Blackford and Gilbert, 2007), (Hofmann et al., 2008c, i.e., Chapter 2), the attribution of pH changes to specific biogeochemical processes has only been done qualitatively. Neglecting minor contributions like primary production and denitrification and the attenuation of gradients due to advective-dispersive transport, the pH profile in the Scheldt estuary is mainly the result of a balance between two biogeochemical reactions, nitrification and oxic mineralisation, which produce protons and CO_2 degassing which consumes protons. This is fully consistent with and supports the findings by Regnier et al. (1997), but our treatment yields more and quantitative information.

The budget of volumetric influences on the proton concentration (Fig. 4.4a; Table 4.5) exhibits the same trumpet like shape (higher values in the upstream region than in the downstream region) as budgets for total ammonium, dissolved inorganic carbon, oxygen, and nitrate (Hofmann et al., 2008c, i.e., Chapter 2). This confirms that high proton turnover is associated to high activity in (kinetically modelled) biogeochemical processes.

Moreover, the budgets for proton production and consumption presented here (Fig. 4.4) are approximately mirror images of the budgets for oxygen sources and sinks (Hofmann et al., 2008c, i.e., Chapter 2). That suggests that proton production and consumption are inversely correlated with oxygen production or consumption. The underlying cause is that oxygen consumption reactions transfer electrons to the oxygen atoms producing reduced oxygen (for example in nitrate or in water). The chemical species that is oxidised (for example the nitrogen in ammonia upon nitrification) is electron-rich before the reaction and electron-depleted and bound to oxygen after the reaction. An electron-rich species, however is more prone to bind electron-depleted protons than an electron poor species. Thus there is a general trend that upon oxidation of a chemical species the electron-depleted protons are produced, and this provides a direct link between the oxygen and the proton budgets in our model.

While CO_2 degassing accounts for the largest total proton turnover per year in the whole estuary, this process acts as a "buffer" for the effects of other processes on the proton concentration, since its magnitude is very sensitive to the current pH of the system. The same holds for the influence of advective-dispersive transport with its buffering character being so pronounced that it changes sign along the estuary. This entails that, given a certain freshwater flow and certain boundary conditions, nitrification and to a lesser extent oxic mineralisation and primary production are the prime factors influencing the pH profile along the estuary, while CO_2 degassing and advective-dispersive transport counteract their effects. This is consistent with findings of Vanderborght et al. (2002) who also identify nitrification in the Scheldt as a process influencing CO_2 degassing via the pH.

The influences of changes in the dissociation constants are several orders of magnitude smaller than the influences of kinetic processes on the proton concentration (Tables 4.5 and 4.6). Therefore, when describing the factors that govern the order of magnitude of the proton concentration of a system, they can be neglected. However, to describe the pH accurately, i.e. more accurate than 0.1 pH units, they should be included. This is especially important for modelling the proton concentration explicitly over a longer period of time, since deviations in $\frac{d[H^+]}{dt}$ are likely to accumulate.

4.4.2. Factors responsible for the change in the mean estuarine pH from 2001 to 2004

Given certain freshwater flow and boundary conditions, advective-dispersive transport mainly "buffers" the effects of other processes on pH within and along averaged estuarine profiles. Nonetheless, interannual changes in advective-dispersive transport due to changes in freshwater flow and boundary conditions are the driving forces for changes in the estuarine mean pH over the years 2001 to 2004.

The general increase in mean estuarine pH from 2001 to 2004 can be attributed to changes in the freshwater flow Q, consistent with Hofmann et al. (2008c, i.e., Chapter 2). Changes in the boundary conditions enforce this general trend and account for small irregularities.

Moreover, changes in freshwater flow and boundary conditions influence the estuarine pH not only "directly" via influences on $[\sum CO_2]$ and [TA], but also "indirectly" by influencing $[\sum NH_4^+]$ which in turn influences the nitrification rates in the estuary. This "indirect" pathway is about half as important as the "direct" influences via $[\sum CO_2]$ and [TA].

The effect of changes in freshwater flow for S, which decreases the pH instead of increasing it, may in part be an artefact specific to the used model implementation as [TA] boundary conditions are calculated from $[\sum CO_2]$ and pH boundary forcing values and S of the first and last model box. This entails that [TA] boundary conditions also slightly change with changes of S in the model, exaggerating the effect of changes in S on the proton concentration.

4.4.3. Synopsis

The main factors governing the pH in the heterotrophic, turbid, tidal Scheldt estuary can be summarised as given in Fig. 4.8. Within the estuary, i.e. with given boundary conditions and freshwater flow, the dependencies depicted with red arrows govern the pH: mainly nitrification and oxic mineralisation (both producing protons) and primary production (consuming protons) influence the proton concentration, an effect which is "buffered" by the effect of CO_2 degassing and advective-dispersive transport. Considering changes of the mean pH in the estuary over the years 2001 to 2004 the dependencies depicted with blue arrows are the governing factors. Changes in boundary conditions and freshwater flow mainly influence $[\sum CO_2]$ and [TA] which can be considered a "direct" effect on the proton concentration. However, changes in boundary conditions and freshwater flow also change $[\sum NH_4^+]$ which in turn influences the effect of nitrification, an "indirect" effect on the proton concentration. This "indirect" effect of changes in boundary conditions and freshwater flow is significant as it amounts to about 50% of the "direct" effect.

4.5. Conclusions

1. A method to quantify the influences of kinetically modelled processes on the pH of a system with time variable acid-base dissociation constants was presented and verified against an existing pH modelling approach.

2. By applying this method to a model of the Scheldt estuary we have identified nitrification as the main process governing the pH profile along the estuary while CO_2 degassing and

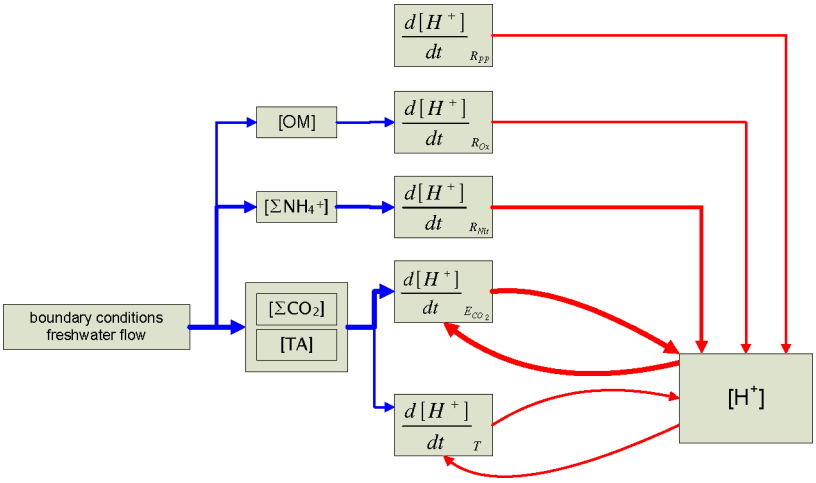

Figure 4.8.: Simplified scheme of the factors governing the pH in a heterotrophic, turbid, tidal estuary: the Scheldt estuary. An arrow pointing from X to Y means: "X influences Y".

advective-dispersive transport (given a certain freshwater flow and certain boundary conditions) "buffer" its effect. However, CO_2 degassing accounts for the largest total proton turnover per year in the whole estuary.

3. A clear inverse correlation between oxygen and proton turnover was found, consistent with theoretical considerations of redox chemistry.

4. While the influences of changes in the dissociation constants might be neglected in approximate whole estuarine budgets, they are important to correctly model the proton concentration explicitly in systems where the acid-base dissociation constants are assumed to be variable over time.

5. The main driver of changes in the mean estuarine pH from 2001 to 2004 is a changing freshwater flow. The pH is influenced "directly" via $[\sum CO_2]$ and [TA] and also – to a significant amount – "indirectly" via $[\sum NH_4^+]$ and the nitrification rates in the estuary.

4.6. Appendix

4.6.1. Partial derivatives

4.6.1.1. Partial derivatives of [TA] with respect to equilibrium invariants

For the work presented here, the partial derivatives of [TA] with respect to the equilibrium invariants (i.e. the terms $\frac{\partial[\mathrm{TA}]}{\partial[\mathrm{X}_j]}$) have been calculated analytically:

$$\frac{\partial[\mathrm{TA}]}{\partial[\sum \mathrm{CO_2}]} = \frac{[\mathrm{H^+}]\mathrm{K_1^*}+2\mathrm{K_1^*K_2^*}}{[\mathrm{H^+}]^2+[\mathrm{H^+}]\mathrm{K_1^*}+\mathrm{K_1^*K_2^*}} \tag{23}$$

$$\frac{\partial[\mathrm{TA}]}{\partial[\sum \mathrm{B(OH)_3}]} = \frac{K^*_{\mathrm{B(OH)_3}}}{[\mathrm{H^+}]+\mathrm{K^*_{B(OH)_3}}} \tag{24}$$

$$\frac{\partial[\mathrm{TA}]}{\partial[\sum \mathrm{NH_4^+}]} = \frac{K^*_{\mathrm{NH_4^+}}}{[\mathrm{H^+}]+\mathrm{K^*_{NH_4^+}}} \tag{25}$$

$$\frac{\partial[\mathrm{TA}]}{\partial[\sum \mathrm{HSO_4^-}]} = -\frac{[\mathrm{H^+}]}{[\mathrm{H^+}]+\mathrm{K^*_{HSO_4^-}}} \tag{26}$$

$$\frac{\partial[\mathrm{TA}]}{\partial[\sum \mathrm{HF}]} = -\frac{[\mathrm{H^+}]}{[\mathrm{H^+}]+\mathrm{K_F^*}} \tag{27}$$

$$\frac{\partial[\mathrm{TA}]}{\partial[\mathrm{H^+}]} = \frac{\partial[\mathrm{HCO_3^-}]}{\partial[\mathrm{H^+}]}+2\frac{\partial[\mathrm{CO_3^{2-}}]}{\partial[\mathrm{H^+}]}+\frac{\partial[\mathrm{B(OH)_4^-}]}{\partial[\mathrm{H^+}]}+\frac{\partial[\mathrm{OH^-}]}{\partial[\mathrm{H^+}]}+\frac{\partial[\mathrm{NH_3}]}{\partial[\mathrm{H^+}]}-\frac{\partial[\mathrm{H^+}]}{\partial[\mathrm{H^+}]}-\frac{\partial[\mathrm{HSO_4^-}]}{\partial[\mathrm{H^+}]}-\frac{\partial[\mathrm{HF}]}{\partial[\mathrm{H^+}]} \tag{28}$$

$$\frac{\partial[\mathrm{HCO_3^-}]}{\partial[\mathrm{H^+}]} = \left(\frac{K_1^*}{[\mathrm{H^+}]\mathrm{K_1^*}+\mathrm{K_1^*K_2^*}+[\mathrm{H^+}]^2}-\frac{[\mathrm{H^+}]\mathrm{K_1^*}\left(2[\mathrm{H^+}]+\mathrm{K_1^*}\right)}{\left([\mathrm{H^+}]\mathrm{K_1^*}+\mathrm{K_1^*K_2^*}+[\mathrm{H^+}]^2\right)^2}\right)[\textstyle\sum \mathrm{CO_2}] \tag{29}$$

$$\frac{\partial[\mathrm{CO_3^{2-}}]}{\partial[\mathrm{H^+}]} = -\frac{K_1^*K_2^*\left(2[\mathrm{H^+}]+\mathrm{K_1^*}\right)}{\left([\mathrm{H^+}]\mathrm{K_1^*}+\mathrm{K_1^*K_2^*}+[\mathrm{H^+}]^2\right)^2}[\textstyle\sum \mathrm{CO_2}] \tag{30}$$

$$\frac{\partial[\mathrm{B(OH)_4^-}]}{\partial[\mathrm{H^+}]} = -\frac{K^*_{\mathrm{B(OH)_3}}}{([\mathrm{H^+}]+\mathrm{K^*_{B(OH)_3}})^2}[\textstyle\sum \mathrm{B(OH)_3}] \tag{31}$$

$$\frac{\partial[\mathrm{OH^-}]}{\partial[\mathrm{H^+}]} = -\frac{K_W^*}{[\mathrm{H^+}]^2} \tag{32}$$

$$\frac{\partial[\mathrm{NH_3}]}{\partial[\mathrm{H^+}]} = -\frac{K^*_{\mathrm{NH_4^+}}}{([\mathrm{H^+}]+\mathrm{K^*_{NH_4^+}})^2}[\textstyle\sum \mathrm{NH_4^+}] \tag{33}$$

$$\frac{\partial[\mathrm{H^+}]}{\partial[\mathrm{H^+}]} = 1 \tag{34}$$

$$\frac{\partial[\mathrm{HSO_4^-}]}{\partial[\mathrm{H^+}]} = \left(\frac{1}{[\mathrm{H^+}]+\mathrm{K^*_{HSO_4^-}}}-\frac{K^*_{\mathrm{HSO_4^-}}}{([\mathrm{H^+}]+\mathrm{K^*_{HSO_4^-}})^2}\right)[\textstyle\sum \mathrm{HSO_4^-}] \tag{35}$$

$$\frac{\partial[\mathrm{HF}]}{\partial[\mathrm{H^+}]} = \left(\frac{1}{[\mathrm{H^+}]+\mathrm{K^*_{HF}}}-\frac{K^*_{\mathrm{HF}}}{([\mathrm{H^+}]+\mathrm{K^*_{HF}})^2}\right)[\textstyle\sum \mathrm{HF}] \tag{36}$$

Note that this list is system specific, e.g. since H_2SO_4 dissociation is not considered an acid-base reaction in our system, HSO_4^- is considered a monoprotic acid.

4.6.1.2. Partial derivatives with respect to and of the dissociation constants

In general, the terms $\sum_i \left(\frac{\partial \mathrm{TA}}{\partial K_i^*}\frac{\partial K_i^*}{\partial S}\right)$, $\sum_i \left(\frac{\partial \mathrm{TA}}{\partial K_i^*}\frac{\partial K_i^*}{\partial T}\right)$, $\sum_i \left(\frac{\partial[\mathrm{TA}]}{\partial[K_i^*]}\frac{\partial K_i^*}{\partial[\sum \mathrm{HSO_4^-}]}\right)$, and $\sum_i \left(\frac{\partial[\mathrm{TA}]}{\partial[K_i^*]}\frac{\partial K_i^*}{\partial[\sum \mathrm{HF}]}\right)$ can be evaluated analytically.

Consider a system where total alkalinity equals carbonate alkalinity

$$[\mathrm{TA}]=[\mathrm{HCO_3^-}]+2[\mathrm{CO_3^{2-}}] \tag{37}$$

$$[\mathrm{TA}]=\frac{[\mathrm{H^+}]\mathrm{K_1^*}+2\mathrm{K_1^*K_2^*}}{[\mathrm{H^+}]^2+[\mathrm{H^+}]\mathrm{K_1^*}+\mathrm{K_1^*K_2^*}}[\sum \mathrm{CO_2}] \tag{38}$$

This means

$$\sum_i\left(\frac{\partial \mathrm{TA}}{\partial K_i^*}\frac{\partial K_i^*}{\partial v}\right) = \frac{\partial \mathrm{TA}}{\partial K_1^*}\frac{\partial K_1^*}{\partial v}+\frac{\partial \mathrm{TA}}{\partial K_2^*}\frac{\partial K_2^*}{\partial v} \tag{39}$$

with $v\in\{T,S,[\sum \mathrm{HSO_4^-}],[\sum \mathrm{HF}]\}$ and

$$\frac{\partial \mathrm{TA}}{\partial K_1^*} = \left(\frac{[\mathrm{H^+}]+2\mathrm{K_2^*}}{[\mathrm{H^+}]\mathrm{K_1^*}+\mathrm{K_1^*K_2^*}+[\mathrm{H^+}]^2}-\frac{([\mathrm{H^+}]+\mathrm{K_2^*})([\mathrm{H^+}]\mathrm{K_1^*}+2\mathrm{K_1^*K_2^*})}{\left([\mathrm{H^+}]\mathrm{K_1^*}+\mathrm{K_1^*K_2^*}+[\mathrm{H^+}]^2\right)^2}\right)[\sum \mathrm{CO_2}] \tag{40}$$

$$\frac{\partial \mathrm{TA}}{\partial K_2^*} = \left(\frac{2K_1^*}{[\mathrm{H^+}]\mathrm{K_1^*}+\mathrm{K_1^*K_2^*}+[\mathrm{H^+}]^2}-\frac{K_1^*([\mathrm{H^+}]\mathrm{K_1^*}+2\mathrm{K_1^*K_2^*})}{\left([\mathrm{H^+}]\mathrm{K_1^*}+\mathrm{K_1^*K_2^*}+[\mathrm{H^+}]^2\right)^2}\right)[\sum \mathrm{CO_2}] \tag{41}$$

K_1^* and K_2^* can be calculated from temperature (T, in Kelvin) and salinity (S), following e.g. Roy et al. (1993b), in the form

$$K_1^* = e^{\left(a_1+\frac{a_2}{T}+a_3\ln(T)+\left(a_4+\frac{a_5}{T}\right)\sqrt{S}+a_6 S+a_7 S^{\frac{3}{2}}\right)} \tag{42}$$

$$K_2^* = e^{\left(b_1+\frac{b_2}{T}+b_3\ln(T)+\left(b_4+\frac{b_5}{T}\right)\sqrt{S}+b_6 S+b_7 S^{\frac{3}{2}}\right)} \tag{43}$$

which allows to write

$$\frac{\partial K_1^*}{\partial T} = K_1^*\frac{\partial[\ln(K_1^*)]}{\partial[T]} = K_1^*\left(\frac{a_3}{T}-\frac{a_2+a_5\sqrt{S}}{T^2}\right) \tag{44}$$

$$\frac{\partial[K_2^*]}{\partial[T]} = K_2^*\frac{\partial[\ln(K_2^*)]}{\partial[T]} = K_2^*\left(\frac{b_3}{T}-\frac{b_2+b_5\sqrt{S}}{T^2}\right) \tag{45}$$

$$\frac{\partial[K_1^*]}{\partial[S]} = K_1^*\frac{\partial[\ln(K_1^*)]}{\partial[S]} = K_1^*\left(a_6+\frac{3a_7\sqrt{S}}{2}+\frac{a_4+\frac{a_5}{T}}{2\sqrt{S}}\right) \tag{46}$$

$$\frac{\partial[K_2^*]}{\partial[S]} = K_2^*\frac{\partial[\ln(K_2^*)]}{\partial[S]} = K_2^*\left(b_6+\frac{3b_7\sqrt{S}}{2}+\frac{b_4+\frac{b_5}{T}}{2\sqrt{S}}\right) \tag{47}$$

Without loss of generality, we assume K_1^* and K_2^* to be calculated on the seawater pH scale and then converted to the free proton scale. According to Dickson (1984) and Zeebe and Wolf-Gladrow (2001)

$$K_i^{*,\mathrm{free}} = K_i^{*,\mathrm{SWS}}\Big/\left(1+\frac{[\sum \mathrm{HSO_4^-}]}{K_{\mathrm{HSO_4^-}}^{*,\mathrm{free}}}+\frac{[\sum \mathrm{HF}]}{K_{\mathrm{HF}}^{*,\mathrm{free}}}\right) \tag{48}$$

with $K_{\mathrm{HSO_4^-}}^{*,\mathrm{free}}$ and $K_{\mathrm{HF}}^{*,\mathrm{free}}$ being calculated on the free proton scale directly. This leads to

$$\frac{\partial K_i^{*,\mathrm{free}}}{\partial[\sum \mathrm{HSO_4^-}]}=-\left(K_i^{*,\mathrm{SWS}}\Big/\left(K_{\mathrm{HSO_4^-}}^{*,\mathrm{free}}\left(1+\frac{[\sum \mathrm{HSO_4^-}]}{K_{\mathrm{HSO_4^-}}^{*,\mathrm{free}}}+\frac{[\sum \mathrm{HF}]}{K_{\mathrm{HF}}^{*,\mathrm{free}}}\right)^2\right)\right) \tag{49}$$

$$\frac{\partial K_i^{*,\mathrm{free}}}{\partial[\sum \mathrm{HF}]} = -\left(K_i^{*,\mathrm{SWS}} \Big/ \left(K_{\mathrm{HF}}^{*,\mathrm{free}} \left(1 + \frac{[\sum \mathrm{HSO}_4^-]}{K_{\mathrm{HSO}_4^-}^{*,\mathrm{free}}} + \frac{[\sum \mathrm{HF}]}{K_{\mathrm{HF}}^{*,\mathrm{free}}} \right)^2 \right) \right) \tag{50}$$

The above shows that even with the simplest possible example, calculating $\sum_i \left(\frac{\partial \mathrm{TA}}{\partial K_i^*} \frac{\partial K_i^*}{\partial S} \right)$, $\sum_i \left(\frac{\partial \mathrm{TA}}{\partial K_i^*} \frac{\partial K_i^*}{\partial T} \right)$, $\sum_i \left(\frac{\partial [\mathrm{TA}]}{\partial [K_i^*]} \frac{\partial K_i^*}{\partial [\sum \mathrm{HSO}_4^-]} \right)$, and $\sum_i \left(\frac{\partial [\mathrm{TA}]}{\partial [K_i^*]} \frac{\partial K_i^*}{\partial [\sum \mathrm{HF}]} \right)$ analytically yields lengthy expressions. These become increasingly more intractable as the definition of [TA] becomes more complex.

Therefore, we decided to calculate these terms numerically by calculating [TA] twice with small disturbances of the independent variable

$$\sum_i \left(\frac{\partial \mathrm{TA}}{\partial K_i^*} \frac{\partial K_i^*}{\partial S} \right) = \Big(TA([\mathrm{H}^+], \mathrm{X}, \mathrm{K}^*(\mathrm{S}+\epsilon_{\mathrm{S}}, \mathrm{T}, [\sum \mathrm{HSO}_4^-], [\sum \mathrm{HF}])) \tag{51}$$

$$- TA([\mathrm{H}^+], \mathrm{X}, \mathrm{K}^*(\mathrm{S}-\epsilon_{\mathrm{S}}, \mathrm{T}, [\sum \mathrm{HSO}_4^-], [\sum \mathrm{HF}])) \Big) / 2\epsilon_{\mathrm{S}} \tag{52}$$

$$\sum_i \left(\frac{\partial \mathrm{TA}}{\partial K_i^*} \frac{\partial K_i^*}{\partial T} \right) = \Big(TA([\mathrm{H}^+], \mathrm{X}, \mathrm{K}^*(\mathrm{S}, \mathrm{T}+\epsilon_{\mathrm{T}}, [\sum \mathrm{HSO}_4^-], [\sum \mathrm{HF}])) \tag{53}$$

$$- TA([\mathrm{H}^+], \mathrm{X}, \mathrm{K}^*(\mathrm{S}, \mathrm{T}-\epsilon_{\mathrm{T}}, [\sum \mathrm{HSO}_4^-], [\sum \mathrm{HF}])) \Big) / 2\epsilon_{\mathrm{T}} \tag{54}$$

$$\sum_i \left(\frac{\partial \mathrm{TA}}{\partial K_i^*} \frac{\partial K_i^*}{\partial [\sum \mathrm{HSO}_4^-]} \right) = \Big(TA([\mathrm{H}^+], \mathrm{X}, \mathrm{K}^*(\mathrm{S}, \mathrm{T}, [\sum \mathrm{HSO}_4^-] + \epsilon_{[\sum \mathrm{HSO}_4^-]}, [\sum \mathrm{HF}])) \tag{55}$$

$$- TA([\mathrm{H}^+], \mathrm{X}, \mathrm{K}^*(\mathrm{S}, \mathrm{T}, [\sum \mathrm{HSO}_4^-] - \epsilon_{[\sum \mathrm{HSO}_4^-]}, [\sum \mathrm{HF}])) \Big) / 2\epsilon_{\mathrm{S}} \tag{56}$$

$$\sum_i \left(\frac{\partial \mathrm{TA}}{\partial K_i^*} \frac{\partial K_i^*}{\partial [\sum \mathrm{HF}]} \right) = \Big(TA([\mathrm{H}^+], \mathrm{X}, \mathrm{K}^*(\mathrm{S}, \mathrm{T}, [\sum \mathrm{HSO}_4^-], [\sum \mathrm{HF}] + \epsilon_{[\sum \mathrm{HF}]})) \tag{57}$$

$$- TA([\mathrm{H}^+], \mathrm{X}, \mathrm{K}^*(\mathrm{S}, \mathrm{T}, [\sum \mathrm{HSO}_4^-], [\sum \mathrm{HF}] - \epsilon_{[\sum \mathrm{HF}]})) \Big) / 2\epsilon_{\mathrm{T}} \tag{58}$$

with $\epsilon_v = 0.1v \forall v \in \{T, S, [\sum \mathrm{HSO}_4^-], [\sum \mathrm{HF}]\}$. Note that $[\sum \mathrm{HSO}_4^-]$ and $[\sum \mathrm{HF}]$ are only perturbed for calculating the dissociation constants and kept at their normal values when they serve as equilibrium invariants (total quantities) for calculating $[\mathrm{HSO}_4^+]$ and [HF].

5. Buffering, stoichiometry, and the sensitivity of pH to biogeochemical and physical processes: a proton-based model perspective

A. F. Hofmann, J. J. Middelburg, K. Soetaert, D. A. Wolf-Gladrow, and F. J. R. Meysman
(submitted to Geochimica et Cosmochimica Acta)

Abstract

Mechanistic understanding of factors governing pH is essential, given growing concern about ocean acidification. The classical approach to carbonate chemistry and pH calculations is centred around the alkalinity concept. In this publication, the classical approach is taken one step further: the influences of biogeochemical and physical processes on the pH are calculated directly, without the detour of alkalinity. The influence of a given process on pH is expressed by its process rate, modulated by a sensitivity factor. Here, we provide the necessary tools and procedures to calculate this sensitivity factor analytically for an arbitry process. Moreover, we show that the sensitivity can be decomposed as the ratio of a particular stoichiometric coefficient of protons over a buffer factor. The stoichiometric coefficient can be derived by describing the process using a *fractional reaction equation at ambient pH* and it represents the protons that are released by the process without accounting for re-equilibration. The presented approach thus provides a chemical interpretation of the mechanisms underlying pH changes in aquatic systems. Applying the concept of buffer capacity and pH sensitivities to an averaged global ocean shows that towards the end of the century the ocean will be around four times less buffered than it is today. This demonstrates how the concepts and tools presented here can make a complementary contribution to the existing modelling approaches of ocean acidification.

5.1. Introduction

The antropogenic release of carbon dioxide to the atmosphere leads to acidification of the global surface waters (IPCC, 2007; Zeebe et al., 2008) which is likely to have an adverse effect on aquatic ecosystems (Orr et al., 2005; Kleypas et al., 2006; Gazeau et al., 2007; Guinotte and Fabry, 2008). In response, there is currently a large effort by the scientific community to better understand past, present and future changes in the pH of natural waters. A crucial task is to quantify how large those changes are and to better understand how biogeochemical processes are driving or modulating these pH changes. Therefore, over the last few years, a range of modelling approaches have been advanced that describe the pH evolution of open waters (e.g. Follows et al., 2006; Soetaert et al., 2007; Wolf-Gladrow et al., 2007), (Hofmann et al., 2008a, i.e., Chapter 3) as well as interstitial pore water in sediments (e.g. Marinelli and Boudreau, 1996; Boudreau, 1996a; Gehlen et al., 1999; Luff et al., 2001; Jourabchi et al., 2005).

The classical approach to carbonate chemistry and pH calculations in natural waters is centred around the alkalinity concept (Morel and Hering, 1993; Stumm and Morgan, 1996; Zeebe and Wolf-Gladrow, 2001). To quantify pH changes, one essentially uses a two-step approach. First, one quantifies the influence of biogeochemical processes on the alkalinity, which then results in a suitable alkalinity change for the system at hand. In a second step, one translates this alkalinity change into a corresponding pH change using a procedure that typically involves a pH equilibration algorithm. In essence, one uses the alkalinity as a mediator between biogeochemical processes on the one hand and the observed or modelled pH changes on the other hand. However, because of this two-step process, there is no direct link between the biogeochemical processes on the one hand, and pH changes on the other hand. In other words, the current approach to pH modelling does not allow for a direct quantification of the influence of an individual biogeochemical process on the proton concentration.

In this paper, we propose an extension of the current alkalinity centered approach, which puts protons at the center of attention, and which enables a direct quantification of the effects of biogeochemical processes on pH. The central idea is that the total rate of change of protons can be decomposed as a linear combination of the biogeochemical process rates. The coefficients in this expression quantify a *sensitivity* of the pH to each biogeochemical process, which determines how strongly this biogeochemical process will influence the pH. This way, one can directly compare the influences of different processes on the pH.

This paper is an extension and generalization of the pH modelling framework detailed in Hofmann et al. (2008a, i.e., Chapter 3), which itself was based on earlier work by Jourabchi et al. (2005), Soetaert et al. (2007) and Wolf-Gladrow et al. (2007). In Hofmann et al. (2008a, i.e., Chapter 3), we primarily concentrated on the numerical aspects of pH modelling, while here, we principally focus on concepts and chemical interpretation. To promote understanding, and to keep the mathematical expressions within reasonable limits, we will outline our approach by means of a simple example, which only incorporates a restricted number of processes ($CaCO_3$ precipitation, CO_2 exchange across the air-water interface, and the carbonate acid-base system). The approach is, however, entirely general and can be extended to any set of reaction and transport processes as well as to any number of acid-base systems. These generalizations are presented in the Appendices.

5.2. Two pH modelling approaches

5.2.1. Problem statement

Assume that on a given day, a water reservoir is sampled and total alkalinity ([TA]), dissolved inorganic carbon ($[\sum CO_2]$) as well as the pH are measured. Twenty days later, the reservoir is sampled again, and the measurements are repeated. The acquired data are given in Table (5.1).

	t = 0 d	t = 20 d	Δ	unit
[TA]	2200	1963	-237	μmol kg^{-1}
$[\sum CO_2]$	2000	1864	-136	μmol kg^{-1}
pH	8.165	7.923	-0.242	-

Table 5.1.: Parameters of the example water reservoir at the begin and the end of a 20 day period; Note that throughout this paper, the pH is defined on the free hydrogen ion concentration scale (Dickson, 1981; Zeebe and Wolf-Gladrow, 2001): $pH = -\log([H^+])$ and hence the term "proton concentration" will refer to the concentration of the free hydrogen ion.

To better understand the observed pH changes, a model can be developed which describes the pH evolution over the 20 day observational period. From previous studies, it is known that the pH chemistry of the reservoir is mainly influenced by $CaCO_3$ precipitation and CO_2 exchange across the air-water interface. These are the two dominant "slow" kinetic processes that drive the biogeochemical changes in the reservoir over a time scale of days. They can be represented by the reaction equations

$$Ca^{2+} + CO_3^{2-} \rightarrow CaCO_3 \quad (1)$$

$$CO_2(g) \rightleftharpoons CO_2 \quad (2)$$

where $CO_2(g)$ represents CO_2 in the atmosphere. In addition, the pH chemistry will also depend on a number of "fast" acid-base dissociation reactions, with characteristic time scales of less than a minute (Zeebe and Wolf-Gladrow, 2001, discuss these timescales in detail). To keep the model suitably simple, only the carbonate system is accounted for

$$CO_2 + H_2O \rightleftharpoons HCO_3^- + H^+ \quad (3)$$

$$HCO_3^- \rightleftharpoons CO_3^{2-} + H^+ \quad (4)$$

The reaction equations (1) to (4) provide a conceptual model of the water chemistry inside the reservoir. This model needs to be translated into a suitable set of differential equations, that not only reproduces the measured values at the end of the 20 day period, but also answers the following two research questions:

1. How did the pH evolve in between the sampling times?
2. Which of the two slow kinetic "driving" processes (calcite precipitation or CO_2 exchange) affects the pH change the most?

Clearly, the primary goal of this model is to predict the evolution of the pH, or equally the proton concentration, as a function of time. Hence, formally, the model should include an equation of the form

$$\frac{d[H^+]}{dt} = f(\mathbf{R}_P, \mathbf{R}_C) \quad (5)$$

where $\mathbf{R}_P$ is the net forward rate of carbonate precipitation and $\mathbf{R}_C$ denotes the net rate of CO_2 exchange. The pH evolution equation (5) expresses the rate of change of the proton concentration as a function of the rates of the "driving" processes. It is important to note that the right hand side of this equation only depends on the rates of the slow kinetic processes. This is because, on the relatively long time-scale of the model, i.e., days, only carbonate precipitation and CO_2 exchange are "driving" the concentration changes within the reservoir. The fast dissociation reactions can be assumed in thermodynamic equilibrium at all times, and as a result, their net forward rates become implicitly dependent on the rates of the slow kinetic processes. A more general and detailed discussion of this important aspect is given in Appendix 5.7.1.

When available, the pH evolution equation (5) certainly is a valuable tool to analyze pH changes in natural systems. It directly links the pH change (the left hand side) to the biogeochemical processes that drive this pH change (the right hand side). However, a key problem with the current approaches to pH modelling is that an equation like (5) is not made available in an explicit form. This is because the conventional approach to carbonate chemistry and pH calculations in natural waters is focused on alkalinity rather than protons. In other words, one explicitly quantifies the effect of biogeochemical processes on alkalinity, but their concomitant effect on protons is only indirectly accounted for. In the next section, we show how a pH model for our reservoir is constructed following the conventional "alkalinity centered" procedure. In a subsequent section, we will show how this conventional modelling approach can be extended, such that an explicit pH evolution equation like Eq. (5) is obtained.

5.2.2. The implicit pH modelling approach

The construction of a biogeochemical model traditionally starts by listing the mass balance equations for the relevant chemical species in the system. In our example, we will track the concentrations of one[1] kinetic species (i.e., species that only participates in slow kinetic processes: $[CaCO_3]$) and four equilibrium species (i.e., species that participate in one of the fast equilibrium reactions: $[CO_2]$, $[HCO_3^-]$, $[CO_3^{2-}]$, and $[H^+]$). The differential mass balance equations for these species are listed in sections (a1) and (a2) of Table (5.2).

A first problem that needs to be resolved is that the mass balances for the equilibrium species still contain the net forward reaction rates of the fast equilibrium reactions, which are not explicitly known. These reactions are not modelled via kinetic expressions, but are assumed to reside in thermodynamic equilibrium at all times. This makes each of their net forward rates an implicit function of the rates of the slow kinetically modelled processes (see also Appendix 5.7.1). Yet, through a suitable linear combination, known as a *transformation into canonical form*, these equilibrium rates can be removed from the equation set (Lichtner, 1996; Meysman, 2001), (Hofmann et al., 2008a, i.e., Chapter 3). As a result, one obtains the reduced equation set (see sections (b) and (c) in Table 5.2 for the derivation of these equations)

$$\frac{d[\mathrm{TA}]}{dt} = -2\mathbf{R}_P \tag{6}$$

$$\frac{d[\sum \mathrm{CO}_2]}{dt} = \mathbf{R}_C - \mathbf{R}_P \tag{7}$$

[1] $[Ca^{2+}]$ is assumed constant. If it was dynamically modelled, it would be a kinetic species as well, since it does not participate in any equilibrium reactions.

Rather than the dissociated species, these mass balance equations now feature the *total quantities* alkalinity ([TA]) and dissolved inorganic carbon ($[\sum CO_2]$). These equations describe the time evolution of [TA] and $[\sum CO_2]$ and form the core of the conventional "alkalinity-centred" approach to pH modeling. Both the [TA] and $[\sum CO_2]$ changes are expressed as a function of the rates of the driving kinetic processes (here $\mathbf{R}_P$ and $\mathbf{R}_C$). Employing suitable kinetic rate laws for the kinetic processes, these evolution equations can be integrated. Rate expressions for carbonate precipitation and CO_2 exchange for our example are provided in section (e) of Table (5.2).

Technically, the total quantities [TA] and $[\sum CO_2]$ are termed *invariant* with respect to the fast equilibrium reactions, because they are no longer influenced by the underlying acid-base equilibria (and thus they are also invariant to temperature and pressure changes that affect these equilibria[2]). Note that in the usual model development procedure, one will not explicitly consider the transformation into canonical form. Instead, the evolution equations for [TA] and $[\sum CO_2]$ (Eqs. 6 and 7) are immediately written, while the specific form of the alkalinity in Eq. (16) is postulated (see Dickson, 1981; Wolf-Gladrow et al., 2007) rather than derived[3].

Table (5.2) details all necessary information, and so, the model can be solved. The direct integration of the evolution equations for [TA] and $[\sum CO_2]$ (Eqs. 6 and 7) should allow for a calculation of [TA](t) and $[\sum CO_2](t)$ at any future time t starting from some initial values $[TA](t_0)$ and $[\sum CO_2](t_0)$. However, such a direct integration is not possible. The problem is that the kinetic rate expressions are not specified in terms of [TA] and $[\sum CO_2]$, but feature the concentrations of the equilibrium species $[CO_2]$ and $[CO_3^{2-}]$.

To overcome this problem, numerical pH modelling procedures typically use a two-step approach (e.g. Ben-Yaakov, 1970; Culberson, 1980; Luff et al., 2001; Follows et al., 2006). This two step procedure includes an additional "equilibration step". During every timestep of the numerical integration of the evolution equations for alkalinity and dissolved inorganic carbon (Eqs. 6 and 7), the current values [TA](t) and $[\sum CO_2](t)$ (starting with $[TA](t_0)$ and $[\sum CO_2](t_0)$ in the first timestep), are used to calculate a full speciation, i.e., to calculate the concentrations of all equilibrium species. For our example, those equilibrium species concentrations are the concentrations of all three carbonate species and the proton concentration. Because of the non-linearity of the equilibrium mass action equations in the proton concentration $[H^+]$, which is an unknown here, this calculation must be performed using a numerical procedure (e.g. numerical root finding). The concentrations of the equilibrium species are then used to calculate the rates of all kinetically modelled processes (here $[CO_2](t)$ is used

[2] [TA] is not invariant with respect to changes in S. This is because the borate system is part of salinity and therefore the total borate concentration always changes simultaneously with S. However, from the given equations one can infer that [TA] is invariant with respect to the effects of changing S on the acid-base dissociation constants in the system.

[3] Here, we explicitly include the transformation into canonical form in Table (5.2), because it demonstrates the implicit logic that lies behind this procedure. It shows one does not need to postulate the definition of alkalinity as such. The alkalinity is essentially a derived quantity, whose specific form directly follows from the linear combination of the mass balances of the equilibrium species in the biogeochemical model. Obviously, the linear combination is done deliberately in a certain way to obtain a subset of Dickson's (Dickson, 1981) total alkalinity in order to be consistent with other works and alkalinity measurement techniques (Gran, 1952; Hansson and Jagner, 1973; Dickson, 1981; DOE, 1994; Anderson et al., 1999; Dickson et al., 2007).

(a1) The mass balance for the kinetic species is:

$$\frac{d[\mathrm{CaCO_3}]}{dt} = \mathbf{R}_P \tag{8}$$

(a2) The mass balances for the equilibrium species are:

$$\frac{d[\mathrm{CO_2}]}{dt} = -\mathbf{R}_{\mathrm{CO_2diss}} + \mathbf{R}_C \tag{9}$$

$$\frac{d[\mathrm{HCO_3^-}]}{dt} = \mathbf{R}_{\mathrm{CO_2diss}} - \mathbf{R}_{\mathrm{HCO_3^-diss}} \tag{10}$$

$$\frac{d[\mathrm{CO_3^{2-}}]}{dt} = \mathbf{R}_{\mathrm{HCO_3^-diss}} - \mathbf{R}_P \tag{11}$$

$$\frac{d[\mathrm{H^+}]}{dt} = \mathbf{R}_{\mathrm{CO_2diss}} + \mathbf{R}_{\mathrm{HCO_3^-diss}} \tag{12}$$

(b) Removing the net forward rates of the fast processes by linear combination provides:

$$(8) + 2\,(9) - (10) = \frac{d\left([\mathrm{HCO_3^-}] + 2[\mathrm{CO_3^{2-}}] - [\mathrm{H^+}]\right)}{dt} = -2\mathbf{R}_P \tag{13}$$

$$(7) + (8) + (9) = \frac{d\left([\mathrm{CO_2}] + [\mathrm{HCO_3^-}] + [\mathrm{CO_3^{2-}}]\right)}{dt} = \mathbf{R}_C - \mathbf{R}_P \tag{14}$$

$$\tag{15}$$

(c) The total quantities or equilibrium invariants are thus defined as:

$$[\mathrm{TA}] = [\mathrm{HCO_3^-}] + 2[\mathrm{CO_3^{2-}}] - [\mathrm{H^+}] \tag{16}$$

$$[\textstyle\sum \mathrm{CO_2}] = [\mathrm{CO_2}] + [\mathrm{HCO_3^-}] + [\mathrm{CO_3^{2-}}] \tag{17}$$

(d) The equilibrium mass action equations are:

$$K_1^* = \frac{[\mathrm{H^+}][\mathrm{HCO_3^-}]}{[\mathrm{CO_2}]} \tag{18}$$

$$K_2^* = \frac{[\mathrm{H^+}][\mathrm{CO_3^{2-}}]}{[\mathrm{HCO_3^-}]} \tag{19}$$

(e) The kinetic rate laws are:

$$\mathbf{R}_P = k_P\,(1-\Omega)^n \tag{20}$$

$$\mathbf{R}_C = k_C\,([\mathrm{CO_2}]_{sat} - [\mathrm{CO_2}]) \tag{21}$$

Table 5.2.: *The pH model development procedure (see Hofmann et al., 2008a, i.e., Chapter 3, for details)*: **(a)** The mass conservation equations for all relevant chemical species are listed. A distinction is made between kinetic species and equilibrium species. The mass balances of the equilibrium species contain at least one rate of a fast "equilibrium" reaction. **(b)** By a suitable linear combination, the rates of the fast equilibrium reactions can be removed from the differential equations of the equilibrium species. We arrive at a reduced equation set where the number of transformed equations (2) always equals the original number of mass balances (4) minus the number of equilibrium reactions (2). **(c)** The definition of [TA] and $[\sum \mathrm{CO_2}]$ follows from the transformed equations. **(d)** The transformed equations themselves are not sufficient for a complete model statement since the system would be underdetermined. We need to add the equilibrium mass action laws for the fast reactions in order to close the model formulation. The K^*'s denote stoichiometric equilibrium constants, as opposed to thermodynamic or hybrid equilibrium constants; see Zeebe and Wolf-Gladrow (2001) for a discussion of different types of equilibrium constants **(e)** Rate laws for the slow "kinetic" reactions. $\Omega = [\mathrm{Ca^{2+}}][\mathrm{CO_3^{2-}}]/K^*_{spc}$ is the calcite saturation state of the water with K^*_{spc} being the stoichiometric solubility product for calcite.

to calculate $\mathbf{R}_C(t)$, and $[CO_3^{2-}](t)$ is used to calculate $\mathbf{R}_P(t)$). Those rates, in turn, are employed for the numerical integration of the evolution equations for [TA] and $[\sum CO_2]$ (Eqs. 6 and 7) over some time step Δt to arrive at $[TA](t + \Delta t)$ and $[\sum CO_2](t + \Delta t)$.

By repeating this two-step procedure for a suitable sequence of time steps, one eventually obtains the evolution of [TA], $[\sum CO_2]$ and pH over the desired time interval. The simulated pH evolution is not directly obtained from an evolution equation like Eq. (5). Instead, the pH is implicitly determined from the time evolution of the [TA] and $[\sum CO_2]$. Therefore, we call this the *implicit pH modelling approach* (in Hofmann et al. (2008a, i.e., Chapter 3) this approach was called *operator splitting approach* because of the two-step procedure). Figure (5.1) shows the results of this implicit modelling procedure for our water reservoir over the 20 day period[4]. The parameter values that were used are summarized in Table (5.3).

Symbol	Value	Units	Reference
S	35	-	
T	15	C	
K_1^*	9.386	μmol kg^{-1}	(Roy et al., 1993b)
K_2^*	6.685 10^{-4}	μmol kg^{-1}	(Roy et al., 1993b)
$[Ca^{2+}]$	1.028 10^4	μmol kg^{-1}	(DOE, 1994)
K_{spc}^*	4.315 10^5	(μmol kg^{-1})^2	(Mucci, 1983)
k_P	1.0	μmol kg^{-1}	
n	2.0	-	
$K0_{CO_2}$	3.746 10^4	μmol kg^{-1}atm^{-1}	(Weiss, 1974)
pCO_2	383.0	μatm	(Guinotte and Fabry, 2008)
k_C	0.5	d^{-1}	

Table 5.3.: Parameter values used in the model of the water reservoir.

As shown by the pH evolution in Fig. (5.1), the implicit modelling procedure is able to predict how the pH changes over time, and so it is able to answer our first research question ("How did the pH evolve in between the sampling times?"). That means, to model the pH dynamics, one does not need an explicit evolution equation like Eq. (5). Yet, the absence of such an evolution equation also has an important disadvantage: the implicit pH modelling approach is not able to answer our second question ("Which one of the slow kinetic processes affected the pH change the most?"). We are not able to check whether carbonate precipitation or CO_2 exchange is the main responsible process for the observed pH changes. In the implicit pH modelling approach, the link between kinetic processes and pH changes is obscured by the numerical equilibration step.

5.2.3. The explicit pH modelling approach

An evolution equation of the form of Eq. (5) would be a valuable tool to improve our understanding of pH changes in natural waters. It shows how different kinetic processes separately contribute to the pH change. The derivation of such an equation is rather straightforward. At equilibrium, it is well known that all quantities in the carbonate system ([TA], $[\sum CO_2]$,

[4] All model implementations discussed in this paper have been coded in the statistical programming language `R` (R Development Core Team, 2005) using the packages `deSolve` (Soetaert et al., 2008) and `AquaEnv` (Hofmann et al., 2008b). The code can be obtained from the corresponding author.

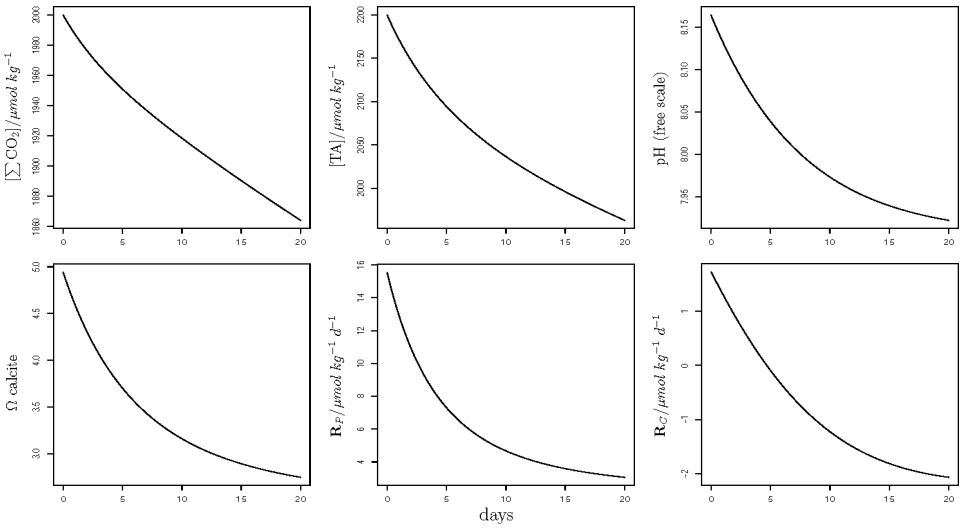

Figure 5.1.: Changes in key variables of the example system over the course of 20 days, calculated with the implicit pH modelling approach.

$[CO_2]$, $[HCO_3^-]$, $[CO_3^{2-}]$, and $[H^+]$) can be calculated from any combination of two components from this list. Taking the proton and $[\sum CO_2]$ concentrations as the primary components, we can express alkalinity [TA] as a function of these two components

$$[TA] = [TA]\left([\textstyle\sum CO_2], [H^+]\right) = \left(\alpha_1\left([H^+]\right) + 2\,\alpha_2\left([H^+]\right)\right)[\textstyle\sum CO_2] - [H^+] \tag{22}$$

where we introduced the ionization fractions α_i as functions of the proton concentration $[H^+]$ in the usual way (Skoog and West, 1982; Stumm and Morgan, 1996)

$$\alpha_0 = \frac{[CO_2]}{[\sum CO_2]} = \frac{[H^+]^2}{[H^+]^2 + K_1^*[H^+] + K_1^*K_2^*} \tag{23}$$

$$\alpha_1 = \frac{[HCO_3^-]}{[\sum CO_2]} = \frac{K_1^*[H^+]}{[H^+]^2 + K_1^*[H^+] + K_1^*K_2^*} \tag{24}$$

$$\alpha_2 = \frac{[CO_3^{2-}]}{[\sum CO_2]} = \frac{K_1^*K_2^*}{[H^+]^2 + K_1^*[H^+] + K_1^*K_2^*} \tag{25}$$

Both $[\sum CO_2]$ and $[H^+]$ are functions of time, while the equilibrium constants K_1^* and K_2^* are considered constant over time (Hofmann et al. (2009a, i.e., Chapter 4) describe an explicit pH modelling approach with time variable K^*'s). So differentiating both the left and right hand side of Eq. (22) with respect to time by applying the chain rule of differentiation, one immediately arrives at[5]

$$\frac{d[TA]}{dt} = \left(\frac{\partial[TA]}{\partial[H^+]}\right)\frac{d[H^+]}{dt} + \left(\frac{\partial[TA]}{\partial[\sum CO_2]}\right)\frac{d[\sum CO_2]}{dt} \tag{26}$$

[5]Note that this procedure is equivalent to constructing the total differential of [TA] as function of $[\sum CO_2]$ and $[H^+]$ and then dividing it by dt.

A simple rearrangement of terms directly provides following expression for the rate of change of the proton concentration

$$\frac{d[\mathrm{H}^+]}{dt} = \frac{1}{\left(\frac{\partial[\mathrm{TA}]}{\partial[\mathrm{H}^+]}\right)}\left(\frac{d[\mathrm{TA}]}{dt} - \left(\frac{\partial[\mathrm{TA}]}{\partial[\sum \mathrm{CO}_2]}\right)\frac{d[\sum \mathrm{CO}_2]}{dt}\right) \tag{27}$$

This expression features the rate of change of both alkalinity and $[\sum \mathrm{CO}_2]$. However, these terms were already known from the evolution equations of these quantities (Eqs.(6) and (7)). Accordingly, upon substitution, we finally arrive at

$$\frac{d[\mathrm{H}^+]}{dt} = S_P \mathbf{R}_P + S_C \mathbf{R}_C \tag{28}$$

with

$$S_P = \frac{1}{\left(\frac{\partial[\mathrm{TA}]}{\partial[\mathrm{H}^+]}\right)}\left(-2 + \frac{\partial[\mathrm{TA}]}{\partial[\sum \mathrm{CO}_2]}\right) \tag{29}$$

$$S_C = \frac{1}{\left(\frac{\partial[\mathrm{TA}]}{\partial[\mathrm{H}^+]}\right)}\left(-\frac{\partial[\mathrm{TA}]}{\partial[\sum \mathrm{CO}_2]}\right) \tag{30}$$

Equation (28) matches the pH evolution equation (5). The terms S_P and S_C will be called the *sensitivity* of pH with respect to $CaCO_3$ precipitation and CO_2 exchange respectively. An important aspect is that these sensitivities can be calculated in a closed analytical form: although the calculation of $[\mathrm{H}^+]$ from $[\sum \mathrm{CO}_2]$ and [TA] requires a numerical solution, the partial derivatives in Eqs. (29) and (30) can be analytically calculated from the expression for the alkalinity Eq. (22).

Equation (28) provides a true evolution equation for the proton concentration (i.e., the pH). This differential equation can be directly integrated together with the evolution equation for $[\sum \mathrm{CO}_2]$ (Eq. (7)). This immediately provides the evolution of $[\sum \mathrm{CO}_2]$ and pH over the desired time interval. Direct integration thus allows us to calculate the values of $[\mathrm{H}^+](t)$ and $[\sum \mathrm{CO}_2](t)$ at any future time t starting from the initial values $[\mathrm{H}^+](t_0)$ and $[\sum \mathrm{CO}_2](t_0)$. The concentrations for the other components of the carbonate system (that is, [TA], $[CO_2]$, $[HCO_3^-]$, $[CO_3^{2-}]$) can be calculated analytically from $[\mathrm{H}^+](t)$ and $[\sum \mathrm{CO}_2](t)$. This means that the numerical solution of a nonlinear equation system in every timestep is no longer required[6]. Because an explicit evolution equation for the proton concentration is integrated, we call this the *explicit pH modelling approach* (in Hofmann et al. (2008a, i.e., Chapter 3) this approach was called *direct substitution approach* because of the substitution of the alkalinity evolution equation by the proton evolution equation).

Apart from the direct integration, the explicit modelling approach also has an important conceptual advantage in terms of understanding pH changes. The analytical expressions for the sensitivities S_P and S_C allow a systematic investigation of how biogeochemical and physical processes influence pH. The pH evolution equation (28) specifies that the influence of a given process on the pH can always be decomposed as a modulating factor, which is the sensitivity

[6] This is the case since the equilibrium mass action equations are only nonlinear with respect to the variable $[\mathrm{H}^+]$, which is now part of the direct integration and therefore not an unknown any more.

of the pH with respect to that process, times the process rate. Processes may have high rates, but a low sensitivity, and vice versa. Accordingly, to examine the overall influence of a kinetic process on the pH, one must look at the combination of both sensitivity and process rate.

The sensitivities S_P and S_C as well as their products with the associated reaction rates R_P and R_C, respectively, are shown for our water reservoir problem in Fig. (5.2). Both the sensitivities as well as the reaction rates change over time. When averaged over the 20 day period, the sensitivity for carbonate precipitation is roughly the same as that for CO_2 air-water exchange. However, the rate of carbonate precipitation (expressed per mole of C) is one order of magnitude higher than the rate of CO_2 air-sea exchange. Accordingly, we can conclude that carbonate precipitation is the dominant process influencing the pH in our water reservoir system over the observed 20 day time period.

In summary, the explicit modelling approach is able to answer our first research question ("How did the pH evolve in between the sampling times?"), as well as the second one ("Which one of the slow kinetic processes affected the pH change the most?").

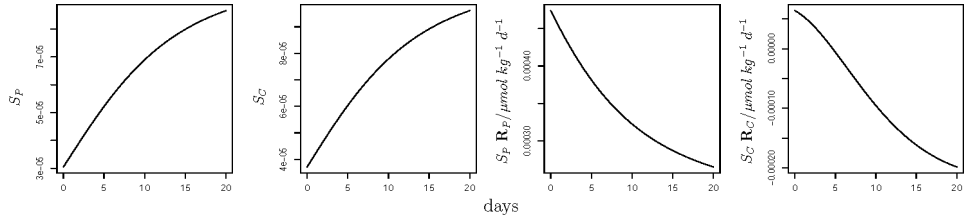

Figure 5.2.: The sensitivities of the pH to calcite precipitation and CO_2 air-water exchange and the overall influences of both processes on the pH (i.e., the product of their rate and the respective sensitivity of the pH) in the example system over the course of 20 days. The sensitivities are dimensionless quantities. The consistency between the explicit and the implicit pH modelling approach has been confirmed for the given example model: the obtained temporal pH profiles are identical.

5.3. The link between pH sensitivities and buffering capacity

Above, we have derived the explicit pH modelling approach as an extension of the conventional implicit pH modelling approach. It is clear that the explicit pH modelling approach can provide valuable insight into pH dynamics. Yet, until now, our derivation has been a pure mathematical recipe without a clear interpretation in terms of water chemistry. How can we interpret the above sensitivities in terms of the mechanisms that are affecting the pH? What is the role of the "slow" kinetic processes as opposed to the role of the "fast" acid-base reactions? In the following, we will discuss a method that derives the pH evolution equation Eq. (28) directly starting from the stoichiometry of the kinetic processes thus providing a direct chemical interpretation of this equation.

5.3.1. Step 1: The proton release rate at ambient pH

Following the classical textbook definition, the production rate of a particular chemical species due to a given chemical reaction simply equals the reaction rate times the stoichiometric coefficient ν of the chemical species in the reaction equation. This also applies to protons, and so in our example, the total release rate of protons would become

$$\nu^P_{H^+}\mathbf{R}_P + \nu^C_{H^+}\mathbf{R}_C \tag{31}$$

where $\nu^P_{H^+}$ and $\nu^C_{H^+}$ represent the stoichiometric coefficients for H^+ in the associated reaction equations for calcite precipitation and CO_2 air-water exchange. However, this is a too simplistic perspective. When literally applying this idea to the specific reaction equations used in our model formulation (i.e., Eqs. (1) and (2)), it would imply that there are no protons released, since $\nu^P_{H^+} = \nu^C_{H^+} = 0$. Obviously, this cannot be true, and the reason for this discrepancy is the inevitable arbitrariness connected with writing stoichiometric reaction equations. Indeed, instead of Eq. (1), the reaction equation for calcium carbonate precipitation can also be written in the alternative forms

$$Ca^{2+} + HCO_3^- \rightarrow CaCO_3 + H^+ \tag{32}$$
$$Ca^{2+} + H_2O + CO_2 \rightarrow CaCO_3 + 2H^+ \tag{33}$$

Note that these reaction equations do produce protons, and hence, the stoichiometric coefficient $\nu^P_{H^+}$ would become 1 and 2 respectively. We refer to the reaction equations (1), (32) and (33) as *integer reaction equations*, since all stoichiometric coefficients are integers. These integer reaction equations are, however, not the only possible alternatives. Any linear combination of reaction equations (1), (32) and (33) of the form

$$Ca^{2+} + c_1CO_2 + c_2HCO_3^- + c_3CO_3^{2-} + c_1H_2O \rightarrow CaCO_3 + (2c_1 + c_2)H^+ \tag{34}$$

is stoichiometrically correct, i.e., contains the same number of atoms for each element and the same amount of charge on the left and on the right hand side, provided the coefficients are constrained by $c_1 + c_2 + c_3 = \nu_{CaCO3} = 1$. Here, the coefficients c_1, c_2, and c_3 are not necessarily integers but fractions, and so, we call Eq. (34) a *fractional reaction equation*.

Effectively, Eq. (34) provides an infinite number of possibilities to write the reaction equation of carbonate precipitation, with an associated infinite number of possibilities for the stoichiometric coefficient $\nu^P_{H^+} = 2c_1 + c_2$. From this infinite set, there is, however, one set of coefficients c_i that has a particular chemical meaning. The ambient pH of the solution induces a specific partitioning of $[\sum CO_2]$ into $[CO_2]$, $[HCO_3^-]$, and $[CO_3^{2-}]$. If we substitute the ionization fractions α_i as the coefficients c_i into Eq. (34), we obtain an equation which describes the proton release of calcium carbonate precipitation at the ambient pH of the system.

$$Ca^{2+} + \alpha_0CO_2 + \alpha_1HCO_3^- + \alpha_2CO_3^{2-} + \alpha_0H_2O \rightarrow CaCO_3 + (2\alpha_0 + \alpha_1)H^+ \tag{35}$$

We refer to Eq. (35) as the *fractional reaction equation at ambient pH* for calcium carbonate precipitation. When CO_2 air-water exchange is written in the way of a chemical reaction

$$CO_2(g) \rightleftharpoons CO_2 \tag{36}$$

we can derive a fractional reaction equation at the ambient pH for CO_2 air-water exchange in much the same way

$$CO_2(g) \rightleftharpoons \alpha_0 CO_2 + \alpha_1 HCO_3^- + \alpha_2 CO_3^{2-} - (\alpha_1 + \alpha_2)\, H_2O + (\alpha_1 + 2\alpha_2)\, H^+ \tag{37}$$

Appendices 5.7.2 and 5.7.3 provide recipes to derive the fractional reaction equation at the ambient pH for any reaction process, including transport processes. From Eqs. (35) and (37) the *proton release rate at ambient pH* for our system is derived as

$$\nu^P_{H^+}\mathbf{R}_P + \nu^C_{H^+}\mathbf{R}_C = (2\alpha_0 + \alpha_1)\mathbf{R}_P + (\alpha_1 + 2\alpha_2)\mathbf{R}_C \tag{38}$$

This quantity represents the production rate of protons at a given pH that results from carbonate precipitation and CO_2 exchange, without re-equilibration by acid-base reactions. In other words, it assumes that the ionization fractions α_i for all species stay constant at values that are calculated using the pH at the start of the reaction (see Eqs. (23)-(25)).

5.3.2. Step 2: Accounting for re-equilibration

In a non-buffered system (i.e., without "fast" acid-base reactions), the rate of change of protons in solution can be equated to the proton release rate at ambient pH. However, in a buffered system, this assumption is no longer valid because of *re-equilibration* by the acid-base reactions. According to the principle of Le Chatelier-Braun, re-equilibration will always counteract the proton release by kinetic reactions. This implies that the actual rate of change of protons must always be smaller than the non-buffered rate. This can be expressed by

$$\frac{d[H^+]}{dt} = \frac{\nu^P_{H^+}}{\beta}\mathbf{R}_P + \frac{\nu^C_{H^+}}{\beta}\mathbf{R}_C \tag{39}$$

where the newly introduced *buffer factor* $\beta \geq 1$ implements the modulating influence of buffering. In essence, the presence of β in Eq. (39) will diminish the amplitude of any pH variations induced by the proton release rate at ambient pH. Starting from the definition of the stoichiometric coefficients $\nu^P_{H^+}$ and $\nu^C_{H^+}$ in Eq.(38), using the definition of alkalinity Eq.(22), and knowing that $\alpha_0 + \alpha_1 + \alpha_2 = 1$, one can easily prove that

$$\nu^P_{H^+} \equiv 2\alpha_0 + \alpha_1 = 2 - \frac{\partial[TA]}{\partial[\sum CO_2]} \tag{40}$$

$$\nu^C_{H^+} \equiv \alpha_1 + 2\alpha_2 = \frac{\partial[TA]}{\partial[\sum CO_2]} \tag{41}$$

Comparing the corresponding terms in the evolution equations (39) and (28), this means one can express the pH sensitivities as

$$S_P = \frac{\nu^P_{H^+}}{\beta} \tag{42}$$

$$S_C = \frac{\nu^C_{H^+}}{\beta} \tag{43}$$

Accordingly, the buffer factor is defined by

$$\beta \equiv -\frac{\partial[TA]}{\partial[H^+]} \tag{44}$$

This expression is true in general for an arbitrarily complex biogeochemical system. For our example reservoir system, the buffer factor takes on the explicit form[7]

$$\begin{aligned}\beta =& 1 - \left(\frac{\mathrm{d}\alpha_1}{\mathrm{d}[\mathrm{H}^+]} + 2\frac{\mathrm{d}\alpha_2}{\mathrm{d}[\mathrm{H}^+]} \right) [\textstyle\sum \mathrm{CO}_2] \\ =& 1 + K_1^* \left(\frac{[\mathrm{H}^+]^2 + 4\,[\mathrm{H}^+]\,\mathrm{K}_2^* + \mathrm{K}_1^*\,\mathrm{K}_2^* - 2\,[\mathrm{H}^+]\,\mathrm{K}_1^*}{\left([\mathrm{H}^+]^2 + [\mathrm{H}^+]\,\mathrm{K}_1^* + \mathrm{K}_1^*\,\mathrm{K}_2^*\right)^2} \right) [\textstyle\sum \mathrm{CO}_2] \geq 1 \end{aligned} \tag{45}$$

A closer examination of this expression confirms that β truly describes chemical buffering. In our reservoir, the only chemical buffering capacity comes from the carbonate system, as represented by the $[\sum \mathrm{CO}_2]$ concentration. When there is no carbonate ($[\sum \mathrm{CO}_2] = 0$), the solution has no buffering capacity. In this case, the buffer factor becomes one, and the protons released at ambient pH will contribute to the pH change in an unmodulated fashion. In contrast, when the carbonate concentration is very large ($[\sum \mathrm{CO}_2] \mapsto \infty$), the solution has an infinite buffering capacity ($\beta \mapsto \infty$, because the factor between brackets in front of $[\sum \mathrm{CO}_2]$ is always negative). Hence, the rate of change of protons vanishes, and the solution is buffered in such a way that it will no longer experience pH changes.

The specific form of the sensitivities (Eqs. (42) and (43)) clarifies the roles of the slow kinetic processes and the fast equilibrium reactions. The proton release at ambient pH, represented by the stoichiometric coefficient of the proton ν_{H^+}, is characteristic for each slow kinetic process. The subsequent re-equilibration, expressed by the buffer factor in the denominator, is dependent on the acid-base systems and thus on the fast equilibrium reactions of the system. This buffer factor attenuates the pH change induced by the proton release at ambient pH of the slow kinetic process.

Figure (5.3) displays the stoichiometric coefficients ν_{H^+} and the buffer factor in our example system. Calcium carbonate precipitation produces a little less than one mole of protons per mole of $CaCO_3$ precipitated. Similarly, CO_2 exchange produces a little more than one mole of protons per one mole of CO_2 taken up by the water. Accordingly, the stoichiometric coefficients for calcite precipitation and CO_2 exchange are approximately the same. This is not readily obvious from our original reaction equations Eqs. (1) and (2), where neither calcite precipitation nor CO_2 air-water exchange seem to produce or consume any protons. The buffer factor decreases over the 20 day period, which implies that the system becomes increasingly more sensitive to proton production (or consumption). This is consistent with increasing sensitivities (Fig 5.2).

5.4. Generalisation

Appendix 5.7.4 details the fractional stoichiometric approach and its connection to the explicit pH modelling approach for an arbitrary complex system, i.e. featuring an arbitrary number of total quantities and reactions.

[7] Note that α_1 and α_2 are - as are all ionization fractions - functions of the single variable H^+ if the dissocation constants are assumed constant over time. This means the derivatives of both ionization fractions in Eq (45) signify ordinary derivatives in Leibnitz notation instead of partial derivatives.

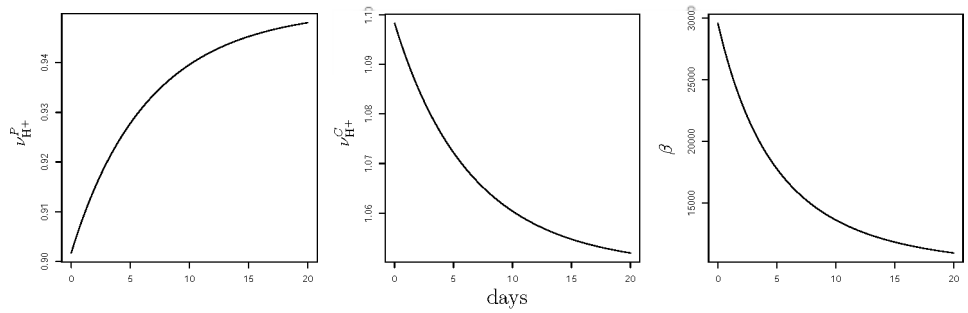

Figure 5.3.: The stoichiometric coefficients for the proton in the fractional stoichiometric equations at ambient pH of the modelled kinetic processes and the buffer factor for our example system. All three are dimensionless quantities.

5.4.1. The sensitivity of pH to biogeochemical and physical processes

For an arbitrary set of biogeochemical process, the evolution equation for the proton concentration becomes

$$\frac{d[\mathrm{H}^+]}{dt} = \sum_X S_X \mathbf{R}_X \tag{46}$$

where $\mathbf{R}_X$ denotes the rate of an arbitrary physical or biogeochemical process and where the sensitivity of the pH to the respective process is expressed as

$$S_X = \frac{\nu^X_{\mathrm{H}^+}}{\beta} \tag{47}$$

with $\nu^X_{\mathrm{H}^+}$ being the stoichiometric coefficient for the proton in the fractional reaction equation at ambient pH for process X. The sensitivity of pH to physical transport processes can also be expressed this way if they are written as chemical reactions. CO_2 air-sea exchange was already treated like this in section (5.3), and Appendix (5.7.3) details how transport and mixing of water masses can be treated in the same way.

5.4.2. The buffer factor

The buffer factor β introduced in the previous sections can be readily generalized as well. When accounting for all relevant acid-base systems in natural seawater (Dickson, 1981) and some more that might be relevant in samples of extreme aquatic environments (Soetaert et al., 2007), the alkalinity becomes

$$\begin{aligned}[\mathrm{TA}] =& [\mathrm{HCO_3^-}] + 2[\mathrm{CO_3^{2-}}] + [\mathrm{OH^-}] + [\mathrm{B(OH)_4^-}] + [\mathrm{HPO_4^{2-}}] + 2[\mathrm{PO_4^{3-}}] + [\mathrm{H_3SiO_4^-}] \\ &+ 2[\mathrm{H_2SiO_4^{2-}}] + [\mathrm{NH_3}] + [\mathrm{HS^-}] + 2[\mathrm{S^{2-}}] \\ &- [\mathrm{H^+}] - [\mathrm{H_3PO_4}] - [\mathrm{HSO_4^-}] - [\mathrm{HF}] - [\mathrm{HNO_3}] - [\mathrm{HNO_2}] - 2[\mathrm{H_2SO_4}]\end{aligned} \tag{48}$$

The associated buffer factor can then be derived as

$$\begin{aligned}\beta &= -\frac{\partial[\mathrm{TA}]}{\partial[\mathrm{H^+}]}\\ &= 1 + \frac{K_\mathrm{W}^*}{[\mathrm{H^+}]^2} - \left(\frac{\mathrm{d}\alpha_1^\mathrm{C}}{\mathrm{d}[\mathrm{H^+}]} + 2\frac{\mathrm{d}\alpha_2^\mathrm{C}}{\mathrm{d}[\mathrm{H^+}]}\right)\left[\sum \mathrm{CO_2}\right] - \frac{\mathrm{d}\alpha_1^\mathrm{B}}{\mathrm{d}[\mathrm{H^+}]}\left[\sum \mathrm{B(OH)_3}\right]\\ &\quad - \left(\frac{\mathrm{d}\alpha_2^\mathrm{P}}{\mathrm{d}[\mathrm{H^+}]} + 2\frac{\mathrm{d}\alpha_3^\mathrm{P}}{\mathrm{d}[\mathrm{H^+}]} - \frac{\mathrm{d}\alpha_0^\mathrm{P}}{\mathrm{dH^+}}\right)\left[\sum \mathrm{H_3PO_4}\right] - \left(\frac{\mathrm{d}\alpha_1^\mathrm{Si}}{\mathrm{d}[\mathrm{H^+}]} + 2\frac{\mathrm{d}\alpha_2^\mathrm{Si}}{\mathrm{d}[\mathrm{H^+}]}\right)\left[\sum \mathrm{H_4SiO_4}\right]\\ &\quad - \frac{\mathrm{d}\alpha_1^\mathrm{NH}}{\mathrm{d}[\mathrm{H^+}]}\left[\sum \mathrm{NH_4^+}\right] - \left(\frac{\mathrm{d}\alpha_1^\mathrm{S}}{\mathrm{dH^+}} + 2\frac{\mathrm{d}\alpha_2^\mathrm{S}}{\mathrm{d}[\mathrm{H^+}]}\right)\left[\sum \mathrm{H_2S}\right] + \left(\frac{\mathrm{d}\alpha_1^\mathrm{SO}}{\mathrm{dH^+}} + 2\frac{\mathrm{d}\alpha_0^\mathrm{SO}}{\mathrm{d}[\mathrm{H^+}]}\right)\left[\sum \mathrm{H_2SO_4}\right]\\ &\quad + \frac{\mathrm{d}\alpha_0^\mathrm{F}}{\mathrm{d}[\mathrm{H^+}]}\left[\sum \mathrm{HF}\right] + \frac{\mathrm{d}\alpha_0^{\mathrm{NO_3}}}{\mathrm{d}[\mathrm{H^+}]}\left[\sum \mathrm{HNO_3}\right] + \frac{\mathrm{d}\alpha_0^{\mathrm{NO_2}}}{\mathrm{d}[\mathrm{H^+}]}\left[\sum \mathrm{HNO_2}\right]\end{aligned} \tag{49}$$

Written in the form of equation (49), the buffer factor now receives contributions from all acid base systems present and it becomes obvious that our buffer factor is similar to the *buffer capacity* defined by Morel and Hering (1993) and the *buffer intensity* as given in Stumm and Morgan (1996). However, our quantity is defined as derivative with respect to the proton concentration while theirs are defined as derivatives with respect to the pH. Frankignoulle (1994) defined a set of chemical buffer factors dealing with the exchange of different chemical species. One of his buffer factors deals with the addition or consumption of protons via a strong acid or base. This quantity is equivalent to the inverse of the buffer capacity or the buffer intensity mentioned above and thus comparable to our buffer factor. However, Frankignoulle (1994) failed to realize that the buffer factor dealing with protons suffices to describe any change to the system as long as fractional stoichiometry at ambient pH is employed.

5.5. A real world example: antropogenic CO_2 uptake

In the past and particularly in recent years a lot of effort has been put into modelling the uptake of antropogenic CO_2 by global oceans and resulting ocean acidification (e.g. MacIntyre, 1978; Archer, 1995; Archer et al., 1998; Archer, 1999; Orr et al., 2001b,a; Prentice et al., 2001; Caldeira and Wickett, 2003, 2005; Sarmiento and Gruber, 2006; Blackford and Gilbert, 2007; IPCC, 2007; Zachos et al., 2008; Zeebe et al., 2008). Complementary to those efforts, our concepts of buffer factor and pH sensitivities can be applied to ocean acidification scenarios.

Assuming a mean global ocean surface water composition as given in Tab. 5.4, and assuming that $[\sum \mathrm{CO_2}]$ increases from 2040 μmol kg^{-1}to 2260 μmol kg^{-1}due to oceanic uptake of antropogenic CO_2, one can calculate that the free scale pH at 25 C drops by around 0.4 pH units from 8.2 to 7.8 (Fig. (5.4) left hand side). This pH drop is consistent with projected decreases in oceanic pH due to the uptake of antropogenic CO_2 by the end of the 21$^{\mathrm{st}}$ century (IPCC, 2007; Guinotte and Fabry, 2008). Now, one can plot the average β of the global surface ocean as a function of the free scale pH until the end of the century (Fig. (5.4)). It becomes obvious that β values at present pH are around 4 times higher than the values at a pH of 7.8. This means, considering CO_2 input alone, by the end of the century, the global ocean will be around 4 times less buffered than it is now which makes it more susceptible to pH changes by further input of acids or the input of bases. This suggests synergistic interactions

between CO_2 based and non CO_2 based ocean acidification like atmospheric deposition of N and S. Such synergistic interactions require further study, especially because projected N and S deposition rates are increasing for decades to come (Doney et al., 2007; Duce et al., 2008).

$[\sum CO_2]$	=	2040.0
$[TA]$	=	2400.0
$[\sum B(OH)_3]$	=	420.0
$[\sum H_3PO_4]$	=	0.6
$[\sum Si(OH)_4]$	=	8.2
$[\sum NH_4^+]$	=	1.0
$[\sum H_2S]$	=	0.1
$[\sum H_2SO_4]$	=	28240.0
$[\sum HF]$	=	70
$[\sum HNO_3]$	=	6.1
$[\sum HNO_2]$	=	0.1
pH (free scale)	=	8.2

Table 5.4.: Approximate composition of the current global ocean. All values are in μmol kg^{-1}. The values for $[\sum CO_2]$, $[\sum B(OH)_3]$, $[\sum H_2SO_4]$, and $[\sum HF]$ have been calculated as functions of salinity S=35 as given in DOE (1994) and Dickson et al. (2007); values for $[\sum H_3PO_4]$, $[\sum HNO_3]$, and $[\sum Si(OH)_4]$ are surface values from the Levitus et al. (1998) dataset as restated in Sarmiento and Gruber (p. 226, 2006); the values for $[\sum HNO_2]$, $[\sum H_2S]$, and $[\sum NH_4^+]$ are values typical for the Atlantic Ocean taken from Soetaert et al. (2007). The free scale pH has been calculated at T=25 C.

To illustrate the power and instructiveness of our approach, we derived the sensitivities of the pH to primary production and oxic mineralisation (see fractional reaction equations in Appendix 5.7.2), in addition to the sensitivities of pH to CO_2 air water exchange (using Eq. (37)) and calcium carbonate precipitation (using Eq. (35)). Those sensitivities can be expressed as given in Table (5.5).

calcite precipitation	S_P	=	$\frac{\nu^P_{H^+}}{\beta}$	= $\frac{2\,\alpha_0^C + \alpha_1^C}{\beta}$
CO_2 air water exchange	S_C	=	$\frac{\nu^C_{H^+}}{\beta}$	= $\frac{\alpha_1^C + 2\,\alpha_2^C}{\beta}$
primary production	S_{PP}	=	$\frac{\nu^{PP}_{H^+}}{\beta}$	= $\frac{\alpha_0^{NH}\gamma^{-1} - \alpha_1^C - 2\,\alpha_2^C}{\beta}$
oxic mineralisation	S_{Ox}	=	$\frac{\nu^{Ox}_{H^+}}{\beta}$	= $\frac{\alpha_1^C + 2\,\alpha_2^C - \alpha_0^{NH}\gamma^{-1}}{\beta}$

Table 5.5.: Sensitivities of the pH to a selection of processes relevant in the global ocean. All processes are normalized to 1 mol of carbon processed. $\gamma = \frac{106}{16}$ is the Redfield $\frac{C}{N}$ ratio.

With the buffer factor β and all ionization fractions (α values) calculated with quantities given in Tab (5.4) one can calculate numerical values for the stoichiometric coefficients ν_{H^+} of the proton in the fractional reaction equations at ambient pH of the given processes as well as for the sensitivities S of the pH to those processes for the current and future ($[\sum CO_2]$ concentration increased to 2260 μmol kg^{-1}; $\approx$ year 2100) state of the global ocean (Tab. (5.6)).

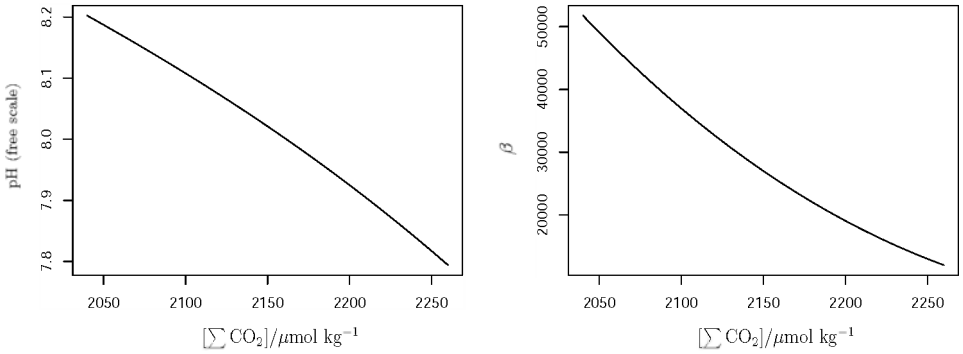

Figure 5.4.: Changes in mean global oceanic free scale pH (calculated at T=25 C) and the buffer factor β when $[\sum CO_2]$ changes linearly from 2040 to 2260 μmol kg^{-1}. The drop in free scale pH from 8.2 to 7.8 is consistent with projected declines in oceanic pH due to the uptake of antropogenic CO_2 by the end of the 21st century (IPCC, 2007; Guinotte and Fabry, 2008).

	present situation ($\beta \approx 51763$)		approx. yr. 2100 ($\beta \approx 12014$)	
	ν_{H^+}	S	ν_{H^+}	S
calcite precipitation	0.88	$1.69\ 10^{-5}$	0.96	$7.99\ 10^{-5}$
CO_2 air water exchange	1.12	$2.17\ 10^{-5}$	1.04	$8.66\ 10^{-5}$
primary production	-0.98	$-1.90\ 10^{-5}$	-0.89	$-7.43\ 10^{-5}$
oxic mineralisation	0.98	$1.90\ 10^{-5}$	0.89	$7.43\ 10^{-5}$

Table 5.6.: Numerical values for the stoichiometric coefficients of the proton in the fractional reaction equations at ambient pH (ν_{H^+}) for the given processes and the sensitivities of the pH (S) to those processes for the present situation ($[\sum CO_2] = 2040$ μmol kg^{-1}) and the future scenario ($[\sum CO_2] = 2260$ μmol kg^{-1}; $\approx$ year 2100).

The first observation is that the pH is around 4 times more sensitive to all of the processes in the future scenario than at present. This is a direct result of the decreasing buffer factor β (see above). Furthermore, in the present situation, the pH is most sensitive to the exchange of carbon with the atmosphere, and the least sensitive to carbonate precipitation. The sensitivitiy of the pH to carbon production or mineralization lies between the two other sensitivities. In the future scenario, however, the situation has changed. While the pH will still be most sensitive to the exchange of carbon with the atmosphere, it will be least sensitive to the production or mineralisation of organic carbon. The pH's sensitivity to calcite precipitation will be larger than its sensitivity to primary production and oxic mineralisation[8].

Calculations of this type are not only helpful to guide experimental scientists to select processes that the pH will be most sensitive to, but they are also useful to Earth System modellers

[8]Note that the sensitivities of all four processes can be directly compared, since all four reaction equations are normalized to carbon.

to decide whether or not to include certain processes in pH models for the future ocean.

5.6. Summary and conclusions

The main limitation of the classical implicit alkalinity centered pH modelling approach (Ben-Yaakov, 1970; Culberson, 1980; Luff et al., 2001; Follows et al., 2006) is that it does not allow for an individual quantification of the influences of "driving" biogeochemical or physical processes that are responsible for pH changes. Here we present an explicit pH modelling approach which does allow such a quantification: a rate of change for the proton concentration is calculated as an explicit function of the rates of the modelled driving processes modulated by a process specific sensitivity of the pH.

The process specific sensitivities of the pH aggregate both, the influence of the driving process in question, and the influences of the acid-base reactions in the system. This can be understood by considering a two step process where protons are produced by the driving processes directly, as in an unbuffered system, and subsequently the system is re-equilibrated. The sensitivity of the pH with respect to a driving process can thus be expressed as a quotient of the stoichiometric coefficient ν_{H^+} for the proton in the fractional reaction equation at ambient pH of the driving process over the buffer factor β. ν_{H^+} is a quantitiy that represents the direct proton production by the driving process, without re-equilibration, and β is a quantity that represents the attenuation of the pH changes by the set of acid-base reactions.

The buffer factor β is similar to buffer quantities as defined by Morel and Hering (1993), Frankignoulle (1994), and Stumm and Morgan (1996), while the definition for ν_{H^+} contains the well-known ionization fractions (Skoog and West, 1982; Stumm and Morgan, 1996).

We applied the concept of buffer factor and pH sensitivities to a scenario of ocean acidification, assuming an average composition of the global surface ocean. This shows that the buffer factor of surface ocean water will be about four times less at the end of the century than it is now. The global ocean pH becomes thus substantially more sensitive to the addition of acids, such as the uptake of antropogenic CO_2, but also the atmospheric input of sulfurous and nitrogenic compounds (see e.g. Doney et al., 2007; Duce et al., 2008). Overall, we show that the influence of an oceanic processes (like calcification, primary production, etc.) on the pH is governed by the product of pH sensitivity and process rate. Therefore, it is not only important to investigate how rates of these processes will change, but also how the associated sensitivity factors will change. In this paper, we provide the necessary theory and tools to do so, especially under future scenarios of ocean acidification. Accordingly, the remaining challenge becomes to predict the process rates in the future ocean, and how these will be influenced by ocean chemistry changes. This is currently an active field of investigation (e.g. Orr et al., 2005; Kleypas et al., 2006; Gazeau et al., 2007; Guinotte and Fabry, 2008). Furthermore, we believe that the concepts and tools presented here can make a complementary contribution to present modelling approaches of ocean acidification (e.g. Caldeira and Wickett, 2003, 2005; Orr et al., 2005; Blackford and Gilbert, 2007; Zachos et al., 2008; Zeebe et al., 2008).

5.7. Appendix

5.7.1. Time scales and the equilibrium assumption

The pH chemistry of natural waters is influenced by processes that act on very different time scales. Based on relaxation time, one can distinguish two groups of processes. On the one hand, there are the various acid-base dissociation systems (carbonate, borate, silicate, etc.) that relax to equilibrium on time scales of less than minutes (Zeebe and Wolf-Gladrow, 2001). The net forward rate of these fast processes is denoted as $\mathbf{R}_i^{fast}$. On the other hand, natural systems will typically include a set of comparatively slow kinetic processes that have much greater relaxation times, ranging from hours to years. These could include chemical reactions, such as calcium carbonate precipitation or dissolution, as well as physical transport, for example the air-water exchange of CO_2. The net forward rate of these slow processes is referred to as $\mathbf{R}_i^{slow}$.

This difference in characteristic time scales has an important consequence in terms of model development. Depending on the time and length scales that are of interest, the formulation of the associated pH model will be different. For small time scales (< 1 min), the disequilibrium of the carbonate and other acid-base systems has to be taken into account. This is for example the case when modelling biogeochemical transformations within the diffusive boundary layer at the ocean-atmosphere interface or in the micro-environment surrounding marine plankton (e.g. Wolf-Gladrow et al., 1999; Zeebe, 2007). On these small time scales, both the slow and the fast processes need to be modelled via suitable kinetic expressions (unless the slow rates can be assumed negligible). As a consequence, the evolution of the proton concentration (or equivalently the pH) will depend on all the process rates and can be described by

$$\frac{d[\mathrm{H}^+]}{dt} = f(\mathbf{R}_1^{fast}, \mathbf{R}_2^{fast}, \ldots, \mathbf{R}_1^{slow}, \mathbf{R}_2^{slow}, \ldots) \tag{50}$$

Often, however, the time scales of interest are considerably larger: hourly, daily, seasonal, yearly or even or multi-decadal changes in pH need to be investigated. These are the situations we will focus upon here. Examples include ocean biogeochemical models, water quality models of lakes and rivers, hydrogeochemical groundwater models, and diagenetic models of sediments. In such cases, the acid-base reactions are "sufficiently" faster than the model time scale, so that these fast reactions can be considered to instantaneously attain thermodynamic equilibrium. In a biogeochemical modelling context, this is known as the *equilibrium assumption*, which basically implies that the forward and backward kinetic rate constants are assumed to be infinitely large but have a well-defined ratio (e.g. Olander, 1960; Aris and Mah, 1963; DiToro, 1976; Saaltink et al., 1998). The resulting models are called *mixed kinetic-equilibrium* models, because they include two types of process descriptions. The fast reactions are described via the algebraic mass action laws of thermodynamic equilibrium, while the slow processes are modelled via suitable differential kinetic rate laws.

An important feature of mixed kinetic-equilibrium models is that the temporal evolution of the system (and hence any pH change) is exclusively driven by the rates of the slow kinetic processes and only the absolute state of the system at any time is influenced by the fast equilibrium reactions. If concentrations are changed by the slow processes, the fast reactions will respond instantaneously according to the principle of Le Chatelier-Braun. This implies

that the net forward rate of the fast reactions must be implicitly dependent on the slow kinetic rates, i.e.

$$\mathbf{R}_i^{fast} = f(\mathbf{R}_j^{slow}) \tag{51}$$

The amount of molecules passing the chemical "pathway" that is presented by the fast equilibrium reaction only depends on the supply or consumption rates of its reactants and products by the slow kinetic reactions, since the reaction step of the fast equilibrium reaction itself is considered to be infinitely fast. Stated alternatively, if all rates $\mathbf{R}_i^{slow}$ were zero, then the pH would not change, i.e., only the slow kinetic processes are driving changes to the system which means for the proton concentration

$$\frac{d[\mathrm{H}^+]}{dt} = f(\mathbf{R}_1^{slow}, \mathbf{R}_2^{slow}, ...) \tag{52}$$

5.7.2. A recipe for fractional reaction equations at ambient pH

Here we describe a procedure to derive the fractional stoichiometric equation at ambient pH starting from an arbitrary reaction equation, without the need to enumerate all possible (integer) reaction equations. In general, each reaction equation one starts with will feature two types of chemical species. *Kinetic species* are species that do not feature in the acid-base reaction equations. In contrast, *equilibrium species* will feature in one or more reaction equations of the acid-base systems. To arrive at the fractional reaction equation at ambient pH one must substitute all equilibrium species except for H^+ in the original equation. This substitution basically involves a replacement of a given equilibrium species by a collection of ionized counterparts in fractions given by the ionization fractions of the respective acid-base system. These ionized counterparts are accompanied by water molecules and protons to balance masses and charge in the reaction equation. The respective amount of water and proton molecules can be found by considering the respective dissociation or association reactions involved.

For the carbonate system, the substitution list is given by:

$$\mathrm{CO_2} : \alpha_0^{\mathrm{C}}\,\mathrm{CO_2} + \alpha_1^{\mathrm{C}}\,(\mathrm{HCO_3^- + H^+ - H_2O}) + \alpha_2^{\mathrm{C}}\left(\mathrm{CO_3^{2-} + 2H^+ - H_2O}\right) \tag{53}$$

$$\mathrm{HCO_3^-} : \alpha_0^{\mathrm{C}}\,(\mathrm{CO_2 - H^+ + H_2O}) + \alpha_1^{\mathrm{C}}\,\mathrm{HCO_3^-} + \alpha_2^{\mathrm{C}}\left(\mathrm{CO_3^{2-} + H^+}\right) \tag{54}$$

$$\mathrm{CO_3^{2-}} : \alpha_0^{\mathrm{C}}\,(\mathrm{CO_2 - 2H^+ + H_2O}) + \alpha_1^{\mathrm{C}}\,(\mathrm{HCO_3^- - H^+}) + \alpha_2^{\mathrm{C}}\,\mathrm{CO_3^{2-}} \tag{55}$$

For the sulphate system, the substitution list is given by:

$$\mathrm{H_2SO_4} : \alpha_0^{\mathrm{SO}}\mathrm{H_2SO_4} + \alpha_1^{\mathrm{SO}}\,(\mathrm{HSO_4^- + H^+}) + \alpha_2^{\mathrm{SO}}\left(\mathrm{SO_4^{2-} + 2H^+}\right) \tag{56}$$

$$\mathrm{HSO_4^-} : \alpha_0^{\mathrm{SO}}\,(\mathrm{H_2SO_4 - H^+}) + \alpha_1^{\mathrm{SO}}\mathrm{HSO_4^-} + \alpha_2^{\mathrm{SO}}\left(\mathrm{SO_4^{2-} + H^+}\right) \tag{57}$$

$$\mathrm{SO_4^{2-}} : \alpha_0^{\mathrm{SO}}\,(\mathrm{H_2SO_4 - 2H^+}) + \alpha_1^{\mathrm{SO}}\,(\mathrm{HSO_4^- - H^+}) + \alpha_2^{\mathrm{SO}}\mathrm{SO_4^{2-}} \tag{58}$$

For the phosphate system, the substitution list is given by:

$$\mathrm{H_3PO_4} : \alpha_0^{\mathrm{P}}\mathrm{H_3PO_4} + \alpha_1^{\mathrm{P}}\,(\mathrm{H_2PO_4^- + H^+}) + \alpha_2^{\mathrm{P}}\left(\mathrm{HPO_4^{2-} + 2H^+}\right) + \alpha_3^{\mathrm{P}}\left(\mathrm{PO_4^{3-} + 3H^+}\right) \tag{59}$$

$$\mathrm{H_2PO_4^-} : \alpha_0^{\mathrm{P}}\,(\mathrm{H_3PO_4 - H^+}) + \alpha_1^{\mathrm{P}}\mathrm{H_2PO_4^-} + \alpha_2^{\mathrm{P}}\left(\mathrm{HPO_4^{2-} + H^+}\right) + \alpha_3^{\mathrm{P}}\left(\mathrm{PO_4^{3-} + 2H^+}\right) \tag{60}$$

$$\mathrm{HPO_4^{2-}} : \alpha_0^{\mathrm{P}}\,(\mathrm{H_3PO_4 - 2H^+}) + \alpha_1^{\mathrm{P}}\,(\mathrm{H_2PO_4^- - H^+}) + \alpha_2^{\mathrm{P}}\mathrm{HPO_4^{2-}} + \alpha_3^{\mathrm{P}}\left(\mathrm{PO_4^{3-} + H^+}\right) \tag{61}$$

$$\mathrm{PO_4^{3-}} : \alpha_0^{\mathrm{P}}\,(\mathrm{H_3PO_4 - 3H^+}) + \alpha_1^{\mathrm{P}}\,(\mathrm{H_2PO_4^- - 2H^+}) + \alpha_2^{\mathrm{P}}\left(\mathrm{HPO_4^{2-} - H^+}\right) + \alpha_3^{\mathrm{P}}\mathrm{PO_4^{3-}} \tag{62}$$

For the ammonia system, the substitution list is given by:

$$\mathrm{NH_4^+} \quad : \quad \alpha_0^{\mathrm{NH}}\,\mathrm{NH_4^+} + \alpha_1^{\mathrm{NH}}\,(\mathrm{NH_3} + \mathrm{H^+}) \tag{63}$$

$$\mathrm{NH_3} \quad : \quad \alpha_0^{\mathrm{NH}}\,(\mathrm{NH_4^+} - \mathrm{H^+}) + \alpha_1^{\mathrm{NH}}\,\mathrm{NH_3} \tag{64}$$

For the water auto dissociation, the substitution list is given by:

$$\mathrm{OH^-} \quad : \quad \mathrm{H_2O} - \mathrm{H^+} \tag{65}$$

The substitution list of other acid-base equilibria can be derived by analogy (As mentioned before: $\mathrm{H^+}$ is the only equilibrium species that does not need to be substituted). Note that the substitution for water auto-dissociation given here is only valid if the ion product of water ($K_W^* = [\mathrm{H^+}]\,[\mathrm{OH^-}]$) is considered and $[\mathrm{H_2O}]$ is assumed constant. If the true dissocation constant of water ($K_{\mathrm{H_2O}}^* = [\mathrm{H^+}]\,[\mathrm{OH^-}]/[\mathrm{H_2O}]$) is considered and $[\mathrm{H_2O}]$ is modelled dynamically, the substitution list has to be derived analoguously to the other acid base systems considering the ionization fractions for $\mathrm{H_2O}$ and $\mathrm{OH^-}$.

The use of these substitution lists can be illustrated by means of simple examples. Assuming a $\frac{\mathrm{C}}{\mathrm{N}}$ ratio of γ, one can devise a simple reaction equation for primary production

$$\mathrm{H_2O} + \mathrm{CO_2} + \frac{1}{\gamma}\mathrm{NH_3} \longrightarrow \mathrm{CH_2O(NH_3)_{\frac{1}{\gamma}}} + \mathrm{O_2} \tag{66}$$

This reaction equation contains two equilibrium species, $\mathrm{CO_2}$ and $\mathrm{NH_3}$, which need to be substituted using Eqs. (53) and (64) respectively to arrive at the fractional reaction equation at ambient pH for primary production

$$\begin{aligned}\left(1 - \alpha_1^{\mathrm{C}} - \alpha_2^{\mathrm{C}}\right)\mathrm{H_2O} + \left(c_1\mathrm{CO_2} + c_2\mathrm{HCO_3^-} + c_3\mathrm{CO_3^{2-}}\right) + \frac{1}{\gamma}\left(\alpha_0^{\mathrm{NH}}\mathrm{NH_4^+} + \alpha_1^{\mathrm{NH}}\mathrm{NH_3}\right) \\ \longrightarrow \mathrm{CH_2O(NH_3)_{\frac{1}{\gamma}}} + \mathrm{O_2} + \left(\frac{c_0^{\mathrm{NH}}}{\gamma} - \alpha_1^{\mathrm{C}} - 2\alpha_2^{\mathrm{C}}\right)\mathrm{H^+}\end{aligned} \tag{67}$$

Similarly, one can express oxic mineralisation as

$$\mathrm{CH_2O(NH_3)_{\frac{1}{\gamma}}} + \mathrm{O_2} \longrightarrow \mathrm{H_2O} + \mathrm{CO_2} + \frac{1}{\gamma}\mathrm{NH_3} \tag{68}$$

and substitute $\mathrm{CO_2}$ and $\mathrm{NH_3}$ to arrive at the fractional reaction equation at ambient pH for oxic mineralisation

$$\begin{aligned}\mathrm{CH_2O(NH_3)_{\frac{1}{\gamma}}} + \mathrm{O_2} \quad \longrightarrow \quad & \left(1 - \alpha_1^{\mathrm{C}} - \alpha_2^{\mathrm{C}}\right)\mathrm{H_2O} + \left(c_1\mathrm{CO_2} + c_2\mathrm{HCO_3} - + c_3\mathrm{CO_3^{2-}}\right) \\ & + \frac{1}{\gamma}\left(\alpha_0^{\mathrm{NH}}\mathrm{NH_4^+} + \alpha_1^{\mathrm{NH}}\mathrm{NH_3}\right) + \left(\alpha_1^{\mathrm{C}} + 2\alpha_2^{\mathrm{C}} - \frac{\alpha_0^{\mathrm{NH}}}{\gamma}\right)\mathrm{H^+}\end{aligned} \tag{69}$$

5.7.3. Transport processes

Physical transport processes can be treated in the same way as biogeochemical reactions by writing them in a way that resembles a chemical reaction. This has been done for $\mathrm{CO_2}$ air-water exchange in Eq. (36) and will be demonstrated here for advective-diffusive transport,

e.g., due to oceaninc mixing.

Assume that the example system described in Sec. (5.2.1) is in contact with another compartement of water, e.g. via an inflow and an outflow similar to a chemostat. Then, the chemical species[9] $[CO_2]$, $[HCO_3^-]$, $[CO_3^{2-}]$, and $[H^+]$ need to be advectively transported in the model. This can be implemented using suitable kinetic expressions of the form $\mathbf{T}_X = Q\,([X]_{outside} - [X])$ with Q being the dilution rate and $[X]_{outside}$ the concentration of species X in the inflowing water.

In the same way as done for CO_2 air-water exchange in Eq. (36) the transport of the four species CO_2, HCO_3^-, CO_3^{2-}, and H^+ can be written in the form of chemical reactions, where the arrow to the right symbolizes the inflow of the respective species and the arrow to the left the outflow. The net forward rate of the given "reaction" for species X is the net inflow of X and is calculated as $\mathbf{T}_X$ as given above.

$$CO_{2\,outside} \rightleftharpoons CO_2 \tag{70}$$
$$HCO_{3\,outside}^- \rightleftharpoons HCO_3^- \tag{71}$$
$$CO_{3\,outside}^{2-} \rightleftharpoons CO_3^{2-} \tag{72}$$
$$H_{outside}^+ \rightleftharpoons H^+ \tag{73}$$

These integer "reaction" equations can be substituted

$$CO_{2\,out} \rightleftharpoons \alpha_0^C\,CO_2 + \alpha_1^C\,(HCO_3^- + H^+ - H_2O) + \alpha_2^C\,(CO_3^{2-} + 2H^+ - H_2O) \tag{74}$$
$$HCO_{3\,out}^- \rightleftharpoons \alpha_0^C\,(CO_2 - H^+ + H_2O) + \alpha_1^C\,HCO_3^- + \alpha_2^C\,(CO_3^{2-} + H^+) \tag{75}$$
$$CO_{3\,out}^{2-} \rightleftharpoons \alpha_0^C\,(CO_2 - 2H^+ + H_2O) + \alpha_1^C\,(HCO_3^- - H^+) + \alpha_2^C\,CO_3^{2-} \tag{76}$$
$$H_{out}^+ \rightleftharpoons H^+ \tag{77}$$

Which gives the sensitivities of the pH with respect to the four transport processes

$$S_{\mathbf{T}_{CO_2}} = \frac{\alpha_1^C + 2\,\alpha_2^C}{\beta} \tag{78}$$
$$S_{\mathbf{T}_{HCO_3^-}} = \frac{-\alpha_0^C + \alpha_2^C}{\beta} \tag{79}$$
$$S_{\mathbf{T}_{CO_3^{2-}}} = \frac{-2\,\alpha_0^C + \alpha_1^C}{\beta} \tag{80}$$
$$S_{\mathbf{T}_{H^+}} = \frac{1}{\beta} \tag{81}$$

Note that, since the transport of every chemical species is considered separately, this approach allows for differential transport between compartements, i.e. transport with different (molecular) diffusion constants, as is the case in porewaters of sediments (Boudreau, 1996a).

However, in a model without differential transport, the total quantities (here $[\sum CO_2]$ and $[TA]$) can be transported directly

$$\mathbf{T}_{[\sum CO_2]} = \mathbf{T}_{CO_2} + \mathbf{T}_{HCO_3^-} + \mathbf{T}_{CO_3^{2-}} = Q\,\left([\sum CO_2]_{outside} - [\sum CO_2]\right) \tag{82}$$
$$\mathbf{T}_{[TA]} = \mathbf{T}_{HCO_3^-} + 2\,\mathbf{T}_{CO_3^{2-}} - \mathbf{T}_{H^+} = Q\,([TA]_{outside} - [TA]) \tag{83}$$

[9] Note that if water auto-dissociation would be considered in the model, OH^- needs to be transported as well.

In this case, an equation analogous to Eq. (27) can be used to directly calculate the combined influence of all transport processes on the pH (see also Hofmann et al., 2008a, 2009a, i.e., Chapters 3, 4).

$$\frac{d[\mathrm{H^+}]}{dt}_{\text{(due to transport)}} = \frac{1}{\left(\frac{\partial[\mathrm{TA}]}{\partial[\mathrm{H^+}]}\right)}\left(\mathbf{T}_{[\mathrm{TA}]} - \left(\frac{\partial[\mathrm{TA}]}{\partial[\sum \mathrm{CO_2}]}\right)\mathbf{T}_{[\sum \mathrm{CO_2}]}\right) \tag{84}$$

5.7.4. Treatment of an arbitrary complex biogeochemical system

Consider a system with M kinetically modelled processes (index i=1,2, ..., M), and N total quantities X (index j = 1,2, ... N), other than alkalinity. The resulting evolution equations for this system can be written in the general form

$$\frac{d[\mathrm{TA}]}{dt} = \sum_i \nu^i_{[\mathrm{TA}]}\mathbf{R}_i \tag{85}$$

$$\frac{d\mathrm{X_j}}{dt} = \sum_i \nu^i_{X_j}\mathbf{R}_i \tag{86}$$

where ν^i_{TA} is the stoichiometric coefficient for the alkalinity associated with process i, $\nu^i_{\mathrm{X}_j}$ is the stoichiometric coefficient for X_j associated with process i, and $\mathbf{R}_i$ is the rate of process i. According to fractional stoichiometry, the resulting total rate of change of the proton concentration becomes

$$\frac{d[\mathrm{H^+}]}{dt} = \frac{1}{\left(-\frac{\partial[\mathrm{TA}]}{\partial[\mathrm{H^+}]}\right)}\sum_i \nu^i_{\mathrm{H^+}}\mathbf{R}_i \tag{87}$$

According to the explicit pH modelling approach (see also Hofmann et al., 2008a, i.e., Chapter 3) the total rate of change of proton concentration is derived as

$$\frac{d[\mathrm{H^+}]}{dt} = \frac{1}{\left(\frac{\partial[\mathrm{TA}]}{\partial[\mathrm{H^+}]}\right)}\left(\frac{d[\mathrm{TA}]}{dt} - \sum_j \frac{\partial[\mathrm{TA}]}{\partial \mathrm{X}_j}\frac{d\mathrm{X}_j}{dt}\right) \tag{88}$$

Upon substitution of the evolution equations for the total quantities (here (6) and (7)) into this equation one finds

$$\frac{d[\mathrm{H^+}]}{dt} = \frac{1}{\left(\frac{\partial[\mathrm{TA}]}{\partial[\mathrm{H^+}]}\right)}\sum_i\left(\nu^i_{[\mathrm{TA}]} - \sum_j \frac{\partial[\mathrm{TA}]}{\partial \mathrm{X}_j}\nu^i_{\mathrm{X}_j}\right)\mathbf{R}_i \tag{89}$$

Knowing that the sum of all ionization fractions for each total quantity X_j is 1, it can be shown in general that

$$\nu^i_{[\mathrm{TA}]} - \sum_j \frac{\partial[\mathrm{TA}]}{\partial \mathrm{X}_j}\nu^i_{\mathrm{X}_j} = -\nu^i_{\mathrm{H^+}} \tag{90}$$

for all processes i. This provides a direct link between the stoichiometric coefficients of total quantities and the stoichiometric coefficient of protons in the fractional reaction equation at ambient pH. For any process, the negative of the stoichiometric coefficient for protons in the fractional reaction equation at ambient pH is the stoichiometric coefficient of total alkalinity minus the sum of the stoichiometric coefficients of all other total quantities X_j, each weighted with the partial derivative of total alkalinity with respect to X_j.

6. AquaEnv - an Aquatic acid-base modelling Environment in R

A. F. Hofmann, K. Soetaert, J. J. Middelburg, and F. J. R. Meysman
(submitted to Aquatic Geochemistry)

Abstract

AquaEnv is an integrated software package for aquatic chemical model generation focused on ocean acidification and antropogenic CO_2 uptake. However, the package is not restricted to the oceans: it calculates, converts, and visualizes information necessary to describe pH, related CO_2 air-water exchange, as well as aquatic acid-base chemistry in general for marine, estuarine or freshwater systems. AquaEnv is implemented in the open source programming language R and its functionality can be seamlessly integrated into reactive-transport models. Additionally, AquaEnv provides a routine to simulate and investigate titrations of water samples with a strong acid or base, as well as a routine that allows for a determination of total alkalinity and total carbonate values from recorded titration curves using non linear curve-fitting.

6.1. Introduction

With increasing concerns about climate change and ocean acidification (Caldeira and Wickett, 2003; Royal Society, 2005; IPCC, 2007; Gazeau et al., 2007; Guinotte and Fabry, 2008; Doney et al., 2009), there is a strong demand for computational tools that enable a quantitative description of the acid base chemistry of natural waters. These tools are needed from both a modelling point of view as well as from an experimental perspective. Due to increasing complexity in model descriptions of aquatic ecosystems, biogeochemical models now often require the capability of pH prediction and full acid-base speciation (Luff et al., 2001; Caldeira and Wickett, 2005; Jourabchi et al., 2005; Vanderborght et al., 2007; Doney et al., 2007; Blackford and Gilbert, 2007; Zeebe et al., 2008; Aloisi, 2008), (Hofmann et al., 2008a, i.e., Chapter 3), (Hofmann et al., 2009a, i.e., Chapter 4). However, computational tools that describe acid-base speciation are also of interest to observational and experimental scientists: current methods to calculate total alkalinity (and total inorganic carbonate) from measured titration curves, are based on fitting numerical models of the acid-base chemistry of the given water sample (Dickson, 1981; DOE, 1994; Anderson et al., 1999; Dickson et al., 2007).

Currently, there are two computational tools available that describe the acid-base chemistry of natural waters and the ocean carbon system in particular: the CO_2SYS program (Lewis and Wallace, 1998; Pierrot et al., 2006) and the extension package seacarb (Lavigne et al., 2008) for the open-source programming language R (R Development Core Team, 2005). Both programs perform two basic tasks:

1. The calculation of various physical parameters (dissociation constants, solubility constants of calcite and aragonite, Henry's constant of CO_2, etc.) as a function of temperature, salinity and pressure

2. The calculation of pH, the associated acid-base speciation, and the saturation state with respect to calcite and aragonite.

CO_2SYS is historically the oldest program, but has a limited scope and is mainly focused on the ocean carbonate system. Only the phosphate and silicate systems are additionally incorporated as acid-base equilibria, while only the carbonate speciation is provided in the output. Furthermore, the CO_2SYS program is distributed either as a compiled Microsoft DOS program (Lewis and Wallace, 1998) or as a Microsoft Excel spreadsheet (Pierrot et al., 2006), which makes the program static and inflexible. This way, CO_2SYS is difficult to link to an external biogeochemical model code. The package `seacarb` is much better in this respect, as it is implemented in the open-source programming language R. The R framework provides vast capabilities of preprocessing, statistical postprocessing, and visualization of data. Recently, R has also evolved into a suitable platform for biogeochemical model development (Soetaert and Herman, 2009), as powerful packages for numerical integration of differential equations (e.g. deSolve Soetaert et al., 2008) and rootfinding (e.g. rootSolve Soetaert, 2008) have been developed. The R platform is excellently suited for rapid prototyping of biogeochemical models, since it combines an interpreted programming language with the possibility to embed legacy FORTRAN code that enables fast numerical calculations.

Here, we report on the new R package AquaEnv that substantially extends the capabilities of both CO_2SYS and `seacarb`. Compared to the `seacarb` package, AquaEnv calculates a

number of additional quantities, such as the buffer factor, various partial derivatives of total alkalinity, and ionization fractions that are useful for studying and modelling the effect of biogeochemical processes on pH (Hofmann et al., 2008a, 2009a,b, i.e., Chapters 3, 4, 5). In addition, a number of more advanced applications are included. These enable the improved interfacing with numerical biogeochemical models, the generation of "in silico" titrations, and the determination of total alkalinity (and total carbonate) values from measured titration curves by nonlinear optimisation (inverse modelling).

6.2. Structure of the AquaEnv package and an *aquaenv* object

The functionality in the `seacarb` package is established by calls to separate R functions. Rather than implementing a procedure oriented approach, AquaEnv adopts elements of object oriented programming. All functionality is contained within one generic function, termed `aquaenv`, which creates structured objects of the *aquaenv* class (encoded as an R list with multiple elements), termed "*aquaenv* objects" in what follows. Elements within an *aquaenv* object contain all information (physical parameters, acid-base dissociation constants, chemical speciation, partial derivatives, etc.) that can be calculated from the given input parameters. When the user enters too few (underdetermined system) or too many input parameters (overdetermined system), an error message is displayed. Information is obtained by selecting the appropriate element from the *aquaenv* object. At the same time, AquaEnv also includes separate functions that calculate quantities like acid-base dissociation constants.

Once created, *aquaenv* objects can be used in generic plotting and data processing commands, that have been specifically created for the *aquaenv* class. *aquaenv* objects can be converted to an R `data.frame`, which can be further post-processed with standard R routines. Similarly, an R `data.frame` can be converted to an *aquaenv* object, for the use of *aquaenv* object specific plotting facilities provided in AquaEnv. Furthermore, the *aquaenv* objects can be used as input argument supplying initial conditions in the `titration` and `TAfit` functions, which respectively simulate an in silico titration and perform the inverse modelling of titration data to obtain total alkalinity values.

Appendix 6.6.2 details the complete structure of an *aquaenv* object. For each element, the name, physical units and a short explanation are listed. Appendix 6.6.2 also includes an annotated account of the literature references upon which the calculation procedures are based. Appendix 6.6.3 gives all relevant mathematical formulae as well as physical and chemical constants used for calculation of elements of an *aquaenv* object.

6.3. Basic applications

6.3.1. Physical and chemical parameters

AquaEnv provides routines that calculate the key physical and chemical parameters involved in the acid-base chemistry of natural waters. These include the stoichiometric equilibrium constants (K^*) for the major acid base systems (carbonate, ammonia, sulfide, nitrate, nitrite, phosphate, silicate, borate, sulfate, and fluoride), the ion product of water, the Henry's

constants (K_0) that govern the solubility of CO_2 and O_2, as well as the solubility products (K_{sp}) for calcite and aragonite. These parameters are all calculated according to a standard (S, t, p) format, i.e., as a function of salinity (S), temperature in C (t), and the gauge pressure or applied pressure (p) which represents the total pressure (P) minus the atmospheric pressure (P_a) (Millero et al., 2008; Feistel, 2008). Instead of the gauge pressure p also the total pressure P or the water depth d can be given as input parameters. All required mathematical expressions were compiled from various sources in literature as discussed in Appendices 6.6.2 and 6.6.3. Our goal was to arrive at an internally consistent parameter set, where all quantities are expressed using the same concentration units and the same pH scale (molinity and free pH scale - see discussion below). To achieve this, appropriate conversions were applied, using auxiliary variables like seawater density calculated as a function of salinity and temperature, and ionic strength calculated as a function of salinity (see Appendix 6.6.3). These auxiliary variables are also stored as elements in *aquaenv* objects and can thus be accessed by the user (As mentioned, a full list of names of elements contained in *aquaenv* objects is given in Appendix 6.6.2).

6.3.2. Seawater composition

For some biogeochemical applications, the detailed ionic composition of seawater is required. AquaEnv calculates this composition from salinity (according to DOE, 1994; Dickson et al., 2007), determining the total borate concentration ($[\sum B(OH)_3]$), the total sulfate concentration ($[\sum H_2SO_4]$), the total fluoride concentration ($[\sum HF]$), and the ion concentrations of Cl^-, Br^-, Na^+, Mg^{2+}, Ca^{2+}, K^+, and Sr^{2+}. Note that the values for $[\sum B(OH)_3]$, $[\sum H_2SO_4]$, $[\sum HF]$ can also be given as input upon construction of an *aquaenv* object, and in that case, they override the default values calculated from salinity.

6.3.3. pH scales and unit conversions

Acid-base calculations are always characterized by a specific choice of the concentration unit (molarity = mol/l, molality = mol/kg-H_2O, or molinity = mol/kg-solution) and the pH scale (free scale, total scale, seawater scale, and NBS scale, - see discussion on pH scales in Dickson (1984) and Zeebe and Wolf-Gladrow (2001)). To ensure the accuracy and consistency of the calculations, it is vital to consider the issue of concentration units and pH scales. Often, it is only specified that calculations are performed in gravimetric units (i.e., mol/kg). However, with increasing salinity, the difference between the two gravimetric units, molality and molinity, becomes significant, and so, the choice of concentration units must be made explicit. Similarly, the differences between pH scales are significant, especially at higher salinities (Zeebe and Wolf-Gladrow, 2001). Each pH scale is linked to its own specific set of values for the stoichiometric equilibrium constants. Using a mixture of pH scales for equilibrium constants (K^*) and pH values thus will lead to erroneous speciation calculations.

In AquaEnv, the input, output, and internal calculations are all stated in SI units (except for the pressure unit, which is bar instead of Pascal), molinity, and on the free pH scale. Both the input parameters and the elements of an *aquaenv* object can be converted between different concentration units and pH scales using the generic AquaEnv function `convert`. Furthermore, the factors for conversion between molality and molinity (`molal2molin`) and between the free, total and seawater pH scale (`free2tot`, `free2sws`, etr.) are elements of an

aquaenv object. The mathematical relations underlying these conversion functions are also detailed in Appendix 6.6.3.

The conversion from and to the NBS pH scale (mostly used in fresh and brackish waters) requires the activity coefficient for protons in solution (Durst, 1975; Dickson, 1981; Zeebe and Wolf-Gladrow, 2001). In AquaEnv we opted for a simple and direct, albeit approximative approach: we implemented the Davies equation (as stated in Zeebe and Wolf-Gladrow, 2001) to calculate the proton activity coefficient rather than coding a detailed ion interaction model (like, e.g., provided in Millero and Pierrot, 1998). The Davies equation is valid up to an ionic strength of I=0.5 mol/kg-H_2O (Zeebe et al., 2008), and hence, up to a salinity S of ~ 25. Above this salinity, the conversion from and to the NBS pH scale as implemented in AquaEnv should be regarded as approximate.

6.3.4. Acid-base speciation calculations

Given suitable input parameters, AquaEnv calculates the full speciation of all acid-base systems in the solution at hand. As output, one obtains an *aquaenv* object containing the concentrations of all dissociated species in the system, the related ionization fractions (i.e., the ratios of dissociated concentrations over total concentrations), the partial pressure of CO_2, as well as the saturation state $\Omega = [Ca^{2+}][CO_3^{2-}]/K_{sp}$ for calcite and aragonite.

The speciation calculation consist essentially of two steps: the pH is first computed numerically, followed by the analytical calculations that describe the speciation. Numerically, the pH calculation comes down to the solution of a set of non-linear algebraic equations as determined by the mass action equations of the acid-base systems. In AquaEnv, this non-linear system is solved using the iterative approximation approach described in Follows et al. (2006), which is based on the repeated analytical solution of a quadratic equation derived from the mass action equations of the carbonate system only. In cases where this approach does not converge, e.g. in cases with very low or zero total dissolved inorganic carbon concentration ($[\sum CO_2]$), the R function `uniroot` is employed which implements an interval based root finding algorithm. If only the pH needs to be calculated without a full speciation, one can set the flag `speciation` to `FALSE`.

A full speciation is calculated from salinity, temperature, and pressure (determining the stoichiometric equilibrium constants), the total concentrations associated with acid-base systems present ($[\sum CO_2]$, $[\sum NH_4^+]$, $[\sum H_2S]$, $[\sum HNO_3]$, $[\sum HNO_2]$, $[\sum H_3PO_4]$, $[\sum Si(OH)_4]$, $[\sum B(OH)_3]$, $[\sum H_2SO_4]$, $[\sum HF]$), as well as total alkalinity ([TA]), or pH, or the carbon dioxide partial pressure (pCO_2), or the carbon dioxide concentration ($[CO_2]$). Some of the quantities above have default values and do not need to be supplied.

Furthermore, it is possible to calculate $[\sum CO_2]$ and a full speciation from a suitable set of input parameters. To that end, the input value `NULL` needs to be assigned to the argument `SumCO2` and one of the pairs pH and $[CO_2]$, pH and pCO_2, pH and [TA], [TA] and $[CO_2]$, or [TA] and pCO_2 needs to be supplied.

6.3.5. Buffer factor, partial derivatives of total alkalinity, and Revelle factor

Theory states that total alkalinity can be specified as a function of the proton concentration and both the total concentrations and the dissociation constants (K_i^*) of the various acid-base systems.

$$[TA] = f([H^+],\ [\sum CO_2],\ [\sum NH_4^+],\ [\sum H_2S],\ ...,\ K_i^*) \tag{1}$$

Recently, it has been shown that the partial derivatives of this expression are crucial in the description of pH chemistry of natural waters (Hofmann et al., 2008a, 2009a,b, i.e., Chapters 3, 4, 5). In particular, they play a key role in the construction of pH models. The most important partial derivative is the buffer factor β, which is related to buffer quantities introduced by Morel and Hering (1993), Frankignoulle (1994), and Stumm and Morgan (1996), but is defined differently

$$\beta = -\frac{\partial[TA]}{\partial[H^+]} \tag{2}$$

Similarly, the partial derivatives of alkalinity with respect to the concentrations of the other total quantities are important

$$\frac{\partial[TA]}{\partial[\sum CO_2]},\ \frac{\partial[TA]}{\partial[\sum NH_4^+]},\ \frac{\partial[TA]}{\partial[\sum H_2S]},\ ... \tag{3}$$

In AquaEnv, all these partial derivatives are calculated via analytical expressions and are accessible to the user as elements of an *aquaenv* object.

Furthermore, [TA] is a function of the dissociation constants (K_i^*) of the various acid-base systems which, in turn, are functions of salinity S, temperature t and pressure p. Hofmann et al. (2009a, i.e., Chapter 4) show that if these dissociation constants are calculated on one pH scale and then converted to another pH scale, they become functions of $[\sum H_2SO_4]$ and $[\sum HF]$ as well. In general

$$K_i^* = f(S,\ t,\ p,\ [\sum H_2SO_4],\ [\sum HF]) \tag{4}$$

Hofmann et al. (2009a, i.e., Chapter 4) show that the products of the partial derivatives of [TA] with respect to the dissociation constants K_i^* and the partial derivative of the dissociation constants K_i^* with respect to one of their variables are needed for their explicit pH modelling approach. Therefore, AquaEnv numerically calculates

$$\sum_i \frac{\partial[TA]}{\partial K_i^*}\frac{\partial K_i^*}{\partial S},\ \sum_i \frac{\partial[TA]}{\partial K_i^*}\frac{\partial K_i^*}{\partial t},\ \sum_i \frac{\partial[TA]}{\partial K_i^*}\frac{\partial K_i^*}{\partial p},\ \sum_i \frac{\partial[TA]}{\partial K_i^*}\frac{\partial K_i^*}{\partial[\sum H_2SO_4]},\ \sum_i \frac{\partial[TA]}{\partial K_i^*}\frac{\partial K_i^*}{\partial[\sum HF]} \tag{5}$$

and provides these quantities as elements of an *aquaenv* object. Furthermore, as a related quantity, the well known Revelle factor (e.g. Zeebe and Wolf-Gladrow, 2001), which is defined as

$$RF_0 = \left(\frac{d[CO_2]}{[CO_2]} \Big/ \frac{d[\sum CO_2]}{[\sum CO_2]}\right)_{[TA]=\text{const.}} \tag{6}$$

is numerically calculated in AquaEnv and provided as element of an *aquaenv* object.

Details of how to use the partial derivatives of total alkalinity in reactive-transport models are given in (Hofmann et al., 2008a, 2009a,b, i.e., Chapters 3, 4, 5). Furthermore, section 6.4.1 provides simple example models employing some of these quantities.

6.3.6. Sensitivity analysis

One of the input variables for the function aquaenv may be a vector. All other input variables are then assumed to be constant. As a result, an *aquaenv* object is created which contains vectors of the respective elements as functions of the input vector. Together with the plotting functionality specific for *aquaenv* objects, this enables a simple form of sensitivity analysis and its visualisation. Figure 6.1 shows how AquaEnv can be used to visualize how salinity variations in estuaries change the carbonate speciation (and pH; not shown).

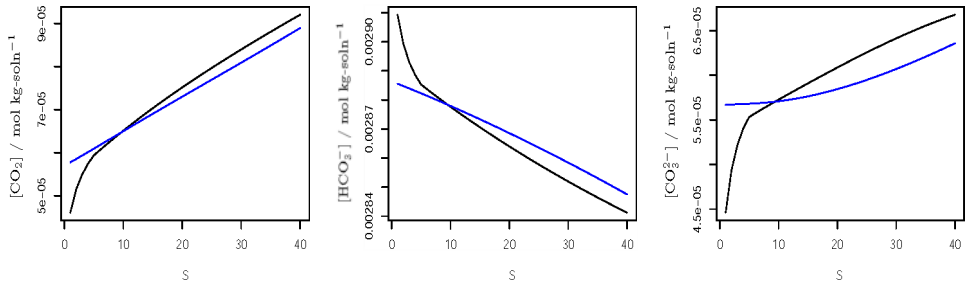

Figure 6.1.: Using AquaEnv to visualize the sensitivity of the carbonate speciation towards changes in salinity S. Black line: using a salinity dependence for the first and second dissociation constants of the carbonate system as given in Roy et al. (1993b) with a freshwater formulation for salinities below 5, as advised in Millero (1995) (these functions are used by default in AquaEnv). Blue line: using a salinity dependence for the first and second dissociation constants of the carbonate system as given in Lueker et al. (2000), as advised in Dickson et al. (2007) (these functions can be used in AquaEnv by setting the flag k1k2 to the value "lueker"). Note that [TA] and $[\sum CO_2]$ have been kept constant at 0.003 mol/kg-solution. Note further that $[\sum B(OH)_3]$, $[\sum H_2SO_4]$, and $[\sum HF]$ are calculated from salinity. The plotted effect of changes in S on the carbonate speciation is thus twofold: via the salinity dependency of the dissociation constants and via the salinity dependency of $[\sum B(OH)_3]$, $[\sum H_2SO_4]$, and $[\sum HF]$.

6.3.7. Data visualization

The plot.aquaenv function is the generic plotting method for *aquaenv* objects. (Within the R object oriented programming environment this function can be called as plot without the .aquaenv suffix.) This plotting method visualizes the information contained in an *aquaenv* object in a multifunctional way. It (1) can be used to visualize the sensitivity of a system

with respect to changes in one input parameter (Figure 6.1). (2) The `plot.aquaenv` function can be used to create Bjerrum plots which are the classical textbook way of displaying the speciation of acid-base systems as a function of pH (e.g. Zeebe and Wolf-Gladrow, 2001). Section 6.4.2 provides examples of how Bjerrum plots can be created with the `plot.aquaenv` function. (3) `plot.aquaenv` can generate "cumulative" plots that attribute the total rate of change of protons to different processes. Section 6.4.1 provides an example for this cumulative plotting functionality. The usage and syntax of the `plot.aquaenv` function is detailed in its R help file as well as in the package vignette of AquaEnv.

6.4. Advanced applications

6.4.1. AquaEnv in reactive transport models

When simulating the biogeochemistry of natural waters, one often needs to explicitly deal with pH dynamics. As a result, the corresponding reactive transport models need to include an acid-base speciation routine as a subcomponent. The function `aquaenv` fits this purpose. At each timestep of a dynamic model, `aquaenv` can calculate the desired information related to the "acid-base state" of the system (physical parameters, speciation, buffer capacity, partial derivatives etc.). We will show the use of `aquaenv` by means of a simple example model of an aquatic system.

Over a time scale of days, the pH chemistry of a water reservoir is known to be influenced by two processes: $CaCO_3$ precipitation and CO_2 exchange across the air-water interface. These two dominant processes can be represented by the reaction equations

$$Ca^{2+} + CO_3^{2-} \rightarrow CaCO_3 \tag{7}$$

$$CO_2(g) \rightleftharpoons CO_2 \tag{8}$$

The associated kinetic rate laws are:

$$\mathbf{R}_P = k_P (1 - \Omega)^n \tag{9}$$

$$\mathbf{R}_C = k_C ([CO_2]_{sat} - [CO_2]) \tag{10}$$

In addition, the pH chemistry will also depend on a number of "fast" acid-base dissociation reactions, with characteristic time scales of less than a minute (Zeebe and Wolf-Gladrow, 2001). To keep the model suitably simple, only the carbonate system is accounted for

$$CO_2 + H_2O \rightleftharpoons HCO_3^- + H^+ \tag{11}$$

$$HCO_3^- \rightleftharpoons CO_3^{2-} + H^+ \tag{12}$$

The equilibrium mass action equations for these two acid-base reactions are, respectively:

$$K^*_{CO_2} = \frac{[H^+][HCO_3^-]}{[CO_2]} \tag{13}$$

$$K^*_{HCO_3^-} = \frac{[H^+][CO_3^{2-}]}{[HCO_3^-]} \tag{14}$$

As detailed in Hofmann et al. (2009b, i.e., Chapter 5), there are two main model approaches to arrive at the pH evolution of the water reservoir. In the "alkalinity centered" or "implicit

pH modelling approach", one focuses on the effect of the kinetic processes on alkalinity ([TA]) and the total carbonate concentration ($[\sum CO_2]$) in the system. As a result, one obtains two differential equations describing the evolution of [TA] and $[\sum CO_2]$

$$\frac{d[\mathrm{TA}]}{dt} = -2\mathbf{R}_P \tag{15}$$

$$\frac{d[\sum CO_2]}{dt} = \mathbf{R}_C - \mathbf{R}_P \tag{16}$$

Since the kinetic rate laws (Eqs. (9) and (10)) feature concentrations of dissociated species, the integration of Eqs. (15) and (16) requires a two-step approach (e.g. Luff et al., 2001; Follows et al., 2006). Starting with initial values for [TA] and $[\sum CO_2]$, one performs an "equilibration step" that calculates the concentrations of all dissociated species as a function of [TA] and $[\sum CO_2]$. Subsequently, an "integration step" is performed: the kinetic rate terms, which feature the concentrations of the dissociated species $[CO_2]$ and $[CO_3^{2-}]$ are calculated, and the resulting rates of change of [TA] and $[\sum CO_2]$ are passed on to the integrator which returns new values for [TA] and $[\sum CO_2]$. Those new values, in turn, can be used for another "equilibration step". By repeating this two-step procedure for a suitable sequence of time steps, one eventually obtains the evolution of [TA], $[\sum CO_2]$, pH and all dissociated species over the desired time interval. The function `aquaenv` can be invoked to conveniently perform the "equilibration step": with one function call, the pH and a full speciation is calculated.

An alternative approach to pH modelling was recently proposed (Hofmann et al., 2008a, 2009b, i.e., Chapters 3, 4). The method was termed the "proton-centered" or "explicit" pH modelling approach, as it is based on an explicit evolution equation for the proton concentration. Rather than using an evolution equation for alkalinity, one integrates following differential equation for the proton concentration

$$\frac{d[\mathrm{H}^+]}{dt} = S_P\mathbf{R}_P + S_C\mathbf{R}_C \tag{17}$$

The quantities S_P and S_C are respectively termed the *sensitivities* of pH with respect to $CaCO_3$ precipitation and CO_2 exchange. They are defined as

$$S_P = \frac{1}{\left(\frac{\partial[\mathrm{TA}]}{\partial \mathrm{H}^+}\right)}\left(-2 + \frac{\partial[\mathrm{TA}]}{\partial[\sum CO_2]}\right) \tag{18}$$

$$S_C = \frac{1}{\left(\frac{\partial[\mathrm{TA}]}{\partial \mathrm{H}^+}\right)}\left(-\frac{\partial[\mathrm{TA}]}{\partial[\sum CO_2]}\right) \tag{19}$$

The sensitivities thus feature partial derivatives of total alkalinity [TA], which are calculated in a closed analytical form by the function `aquaenv`.

Hofmann et al. (2009b, i.e., Chapter 5) show that the sensitivities of pH with respect to biogeochemical processes can also be expressed using ionization fractions (Skoog and West, 1982; Stumm and Morgan, 1996), here of the carbonate system ($c_1 = [CO_2]/[\sum CO_2]$, $c_2 = [HCO_3^-]/[\sum CO_2]$, $c_3 = [CO_3^{2-}]/[\sum CO_2]$)

$$S_P = \frac{1}{\left(-\frac{\partial[\mathrm{TA}]}{\partial[\sum \mathrm{CO_2}]}\right)} (2c_1 + c_2) \quad (20)$$

$$S_C = \frac{1}{\left(-\frac{\partial[\mathrm{TA}]}{\partial[\sum \mathrm{CO_2}]}\right)} (c_2 + 2c_3) \quad (21)$$

Ionization fractions are calculated by the function `aquaenv` as well.

The full implementation of the implicit and explicit pH modelling approaches into R code using the `aquaenv` function is detailed in Appendix 6.6.1.1. The implicit and explicit pH modelling approaches provide exactly the same evolution of pH, alkalinity, the total carbonate concentration, and all other quantities as a function of time (Fig (6.2)). However, the explicit modelling approach has the important conceptual advantage that it allows a systematic investigation of the sensitivity of pH to the associated biogeochemical processes. Equation (17) specifies that the influence of a given process on pH can always be decomposed as a modulating factor, which is the sensitivity of pH with respect to that process, times the process rate. This way, one can attribute the observed pH changes in a given system to particular processes. Using the `plot.aquaenv` function, this can be illustrated in a cumulative plot (Fig (6.3)).

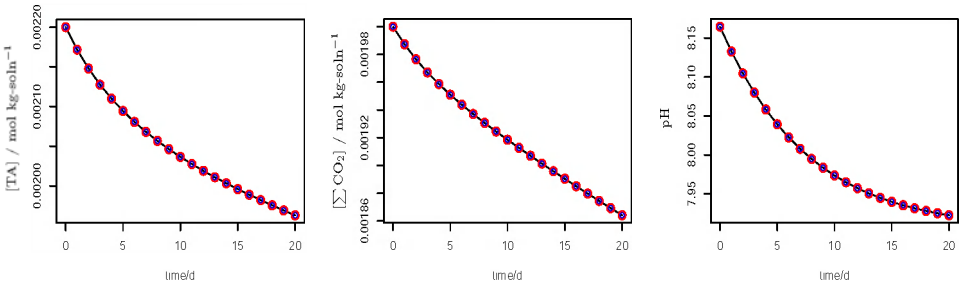

Figure 6.2.: Comparison of the results of the implicit and explicit pH modelling approaches using the function `aquaenv`. Black line: implicit approach, Blue circles: explicit approach expressing sensitivities of pH with partial derivatives (Eqs. (18) and (19)), Red circles: explicit approach expressing sensitivities of pH using ionization fractions (Eqs. (20) and (21)). Initial values and model parameters are given in the R code in Appendix 6.6.1.1

6.4.2. Titration simulation

In aquatic chemistry, one important experimental procedure is titration. The function `titration` within AquaEnv provides a tool to simulate titrations, i.e., to perform "in silico" titrations. The archetypal titration procedure involves an initial water sample to which concentrated monoprotic acid or base is added in a stepwise fashion. The `titration` function in AquaEnv describes how the composition of a water sample changes due to the addition of titrant solution which can be either a strong acid (typically HCl) or a strong base (typically

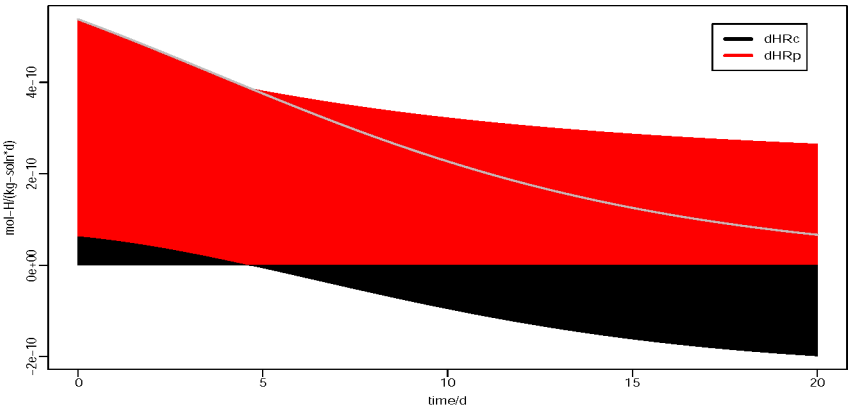

Figure 6.3.: Cumulative plot of the influences of kinetically modelled processes on the pH using the function `plot.aquaenv`. The gray line represents the net rate of change of the proton concentration over time and the coloured areas signify gross rates due to the two processes calcium carbonate precipitation and CO_2 air-sea exchange adding up to the net rate.

NaOH). Titration with multiprotic acids is not accounted for.

To simulate a titration using AquaEnv, one proceeds in two steps. First, the composition of the initial water sample has to specified. This is done via creating an *aquaenv* object by specifying salinity, temperature, and pressure, as well as the initial pH (or equally [TA]), and the concentrations of all total quantities. This *aquaenv* object describing the initial conditions will be the first argument of the function `titration`. As further arguments, one has to specify the mass of the initial sample solution (`mass_sample`), the concentration of the titrant (`conc_titrant`), the salinity of the titrant solution (`S_titrant`), the total mass of titrant solution added (`mass_titrant`), the number of titration steps (`steps`), and the type of the titrant (either a strong acid indicated by "HCl", or a strong base indicated by "NaOH" as values for the argument `type` with the default value "HCl"). Note that the titration simulation accounts for changes in the salinity of the titrated solution due to dilution of the original sample by the titrant (which may influence acid-base equilibria), as well as for volume changes and thus also the dilution of concentrations ($[\sum CO_2]$, etc.) due to the addition of titrant. The logical flag `seawater_titrant` decides whether the titrant contains borate, sulfate and fluoride (titration with natural seawater), or not (titration with artificial seawater). The usage and syntax of the `titration` function is detailed in its R help file as well as in the package vignette of AquaEnv. Example titrations expressed in R code are given in Appendix 6.6.1.2.

Results can be visualized by plotting pH and speciation against the amount of titrant added or any other variable in the *aquaenv* object (Figure 6.4). However, an *aquaenv* object containing an in silico titration can also be visualized via Bjerrum plots (Figure 6.5). The respective calls to the function `plot.aquaenv` are given in Appendix 6.6.1.2.

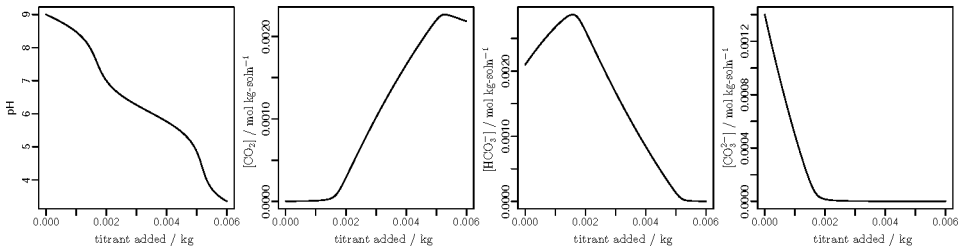

Figure 6.4.: Visualizing the results of an in silico titration. Note that the CO_2 concentration declines towards the right of the plot. This is due to the fact that the `titration` function takes into account the dilution of the dissolved inorganic carbonate concentration due to the addition of titrant.

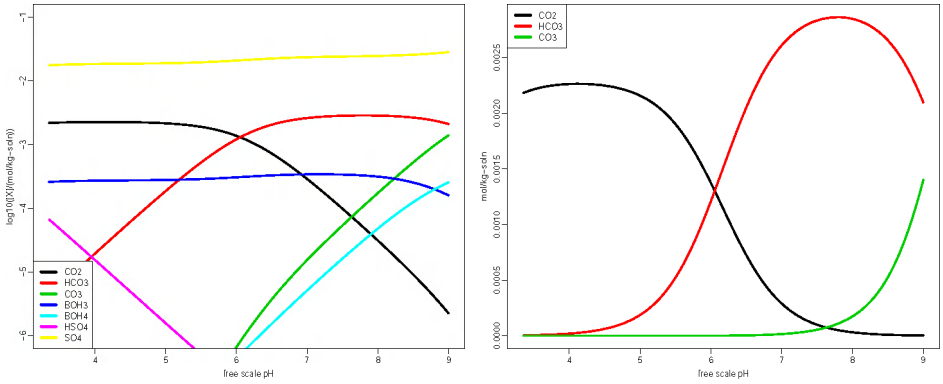

Figure 6.5.: Left panel: Bjerrum plot of a selection of concentrations of dissociated species in the example in silico titration, concentrations are plotted on logarithmic scale. Right panel: Bjerrum-like plot, concentrations are not plotted on logarithmic scale.

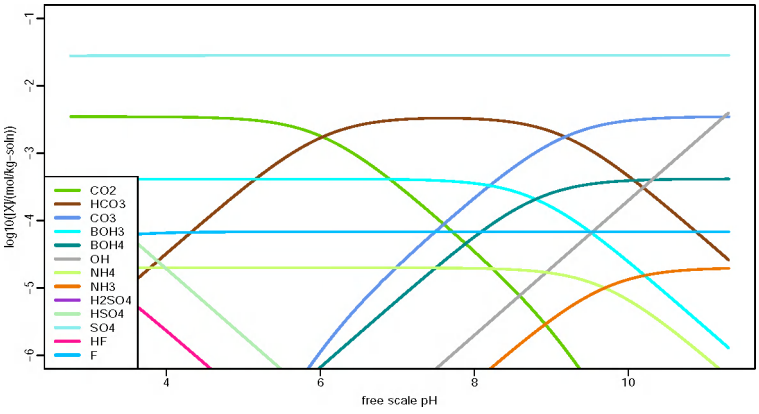

Figure 6.6.: Classical textbook Bjerrum plot using an in silico titration object

The plots in Figure 6.5 differ from the classical textbook Bjerrum graphs (e.g. Zeebe and Wolf-Gladrow, 2001) since the effect of dilution due to the addition of titrant is accounted for. When simulating a titration with a rather large volume and a concentrated titrant, the volume and salinity corrections are only minor, and one obtains the classical Bjerrum graphs known from textbooks (see Figure 6.6 and example titration 2 in Appendix 6.6.1.2).

6.4.3. Titration data analysis: obtaining total alkalinity and total carbonate from titration data

The function `TAfit` is based on a method described in DOE (1994) and Dickson et al. (2007), makes use of the in silico titration function `titration` provided in AquaEnv, and allows for determining total alkalinity ([TA]), the total dissolved inorganic carbon concentration[1] ($[\sum CO_2]$), as well as the electrode standard potential (E_0) and the first dissociation constant of the carbonate system ($K^*_{CO_2}$) from measured titration curves (pH versus the mass of titrant added) using an inverse modelling procedure. The Levenberg-Marquardt least squares optimization algorithm as provided in the R package minpack.lm (Elzhov and Mullen, 2008) is employed to match calculated and measured titration curves.

The underlying principle of `TAfit` is simple: it generates an in silico titration curve (using an initial *aquaenv* object and the supplied parameters `conc_titrant`, `mass_sample`, `S_titrant`, and `seawater_titrant` which are passed on to the function `titration`) with arbitrary values for [TA], $[\sum CO_2]$, and E_0 (if an electrode potential curve is used). This in silico titration curve is then compared to the measured curve. In an iterative least-squares procedure, the arbitrary values for [TA], $[\sum CO_2]$, and E_0 are then refined to the "best-fitting" values by matching the calculated and the measured titration curve (by setting the flag `verbose` to `TRUE`, the fitting process can be visualized while it is performed). Note that, although `TAfit` always returns values for [TA] and $[\sum CO_2]$, the $[\sum CO_2]$ value only reflects the value of the original sample if the titration is conducted in a closed vessel to prevent equilibration with the air. Due to uncertainties in the first dissociation constant of the carbonate system $K^*_{CO_2}$, it is sometimes advised to fit this constant in the iterative least-squares procedure as well (this can be specified in `TAfit` via the logical flag `K_CO2fit`). All other dissociation constants are calculated from salinity, temperature, and pressure. This curve fitting procedure was introduced by Dickson (1981), restated in DOE (1994) and Dickson et al. (2007), and mentioned in Anderson et al. (1999) and Zeebe and Wolf-Gladrow (2001). Additionally, Dickson et al. (2007) employ a variant of this method: a [TA] value is obtained by fitting only a part of the total titration curve after the sample has been acidified to expel all carbonate from the solution. The function `TAfit` is also capable of fitting only a part of a titration curve: with the argument `datxbegin` the amount of titrant added to acidify the sample before the actual titration can be specified. The usage and syntax of the `TAfit` function is detailed in its R help file as well as in the package vignette of AquaEnv.

For computational reasons, Johansson and Wedborg (1982) and Anderson et al. (1999) suggested to switch the dependent and independent variables, i.e., to calculate a theoretical vector of titrant masses instead of a vector of theoretical pH or E values while calculating the in silico

[1] Although it is possible to also determine total dissolved inorganic carbonate concentrations from closed-cell titration data analysis, Dickson et al. (2007) recommend a more accurate method based on expelling all dissolved inorganic carbon in a sample as gaseous CO_2 via acidification and subsequent gas analysis.

titration curve. This has the advantage that one does not need to solve a non linear equation system for the pH at every point of every in silico titration. However, due to the fact that in curve fitting algorithms the sum of squares of errors in the dependent variable is minimized, while errors in the independent variable are disregarded, Anderson et al. (1999) concluded that in principle the pH (or E) values would be the best choice as dependent variable, as their associated measurement uncertainty is larger than the measurement uncertainty for the amount of titrant added. Since nowadays computational power is not limiting anymore, we implemented the `TAfit` function of AquaEnv such that pH or E serve as dependent variables.

The functioning of `TAfit` is illustrated with a simple example. Dickson (1981) provided a benchmark test for total alkalinity fitting programs in the form of a synthetic dataset. This dataset is included in AquaEnv as the object `sample_dickson1981`. Dickson (1981) uses fixed values for the equilibrium constants instead of calculating them as functions of salinity and temperature. `TAfit` allows for providing fixed values for the main dissociation constants, so the values given in Dickson (1981) can be used for the fitting procedure. As shown in the script and associated output given in Appendix 6.6.1.3, the values for [TA] and $[\sum CO_2]$ returned by the function `TAfit` are exactly the same as given in Dickson (1981), i.e., the fitting procedure yields the correct values.

6.5. Summary

The R-package AquaEnv provides an integrated framework for acid-base speciation calculations and pH modelling. AquaEnv extends the functionality and application domain of packages like CO_2SYS (Lewis and Wallace, 1998; Pierrot et al., 2006) and seacarb (Lavigne et al., 2008). The package is not only applicable to seawater, but also to brackish and freshwater environments, and it not only deals with carbonate chemistry, but also includes a large selection of other relevant acid base systems in natural waters. We adopted an object oriented programming style by letting the function `aquaenv` create objects of a certain class which then can be visualized and processed with the functions `plot` and `convert`, but can also be exported to an R `data.frame` for further processing. AquaEnv allows a seamless integration with complex biogeochemical models, and provides functions that allow to simulate titrations and to calculate alkalinity and total carbonate values from titration data.

6.6. Appendix

6.6.1. **AquaEnv** example scripts

6.6.1.1. pH modelling using the implicit and explicit approaches

```
########################################
#### IMPLICIT approach #################
########################################
require(AquaEnv)
what   <- c("SumCO2", "TA", "Rc", "Rp", "omega_calcite", "pH")

parameters <- list(
                  S          = 35        , # psu
                  t          = 15        , # degrees C

                  SumCO2_t0   = 0.002    , # mol/kg-soln
                  TA_t0       = 0.0022   , # mol/kg-soln

                  kc          = 0.5      , # 1/d
                  kp          = 0.000001 , # mol/(kg-soln*d)
                  n           = 2.0      , # -

                  modeltime   = 20       , # d
                  outputsteps = 20
                 )

implicit.pH.model <- function(timestep, currentstate, parameters)
  {
    with(as.list(c(currentstate,parameters)),
         {
           ae    <- aquaenv(S=S, t=t, SumCO2=SumCO2, TA=TA,
                            SumSiOH4=0, SumBOH3=0, SumH2SO4=0, SumHF=0)

           Rc      <- kc * ((ae$CO2_sat) - (ae$CO2))
           Rp      <- kp * (1-ae$omega_calcite)^n

           dSumCO2 <- Rc - Rp
           dTA     <- -2*Rp

           ratesofchanges <- c(dSumCO2, dTA)
           processrates   <- c(Rc=Rc, Rp=Rp)
           return(list(ratesofchanges, list(processrates, ae)))
         })
  }

with (as.list(parameters),
      {
```

```
        initialstate <<- c(SumCO2=SumCO2_t0, TA=TA_t0)
        times        <<- seq(0,modeltime,(modeltime/outputsteps))
        output       <<- as.data.frame(vode(initialstate,times,
                                    implicit.pH.model,parameters, hmax=1))
      })

plot(aquaenv(ae=output, from.data.frame=TRUE), xval=output$time, xlab="",
      mfrow=c(2,3), size=c(15,7), what=what)



##############################################################################
# EXPLICIT approach expressing sensitivities of pH with partial derivatives #
##############################################################################
what   <- c("SumCO2", "TA", "Rc", "Rp", "omega_calcite",
            "pH", "dHRc", "dHRp")

explicit.pH.model <- function(timestep, currentstate, parameters)
  {
     with(as.list(c(currentstate, parameters)),
          {
            ae <- aquaenv(S=S, t=t, SumCO2=SumCO2, pH=-log10(H),
                          SumBOH3=0, SumH2SO4=0, SumHF=0, dsa=TRUE)

            Rc <- kc * ((ae$CO2_sat) - (ae$CO2))
            Rp <- kp * (1 - ae$omega_calcite)^n

            dSumCO2 <- Rc - Rp

            dHRp    <- ((-2 + ae$dTAdSumCO2)/ae$dTAdH)*Rp
            dHRc    <- ((-ae$dTAdSumCO2)/ae$dTAdH)*Rc
            dH      <- dHRc + dHRp

            ratesofchanges <- c(dSumCO2, dH)
            processrates   <- c(Rc=Rc, Rp=Rp)
            outputvars     <- c(dHRc=dHRc, dHRp=dHRp)

            return(list(ratesofchanges, list(processrates, outputvars, ae)))
          })
  }

with (as.list(parameters),
      {
        aetmp <- aquaenv(S=S, t=t, SumCO2=SumCO2_t0, TA=TA_t0,
                         SumSiOH4=0, SumBOH3=0, SumH2SO4=0, SumHF=0)
        H_t0  <- 10^(-aetmp$pH)
```

```
        initialstate <<- c(SumCO2=SumCO2_t0, H=H_t0)
        times        <<- seq(0,modeltime,(modeltime/outputsteps))
        output       <<- as.data.frame(vode(initialstate,times,
                                            explicit.pH.model,
                                            parameters, hmax=1))
      })

plot(aquaenv(ae=output, from.data.frame=TRUE), xval=output$time,
     xlab="time/d", mfrow=c(3,3), size=c(15,10), what=what)



##############################################################################
# EXPLICIT approach expressing sensitivities of pH w. ionization fractions #
##############################################################################
explicit.pH.model <- function(timestep, currentstate, parameters)
  {
     with(as.list(c(currentstate, parameters)),
          {
            ae <- aquaenv(S=S, t=t, SumCO2=SumCO2, pH=-log10(H),
                          SumBOH3=0, SumH2SO4=0, SumHF=0, dsa=TRUE)

            Rc <- kc * ((ae$CO2_sat) - (ae$CO2))
            Rp <- kp * (1 - ae$omega_calcite)^n

            dSumCO2 <- Rc - Rp

            dHRc <- ((ae$c2 + 2*ae$c3)/(-ae$dTAdH))*Rc
            dHRp <- ((2*ae$c1 + ae$c2)/(-ae$dTAdH))*Rp
            dH   <- dHRc + dHRp

            ratesofchanges <- c(dSumCO2, dH)
            processrates   <- c(Rc=Rc, Rp=Rp)
            outputvars     <- c(dHRc=dHRc, dHRp=dHRp)

            return(list(ratesofchanges, list(processrates, outputvars, ae)))
          })
  }

with (as.list(parameters),
      {
        aetmp <- aquaenv(S=S, t=t, SumCO2=SumCO2_t0, TA=TA_t0,
                         SumSiOH4=0, SumBOH3=0, SumH2SO4=0, SumHF=0)
        H_t0  <- 10^(-aetmp$pH)

        initialstate <<- c(SumCO2=SumCO2_t0, H=H_t0)
        times        <<- seq(0,modeltime,(modeltime/outputsteps))
```

```
        output       <<- as.data.frame(vode(initialstate,times,
    explicit.pH.model,
                                            parameters, hmax=1))
      })

plot(aquaenv(ae=output, from.data.frame=TRUE), xval=output$time,
     xlab="time/d", mfrow=c(3,3), size=c(15,10), what=what)

what <- c("dHRc", "dHRp")
plot(aquaenv(ae=output, from.data.frame=TRUE), xval=output$time,
     xlab="time/d", what=what, ylab="mol-H/(kg-soln*d)",
     legendposition="topright", cumulative=TRUE, size=c(10,6))
```

6.6.1.2. Titration simulations

```
########################################
#### example titration 1 #################
########################################
require(AquaEnv)
initial_sample      <- aquaenv(S=35, t=15, SumCO2=0.0035, SumNH4=2e-05, pH=9)
virtual_titration   <- titration(initial_sample, mass_sample=0.01,
                                 mass_titrant=0.006, conc_titrant=0.01,
                                 S_titrant=0.5, steps=100)


# plot against the amount of titrant added
########################################
what <- c("pH", "CO2", "HCO3", "CO3")
plot(virtual_titration, xval=virtual_titration$delta_mass_titrant,
     xlab="titrant added / kg", what=what, mfrow=c(1,4), size=c(10,2.5))

# Bjerrum plot
##############
what <- c("CO2", "HCO3", "CO3", "BOH3", "BOH4", "HSO4", "SO4")
plot(virtual_titration, what=what, bjerrum=TRUE, log=TRUE, ylim=c(-6, -1),
     legendinset=0, lwd=3, size=c(9,7))

# Bjerrum-like plot
###################
what <- c("CO2", "HCO3", "CO3")
plot(virtual_titration, what=what, bjerrum=TRUE, legendinset=0,
     legendpos="topleft", lwd=3, size=c(9,7))


#################################################################
#### example titration 2: classical textbook Bjerrum plots #####
#################################################################
```

```
initial_sample    <- aquaenv(S=35, t=15, SumCO2=0.0035, SumNH4=0.00002,
                             pH=11.3)
virtual_titration <- titration(initial_sample, mass_sample=100,
                               mass_titrant=0.45, conc_titrant=3,
                               S_titrant=0.5, steps=100)
what  <- c("CO2", "HCO3", "CO3", "BOH3", "BOH4", "OH", "NH4",
           "NH3", "H2SO4", "HSO4", "SO4", "HF", "F")
palette <- colors()[seq(50,150,6)]
plot(virtual_titration, what=what, bjerrum=TRUE, log=TRUE, ylim=c(-6,-1),
     legendinset=0, lwd=3, palette=palette, size=c(10,6))
```

6.6.1.3. Determining [TA] from titration curves

```
require(AquaEnv)
sample     <- cbind(sample_dickson1981[, 1]/1000, sample_dickson1981[, 2])
dicksonfit <- TAfit(aquaenv(t=25, S=35, SumBOH3=0.00042, SumH2SO4=0.02824,
                    SumHF=7e-05, k_w=4.32e-14, k_co2=1e-06, k_hco3=8.2e-10,
                    k_boh3=1.78e-09, k_hso4=(1/12.3), k_hf=(1/408)), sample,
                    conc_titrant=0.3, mass_sample=0.2, S_titrant=14.835,
                    k_w=4.32e-14, k_co2=1e-06, k_hco3=8.2e-10,
                    k_boh3=1.78e-09, k_hso4=(1/12.3), k_hf=(1/408))
dicksonfit

$TA
[1] 0.00245
attr(,"unit")
[1] "mol/kg-soln"

$SumCO2
[1] 0.0022
attr(,"unit")
[1] "mol/kg-soln"

$sumofsquares
[1] 3.279302e-12
```

6.6.2. Elements of an *aquaenv* object

Maximally, i.e., if enough input data is supplied to define the pH of the system and the flags `speciation`, `dsa`, and `revelle` are `TRUE` while the flag `skeleton` is `FALSE`, an *aquaenv* object contains the following elements

element	unit	explanation
`S`	"psu" (no unit)	salinity
`t`	C	temperature
`p`	bar	gauge pressure (total pressure minus atmospheric pressure Feistel, 2008)
`T`	K	absolute temperature
`Cl`	‰	chlorinity
`I`	mol/kg-H_2O	ionic strength
`P`	bar	total pressure
`Pa`	bar	atmospheric pressure
`d`	m	depth
`density`	kg/m^3	(seawater) density
`SumCO2`	mol/kg-soln	$[\sum CO_2]$, total dissolved inorganic carbon concentration
`SumNH4`	mol/kg-soln	$[\sum NH_4^+]$, total ammonium concentration
`SumH2S`	mol/kg-soln	$[\sum H_2S]$, total sulfide concentration
`SumHNO3`	mol/kg-soln	$[\sum HNO_3]$, total nitrate concentration
`SumHNO2`	mol/kg-soln	$[\sum HNO_2]$, total nitrite concentration
`SumH3PO4`	mol/kg-soln	$[\sum H_3PO_4]$, total phosphate concentration
`SumSiOH4`	mol/kg-soln	$[\sum Si(OH)_4]$, total silicate concentration
`SumBOH3`	mol/kg-soln	$[\sum B(OH)_3]$, total borates concentration
`SumH2SO4`	mol/kg-soln	$[\sum H_2SO_4]$, total sulfate concentration
`SumHF`	mol/kg-soln	$[\sum HF]$, total fluoride concentration
`SumBr`	mol/kg-soln	$[\sum HBr]$, total bromide concentration
`ClConc`	mol/kg-soln	$[Cl^-]$, chloride concentration
`Na`	mol/kg-soln	$[Na^+]$, sodium concentration
`Mg`	mol/kg-soln	$[Mg^{2+}]$, magnesium concentration
`Ca`	mol/kg-soln	$[Ca^{2+}]$, calcium concentration
`K`	mol/kg-soln	$[K^+]$, potassium concentration
`Sr`	mol/kg-soln	$[Sr^{2+}]$, strontium concentration
`molal2molin`	(mol/kg-soln)/(mol/kg-H2O)	concentration conversion factor: from molality to molinity
`free2tot`	-	pH conversion factor: free scale to total scale
`free2sws`	-	pH conversion factor: free scale to sawater scale
`tot2free`	-	pH conversion factor: total scale to free scale
`tot2sws`	-	pH conversion factor: total scale to seawater scale
`sws2free`	-	pH conversion factor: seawater scale to free scale
`sws2tot`	-	pH conversion factor: seawater scale to total scale
`K0_CO2`	mol/(kg-soln*atm)	Henry's constant for CO_2
`K0_O2`	mol/(kg-soln*atm)	Henry's constant for O_2
`CO2_sat`	mol/kg-soln	CO_2 saturation concentration at an atmospheric partial pressure/fugacity of Fugacity CO2
`O2_sat`	mol/kg-soln	O_2 saturation concentration at an atmospheric partial pressure/fugacity of Fugacity O2
`K_W`	(mol/kg-soln)^2, free pH scale	stoichiometric equilibrium ion product of H_2O: $K^*_W = [H^+][OH-]$
`K_HSO4`	mol/kg-soln, free pH scale	stoichiometric equilibrium constant $K^*_{HSO_4^-} = [H^+][SO_4^{2-}]/[HSO_4^-]$
`K_HF`	mol/kg-soln, free pH scale	stoichiometric equilibrium constant $K^*_{HF} = [H^+][F^-]/[HF]$
`K_CO2`	mol/kg-soln, free pH scale	stoichiometric equilibrium constant $K^*_{CO_2} = [H^+][HCO_3^-]/[CO_2]$

K_HCO3	mol/kg-soln, free pH scale	stoichiometric equilibrium constant $K^*_{HCO_3^-} = [H^+][CO_3^{2-}]/[HCO_3^-]$
K_BOH3	mol/kg-soln, free pH scale	stoichiometric equilibrium constant $K^*_{B(OH)_3} = [H^+][B(OH)_4^-]/[B(OH)_3]$
K_NH4	mol/kg-soln, free pH scale	stoichiometric equilibrium constant $K^*_{NH_4^+} = [H^+][NH_3]/[NH_4^+]$
K_H2S	mol/kg-soln, free pH scale	stoichiometric equilibrium constant $K^*_{H_2S} = [H^+][HS^-]/[H_2S]$
K_H3PO4	mol/kg-soln, free pH scale	stoichiometric equilibrium constant $K^*_{H_3PO_4} = [H^+][H_2PO_4^-]/[H_3PO_4]$
K_H2PO4	mol/kg-soln, free pH scale	stoichiometric equilibrium constant $K^*_{H_2PO_4^-} = [H^+][HPO_4^{2-}]/[H_2PO_4^-]$
K_HPO4	mol/kg-soln, free pH scale	stoichiometric equilibrium constant $K^*_{HPO_4^{2-}} = [H^+][PO_4^{3-}]/[HPO_4^{2-}]$
K_SiOH4	mol/kg-soln, free pH scale	stoichiometric equilibrium constant $K^*_{Si(OH)_4} = [H^+][SiO(OH)_3^-]/[Si(OH)_4]$
K_SiOOH3	mol/kg-soln, free pH scale	stoichiometric equilibrium constant $K^*_{SiO(OH)_3^-} = [H^+][SiO_2(OH)_2^{2-}]/[SiO(OH)_3^-]$
K_HNO2	mol/kg-soln; mol/kg-H2O; mol/l	approximate value for equilibrium constant $K^*_{HNO_2} = [H^+][NO_2^-]/[HNO_2]$
K_HNO3	mol/kg-soln; mol/kg-H2O; mol/l	approximate value for equilibrium constant $K^*_{HNO_3} = [H^+][NO_3^-]/[HNO_3]$
K_H2SO4	mol/kg-soln; mol/kg-H2O; mol/l	approximate value for equilibrium constant $K^*_{H_2SO_4} = [H^+][HSO_4^-]/[H_2SO_4]$
K_HS	mol/kg-soln; mol/kg-H2O; mol/l	approximate value for equilibrium constant $K^*_{HS^-} = [H^+][S^{2-}]/[HS^-]$
Ksp_calcite	$(\text{mol/kg-soln})^2$	stoichiometric equilibrium solubility product of calcite $Ksp^*_{\mathbf{cal}} = [Ca^{2+}][CO_3^{2-}]$
Ksp_aragonite	$(\text{mol/kg-soln})^2$	stoichiometric equilibrium solubility product of aragonite $Ksp^*_{\mathbf{ara}} = [Ca^{2+}][CO_3^{2-}]$
TA	mol/kg-soln	[TA], total alkalinity
pH	-, free scale	pH
pCO2	atm,	partial pressure (fugacity) of CO_2 in the water
CO2	mol/kg-soln	$[CO_2]$
HCO3	mol/kg-soln	$[HCO_3^-]$
CO3	mol/kg-soln	$[CO_3^{2-}]$
BOH3	mol/kg-soln	$[B(OH)_3]$
BOH4	mol/kg-soln	$[B(OH)_4^-]$
OH	mol/kg-soln	$[OH^-]$
H3PO4	mol/kg-soln	$[H_3PO_4]$
H2PO4	mol/kg-soln	$[H2PO_4^-]$
HPO4	mol/kg-soln	$[HPO_4^{2-}]$
PO4	mol/kg-soln	$[PO_4^{3-}]$
SiOH4	mol/kg-soln	$[Si(OH)_4]$
SiOOH3	mol/kg-soln	$[SiO(OH)_3^-]$
SiO2OH2	mol/kg-soln	$[SiO_2(OH)_2^{2-}]$
H2S	mol/kg-soln	$[H_2S]$
HS	mol/kg-soln	$[HS^-]$
S2min	mol/kg-soln	$[S^{2-}]$
NH4	mol/kg-soln	$[NH_4^+]$
NH3	mol/kg-soln	$[NH_3]$
H2SO4	mol/kg-soln	$[H_2SO_4]$
HSO4	mol/kg-soln	$[HSO_4^-]$
SO4	mol/kg-soln	$[SO_4^{2-}]$

HF	mol/kg-soln	$[HF]$
F	mol/kg-soln	$[F^-]$
HNO3	mol/kg-soln	$[HNO_3]$
NO3	mol/kg-soln	$[NO_3^-]$
HNO2	mol/kg-soln	$[HNO_2]$
NO2	mol/kg-soln	$[NO_2^-]$
omega_calcite	-	saturation state Ω with respect to calcite
omega_aragonite	-	saturation state Ω with respect to aragonite
revelle	-	Revelle factor RF_0
c1	-	ionization fraction $c_1 = [CO_2]/[\sum CO_2]$
c2	-	ionization fraction $c_2 = [HCO_3^-]/[\sum CO_2]$
c3	-	ionization fraction $c_3 = [CO_3^{2-}]/[\sum CO_2]$
dTAdSumCO2	-	$\frac{\partial[TA]}{[\partial \sum CO_2]}$ with $[TA] = f([H^+], [\sum CO_2], ...)$
b1	-	ionization fraction $b_1 = [B(OH)_3]/[\sum B(OH)_3]$
b2	-	ionization fraction $b_2 = [B(OH)_4^-]/[\sum B(OH)_3]$
dTAdSumBOH3	-	$\frac{\partial[TA]}{[\partial \sum B(OH)_3]}$ with $[TA] = f([H^+], [\sum CO_2], ...)$
so1	-	ionization fraction $so_1 = [H_2SO_4]/[\sum H_2SO_4]$
so2	-	ionization fraction $so_2 = [HSO_4^-]/[\sum H_2SO_4]$
so3	-	ionization fraction $so_3 = [SO_4^{2-}]/[\sum H_2SO_4]$
dTAdSumH2SO4	-	$\frac{\partial[TA]}{[\partial \sum H_2SO_4]}$ with $[TA] = f([H^+], [\sum CO_2], ...)$
f1	-	ionization fraction $f_1 = [HF]/[\sum HF]$
f2	-	ionization fraction $f_2 = [F^-]/[\sum HF]$
dTAdSumHF	-	$\frac{\partial[TA]}{[\partial \sum HF]}$ with $[TA] = f([H^+], [\sum CO_2], ...)$
p1	-	ionization fraction $p_1 = [H_3PO_4]/[\sum H_3PO_4]$
p2	-	ionization fraction $p_2 = [H_2PO_4^-]/[\sum H_3PO_4]$
p3	-	ionization fraction $p_3 = [HPO_4^{2-}]/[\sum H_3PO_4]$
p4	-	ionization fraction $p_4 = [PO_4^{3-}]/[\sum H_3PO_4]$
dTAdSumH3PO4	-	$\frac{\partial[TA]}{[\partial \sum H_3PO_4]}$ with $[TA] = f([H^+], [\sum CO_2], ...)$
si1	-	ionization fraction $si_1 = [Si(OH)_4]/[\sum Si(OH)_4]$
si2	-	ionization fraction $si_2 = [SiO(OH)_3]/[\sum Si(OH)_4]$
si3	-	ionization fraction $si_3 = [SiO_2(OH)_2]/[\sum Si(OH)_4]$
dTAdSumSumSiOH4	-	$\frac{\partial[TA]}{[\partial \sum Si(OH)_4]}$ with $[TA] = f([H^+], [\sum CO_2], ...)$
s1	-	ionization fraction $s_1 = [H_2S]/[\sum H_2S]$
s2	-	ionization fraction $s_2 = [HS^-]/[\sum H_2S]$
s3	-	ionization fraction $s_3 = [S^{2-}]/[\sum H_2S]$ Note that we do assume S^{2-} does exist. However, s_3 is very small.
dTAdSumH2S	-	$\frac{\partial[TA]}{[\partial \sum H_2S]}$ with $[TA] = f([H^+], [\sum CO_2], ...)$
n1	-	ionization fraction $n_1 = [NH_4^+]/[\sum NH_4^+]$
n2	-	ionization fraction $n_2 = [NH_3]/[\sum NH_4^+]$
dTAdSumNH4	-	$\frac{\partial[TA]}{[\partial \sum NH_4^+]}$ with $[TA] = f([H^+], [\sum CO_2], ...)$
na1	-	ionization fraction $na_1 = [HNO_3]/[\sum HNO_3]$
na2	-	ionization fraction $na_2 = [NO_3^-]/[\sum HNO_3]$
dTAdSumHNO3	-	$\frac{\partial[TA]}{[\partial \sum HNO_3]}$ with $[TA] = f([H^+], [\sum CO_2], ...)$

ni1	-	ionization fraction $ni_1 = [HNO_2]/[\sum HNO_2]$
ni2	-	ionization fraction $ni_2 = [NO_2^-]/[\sum HNO_2]$
dTAdSumHNO2	-	$\frac{\partial[TA]}{[\partial \sum HNO_2]}$ with $[TA] = f([H^+], [\sum CO_2], ...)$
dTAdH	-	$\frac{\partial[TA]}{[\partial[H^+]}$: buffer factor with $[TA] = f([H^+], [\sum CO_2], ...)$
dTAdKdKdS	-	$\sum_i \frac{\partial[TA]}{\partial K_i^*} \frac{\partial K_i^*}{\partial S}$ with $[TA] = f([H^+], [\sum CO_2], ..., K_i^*)$
dTAdKdKdT	-	$\sum_i \frac{\partial[TA]}{\partial K_i^*} \frac{\partial K_i^*}{\partial t}$ with $[TA] = f([H^+], [\sum CO_2], ..., K_i^*)$
dTAdKdKdp	-	$\sum_i \frac{\partial[TA]}{\partial K_i^*} \frac{\partial K_i^*}{\partial p}$ with $[TA] = f([H^+], [\sum CO_2], ..., K_i^*)$
dTAdKdKdSumH2SO4	-	$\sum_i \frac{\partial[TA]}{\partial K_i^*} \frac{\partial K_i^*}{\partial[\sum H_2SO_4]}$ with $[TA] = f([H^+], [\sum CO_2], ..., K_i^*)$
dTAdKdKdSumHF	-	$\sum_i \frac{\partial[TA]}{\partial K_i^*} \frac{\partial K_i^*}{\partial[\sum HF]}$ with $[TA] = f([H^+], [\sum CO_2], ..., K_i^*)$

For elements that are calculated according to certain literature references, those references are

element	references
p, P, Pa, p	The relation between pressure and depth given in Fofonoff and Millard (1983) is used. The standard value for atmospheric pressure Pa at sea level as well as the definition of total pressure and gauge pressure is taken from Feistel (2008).
Cl	DOE (1994, chapter 5, p. 11), and Zeebe and Wolf-Gladrow (2001, p. 100, footnote 3)
I	DOE (1994, chapter 5, p. 13, 15), Zeebe and Wolf-Gladrow (2001, p.12), and Roy et al. (1993b, p.257). Note that the approximation I/(mol/kg-solution) ≈ 0.0199201 S is given in Millero (1982, p. 428.). This relationship converted into mol/kg-H_2O and the last digits adjusted (from 0.0199201 to 0.019924) results in the formula used here.
density	Millero and Poisson (1981) and DOE (1994, chapter 5, p. 6f).
SumBr, ClConc, Na, Mg, Ca, K, Sr	DOE (1994, chapter 5, p.11)
molal2molin	Roy et al. (1993b, p.257), and DOE (1994, chapter 5, p. 15)
free2tot, tot2free	Dickson (1984, p.2302), DOE (1994, chapter 4, p.16), Zeebe and Wolf-Gladrow (2001, p.57, 261)
free2sws, tot2sws, sws2free, sws2tot	Dickson (1984, p.2303), Zeebe and Wolf-Gladrow (2001, p.57)
K0_CO2	Weiss (1974), DOE (1994, chapter 5, p. 13) (here it is stated that the unit is mol/(kg-solution*atm)), Millero (1995, p.663), Zeebe and Wolf-Gladrow (2001, p.257)
K0_O2	derived from a formula for the oxygen saturation concentration in ml-O_2/kg-solution by Weiss (1970) using the first virial coefficient of oxygen (Atkins, 1996, p. 41, 1029) and the atmospheric oxygen fugacity (Williams, 2004)
K_W	Millero (1995, p.670) (**original reference**, but slightly different formula for seawater pH), DOE (1994, chapter 5, p. 18) (not the original reference! DOE (1994) cites in an update from 1997 Millero (1995)! However the version of the formula used here is the one converted to total pH scale given in DOE (1994)), and Zeebe and Wolf-Gladrow (2001, p. 258). Constant type (stoichiometric), pH scale (total, converted to free here) , and concentration unit (mol/kg-solution squared): DOE (1994, chapter 5, p. 12,18), pH scale also in Zeebe and Wolf-Gladrow (2001, p. 258).

K_HSO4	DOE (1994, chapter 5 page 13), Zeebe and Wolf-Gladrow (2001, p. 260), Dickson (1990b) (original reference). Constant type (stoichiometric), pH scale (free) , and concentration unit (mol/kg-H_2O converted to mol/kg-solution here): DOE (1994, chapter 5, p. 13).
K_HF	Dickson and Riley (1979a, p. 91) (original reference), DOE (1994, c. 5, p. 15), Roy et al. (1993b, p. 257), Dickson and Millero (1987, p. 1783), Millero (1995, p. 664), Zeebe and Wolf-Gladrow (2001, p. 260) (converted to molinty and total scale). Constant type (stoichiometric), pH scale (free) , and concentration unit (mol/kg-H_2O converted to mol/kg-solution here): DOE (1994, chapter 5, p. 15, 16). In AquaEnv, it is also possible to use the constant according to Perez and Fraga (1987).
K_CO2, K_HCO3	Roy et al. (1993b, p. 254) (original reference), DOE (1994, chapter 5, p.14) (in a version converted to mol/kg-H_2O), Millero (1995, p. 664), Zeebe and Wolf-Gladrow (2001, p. 255). Constant type (stoichiometric) and concentration unit (mol/kg-H_2O converted to mol/kg-solution here): DOE (1994, chapter 5, p. 14, 15), pH scale (total, converted to free here): In DOE (1994, chapter 5, p. 12) the total scale is stated for the formula for high salinities and thus can be inferred for the formula for low salinities. The scale is also indirectly stated for both formulations in the original reference Roy et al. (1993b). Note that in Roy et al. (1993b) a function for fresh water (based on Millero (1979) which in turn is on a temperature relationship from Harned and Davis (1943) and Harned and Scholes (1941) respectively) and a function for seawater is derived. In Millero (1995) it is stated that for S<5 the fresh water formula (based on Millero (1979)) should be used and for S>=5 the seawater formula derived in Roy et al. (1993b). However, both formulations do not always intersect at S=5. The true intersection with respect to salinity S is a function of temperature t. Here, we first calculate this intersection by numerical root finding and then decide which formulation to use. This practise results in a continuous function with respect to S. (Note that there is a typesetting error in Roy et al. (1993b): one of the numerical values for the function for $K^*_{CO_2}$ is given as 310.48919, but correct is 2310.48919. However, in Millero (1995) this value is stated correctly.) In AquaEnv, it is also possible to use the constants according to Lueker et al. (2000).
K_BOH3	Dickson (1990a, p. 763) (original, but mol/kg-H_2O version), DOE (1994, ch. 5, p. 14), Zeebe and Wolf-Gladrow (2001, p. 262), Millero (1995, p.669) (mol/kg-H_2O version) , agrees with data in Roy et al. (1993b). Constant type (stoichiometric) and concentration unit (mol/kg-solution): DOE (1994, chapter 5, p. 14), pH scale (total): DOE (1994, chapter 5, p. 12) and Zeebe and Wolf-Gladrow (2001, p.263).
K_NH4	Millero et al. (1995) (original reference), Millero (1995, p.671). Constant type (stoichiometric) and concentration unit (mol/kg-solution): Millero (1995, p.671), pH scale (seawater, converted to free here): Lewis and Wallace (1998) (in corrections of Millero (1995)).
K_H2S	Millero et al. (1988) (original reference), Millero (1995, p.671). Constant type (stoichiometric) and concentration unit (mol/kg-solution): Millero (1995, p.671), pH scale (seawater, converted to free here): Lewis and Wallace (1998) (in corrections of Millero (1995)).
K_H3PO4, K_H2PO4, K_HPO4	Millero (1995, p.670) (original reference, but formula for seawater scale pH), DOE (1994, ch. 5, p 16,17), agrees with data in Dickson and Riley (1979b). Constant type (stoichiometric), concentration unit (mol/kg-solution), and pH scale (total, converted to free here): DOE (1994, chapter 5, p. 12, 16, 17).
K_SiOH4	Millero et al. (1988) (original reference), DOE (1994, chapter 5, p 17), Millero (1995, p.671) (formula for seawater scale pH) Constant type (stoichiometric), concentration unit (mol/kg-H_2O converted to mol/kg-solution here by omitting the conversion summand ln(1-0.001005 S)), and pH scale (total, converted to free here): DOE (1994, chapter 5, p. 12, 17).
K_SiOOH3	Wischmeyer et al. (2003) (original reference), corrected due to personal communication with Dieter Wolf-Gladrow (one of the authors). The corrected version can be obtained from either Dieter Wolf-Gladrow or Andreas F Hofmann (a.hofmann@nioo.knaw.nl). Constant type (stoichiometric), concentration unit (mol/kg-solution), and pH scale (total, converted to free here): Wischmeyer et al. (2003).

K_HNO2	Constant value, not a function of temperature and salinity! Obtained as a hybrid pk value (featuring the activity of the proton but the concentration of other species (see Zeebe and Wolf-Gladrow (2001) for a treatment of different types of equilibrium constants) in molar concentration (mol/l) on the NBS pH scale (Durst, 1975) from Riordan et al. (2005). Used as an approximation for the stoichiometric $K^*_{HNO_2}$ in mol/kg-solution on the free proton pH scale here.
K_HNO3	Constant value, not a function of temperature and salinity! Obtained from Boudreau (1996a) as restated in Soetaert et al. (2007)
K_H2SO4	Constant value, not a function of temperature and salinity! Obtained as a standard pK value from Atkins (1996, p. 1045). Used as an approximation for the stoichiometric $K^*_{H_2SO_4}$ in mol/kg-solution on the free proton pH scale here.
K_HS	Constant value, not a function of temperature and salinity! Obtained as a standard pK value from Atkins (1996, p. 1045). Used as an approximation for the stoichiometric $K^*_{Hs^-}$ in mol/kg-solution on the free proton pH scale here.
Ksp_calcite, Ksp_aragonite	Mucci (1983) (original reference), Boudreau (1996a). Note that in there are errors in Boudreau (1996a): b_0 for calcite is not 0.7712 but 0.77712 and b_1 for aragonite is not 0.001727 but 0.0017276.
pH	As given in Dickson (1984), p. 2303 (use of "m") and Dickson and Riley (1979b), p. 91f all concentrations appearing in the definition of the total and the seawater pH scale are **molal** (mol/kg-H_2O) concentrations. But in Roy et al. (1993b), p. 257 and in DOE (1994), chapter 4, SOP 6, p. 1 it is stated, that concentrations for the seawater and total pH scale are in mol/kg-solution. To be consistent with DOE (1994) **molin** concentrations (mol/kg-solution) are chosen for calculating the pH.
revelle	Zeebe and Wolf-Gladrow (2001, p.73)
dTAdH, dTAdSumCO2, dTAdSumBOH3, dTAdSumH2SO4, dTAdSumHF, dTAdSumH3PO4, dTAdSumSumSiOH4, dTAdSumH2S, dTAdSumNH4, dTAdSumHNO3, dTAdSumHNO2	Hofmann et al. (2008a, , i.e., Chapter 3)
c1, c2, c3, b1, b2, so1, so2, so3, f1, f2, p1, p2, p3, p4 si1, si2, si3, s1, s2, s3, n1, n2, na1, na2, ni1, ni2	Skoog and West (1982), Stumm and Morgan (1996), Hofmann et al. (2009b, , i.e., Chapter 5)
dTAdKdKdS, dTAdKdKdT, dTAdKdKdp, dTAdKdKdSumH2SO4, dTAdKdKdSumHF	Hofmann et al. (2009a, , i.e., Chapter 4)

The values for K_W, K_HSO4, K_HF, K_CO2, K_HCO3, K_BOH3, K_NH4, K_H2S, K_H3PO4, K_H2PO4, K_HPO4, K_SiOH4, K_SiOOH3, Ksp_calcite, Ksp_aragonite obtained as functions of salinity S and temperature t from the above references (for the formulae see Appendices 6.6.3.7.2 and 6.6.3.8) are pressure corrected using the gauge pressure p according to Millero (1995) with corrections by Lewis and Wallace (1998) (see Appendix 6.6.3.9).

Note that the elements revelle, dTAdKdKdS, dTAdKdKdT, dTAdKdKdp, dTAdKdKdSumH2SO4, and dTAdKdKdSumHF are calculated numerically and therefore their calculation (induced via the

flags `revelle` and `dsa`) is computationally intense. Similarly, calculating `K_CO2` and `K_HCO3` according to Roy et al. (1993b) which means that the intersection of the formulae for high and low salinity as a function of temperature needs to be calculated, is computationally intense.

6.6.3. Constants and formulae

6.6.3.1. Chemical constants used in AquaEnv

6.6.3.1.1. Elements of list `PhysChemConst`

`absZero`	-273.15	C	(Dickson et al., 2007)	absolute zero
`R`	83.14472	$\frac{bar*cm^3}{mol*K}$	(Dickson et al., 2007)	ideal gas constant
`F`	96485.3399	C/mol	(Dickson et al., 2007)	Faraday constant
`e`	79	-	(Zeebe and Wolf-Gladrow, 2001)	relative dielectric constant of seawater
`K_HNO2`	1.584893e-3	mol/l	(Riordan et al., 2005)	approximative dissociation constant of HNO_2, NBS pH scale, hybrid constant
`K_HNO3`	23.44	mol/kg-soln	(Boudreau, 1996a; Soetaert et al., 2007)	approximative dissociation constant of HNO_3, assumed on mol/kg-soln and free pH scale, stoichiometric constant
`K_H2SO4`	100	mol/kg-soln	(Atkins, 1996)	approximative dissociation constant of H_2SO_4, assumed on mol/kg-soln and free pH scale, stoichiometric constant
`K_HS`	1.1e-12	mol/kg-soln	(Atkins, 1996)	approximative dissociation constant of HS, assumed on mol/kg-soln and free pH scale, stoichiometric constant

6.6.3.1.2. Elements of list `Fugacity`

Note that here we do not distinguish between fugacity and the partial pressure.

`CO2`	0.000383	atm	(Borges et al., 2004; Guinotte and Fabry, 2008)	fugacity of CO_2
`O2`	0.20946	atm	(Williams, 2004)	fugacity of O_2

6.6.3.1.3. Elements of list `MeanMolecularMass`

The list `MeanMolecularMass` contains mean molecular masses in g/mol. The list is taken from DOE (1994, chap. 5, p. 3) and Dickson et al. (2007, chap. 5, p. 4).

`Cl`	35.453
`SO4`	96.061
`Br`	79.904
`F`	18.998
`Na`	22.990
`Mg`	24.3050
`Ca`	40.078
`K`	39.098
`Sr`	87.62
`B`	10.811

6.6.3.1.4. Elements of list ConcRelCl

The list ConcRelCl contains relative concentrations[2] of key chemical species in seawater with respect to chlorinity (DOE (1994, chap. 5, p. 11) and Dickson et al. (2007, chap. 5, p. 10)).

Cl	0.99889
SO4	0.1400
Br	0.003473
F	0.000067
Na	0.55661
Mg	0.06626
Ca	0.02127
K	0.0206
Sr	0.00041
B	0.000232

6.6.3.2. Chlorinity Cl as a function of salinity S

Chlorinity Cl (in ‰) is calculated from salinity S using a relation given in DOE (1994, chap. 5, p. 11) and Zeebe and Wolf-Gladrow (2001, p. 100)

$$\mathrm{Cl} = \frac{\mathrm{S}}{1.80655} \tag{22}$$

6.6.3.3. Total concentrations of key chemical species in seawater as a function of chlorinity Cl

As described in DOE (1994, chap. 5, p. 11) and Dickson et al. (2007, chap. 5, p. 10), values in lists MeanMolecularMass and ConcRelCl are used to calculate the total concentration [X] (in mol/kg-soln) of chemical species X in seawater[3] according to the relation

$$[\mathrm{X}] = \frac{\mathrm{ConcRelCl\ X}}{\mathrm{MeanMolecularMass\ X}}\,\mathrm{Cl} \tag{23}$$

6.6.3.4. Ionic strength I as function of salinity S

According to DOE (1994, chapter 5, p. 13, 15), Zeebe and Wolf-Gladrow (2001, p.12), and Roy et al. (1993b, p.257), I (in mol/kg-H_2O) is calculated as

$$\mathrm{I} = \frac{19.924\ \mathrm{S}}{1000 - 1.005\ \mathrm{S}} \tag{24}$$

Note that the approximation I/(mol/kg-solution) ≈ 0.0199201 S is given in Millero (1982, p. 428.). This relationship converted into mol/kg-H_2O and the last digits adjusted (from 0.0199201 to 0.019924) results in the formula used here.

[2] Note that the given values do not sum up to one since chlorinity is defined as grams of chloride equivalents per kg of sample (Kremling, 1999), i.e., it expresses the amount of only the the anions converted to the molecular mass of chloride. Here, however, both anions and cations are listed, and the given values are related to their true molecular weight.

[3] Note that the solution must have seawater composition, otherwise the relation given here is void.

6.6.3.5. Relation between water depth `d` and gauge pressure `p`

Although the relation between gauge pressure `p` (total pressure minus atmospheric pressure, see Feistel (2008)) and water depth `d` can be approximated by

$$\mathtt{p} = 0.101325\,\mathtt{d} \tag{25}$$

since `p` increases per m of water depth `d` by approximately $\frac{1}{10}$ of 1 atm (= 1.01325 bar Dickson et al. (2007, chap. 5, p. 3)), here, the relation given by Fofonoff and Millard (1983) as implemented in Soetaert et al. (2009) is used

$$\mathtt{d} = \frac{(9.72659 + (-2.2512\,10^{-5} + (2.279\,10^{-10} - 1.82\,10^{-15}\,\mathtt{p})\,\mathtt{p})\,\mathtt{p})\,\mathtt{p})}{\mathtt{g} + 1.092\,10^{-6}\,\mathtt{p}} \tag{26}$$

where `p` is the gauge pressure in dbar (deci-bar) and `g` the earth's gravity in m/s^2. `g` is calculated from the latitude `lat` (in degrees, -90 to 90, if not given `lat`=0 is assumed) as given in Fofonoff and Millard (1983) and implemented in Soetaert et al. (2009)

$$\mathtt{g} = 9.780318\,(1 + (0.0052788 + 2.36\,10^{-5}\,\sin(\mathtt{lat}\,\frac{\Pi}{180}))\,\sin(\mathtt{lat}\,\frac{\Pi}{180})) \tag{27}$$

6.6.3.6. Seawater `density` as function of salinity `S` and temperature `t`

According to (Millero and Poisson, 1981) as reprinted in DOE (1994, chap. 5, p. 6f) the density of seawater $\rho_{SeaWater}$ (in $\frac{kg}{m^3}$; `density` in an *aquaenv* object) can be calculated as

$$\begin{aligned}
\rho_{\mathrm{SeaWater}} &= \rho_{\mathrm{Water}} + \mathrm{A}\,\mathtt{S} + \mathrm{B}\,\mathtt{S}^{1.5} + \mathrm{C}\,\mathtt{S}^2 && (28)\\
\mathrm{A} &= 0.824493 - 4.0899\,10^{-3}\,\mathtt{t} + 7.6438\,10^{-5}\,\mathtt{t}^2 - 8.2467\,10^{-7}\,\mathtt{t}^3 && (29)\\
&\quad +5.3875\,10^{-9}\,\mathtt{t}^4 && (30)\\
\mathrm{B} &= -5.72466\,10^{-3} + 1.0227\,10^{-4}\,\mathtt{t} - 1.6546\,10^{-6}\,\mathtt{t}^2 && (31)\\
\mathrm{C} &= 4.8314\,10^{-4} && (32)\\
\rho_{Water} &= 999.842594 + 6.793952\,10^{-2}\,\mathtt{t} - 9.095290\,10^{-3}\,\mathtt{t}^2 && (33)\\
&\quad +1.001685\,10^{-4}\,\mathtt{t}^3 - 1.120083\,10^{-6}\,\mathtt{t}^4 + 6.536332\,10^{-9}\,\mathtt{t}^6 && (34)
\end{aligned}$$

with `t` representing the temperature in C and ρ_{Water} the density of fresh water in in kg/m^3.

6.6.3.7. Gas-exchange constants, dissociation constant, and solubility products as functions of salinity `S`, (absolute) temperature `T`, and gauge pressure `p`

Empirical formulations for the temperature and salinity dependency of all gas exchange constants, equilibrium constants and solubility products calcuated in AquaEnv can be brought into the generic forms

$$\ln\frac{\mathrm{K_X}}{\mathrm{k_0^\circ}} = \mathrm{A} + \frac{\mathrm{B}}{\mathtt{T}} + \mathrm{C}\,\ln(\mathtt{T}) + \mathrm{D}\,\mathtt{T} + \mathrm{E}\,\mathtt{T}^2 \tag{35}$$

or

$$\log_{10}\frac{\mathrm{K_X}}{\mathrm{k_0^\circ}} = \mathrm{A}' + \frac{\mathrm{B}'}{\mathtt{T}} + \mathrm{C}'\,\log_{10}(\mathtt{T}) + \mathrm{D}'\,\mathtt{T} + \mathrm{E}'\,\mathtt{T}^2 \tag{36}$$

with T being the temperature in Kelvin, S the salinity, k_0° the concentration unit of the constant, and A, B, C, D, E, and the respective variables with a prime (') being functions of salinity S. In the following we will give A, B, C, D, and E or A', B', C', D', and E' for each calculated constant.

6.6.3.7.1. Gas-exchange constants (Henry's constants) as functions of salinity S and temperature T

The following table shows the coefficients for Eq. (35) of gas exchange constants in AquaEnv, with fCO_2 being the fugacity (assumed to be equal to the partial pressure) of CO_2.

K0_CO2 : **solubility of CO_2 in seawater**	
A = 0.023517S – 167.81077 B = 9345.17 C = 23.3585 D = $-2.3656\ 10^{-4}$S E = $4.7036\ 10^{-7}$S	CO2_sat = fCO_2 K0_CO2 k_0° = $\left[\frac{mol}{kg\text{–}solution\ atm}\right]$
References: Weiss (1974) (original), DOE (1994, chap. 5, p. 13), Millero (1995, p. 663), Zeebe and Wolf-Gladrow (2001, p. 257), and Dickson et al. (2007, chap. 5, p. 12)	

K0_O2 : **solubility of O_2 in seawater** (**micro**mol per kg-soln and atm)	
A = –846.9975 – 0.037362 S B = 25559.07 C = 146.4813 D = –0.22204 + 0.00016504 S E = $-2.0564\ 10^{-7}$ S	O2_sat = fO_2 K0_O2 k_0° = $\left[\frac{\mu mol}{kg\text{–}solution\ atm}\right]$
References: derived from Weiss (1970), agrees with data in Murray et al. (1969)	

Note that the formulation for K0_O2 has been derived using the formulation for a gravimetric O_2 saturation concentration given in Weiss (1970, Weiss, 1970). It has been converted from ml-O_2/kg-soln to μmol-O_2/kg-soln using the molar volume of O_2 calculated with the virial equation using a first virial coefficient for oxygen at 273.0 Kelvin of –22 cm^3/mol Atkins (1996), a value of 8.314 Nm/(Kelvin mol) for the gas constant R and an ambient pressure of 101300 N/m^2. The expression for the Henry's constant has then been created by dividing the expression for the saturation concentration by fO_2 = 0.20946 atm (Williams, 2004).

6.6.3.7.2. Stoichiometric acid base dissociation constants as functions of salinity S and temperature T

The following table gives the coefficients for Eq. (35) or (36) of stoichiometric acid base dissociation constants in AquaEnv. Note that not mentioned coefficients A to E are zero and note also that given references somtimes contain the formulae in different units or on different pH scales. The formulae provided in this table yield the dissociation constants on different pH scales and concentration units. In AquaEnv, constants that are not already on the free pH scale and in mol/kg-soln are converted to the free pH scale and mol/kg-soln.

K_HSO4 : $HSO_4^- \rightleftharpoons H^+ + SO_4^{2-}$	**free** pH scale
$A = 324.57\sqrt{\left(\frac{I}{m^\circ}\right)} - 771.54\,\frac{I}{m^\circ} + 141.328$ $B = 35474\,\frac{I}{m^\circ} + 1776\left(\frac{I}{m^\circ}\right)^2 - 13856\sqrt{\left(\frac{I}{m^\circ}\right)} - 2698\left(\frac{I}{m^\circ}\right)^{\frac{3}{2}} - 4276.1$ $C = 114.723\,\frac{I}{m^\circ} - 47.986\sqrt{\left(\frac{I}{m^\circ}\right)} - 23.093$	$K\_HSO4 = \frac{[H^+]_F\,[SO_4^{2-}]}{[HSO_4^-]}$ $k^\circ = \frac{mol}{kg\text{-}H_2O}$ $m^\circ = \frac{mol}{kg\text{-}H_2O}$
References: DOE (1994, c. 5, p. 13), Zeebe and Wolf-Gladrow (2001, p. 260), Dickson (1990b) (original)	

K_HF: $HF \rightleftharpoons H^+ + F^-$ ("dickson")	**free** pH scale
$A = 1.525\sqrt{\frac{I}{m^\circ}} - 12.641$ $B = 1590.2$	$K\_HF = \frac{[H^+]_F\,[F^-]}{[HF]}$ $k^\circ = m^\circ = \frac{mol}{kg\text{-}H_2O}$
References: Dickson and Riley (1979a, p. 91) (original), Dickson and Millero (1987, p. 1783), Roy et al. (1993b, p. 257), DOE (1994, c. 5, p. 15), Millero (1995, p. 664), Zeebe and Wolf-Gladrow (2001, p. 260)	

K_HF: $HF \rightleftharpoons H^+ + F^-$ ("perez")	**total** pH scale
$A = -9.68 + 0.111\sqrt{S}$ $B = 874$	$K\_HF = \frac{[H^+]_F\,[F^-]}{[HF]}$ $k^\circ = \frac{mol}{kg\text{-solution}}$
References: Perez and Fraga (1987, p. 91) (original), Dickson et al. (2007, chap. 5, p. 14)	

K_CO2: $CO_2(aq) + H_2O\ (\rightleftharpoons H_2CO_3) \rightleftharpoons H^+ + HCO_3^-$ ("roy"; high salinities: S > 5)	**total** pH scale
$A = 2.83655 - 0.20760841\sqrt{S} + 0.08468345\,S - 0.00654208\,S^{\frac{3}{2}}$ $B = -2307.1266 - 4.0484\sqrt{S}$ $C = -1.5529413$	$K\_CO2 = \frac{[H^+]\,[HCO_3^-]}{[CO_2(aq)]}$ $k^\circ = \frac{mol}{kg\text{-}H_2O}$
References: Roy et al. (1993b, p. 254) (original), DOE (1994, c. 5, p.14), Millero (1995, p. 664), Zeebe and Wolf-Gladrow (2001, p. 255)	

K_CO2: $CO_2(aq) + H_2O$ ($\rightleftharpoons H_2CO_3$) $\rightleftharpoons H^+ + HCO_3^-$ ("roy"; low salinities: $S \leq 5$)	**total** pH scale
$A = 290.9097 - 228.39774\ \sqrt{S} + 54.20871\ S - 3.969101\ S^{\frac{3}{2}} - 0.00258768\ S^2$	
$B = -14554.21 + 9714.36839\ \sqrt{S} - 2310.48919\ S + 170.22169\ S^{\frac{3}{2}}$	K_CO2 $= \frac{[H^+]\,[HCO_3^-]}{[CO_2(aq)]}$
$C = -45.0575 + 34.485796\ \sqrt{S} - 8.19515\ S + 0.60367\ S^{\frac{3}{2}}$	$k^\circ = \frac{mol}{kg\text{-}H_2O}$
References: Roy et al. (1993b, p. 256) (original, based on a temperature dependency restated in Millero (1979), originally given in Harned and Davis (1943). Note that there is a typesetting error in Roy et al. (1993b): the third value for B is 2310.48919, not 310.48919) Millero (1995, p. 664) (the typesetting error is corrected here). Also, here it is mentioned that this formula should be used for $S \leq 5$. Note that both functions do not always intersect at S=5. The true intersection is a function of t, is calculated in AquaEnv, and is used to decide which formula to use.)	

K_CO2: $CO_2(aq) + H_2O$ ($\rightleftharpoons H_2CO_3$) $\rightleftharpoons H^+ + HCO_3^-$ ("lueker")	**total** pH scale
$A' = 61.2172 + 0.011555\ S - 0.0001152\ S^2$	K_CO2 $= \frac{[H^+]\,[HCO_3^-]}{[CO_2(aq)]}$
$B' = -3633.86$	$k^\circ = \frac{mol}{kg\text{-}solution}$
$C' = -9.67770$	
References: Lueker et al. (2000) (original), Dickson et al. (2007, chap. 5, p.13-14)	

K_HCO3: $HCO_3^- \rightleftharpoons H^+ + CO_3^{2-}$ ("roy"; high salinities: $S > 5$)	**total** pH scale
$A = -9.226508 - 0.106901773\ \sqrt{S} + 0.1130822\ S - 0.00846934\ S^{\frac{3}{2}}$	K_HCO3 $= \frac{[H^+]\,[CO_3^{2-}]}{[HCO_3^-]}$
$B = -3351.6106 - 23.9722\ \sqrt{S}$	$k^\circ = \frac{mol}{kg\text{-}H_2O}$
$C = -0.2005743$	
References: Roy et al. (1993b, p. 254) (original), DOE (1994, c. 25, p.15), Millero (1995, p. 664), Zeebe and Wolf-Gladrow (2001, p. 255)	

K_HCO3: $HCO_3^- \rightleftharpoons H^+ + CO_3^{2-}$ ("roy"; low salinities: $S \leq 5$)	**total** pH scale
$A = 207.6548 - 167.69908\ \sqrt{S} + 39.75854\ S - 2.892532\ S^{\frac{3}{2}} - 0.00613142\ S^2$	
$B = -11843.79 + 6551.35253\ \sqrt{S} - 1566.13883\ S + 116.270079\ S^{\frac{3}{2}}$	K_HCO3 $= \frac{[H^+]\,[CO_3^{2-}]}{[HCO_3^-]}$
$C = -33.6485 + 25.928788\ \sqrt{S} - 6.171951\ S + 0.45788501\ S^{\frac{3}{2}}$	$k^\circ = \frac{mol}{kg\text{-}H_2O}$
References: Roy et al. (1993b, p. 256) (original, based on a temperature depencence restated in Millero (1979), originally given in Harned and Scholes (1941)), Millero (1995, p. 664) (here it is mentioned that this formula should be used for $S \leq 5$. Note that both functions do not always intersect at S=5. The true intersection is a function of t, is calculated in AquaEnv, and is used to decide which formula to use.)	

K_HCO3: $HCO_3^- \rightleftharpoons H^+ + CO_3^{2-}$ ("lueker")	**total** pH scale
$A' = -25.9290 + 0.01781\ S - 0.0001122\ S^2$	K_HCO3 $= \frac{[H^+]\,[CO_3^{2-}]}{[HCO_3^-]}$
$B' = -471.78$	$k^\circ = \frac{mol}{kg\text{-}solution}$
$C' = 3.16967$	
References: Lueker et al. (2000) (original), Dickson et al. (2007, chap. 5, p.14)	

K_W: $H_2O \rightleftharpoons H^+ + OH^-$	**total** pH scale
$A = 148.9652 - 5.977\sqrt{S} - 0.01615\,S$ $B = -13847.26 + 118.67\sqrt{S}$ $C = -23.6521 + 1.0495\sqrt{S}$	$K\_W = [H^+][OH^-]$ $k^\circ = \left(\frac{mol}{kg-solution}\right)^2$
References: Millero (1995, p.670) (original), DOE (1994, c. 5, p. 18) (update 1997 cites Millero (1995)), Zeebe and Wolf-Gladrow (2001, p. 258), Dickson et al. (2007, chap. 5, p.16)	

K_BOH3: $B(OH)_3 \rightleftharpoons H^+ + B(OH)_4^-$	**total** pH scale
$A = 148.0248 + 137.1942\sqrt{S} + 1.62142S$ $B = -8966.90 - 2890.53\sqrt{S} - 77.942S + 1.728\,S^{\frac{3}{2}} - 0.0996\,S^2$ $C = -24.4344 - 25.085\sqrt{S} - 0.2474\,S$ $D = 0.053105\sqrt{S}$	$K\_BOH3 = \frac{[H^+][B(OH)_4^-]}{[B(OH)_3]}$ $k^\circ = \frac{mol}{kg-solution}$
References: Dickson (1990a, p. 763) (or.), DOE (1994, c. 5, p. 14), Millero (1995, p. 669), Zeebe and Wolf-Gladrow (2001, p. 262), agrees with data in Roy et al. (1993a)	

K_NH4: $NH_4^+ \rightleftharpoons H^+ + NH_3$	**SWS** pH scale
$A = -0.25444 + 0.46532\sqrt{S} - 0.01992\,S$ $B = -6285.33 - 123.7184\sqrt{S} + 3.17556\,S$ $D = 0.0001635$	$K\_NH4 = \frac{[H^+][NH_3]}{[NH_4^+]}$ $k^\circ = \frac{mol}{kg-solution}$
References: Millero (1995, p. 671), Millero et al. (1995) (original), corrections of Millero (1995) in Lewis and Wallace (1998) give pH scale	

K_H2S: $H_2S \rightleftharpoons H^+ + HS^-$	**total** pH scale
$A = 225.838 + 0.3449\sqrt{S} - 0.0274\,S$ $B = -13275.3$ $C = -34.6435$	$K\_H2S = \frac{[H^+][HS^-]}{[H_2S]}$ $k^\circ = \frac{mol}{kg-solution}$
References: Millero (1995, p. 671), Millero et al. (1988) (original), corrections of Millero (1995) in Lewis and Wallace (1998) give pH scale	

K_H3PO4: $H_3PO_4 \rightleftharpoons H^+ + H_2PO_4^-$	**total** pH scale
$A = 115.525 + 0.69171\sqrt{S} - 0.01844\,S$ $B = -4576.752 - 106.736\sqrt{S} - 0.65643\,S$ $C = -18.453$	$K\_H3PO4 = \frac{[H^+][H_2PO_4^-]}{[H_3PO_4]}$ $k^\circ = \frac{mol}{kg-solution}$
References: DOE (1994, chap. 5, p 16), Millero (1995, p.670), (original) Dickson et al. (2007, chap. 5, p.15) agrees with data in Dickson and Riley (1979b)	

K_H2PO4 : $H_2PO_4^- \rightleftharpoons H^+ + HPO_4^{2-}$	**total** pH scale
$A = 172.0883 + 1.3566\sqrt{S} - 0.05778\,S$ $B = -8814.715 - 160.340\sqrt{S} + 0.37335\,S$ $C = -27.927$	$K\_H2PO4 = \frac{[H^+][HPO_4^{2-}]}{[H_2PO_4^-]}$ $k^\circ = \frac{mol}{kg-solution}$
References: DOE (1994, chap. 5, p 16), Millero (1995, p.670) (original), Dickson et al. (2007, chap. 5, p.15), agrees with data in Dickson and Riley (1979b)	

K_HPO4 : $HPO_4^{2-} \rightleftharpoons H^+ + PO_4^{3-}$	**total** pH scale
$A = -18.141 + 2.81197\ \sqrt{S} - 0.09984\ S$ $B = -3070.75 + 17.27039\ \sqrt{S} - 44.99486\ S$	K_HPO4 $= \frac{[H^+]\,[PO_4^{3-}]}{[HPO_4^{2-}]}$ $k^\circ = \frac{mol}{kg-solution}$
References: DOE (1994, chap. 5, p 17), Millero (1995, p.670) (original), Dickson et al. (2007, chap. 5, p.15), agrees with data in Dickson and Riley (1979b)	

K_SiOH4: $Si(OH)_4 \rightleftharpoons H^+ + SiO(OH)_3^-$	**total** pH scale
$A = 117.385 + 3.5913\ \sqrt{\frac{I}{m^\circ}} - 1.5998\ \frac{I}{m^\circ} + 0.07871\ \left(\frac{I}{m^\circ}\right)^2$ $B = -8904.2 - 458.79\ \sqrt{\frac{I}{m^\circ}} + 188.74\ \frac{I}{m^\circ} - 12.1652\left(\frac{I}{m^\circ}\right)^2$ $C = -19.334$	K_SiOH4 $= \frac{[H^+]\,[SiO(OH)_3^-]}{[Si(OH)_4]}$ $k^\circ = \frac{mol}{kg-H_2O}$ $m^\circ = \frac{mol}{kg-H_2O}$
References: Millero et al. (1988) (original), DOE (1994, chapter 5, p 17), Millero (1995, p.671)	

K_SiOOH3: $SiO(OH)_3^- \rightleftharpoons H^+ + SiO_2(OH)_2^{2-}$	**total** pH scale
$A = 8.96$ $B = -4465.18$ $D = 0.021952$	K_SiOOH3 $= \frac{[H^+]\,[SiO_2(OH)_2^{2-}]}{[SiO(OH)_3^-]}$ $k^\circ = \frac{mol}{kg-H_2O}$
References: Wischmeyer et al. (2003) (original; including corrections by co-author D. Wolf-Gladrow)	

6.6.3.8. Stoichiometric solubility products as functions of salinity S and temperature T

The following table shows the coefficients for Eq. (36) for the stoichiometric solubility products for calcite and aragonite in AquaEnv.

Ksp_calcite : solubility product of calcite	
$A' = -171.9065 - 0.77712\ \sqrt{S} - 0.07711\ S + 0.0041249\ S^{1.5}$ $B' = 2839.319 + 178.34\ \sqrt{S}$ $C' = 71.595$ $D' = -0.077993 + 0.0028426\ \sqrt{S}$	Ksp_cal $= [CO_3^{2-}]\,[Ca^{2+}]$ $k_0^\circ = \left[\left(\frac{mol}{kg-solution}\right)^2\right]$
References: Mucci (1983) (original), Boudreau (1996a, p. 160), (note that the second value for A' is -0.77712 not -0.7712 as cited in Boudreau (1996a))	

Ksp_aragonite : solubility product of aragonite	
$A' = -171.945 - 0.068393\ \sqrt{S} - 0.10018\ S + 0.0059415\ S^{1.5}$ $B' = 2903.293 + 88.135\ \sqrt{S}$ $C' = 71.595$ $D' = -0.077993 + 0.0017276\ \sqrt{S}$	Ksp_ara $= [CO_3^{2-}]\,[Ca^{2+}]$ $k_0^\circ = \left[\left(\frac{mol}{kg-solution}\right)^2\right]$
References: Mucci (1983) (original), Boudreau (1996a, p. 160), (note that the second value for D' is 0.0017276 not 0.001727 as cited in Boudreau (1996a))	

6.6.3.9. Pressure correction of dissociation constants and solubility products

Pressure has an effect on the stoichiometric acid-base dissociation constants and the stoichiometric solubility products given in the previous sections. As described in Millero (1995, p. 675) using corrections and assumptions from Lewis and Wallace (1998, p. A-7) the effect of pressure can be accounted for by the equation[4]:

$$K_{corr} = K \left(-\frac{a_0 + a_1\, t + a_2\, t^2}{R\, T}\, p + \frac{b_0 + b_1\, t + b_2\, t^2}{1000\, R\, T}\, 0.5\, p^2 \right) \quad (37)$$

Where K_{corr} is the pressure corrected constant and K is the uncorrected constant, both on matching units, e.g., mol/kg-soln, `T` is the absolute temperature in Kelvin, `t` is the temperature in C, `R` is the ideal gas constant in (bar cm^3)/(mol Kelvin), and `p` is the gauge pressure (total pressure minus one atm, see Feistel (2008) for a definition) in bar. The a and b coefficients (according to Millero (1995) which is partly a restatement of Millero (1979), corrected by Lewis and Wallace (1998)) for constants in AquaEnv (stored in the data frame `DeltaPcoeffs`) are given in the following table[5].

	a_0	a_1	a_2	b_0	b_1	b_2
K_HSO4	-18.03	0.0466	$0.3160\ 10^{-3}$	- 4.53	0.0900	0
K_HF	-9.78	-0.0090	$-0.9420\ 10^{-3}$	- 3.91	0.0540	0
K_CO2	-25.50	0.1271	$0.0000\ 10^{-3}$	- 3.08	0.0877	0
K_HCO3	-15.82	-0.0219	$0.0000\ 10^{-3}$	1.13	-0.1475	0
K_W	-25.60	0.2324	$-3.6246\ 10^{-3}$	- 5.13	0.0794	0
K_BOH3	-29.48	0.1622	$2.6080\ 10^{-3}$	- 2.84	0.0000	0
K_NH4	-26.43	0.0889	$-0.9050\ 10^{-3}$	- 5.03	0.0814	0
K_H2S	-14.80	0.0020	$-0.4000\ 10^{-3}$	2.89	0.0540	0
K_H3PO4	-14.51	0.1211	$-0.3210\ 10^{-3}$	- 2.67	0.0427	0
K_H2PO4	-23.12	0.1758	$-2.6470\ 10^{-3}$	- 5.15	0.0900	0
K_HPO4	-26.57	0.2020	$-3.0420\ 10^{-3}$	- 4.08	0.0714	0
K_SiOH4	-29.48	0.1622	$2.6080\ 10^{-3}$	- 2.84	0.0000	0
K_SiOOH3	-29.48	0.1622	$2.6080\ 10^{-3}$	- 2.84	0.0000	0
Ksp_calcite	-48.76	0.5304	$0.0000\ 10^{-3}$	-11.76	0.3692	0
Ksp_aragonite	-45.96	0.5304	$0.0000\ 10^{-3}$	-11.76	0.3692	0

6.6.3.10. Conversion factors

The following list gives the basic concentration and pH scale conversion factors used in AquaEnv. All other conversion factors in the function `convert` are calculated from the factors given here. Note that the factors given below are multiplicative factors that can be used to convert dissociation constants or proton concentration values. To convert pH values, one needs to use the negative decadal logarithm of the factors below as an additive term.

[4] It is not stated in Millero (1995) but since this pressure correction is a multiplicative factor, it can be inferred that the unit and pH scale of the corrected constant only depends on the unit and pH scale of the uncorrected constant. This formula thus can be applied to any constant with no respect to its unit and pH scale.

[5] Note that in Lewis and Wallace (1998) it is stated that the *a* values for H_2O and H_2S are *freshwater* values! And that the coefficients for the silicate species are assumed to be the same as the ones for the borate species.

`molal2molin` denotes conversion from mol/kg-H_2O to mol/kg-soln, `free2tot` denotes conversion from the free to the total pH scale, `free2sws` denotes conversion from the free to the seawater pH scale (for a general treatment of the free, total and seawater pH scale see Dickson (1984) and Zeebe and Wolf-Gladrow (2001)), and `free2nbs` denotes conversion from the free to the NBS pH scale (Durst, 1975).

`molal2molin`	(1 - 0.001005 S)	Roy et al. (1993b, p. 257), DOE (1994, chap. 5, p. 15)
`free2tot`	$(1 + \frac{S_T}{K\_HSO4})$	Dickson (1984, p. 2302), DOE (1994, chap. 5, p. 16), Zeebe and Wolf-Gladrow (2001, p. 57, p. 261)
`free2sws`	$(1 + \frac{S_T}{K\_HSO4} + \frac{F_T}{K\_HF})$	Dickson (1984, p. 2303), Zeebe and Wolf-Gladrow (2001)
`free2nbs`	γ_{H^+}	Dickson (1984), Zeebe and Wolf-Gladrow (2001)

In the above table `S` is salinity, $S_T = [SO_4^{2-}] + [HSO_4^-] \approx [SO_4^{2-}]$, $F_T = [HF] + [F^-] \approx [F^-]$, both in mol/kg-soln, and γ_{H^+} is the activity coefficient for the proton. The dissociation constants `K_HSO4` and `K_HF` are on the free pH scale and in mol/kg-soln as well. Note that, as given in Dickson (1984, p. 2303) and Dickson and Riley (1979a, p. 91f) all concentrations appearing in the definition for the total and the seawater pH scale are molal, i.e., mol/kg-H_2O, concentrations. But in Roy et al. (1993b, p. 257) and in DOE (1994, chap. 4, SOP 6, p. 1) it is stated, that concentrations for the seawater and total pH scale are molin, i.e., mol/kg-soln. To be consistent with DOE (1994) mol/kg-soln is chosen here.

6.6.3.11. Activity coefficient for the proton

In AquaEnv a complex ion-interaction model like, e.g., Millero and Pierrot (1998) is not implemented. According to Zeebe and Wolf-Gladrow (2001) the activity coefficient for the proton γ_{H^+} can be approximated by the Davies equation as long as the ionic strength of the solution in question remains below 0.5 mol/kg-H_2O. This means for solutions with a salinity of less than 24.48. Since NBS scale pH values are normally not used for open ocean applications but mainly in brackish and fresh waters, the Davies equation has been assumed to be a sufficient approximation for γ_{H^+}. Important to note, however, is that the conversion from and to the NBS pH scale in AquaEnv for salinities above 24.48 is only an approximation! The Davies equation is used as given in Zeebe and Wolf-Gladrow (2001)

$$\gamma_{H^+} = 10^{-\left(1.82\,10^6\,(\epsilon\,T)^{-\frac{3}{2}}\right)\left(\frac{\sqrt{(I)}}{1+\sqrt{(I)}}-0.2\,I\right)} \tag{38}$$

where ϵ is the relative dielectric constant of seawater (`PhysChemConst e` in AquaEnv), `T` is the temperature in Kelvin, and `I` is the ionic strength in mol/kg-H_2O. Note that the squared charge of the ion before the brackets with the ionic strength terms which is present in the generic form of the Davies equation has been omitted here since for the proton, this factor is 1.

6.6.3.12. The Revelle factor

In Zeebe and Wolf-Gladrow (2001, p.73) the revelle factor is given as

$$\mathrm{RF}_0 = \left(\frac{d[\mathrm{CO_2}]}{[\mathrm{CO_2}]} \Big/ \frac{d[\sum \mathrm{CO_2}]}{[\sum \mathrm{CO_2}]} \right)_{[\mathrm{TA}]=\mathrm{const.}} \tag{39}$$

in AquaEnv, `revelle` is calculated numerically.

6.6.3.13. Partial derivatives of total alkalinity

The values for `dTAdKdKdS`, `dTAdKdKdT`, `dTAdKdKdd`, `dTAdKdKdSumH2SO4`, and `dTAdKdKdSumHF` are calculated numerically as described in Hofmann et al. (2009a, , i.e., Chapter 4).

The values for `dTAdH`, `dTAdSumCO2`, `dTAdSumBOH3`, `dTAdSumH2SO4`, and `dTAdSumHF` are calculated analytically as given in Hofmann et al. (2008a, , i.e., Chapter 3).

7. Conclusions and outlook

Even if some field of science seems to be "thoroughly explored" at first sight, that does not mean that there is no more work to be done and there are no new insights to be gained. pH chemistry is such a field: pioneered over a hundred years ago by people like Svante Arrhenius, Johannes N. Brønsted, and Thomas M. Lowry, it is of such complexity, that even now, in the first decade of the 21^{st} century, it can still sustain a PhD thesis - and I am sure this will not be the last, especially since this thesis raises more questions than it answers, more precisely, it provides the tools to answer new questions.

The mentioned pioneers of pH chemistry mainly were concerned about pH predictions, buffering, titrations, and the like in controlled and sterile experimental setups in beakers in the laboratory - an approach that sometimes is lovingly termed "bucket-chemistry". Nowadays, even in higher education, pH chemistry is still taught mainly based on this approach. However, when considering pH in natural systems, such as rivers, lakes, estuaries and oceans, this approach is often not sufficient. Natural aquatic systems are generally in contact with the atmosphere and exchange between the gaseous and liquid phases as well as atmospheric wet and dry deposition take place at considerable magnitudes, often influencing pH. Furthermore, not only lateral and vertical transport, e.g., in the oceans, but also exchange of chemical substances with the sediments of natural aquatic systems can have an effect on pH. Last but not least there is the biosphere: any natural aquatic system is teeming with life, not only are there plants and animals that are visible to the naked eye, but every liter of natural seawater contains countless multicellular and unicellular microalgae, countless specimens of multicellular and unicellular zooplankton, up to 10^9 bacterial and archeal cells, and around 10^{11} viral particles (Sommer, 1998). They photosynthesize, respire, excrete, nitrify and perform a multitude of other biogeochemical tasks. Most of these processes affect pH. To investigate pH of natural systems in a proper way, it therefore is necessary to step away from a "bucket chemical" approach and consider an open system with a multitude of biogeochemical processes.

Existing approaches to develop biogeochemical pH models for dynamic open systems are "alkalinity centered", meaning the connection between modelled processes and pH changes in the system is expressed and obscured via the detour of alkalinity and numerical solution techniques for nonlinear equation systems. During this thesis we investigated the fundamental connection between biogeochemical and physical process rates and pH changes in a buffered system. We made this connection explicit by introducing an analytical formula for the rate of change of proton concentration. By doing so, we made the transition from the traditional "alkalinity centered" approach of pH modelling towards the "proton centered" approach. An analytical formula for the rate of change of proton concentration makes it possible to quantify the influences of different process on pH in a system where all those processes are proceeding at the same time. Together with the extension for variable acid-base dissociation constants, this approach can be applied to any system with any set of processes, be it biological, chemical or physical. Even advective-diffusive transport processes in sediments with different molecular diffusion coefficients for each single chemical species (differential transport) can be treated. To our knowledge, this has not been possible before.

We furthermore complement our approach with palpable chemical meaning by showing how the explicit expression for the rate of change of proton concentration due to a certain process relates to the stoichiometry of this process. We show that it is possible to construct a certain form of stoichiometric equation, a *fractional reaction equation at ambient pH* for any process, including transport processes. The stoichiometric coefficient for protons in this reaction equation expresses proton consumption or release of the respective process *at ambient pH*, i.e., assuming the chemical speciation of the whole system does not change. In an unbuffered system, this proton release at ambient pH would equal the rate of change of proton concentration over time. In a buffered system, however, this proton release needs to be attenuated via the division by a buffer factor. We establish that this buffer factor is the negative of the partial derivative of total alkalinity with respect to the proton concentration. This quantity can be intuitively understood to express the buffering capacity of a system since it expresses the amount of alkalinity change per proton addition or removal. Since alkalinity is a sum of positive and negative equilibrium species concentrations, i.e. concentrations that depend on acid-base reactions, it is also obvious that our buffer factor depends on the equilibrium acid-base reactions of the system, making their role explicit. We call the quotient of the stoichiometric coefficient for the proton over the buffer factor, the *sensitivity* of pH with respect to the respective process. This sensitivity is the modulating factor with which the process rate needs to be multiplied to arrive at the analytical expression for the rate of change of proton concentration due to a certain process. The fact that the sensitivity of pH with respect to a certain process can be decomposed into a stoichiometric coefficient which is characteristic to the process itself over the buffer factor depending on the acid-base reactions in the system, allows for identification and partitioning of how driving biogeochemical processes and buffering acid-base reactions contribute to an observable pH change.

The use of a buffer factor is not novel, chemical textbooks such as Morel and Hering (1993), Stumm and Morgan (1996) or papers like Frankignoulle (1994) postulate and define similar quantities based on pH. However, in these references, it is either not specified how the defined buffer quantities can be used to estimate effects of processes on the system in general and on pH in particular, or they are limited to the addition of fully dissociated strong acids to the system. Our buffer factor β, however, is consistently derived from the explicit mathematical description of the system, is based on the biogeochemically relevant free proton concentration, and our fractional stoichiometric approach using ionization fractions of acid-base systems provides a clear recipe of how β can be used to assess the influence of any process on pH, not only the addition of strong acids.

Although we used the the Scheldt estuary as the main testbed, our approach was developed with global problems of ocean carbon uptake and acidification in mind. Applying the concept of buffer capacity and pH sensitivities to an averaged global ocean shows that towards the end of the century the global oceans might be between three and four times less buffered than they are today (see also Figure 7.1). This back-of-the-envelope calculation provides a small glimpse of how the concepts and tools presented here can make a complementary contribution to the existing modelling approaches of ocean acidification and global carbon cycling. Calculations and models of this type are not only helpful to guide experimental scientists to identify processes to which pH will be most sensitive, but they are also useful to Earth System modellers to decide whether or not to include certain processes in pH models for the future ocean. Furthermore, it is vital to calculate the - well known - sensitivities of the pH

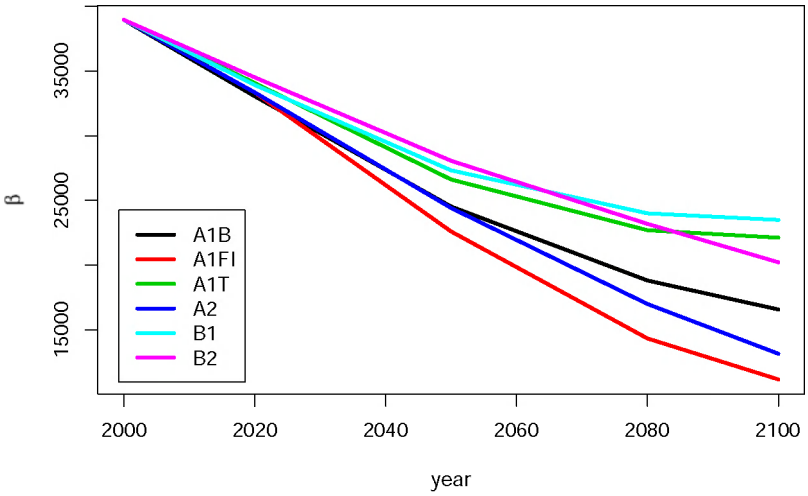

Figure 7.1.: The buffer capacity β of the global ocean: by the end of the century, the global ocean might be up to ≈ 3.5 times less buffered than it is today. β is calculated with concentrations of total quantities as given in Table 5.4, t=15 C, S=35, and pH, assumed to be on the seawater pH scale, taken from the graphic in Figure 1.1 (taken from Meehl et al., 2007) at years 2000, 2020, 2050, 2080 and 2100, for the IPCC scenarios given in the legend (IPCC scenarios are explained in IPCC (2000)).

with respect to certain processes correctly to be able to focus on the real modelling challenge of the coming years: closing the feedback-loop of processes influencing pH and pH influencing processes, with the ultimate goal of getting the rates of the main processes right, which drive ocean acidification and the mitigation of antropogenic CO_2 emissions.

Once the feedback loop of processes influencing pH that also depend on pH is closed, a whole range of questions, even beyond mere predictions of future oceanic pH values, can be addressed. For example, appropriate ecosystem models can be used to investigate ecosystem resilience and alternative steady states for the pH chemistry of any aquatic system, from the smallest pond to the global ocean. To that end, it can be assessed how the effect of, for example local, excursions of pH due to events like phytoplankton blooms or atmospheric deposition of acids or bases on an ecosystem changes with a changing baseline pH. Furthermore, rather unanticipated effects of ocean acidification can be investigated: via the influences of processes on pH, the influences of processes on properties related to pH, such as sound attenuation (Hester et al., 2008) which might be relevant for, e.g., marine mammals, can be quantified.

Moreover, the introduced explicit pH modelling and fractional stoichiometric approach cannot only be applied to questions related to ocean acidification: it can also be used to investigate physiological questions like the control of pH inside the shells of bivalves or within unicellular

organisms. Furthermore, it can be employed in bio-engineering: the concept of pH sensitivities can be used for automated data-mining in databases of physiological pathways to select and rank pathways and associated microbial communities that affect pH in a certain desired way. This can not only be applied to, e.g., wastewater treatment plants, but it can also be used to analyze and optimize pH dependent processes in biochemical food processing reactors or bio-gas fermenters. Last but not least there are medical applications: most processes inside the human body depend on and govern pH in the cytosol of somatic cells as well as interstitial, digestive, and various other body fluids.

In short, as the few examples in the above paragraphs show, this thesis provides a framework of versatile tools that can be used to foster understanding of pH chemistry in natural aqueous solutions in all its facettes.

Part III.

Summary

8. Summary

Along the course of this thesis we (1) developed a one-dimensional ecosystem model of the Scheldt estuary and investigated the estuarine filter function with respect to nitrogen and carbon. Furthermore, we (2) structured, unified and connected existing pH modelling approaches and developed a methodology to quantify the influences of biogeochemical and physical processes on the pH. (3) By applying this methodology to our model of the Scheldt estuary we shed light on the dominant processes governing the yearly averaged longitudinal pH profile along the estuary, as well as the driving forces for interannual changes in the mean estuarine pH. We then (4) further elaborated our pH modelling methodology and added chemical interpretation through explicitly connecting reaction stoichiometry and influences of processes on pH. Finally, we (5) presented a toolbox for quickly developing pH models of natural aquatic systems in the interpreted open-source programming language R.

In **Chapter 2**, we developed a one-dimensional reactive transport model of the Scheldt estuary (The Southern Netherlands and Northern Belgium) and applied it to the years 2001 to 2004. Using this model we calculated volumetric and volume-integrated yearly averaged longitudinal mass balance budgets for total ammonium, dissolved inorganic carbon, dissolved oxygen, and the nitrate concentration. Furthermore, combined whole estuarine yearly averaged budgets for the elements nitrogen and carbon were compiled. We showed that the Scheldt estuary is an active biogeochemical reactor where, all along its path, the transformations occur at a similar magnitude. This is due to the interplay of a decreasing volumetric process activity and an increasing estuarine volume from upstream to downstream. With respect to the nitrogen cycle, the estuary has evolved towards a more and more neutral passage way of total nitrogen, with only 10% of the total imported nitrogen being lost from the estuary to the atmosphere. This is in sharp contrast to the situation in the eighties and seventies where this loss amounted to more than 20% and 40%, respectively. Coinciding with a reduced total nitrogen import in the estuary, this has led to a current total nitrogen export to the North Sea which is smaller than the export in the eighties but still larger than what was observed in the seventies. Moreover, the estuary has a large effect on the nitrogen speciation, especially by transforming ammonium and, indirectly, the imported organic nitrogen to nitrate. Similarly to previous budget estimates, nitrification remains one of the most important oxygen consuming processes in the estuary. The loss of imported carbon in the estuary amounts to about 13%, and occurs through physical ventilation of CO_2 to the atmosphere. Two thirds of this lost C is riverine-borne DIC, one third of the ventilated CO_2 originates from heterotrophic production in the estuary itself. Whilst the estuary remains a significant source of CO_2 to the atmosphere, our results suggest that there is a downward trend in CO_2 degassing from the nineties to our model time period. This result should be considered tentative due to the high degree of uncertainty associated with CO_2 degassing estimates.

In **Chapter 3**, we systematically and consistently derived a succession of methods to model pH, making every step of the model generation process explicit. The chemical structure of the model was used for sucessive reformulations until fast and elegant numerical solutions were possible. Existing pH modelling approaches were identified within this framework and advantages and drawbacks were pointed out. The last reformulation of the system allowed for a way of solving the system that makes it possible to quantify the influence of modelled

kinetic processes on pH. Applying this approach to a simple one box model of the upper Scheldt estuary, we investigated the effects on pH of three theoretical scenarios: halving the waste loading (organic matter) that enters the modelled area, the spill of ten thousand tons of ammonium nitrate due to a ship accident carrying artificial fertilizer, and the spill of ten thousand tons of ammonia, also from a ship spill. While the change in the waste load has minute effects on the pH of the system, the ammonium nitrate spill results in downwards pH excursion of approximately 0.2 pH units, and the spill of ammonia results in an even larger upwards pH excursion of about 1 pH unit. The main process responsible for the pH excursion after the ammonium nitrate spill is nitrification which shows increased rates due to the increased ammonium concentration. For the case of the ammonia spill, the ammonia addition itself is mainly responsible for the pH change. After both spills, the system returns back to a normal state in about two weeks.

In **Chapter 4**, the methodology to quantify the influences of kinetically modelled processes on the pH is extended to a system with (time) variable acid-base dissociation constants. This extension is verified against an existing pH modelling approach. While the influences of changes in the dissociation constants might be neglected in approximate whole estuarine budgets, they are important to explicitly model proton concentrations in systems where the acid-base dissociation constants are assumed to be variable over time, if the accuracy needs to be better than 0.1 pH units. By applying this method to the one-dimensional reaction transport model of the Scheldt estuary developed in Chapter 2, we have identified nitrification as the main process governing the pH profile along the estuary, while CO_2 degassing and advective-dispersive transport buffer the effect of this process. However, CO_2 degassing accounts for the largest total proton turnover per year in the whole estuary. A clear inverse correlation between oxygen and proton turnover was found, consistent with theoretical considerations of redox chemistry. The main driver of changes in the mean estuarine pH from 2001 to 2004 was a changing freshwater flow which influenced pH "directly" via $[\sum CO_2]$ and $[TA]$ and also – to a significant amount – "indirectly" via $[\sum NH_4^+]$ and the nitrification rates.

In **Chapter 5**, the methodology to quantify the influences of kinetically modelled processes on the pH was revisited and investigated in detail. In the previous chapters we primarily concentrated on the numerical aspects of the approach, while here, we principally focused on concepts and chemical interpretation. The central idea is that the total rate of change of protons can be decomposed into a linear combination of the biogeochemical process rates and that the coefficients in this expression quantify a *sensitivity* of the pH to each biogeochemical process. This sensitivity determines how strongly this biogeochemical process will influence the pH. We showed that the process specific sensitivities of the pH aggregate both, the influence of the driving process in question, and the influences of the acid-base reactions in the system. This can be understood by considering a two step process where protons are produced by the driving processes directly, as in an unbuffered system, and subsequently the system is re-equilibrated. The sensitivity of pH with respect to a driving process can thus be expressed as a quotient of the stoichiometric coefficient ν_{H^+} for the proton in the fractional reaction equation at ambient pH of the driving process over the buffer factor β. ν_{H^+} is a quantity that represents the direct proton production by the driving process, without re-equilibration, and β is a quantity that represents the attenuation of the pH changes by the set of acid-base reactions. We furthermore show that this approach is deeply rooted in well known chemical concepts: the buffer factor β is similar to buffer quantities that have been previously defined

in literature and the definition of the stoichiometric coefficient ν_{H^+} contains the well-known ionization fractions. Additionally, we applied the concept of buffer factor and pH sensitivities to a scenario of ocean acidification, assuming an average composition of the global surface ocean and showed that the buffer factor of surface ocean water might be about four times less at the end of the century than it is now. The global ocean pH becomes thus substantially more sensitive to the addition of acids or bases in the future, allowing for synergistic effects between CO_2-induced ocean acidification and non-CO_2-induced ocean acidification (e.g., atmospheric wet and dry deposition of HNO_3 and H_2SO_4). This back-of-the envelope calculation is a simple example of how calculations based on our approach can help to investigate global ocean acidification and global carbon cycling.

In **Chapter 6**, an extension package, called `AquaEnv`, for the interpreted open-source programming language R was introduced which comprises an extensive toolbox for aquatic acid-base modelling that allows for rapid prototyping and the visualization of pH model results for natural aquatic systems as well as for processing and visualizing of measured data. All quantities needed to model the pH according to the methodology described in the previous chapters are coded in the package. `AquaEnv` can also be used to conduct "in silico experiments": it can be used to simulate titrations with either a strong acid or a strong base and the resulting speciation curves can be visualized as Bjerrum plots. Furthermore, the calculation of alkalinity values from measured titration curves via non linear curve fitting has been implemented. `AquaEnv` is a collection of building blocks that have been developed along the course of this thesis, contains some examples of how to use these building blocks, but is intended to be used as just that, a collection of building blocks that scientists can use to build their own pH models.

9. Samenvatting

In deze thesis is (1) een 1-dimensonaal ecosysteemmodel van het Schelde estuarium ontwikkeld en de estuarine filterfunctie met betrekking tot stikstof en koolstof onderzocht. Verder zijn (2) bestaande pH modelleermethodes gestructureerd en geïntegreerd en er is een methodologie ontwikkeld om de invloeden van biogeochemische en fysische processen op de pH waarde te bepalen. Door deze methodologie op het model van het Schelde estuarium toe te passen zijn (3) niet alleen de belangrijkste processen die voor het jaargemiddelde pH profiel langs het estuarium verantwoordelijk zijn bepaald, maar werden ook de drijvende krachten achter interannuele veranderingen van de over het hele estuarium gemiddelde pH verhelderd. Vervolgens is (4) de pH modelleermethodologie verder uitgewerkt en met chemische interpretatie aangevuld door de link tussen reactie stoichiometrie en de invloeden van processen op de pH waarde expliciet te maken. Tenslotte is (5) een "programmeer gereedschapskist" gepresenteerd die het mogelijk maakt met behulp van de geïnterpreteerde open-source programmeertaal R snel en makkelijk pH modellen van natuurlijke aquatische systemen te genereren.

In **Hoofdstuk 2** is een 1-dimensionaal reactie-transport model van het Schelde estuarium (Zuid-Nederland en Noord-Belgie) ontwikkeld en op de jaren 2001 t/m 2004 toegepast. Dit model werd gebruikt om volumetrische en volume-geïntegreerde massa budgetten voor ammoniak + ammonium, voor opgeloste anorganisch koolstof, opgeloste zuurstof en voor de nitraatconcentratie te berekenen. Daarnaast zijn over het jaar en het hele estuarium gemiddelde budgetten voor de elementen stikstof en koolstof berekend. Er wordt aangetoond, dat het Schelde estuarium een actieve biogeochemische reactor is, waarin, langs de gehele lengte, chemische transformaties in dezelfde orde van grootte plaats vinden. Dit is het gevolg van de balans tussen van bovenstrooms naar benedenstrooms afnemende volumetrische proces activiteiten en een van bovenstrooms naar benedenstrooms toenemend estuarien volume. Met betrekking tot de stikstofcyclus is het estuarium tot een vrijwel neutrale transit-zone voor totale stikstof geëvolueerd, waarin maar 10% van de totale geïmporteerde stikstof uit het estuarium naar de atmosfeer gaat. Dit staat in scherp contrast met de jaren tachtig en zeventig, toen dit verlies respectievelijk 20% en 40% bedroeg. Samen met een verminderde import van totale stikstof in het estuarium, resulteert dat in een hedendaags export van stikstof naar de Noordzee die wel lager is dan de export in de jaren tachtig, maar die nog steeds hoger is dan de export die in de jaren zeventig te zien was. Behalve dat heeft het estuarium ook een grote invloed op de stikstof speciatie, in het bijzonder door de transformatie van ammonium en, op indirecte manier, van de geïmporteerde organische stikstof naar nitraat. Net zoals in vroegere schattingen blijft nitrificatie het proces dat het belangrijkst is voor de zuurstofconsumptie in het estuarium. Het verlies van koolstof in het estuarium bedraagt 13% van de import en gebeurt via fysische ventilatie van CO_2 naar de atmosfeer. Twee derde van deze verloren koolstof is afkomstig van fluviatiel DIC en een derde van heterotrofe productie in het estuarium zelf. Hoewel het estuarium een substantiële bron van CO_2 voor de atmosfeer blijft, wijzen onze resultaten erop dat er een neerwaartse trend voor CO_2 uitgassing van de jaren negentig naar de tijdsperiode van ons model bestaat. Dit resultaat moet als tentatief beschouwd worden omdat, er veel onzekerheid aan schattingen van CO_2 uitgassing verbonden is.

In **Hoofdstuk 3** is op systematische en coherente wijze een opeenvolging van methodes

afgeleid om de pH waarde te modelleren en elke stap van het genereren van het model is erbij expliciet gemaakt. De chemische structuur van het model is voor opeenvolgende herformuleringen gebruikt, totdat snelle en elegante numerieke oplossingen mogelijk waren. Bestaande pH modelleermethodes zijn binnen deze beraming geïdentificeerd en de voor- en nadelen zijn aangegeven. De laatste herformulering stelde ons in de gelegenheid, het systeem op een manier op te lossen die het mogelijk maakt, de invloeden van gemodelleerde kinetische processen op de pH waarde te kwantificeren. Door deze methode op een eenvoudig box model van het bovenstrooms gedeelte van het Schelde estuarium toe te passen, zijn de effecten van drie theo- retische scenario's op de pH waarde onderzocht: het halveren van de afvalstoffen lozing (organische stof) in het gemodelleerd gebied, de vervuiling met tienduizend ton ammoniumnitraat door averij aan een schip dat kunstmest vervoert, en de vervuiling met tienduizend ton ammoniak, ook door een scheepsramp. Alhoewel het veranderen van de afvalstofinvoer maar een beperkte invloed op de pH waarde van het systeem heeft, resulteert een lekkage van ammoniumnitraat in een opwaartse excursie van de pH waarde met 0.2 pH eenheden en het uitstromen van ammoniak resulteert in een zelfs nog grotere negatieve excursie. Het proces dat het meest verantwoordelijk voor de pH verandering naar het uitstromen van ammoniumnitraat is, is nitrificatie, die door de verhoogde ammoniumconcentratie een toegenomen reactiesnelheid vertoont. In het geval van ammoniak is de lekkage zelf hoofdzakelijk ervoor verantwoordelijk dat de pH waarde verandert. Voor beide uitstroom scenario's keert het systeem binnen ongeveer twee weken terug naar de uitgangstoestand.

In **Hoofdstuk 4** is de methodologie, om de invloed van kinetisch gemodelleerde processen op de pH waarde te kwantificeren, uitgebreid naar systemen met zuur-base dissociatieconstanten die over de tijd veranderlijk zijn. Deze uitbreiding is aan de hand van een bestaande pH modelleermethode geverifieerd. Alhoewel de veranderingen van dissociatieconstanten voor massa budgetten betreffende het gehele estuarium weinig invloed hebben, zijn ze wel belangrijk voor het expliciete modelleren van de protonenconcentratie in systemen waar zuur-base dissociatieconstanten als veranderlijk over de tijd beschouwd kunnen worden en de nauwkeurigheid beter dan 0.1 pH eenheden moet zijn. Door deze methode op het 1-dimensionale model van het Schelde estuarium, dat in Hoofdstuk 3 ontwikkeld is, toe te passen, is nitrificatie als het proces geïdentificeerd dat het pH profiel langs het estuarium hoofdzakelijk bepaalt, terwijl CO_2 uitgassing en advectief-dispersief transport de invloed van dit proces bufferen. CO_2 uitgassing is echter verantwoordelijk voor de grootste omzet van protonen in het gehele estuarium per jaar. Er is een duidelijke inverse correlatie tussen zuurstof en protonenomzet, wat consistent met theoretische beschouwingen van redoxchemie is. De voornaamste drijvende kracht achter veranderingen van de gemiddelde estuarine pH tussen 2001 en 2004 was een veranderende riviertoevoer welke de pH waarde "direct" via $[\sum CO_2]$ en [TA] beïnvloedde maar ook - op significante schaal - "indirect" via $[\sum NH_4^+]$ en de nitrificatiesnelheden.

In **Hoofdstuk 5** is de methodologie, om de invloeden van kinetisch gemodelleerde processen op de pH waarde te kwantificeren, opnieuw vanuit een ander oogpunt bekeken en tot in het detail uitgezocht. In de voorgaande hoofdstukken was op de numerieke aspecten van de methode geconcentreerd, terwijl hier voornamelijk op concepten en chemische interpretatie gefocust wordt. Het hoofdidee is dat de totale veranderingssnelheid van de protonenconcentratie opgesplitst kan worden in een lineaire combinatie van de biogeochemische reactiesnelheden en dat de coëfficiënten van deze lineaire combinatie een *sensitiviteit* van de pH waarde aangaande elk biogeochemisch proces uitdrukken. Deze sensitiviteit bepaalt hoe sterk het biogeochemische

proces de pH waarde beïnvloedt. Het is aangetoond, dat de proces-specifieke sensitiviteit van de pH waarde zowel de directe invloed van het drijvende proces, als ook de invloeden van de zuur-base reacties in het systeem bevat. Dit is te begrijpen als men twee stappen beschouwt, waar het drijvende proces direct protonen produceert, net zoals in een niet gebufferd systeem, en het systeem vervolgens naar een zuur-base evenwicht terugkeert. De sensitiviteit van de pH waarde met betrekking tot een bepaald proces kan dus als een quotiënt van de stoichiometrische coefficiënt ν_{H^+} voor protonen in de fractionale reactievergelijking bij omgevings pH van het drijvend proces over de buffer factor β uitgedrukt worden. ν_{H^+} is een maat welke de directe protonenproductie door het drijvend proces zonder herequilibratie representeert en β is een maat voor de demping van veranderingen in de pH waarde door zuur-base reacties. Het is ook aangetoond dat deze benadering diep in bekende chemische concepten verankerd is: de buffer factor β is met kwantiteiten welke al eerder in de literatuur gedefinieerd zijn te vergelijken en de definitie van de stoichiometrische coëfficiënt ν_{H^+} bevat de bekende ionisatie fracties. Bovendien is het concept van buffer factor en pH sensitiviteiten op een scenario van mondiale oceaanverzuring toegepast, waar van een gemiddelde samenstelling van de mondiale oppervlakteoceaan uitgegaan wordt, en aangetoond wordt, dat de buffer factor van het oceaan oppervlaktewater tegen het eind van het eeuw mogelijk tot vier keer kleiner is dan nu. De pH waarde van de mondiale oceaan wordt in de toekomst dus substantieel gevoeliger voor het toevoegen van zuur of base, wat synergistische effecten tussen door CO_2 geïnduceerde oceaanverzuring en niet door CO_2 geïnduceerde oceaanverzuring (bijvoorbeeld natte en droge depositie van HNO_3 en H_2SO_4) mogelijk maakt. Deze back-of-the-envelope berekening is een eenvoudig voorbeeld voor manieren van hoe berekeningen die op onze benadering gebaseerd zijn erbij kunnen helpen mondiale oceaanverzuring en de mondiale koolstofcyclus te onderzoeken.

In **Hoofdstuk 6** is AquaEnv, een uitbreidingspakket voor de geïnterpreteerde open-source programmeertaal R, geintroduceerd, welk een brede verzameling van functies voor het aquatische zuur-base modelleren bevat en welk het snelle genereren van prototypen en het bewerken en visualiseren van modelresultaten voor natuurljike aquatische systemen en gemeten data mogelijk maakt. Alle gegevens welke voor de in voorgaande hoofdstukken uitgelegde pH mo-delleermethode nodig zijn, zijn in het pakket gecodeerd. AquaEnv kan ook worden gebruikt om "in silico experimenten" te doen: titraties met een sterk zuur of een sterke base kunnen gesimuleerd worden en de resulterende speciatie curves kunnen als Bjerrum plots worden ge-visualiseerd. Daarnaast werd ook de berekening van alkaliteitswaarden, uitgaande van gemeten titratiecurves en met behulp van niet lineaire curvenoptimisatie, geïmplementeerd. AquaEnv is een verzameling van bouwstenen welke tijdens het werken aan deze thesis ontwikkeld werden. Alhoewel het voorbeelden bevat hoe deze functies te gebruiken zijn, is het toch voornamelijk de bedoeling dat wetenschappers die functies gebruiken om hun eigen pH modellen te bouwen.

10. Zusammenfassung

Im Laufe dieser Doktorarbeit wurde (1) ein eindimensionales Ökosystemmodell des Scheldeästuariums entwickelt und die ästuarine Filterfunktion bezüglich Stickstoff und Kohlenstoff untersucht. Des Weiteren wurden (2) existierende pH Modelliermethoden strukturiert, vereinheitlicht und verbunden. Es wurde außerdem eine Methodologie entwickelt, um die Einflüsse biogeochemischer und physischer Prozesse auf den pH Wert zu quantifizieren. Durch die Anwendung dieser Methodologie auf das Modell des Scheldeästuariums wurde (3) nicht nur ans Licht gebracht, welche Prozesse hauptsächlich das jährlich gemittelte pH Profil entlang des Ästuariums verursachen, sondern es wurden auch die treibenden Kräfte hinter Veränderungen im durchschnittlichen pH Wert des gesamten Ästuariums von Jahr zu Jahr identifiziert. Die entwickelte pH Modelliermethodologie wurde dann (4) weiter ausgearbeitet und mit chemischer Interpretation versehen, d. h. Reaktionsstöchiometrie wurde explizit mit den Einflüssen von Prozessen auf den pH verbunden. Schließlich wurde (5) ein programmiertechnischer Werkzeugkasten präsentiert, der es erlaubt mit der Open-Source Programmiersprache R schnell und einfach pH Modelle von natürlichen aquatischen Systemen zu generieren.

In **Kapitel 2** wurde ein eindimensionales Reaktionstransportmodell des Scheldeästuariums (gelegen im Süden der Niederlande und im Norden Belgiens) entwickelt und auf die Jahre 2001 bis 2004 angewendet. Mit diesem Modell wurden volumetrische und über das Volumen integrierte, jährlich gemittelte Massenbilanzen für Ammoniak und Ammonium gemeinsam, für gelösten anorganischen Kohlenstoff, gelösten Sauerstoff und die Nitratkonzentration entlang des Ästuariums berechnet. Weiterhin wurden kombinierte, jährlich gemittelte Bilanzen für die Elemente Stickstoff und Kohlenstoff aufgestellt. Es wurde gezeigt, daß das Scheldeästuarium ein aktiver biogeochemischer Reaktor ist, in dem entlang seines gesamten Laufes chemische Transformationen in vergleichbarer Grössenordnung ablaufen. Dies ist ein Effekt des Zusammenspiels einer von flussaufwärts nach flussabwärts abnehmenden volumetrischen Aktivität der Prozesse und eines von flussaufwärts nach flussabwärts zunehmenden ästuarinen Volumens. Bezüglich des Stickstoffkreislaufes hat sich das Ästuarium zu einer mehr und mehr neutralen Passage für totalen Stickstoff entwickelt, da nur etwa 10% allen Stickstoffes, der in das Ästuarium importiert wird, an die Atmosphäre verloren gehen. Das steht in scharfem Gegensatz zu der Situation in den Achtzigern und Siebzigern, in denen sich dieser Verlust auf 20% bzw. 40% belief. Zusammen mit einem reduzierten Stickstoffimport in das Ästuarium hat dies zu einem momentanen Export von totalem Stickstoff in die Nordsee geführt, welcher zwar niedriger ist als der Export in den Achtzigern, welcher aber immer noch grösser ist als der Export, der in den Siebzigern zu beobachten war. Darüber hinaus hat das Ästuarium einen großen Einfluß auf die Stickstoffspeziation, vor allem durch die Umsetzung von Ammonium und, auf indirektem Wege, von importiertem organischen Stickstoff zu Nitrat. Ähnlich wie in früheren Schätzungen bleibt Nitrifikation einer der wichtigsten Sauerstoff verbrauchenden Prozesse im Ästuarium. Der Verlust von Kohlenstoff aus dem Ästuarium beläuft sich auf 13% und erfolgt durch physikalische Ventilation von CO_2 in die Atmosphäre. Zwei Drittel des abgegebenen Kohlenstoffes stammt aus fluviatilem DIC und ein Drittel entsteht im Ästuarium selbst durch heterotrophe Produktion. Während das Ästuarium eine wichtige CO_2 Quelle für die Atmosphäre bleibt, legen unsere Resultate nahe, daß von den neunziger Jahren bis zu unserem Modellzeitraum ein Abwärtstrend in der Abgabe von gasförmigem CO_2 aus

dem Ästuarium vorliegt. Dieses Ergebnis sollte allerdings als tentativ betrachtet werden, da ein hoher Grad an Unsicherheit mit Schätzungen von CO_2 Abgaben aus dem Ästuarium an die Atmosphäre verbunden ist.

In **Kapitel 3** wurde eine Abfolge von pH Modelliermethoden systematisch und konsistent hergeleitet, wobei jeder Herleitungsschritt explizit beschrieben wurde. Die chemische Struktur des Modells wurde für aufeinanderfolgende Umformungen verwendet, bis schnelle und elegante numerische Lösungen des Modells möglich waren. Im Rahmen dessen wurden bereits bestehende pH Modelliermethoden identifiziert und ihre Vor- und Nachteile aufgezeigt. Die letzte Umformung des Systems ließ eine Lösung zu, die es erlaubt, die Einflüsse von kinetisch modellierten Prozessen auf den pH Wert zu quantifizieren. Durch die Anwendung auf ein einfaches Box-Modell des oberen Scheldeästuariums wurden die Effekte von drei theoretischen Szenarien auf den pH Wert untersucht: das Halbieren des Schmutzeintrages (organisches Material) in den modellierten Teil des Ästuariums, das Auslaufen von zehntausend Tonnen Ammoniumnitrat aufgrund der Havarie eines Kunstdünger transportierenden Schiffes und das Auslaufen von zehntausend Tonnen Ammoniak, ebenfalls aufgrund einer Schiffshavarie. Während der geänderte Schmutzeintrag praktisch keinen Effekt auf den pH Wert des Systems hat, führt das Auslaufen des Ammoniumnitrates zu einer abwärts gerichteten Auslenkung des pH Wertes von ungefähr 0.2 pH Einheiten. Das Auslaufen des Ammoniaks führt sogar zu einer noch grösseren aufwärts gerichteten Auslenkung des pH Wertes von einer pH Einheit. Nitrifikation, welche aufgrund der gestiegenen Ammoniumkonzentration erhöhte Reaktionsraten zeigt, ist hauptverantwortlich für die pH Veränderung nach dem Ammoniumnitrateintrag in das System. Im Falle des Auslaufens von Ammoniak ist der Ammoniakeintrag in das System selbst der Prozess, der für die pH Veränderung hauptverantwortlich ist. Nach beiden Havarieszenarien kehrt das System nach ungefähr zwei Wochen in den Normalzustand zurück.

In **Kapitel 4** wurde die Methodologie, um die Einflüsse kinetisch modellierter Prozesse auf den pH Wert zu quantifizieren, auf Systeme mit über die Zeit veränderlichen Säure-Basen Dissoziationskonstanten erweitert. Diese Erweiterung wurde anhand einer bestehenden pH Modelliermethode verifiziert. Während die Einflüsse von Veränderungen der Dissoziationskonstanten in approximativen Massenbilanzen des gesamten Ästuariums vernachlässigt werden können, sind sie wichtig, um die Protonenkonzentration in Systemen mit über die Zeit variablen Säure-Basen Dissoziationskonstanten explizit zu modellieren, wenn die Genauigkeit besser als 0.1 pH Einheiten sein soll. Durch die Anwendung dieser Methode auf das eindimensionale Reaktionstransportmodell des Schelde Ästuariums, das in Kapitel 2 entwickelt wurde, wurde Nitrifikation als der das pH Profil entlang des Ästuariums am meisten beeinflussende Prozess identifiziert, während CO_2 Entgasung und advektiv-dispersiver Transport den Effekt dieses Prozesses ausgleichen. Allerdings verursacht CO_2 Entgasung den grössten Protonenumsatz per Jahr im Ästuarium. Es wurde eine deutliche inverse Korrelation zwischen Sauerstoff- und Protonenumsatz gefunden, welche konsistent mit theoretischen Betrachtungen der Redoxchemie ist. Der Haupteinflussfaktor, der Veränderungen des über das gesamte Ästuarium gemittelten pH Wertes über die Jahre 2001 bis 2004 verursachte, ist eine sich verändernde Frischwasserabflussmenge der Schelde, welche den pH Wert sowohl "direkt" über $[\sum CO_2]$ und [TA] als auch - in signifikantem Maße - "indirekt" über $[\sum NH_4^+]$ und die Nitrifikationsraten beeinflusst.

In **Kapitel 5** wurde die Methodologie, um die Einflüsse kinetisch modellierter Prozesse auf den pH Wert zu quantifizieren, wiederholt und bis ins Detail ausgeleuchtet. In den vorhergehenden Kapiteln wurde hauptsächlich der numerische Aspekt der Methode bearbeitet, während der Nachdruck hier auf Konzepte und chemische Interpretation gelegt wurde. Die zentrale Idee ist, daß die Gesamtveränderungsrate der Protonenkonzentration in eine Linearkombination der biogeochemischen Prozessraten aufgeteilt werden kann und daß die Koeffizienten dieser Linearkombination eine *Sensitivität* des pH Wertes gegenüber den entsprechenden biogeochemischen Prozessen quantifizieren. Diese Sensitivität bestimmt, wie stark der entsprechende Prozess den pH Wert beeinflusst. Es wurde gezeigt, daß diese prozessspezifischen Sensitivitäten des pH Wertes sowohl den Einfluss des treibenden Prozesses, als auch die Einflüsse der Säure-Basenreaktionen des Systems beinhalten. Das kann durch die Betrachtung eines zweistufigen Vorgangs verstanden werden, während dessen Protonen direkt durch die treibenden Prozesse produziert werden, wie im ungepufferten Fall, und das System daraufhin zu einem Säure-Basengleichgewicht zurückkehrt. Die Sensitivität des pH Wertes bezüglich eines treibenden Prozesses kann demzufolge als ein Quotient aus dem stöchiometrischen Koeffizient ν_{H^+} für das Proton in der fraktionalen Reaktionsgleichung bei Umgebungs-pH des treibenden Prozesses geteilt durch den Pufferfaktor β ausgedrückt werden. ν_{H^+} repräsentiert die direkte Protonenproduktion durch den treibenden Prozess, ohne Reäquilibrierung, während β die Abschwächung der pH Wert Veraenderungen durch Säure-Basenreaktionen symbolisiert. Es wurde des Weiteren gezeigt, daß diese Vorgehensweise tief in bekannten chemischen Konzepten verwurzelt ist: der Pufferfaktor β ist bereits in der Literatur definierten Puffergrössen ähnlich und die Definition des stöchiometrischen Koeffizienten ν_{H^+} enthält die wohlbekannten Ionisationsbrüche. Zusätzlich wurde das Konzept von Pufferfaktor und Sensitivitäten des pH Wertes auf ein Ozeanversäuerungsszenario angewendet, wobei von einer gemittelten Zusammenstellung globalen Oberflächenozeanwassers ausgegangen wurde. Dabei wurde verdeutlicht, daß der Pufferfaktor von globalem Oberflächenozeanwasser gegen Ende des Jahrhunderts ungefähr um einen Faktor vier kleiner sein könnte, als er jetzt ist. Der globale Ozean wird in der Zukunft also wesentlich anfälliger gegenueber dem Eintrag von Säuren oder Basen sein, was synergistische Effekte zwischen CO_2 induzierter Ozeanversauerung und nicht CO_2 induzierter Ozeanversauerung (z.B. atmosphärische Nass- und Trockendeposition von HNO_3 und H_2SO_4) zur Folge haben kann. Diese grobe Rechnung ist ein einfaches Beispiel dafür, wie auf unserer Methode basierende Berechnungen dabei helfen können, globale Ozeanversauerung und den globalen Kohlenstoffkreislauf zu untersuchen.

In **Kapitel 6** wurde ein AquaEnv genanntes Erweiterungspaket für die interpretierte Open-Source Programmiersprache R vorgestellt, welches eine schnelle Prototypenentwicklung und die Visualisierung der Ergebinsse von pH Modellen für natürliche aquatische Systeme erlaubt und ebenso das Bearbeiten und Visualisieren von gemessenen Daten möglich macht. Alle Grössen die nötig sind, um den pH Wert mittels der in den vorangegangenen Kapiteln beschriebenen Methodologie zu modellieren, sind in dem Paket implementiert. AquaEnv kann auch dazu verwendet werden "in silico" Experimente durchzuführen: es können Titrationen mit entweder einer starken Säure oder einer starken Base simuliert werden und die resultierenden Speziationskurven können als Bjerrumgrafiken dargestellt werden. Ausserdem wurde die Berechnung von totaler Alkalinität anhand gemessener Titrationskurven durch nichtlineare Kurvenanpassung implementiert. AquaEnv ist eine Sammlung von Programmierbausteinen, die im Laufe dieser Doktorarbeit entwickelt wurden. Obwohl es Beispiele enthält, wie diese Bausteine verwendet werden können, ist es jedoch hauptsächlich als eine Sammlung von Funktionen zur Eigenentwicklung von pH Modellen gedacht.

Part IV.

Appendix

A. Determining total alkalinity from titration data - a short overview

There are three major groups of methods how to determine total alkalinity from titration data. (Furthermore, there are methods not based on titration, e.g. a spectrophotometrical method of total alkalinity determination (Roche and Millero, 1998), which will not be treated here.)

1. The backtitration method (Anderson et al., 1999) is a rather crude approximation of the alkalinity of a sample which can be performed with simple equipment. The method consists of removing the dissolved inorganic carbon by boiling, acidifying the sample with hydrochloric acid to around pH 3.5 and then back-titrating it to pH 6 with sodium hydroxide. Total alkalinity is then calculated from the amounts of acid and base needed for the titrations.

2. A whole group of methods is based on the position of specific features of the titration curve of a seawater sample with hydrochloric acid. In such a titration curve (either the volume of the titrant or the mass of the titrant against pH or the electrode potential E, where the mass of the titrant is to be preferred over the volume of the titrant to evade the problem of density variations (Dickson, 1981)), two clear equivalence points are visible (e.g. Dickson, 1981, see also Fig. (A.1)). The mass or volume of titrant needed to reach the first equivalence point (at around a free scale pH of 7.85) is denoted by v_1 and the volume or mass needed to reach the second equivalence point (at a free scale pH of around 4.74) is denoted v_2. In short (Hansson and Jagner, 1973)

$$\mathrm{TA} = v_2 \frac{C_{\mathrm{tit}}}{M_{\mathrm{samp}}} \tag{1}$$

$$\mathrm{DIC} = (v_2 - v_1) \frac{C_{\mathrm{tit}}}{M_{\mathrm{samp}}} \tag{2}$$

where v_1 and v_2 signify masses in this case and C_{tit} is the gravimetric concentration of the titrant while M_{samp} denotes the mass of the sample.

Why this is the case can be understood in a number of easy steps

a) Constructing a *proton condition* (see, e.g., Dickson, 1981; Zeebe and Wolf-Gladrow, 2001; Wolf-Gladrow et al., 2007), i.e. a balance of proton donors and acceptors with respect to the *proton zero level* of each acid base system (the dominant species at the respective pH) for the pH of the second equivalence point (pH $\approx$ 4.74) yields (for a simplified system with only the carbonate, borate, sulfate and fluoride acid-base systems present)

$$[\mathrm{H^+}] + [\mathrm{HSO_4^-}] + [\mathrm{HF}] = [\mathrm{HCO_3^-}] + 2[\mathrm{CO_3^{2-}}] + [\mathrm{B(OH)_4^-}] + [\mathrm{OH^-}] \tag{3}$$

or better

$$[HCO_3^-] + 2[CO_3^{2-}] + [B(OH)_4^-] + [OH^-] - [H^+] - [HSO_4^-] - [HF] = 0 \quad (4)$$

which can be easily recognized as the total alkalinity aquivalence point. (That is the reason why Dickson (1981) defined total alkalinity the way he did.)

b) This, however, means if one has titrated to this second equivalence point (by adding v_2 kilograms of hydrochloric acid with concentration C_{tit} (in mol/kg-soln)), one has completely "neutralized" every mole of the original total alkalinity of the sample ("moles of total alkalinity in the sample" = TA of the initial sample in moles/kg-soln times M_{samp} in kg) That means with on the right hand side of the equations concentrations of the original sample, before the titration

$$C_{tit}\, v_2 = ([HCO_3^-] + 2[CO_3^{2-}] + [B(OH)_4^-] + [OH^-] - [H^+] - [HSO_4^-] - [HF])\, M_{samp} \quad (5)$$

$$C_{tit}\, v_2 = TA\, M_{samp} \quad (6)$$

where TA in Eq. (6) also signifies the total alkalinity of the original sample before the titration. From this follows that one can calculate TA according to Eq. (1) if v_2 is known.

c) The first equivalence point (according to Dickson (1981) mainly due to titration of hydrogencarbon and boric acid) is found at around pH = 7.85. Constructing a proton condition for this pH yields

$$[H^+] + [HSO_4^-] + [HF] + [CO_2] = [CO_3^{2-}] + [B(OH)_4^-] + [OH^-] \quad (7)$$

or better

$$[CO_3^{2-}] - [B(OH)_4^-] - [OH^-] - [H^+] - [HSO_4^-] - [HF] - [CO_2] = 0 \quad (8)$$

This means, again with concentrations before the titration

$$C_{tit}\, v_1 = ([CO_3^{2-}] - [B(OH)_4^-] - [OH^-] - [H^+] - [HSO_4^-] - [HF] - [CO_2])\, M_{samp} \quad (9)$$

As mentioned in Dickson (1981) and originally pointed out by Dyrssen and Sillen (1967), if one subtracts Eq. (9) from Eq (5) one gets (again, with concentrations before the titration)

$$C_{tit}\, (v_2 - v_1) = ([HCO_3^- + [CO_3^{2-}] + [CO_2])\, M_{samp} \quad (10)$$

$$C_{tit}\, (v_2 - v_1) = DIC\, M_{samp} \quad (11)$$

From this follows that one can calculate DIC according to Eq. (2), if v_1 and v_2 are known.

There are several ways of determining v_1 and v_2 to make use of Eqs. (1) and (2) to obtain TA and DIC

a) For the *Gran evaluation* (Gran, 1952) one defines almost linear functions using the dominant reactions in the vincinity of both equivalence points which can then be extrapolated to their roots (=0) to obtain v_1 and v_2 (see Fig. (A.1), top). Those functions are basically defined by the proton conditions at the two equivalence points (Eq. (4) ≈ Gran function F0, Eq. (8) ≈ Gran function F2 or -F1 with the Gran function naming as in Haraldsson et al. (1997)).

b) The main problem with Gran functions is, that they are not perfectly linear amongst others due to dilution effects during the titration (see Fig. (A.1), top). Using a large sample volume and a small volume of highly concentrated titrant eases this problem (see Fig. (A.1), center) but it can be overcome by introducing *modified Gran functions* according to Hansson and Jagner (1973) that take into account volume changes during titration. Due to other reactions and not totally completed main reactions, as well as uncertainties in the electrode standard potential E_0, this modified Gran approach is still not completely accurate. Out of this reason Hansson and Jagner (1973) employed an iterative scheme to obtain sensible values for TA and E_0 (and DIC as Gran function F0 is not used).

c) Furthermore, there is the possibility to obtain the position of the equivalence points, and thus v_1 and v_2, in a mathematical graphical manner. One can record the titration curve, fit a polynomial function through it, and find maxima in the first derivative of this function to localize the equivalence points (see Fig. (A.1), bottom). This can be done visually or by finding the roots of the second derivative of the fitted function. This approach which is inspired by classical analytical chemical methods (Skoog and West, 1982) has the advantage that no mechanistic model for the seawater system is needed and the effects of all minor species are included in the determination of the positions of the equivalence points. However, if the compositon of the sample deviates from the composition of standard seawater to such an extend that the classical two equivalence points cannot be identified, this method is bound to fail.

3. However, there is also a method that does not depend on the specific form of the titration curve (i.e. the position of the equivalence points) but considers the whole titration curve. One can build a mechanistic chemical model of the sample solution, and generate theoretical titration curves with arbitrary values for TA, DIC, and E_0 (if an electrode potential curve is used). In an iterative least-squares procedure, those arbitrary values can be refined to the true values. Due to uncertainties in the first dissociation constant of the carbonate system $K^*_{CO_2}$, it sometimes is advised to fit this dissociation constant in the iterative least-squares procedure as well. All other dissociation constants are calculated from salinity, temperature and pressure. This curve fitting procedure was introduced by Dickson (1981), restated in DOE (1994) and mentioned in Anderson et al. (1999) and Zeebe and Wolf-Gladrow (2001). Dickson et al. (2007) employ a derivative of this method.

   Out of computational reasons, Johansson and Wedborg (1982) and Anderson et al. (1999) suggested to switch the dependent and independent variables, i.e. to calculate a theoretical vector of titrant masses instead of a vector of theoretical pH or E values while calculating the theoretical titration curve. This has the advantage that one does not need to solve a non linear equation system for the pH at every point of every theoretical titration. However, due to the fact that in curve-fitting algorithms the sum of squares in the dependent variable only is minimized, Anderson et al. (1999) conclude that in principle the (experimentally determined) E (or pH) values would be the best choice as dependent variable.

Since in recent years computational power is not limiting anymore, we follow the conclusion of Anderson et al. (1999) and implemented the `TAfit` function of our R package AquaEnv (see above) such that a theoretical titration curve (pH or E as dependent variable) is calculated using the function `titration` and TA, DIC, E_0 (if an E curve is provided), and optionally $K^*_{CO_2}$ are obtained by iterative least squares fitting using the Levenberg-Marquard algorithm as implemented by Elzhov and Mullen (2008) in the R package minpack.lm.

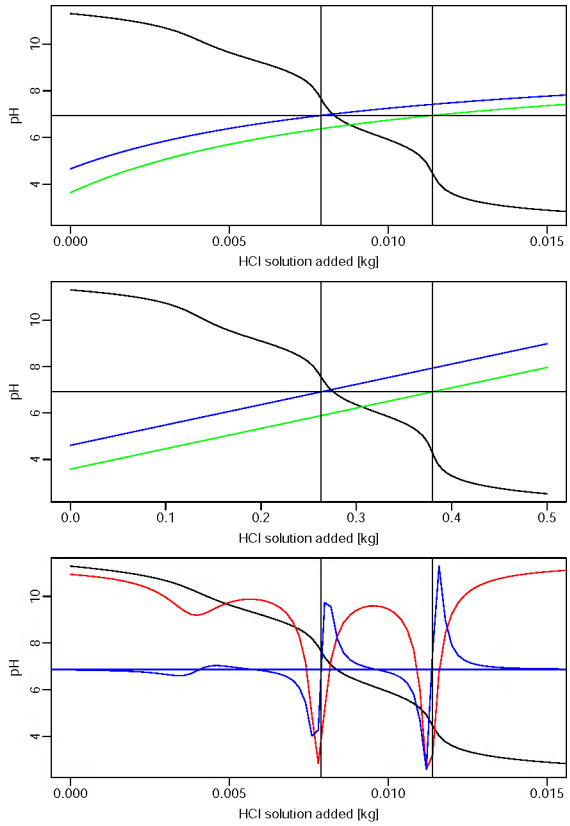

Figure A.1.: Titration curve of standard seawater and its equivalence points. Top: titration with a small sample volume and a large titrant volume of low concentration, Gran functions F0 and F2 (axis not plotted, the horizontal line signifies the zero level); Center: titration with a larger sample volume and a small volume of titrant with high concentration, Gran functions F0 and F2 (axis not plotted, the horizontal line signifies the zero level); Bottom: same titration as on the top, first and second derivative of the curve (axis not plotted). Note that these plots are produced using the `titration` function of the R package AquaEnv. The code that produces these graphs can be found in the vignette of AquaEnv.

B. Curriculum Vitae

First name: Andreas
Middle name: Felix
Last name: Hofmann

Address: Violenlaan 2
4401 HR Yerseke
The Netherlands
Cellular Phone: 0031 6 651974359
E-Mail: a.hofmann@nioo.knaw.nl

Date of birth: 1978 / 09 / 14
Place of birth: Würzburg, Germany
Nationality: German
Marital status: engaged, expecting a child

Webpage: http://www.nioo.knaw.nl/ppages/ahofmann/

Education:

2005/05 - 2009/04:	PhD project at the Netherlands Institute of Ecology
2002/04 - 2005/04:	≈ MSc (German degree: Diplom) in Bioinformatics / Computational Biology at Saarland University, Saarbruecken, Germany (thesis)
1999/11 - 2002/03:	≈ BSc (German degree: Vordiplom) in Biology at Regensburg University, Regensburg, Germany

Peer reviewed publications:

A. F. Hofmann, K. Soetaert, J. J. Middelburg:
Present nitrogen and carbon dynamics in the Scheldt estuary using a novel 1-D model
(Biogeosciences 5, 981-1006, 2008)

A. F. Hofmann, F. J. R. Meysman, K. Soetaert, J. J. Middelburg:
A step-by-step procedure for pH model construction in aquatic systems
(Biogeosciences 5, 227-251, 2008)

K. Soetaert, A. F. Hofmann, J. J. Middelburg, F. J.R. Meysman, J. Greenwood
The effect of biogeochemical processes on pH
(Marine Chemistry 105, 30-51 (reprint: 106, 380-401), 2007)

H. Toll, P. Berger, A. Hofmann, A. Hildebrandt, H. Oberacher, H. P. Lenhof, C. G. Huber
Glycosylation patterns of human chorionic gonadotropin revealed by liquid chromatography–mass spectrometry and bioinformatics
(ELECTROPHORESIS 27, 2734-2746, 2006)

Peer reviews:
A. F. Hofmann
Interactive comment on "Enhanced ocean carbon storage from anaerobic alkalinity generation in coastal sediments" by H. Thomas et al.
(Biogeosciences Discussion 5: S1955-S1962, 2008)

Publications in review:
A. F. Hofmann, F. J. R. Meysman, K. Soeatert, J. J. Middelburg
Factors governing the pH in a heterotrophic, turbid, tidal estuary
(Biogeosciences Discussion, 6, 197-240, 2009)

Submitted publications:
A. F. Hofmann, J.J. Middelburg, K. Soetaert, D. A. Wolf-Gladrow, F. J. R. Meysman
Buffering, stoichiometry, and the sensitivity of pH to biogeochemical and physical processes: a proton-based model perspective
(submitted to Geochimica et Cosmochimica Acta)

A. F. Hofmann, K. Soetaert, J.J. Middelburg, F. J. R. Meysman
AquaEnv - an Aquatic acid-base modelling Environment in R
(submitted to Aquatic Geochemistry; the R package can be found on R-Forge[1] and on CRAN[2])

Publications in preparation:
F. Gazeau, A.R. Nzigou, H. Wood, A.F. Hofmann, J.P. Gattuso, J.J. Middelburg, C. Heip.
Impacts of ocean acidification on the blue mussel, critical assessment of the alkalinity anomaly method
(in preparation)

P. M. J. Herman, A. F. Hofmann, et al.
The spring pH peak in the Wadden sea as a proxy for primary production activity
(working title; in preparation)

PhD courses:

2006/11:	Writing a Scientific Article, in Yerseke, The Netherlands
2006/06:	CARBOOCEAN Modelling Summer School, in Bergen, Norway
2006/05:	Estuarine Ecology, in Yerseke, The Netherlands
2006/03:	Goal Oriented Working and Planning, in Utrecht, The Netherlands
2006/02:	Inverse Problems, in Utrecht, The Netherlands
2005/08:	Aquatic Microbial and Molecular Ecology, in Odense, Denmark

[1] http://r-forge.r-project.org/projects/aquaenv/
[2] http://cran.r-project.org/

Scientific meetings:

2008/06:	AMEMR Symposium 2008 in Plymouth, UK (poster)
2008/05:	10th International Estuarine Biogeochemistry Symposium in Xiamen, China (presentation)
2008/03:	ASLO Ocean Science meeting in Orlando, Florida (USA) (presentation)
2007/12:	3rd annual CARBOOCEAN meeting in Bremen, Germany (at this meeting I presented a poster, gave an oral presentation, and organized a PhD panel session)
2007/02:	NIOO dagen 2007 in Lunteren, The Netherlands
2006/12:	2nd annual CARBOOCEAN meeting on Gran Canaria, Spain
2006/05:	9th International Estuarine Biogeochemistry Symposium in Warnemuende, Germany (poster)
2006/02:	NIOO dagen 2006 in Lunteren, The Netherlands (presentation)
2005/11:	1st annual CARBOOCEAN meeting in Amsterdam, The Netherlands (poster)

Further Qualifications:

2006/09 - 2006/11:	Dutch recreative boat driver's license for inland and coast waters
2005/10 - 2007/05:	Dutch language classes (with examinations and certificate)
1998/06 - 2003/08:	Scuba diving training with examination up to CMAS **
1998/10 - 1999/03:	Bavarian state examination for sports fishers
1998/09 - 1999/09:	German community service: working full-time as an assistant paramedic (with training and examinations)
1994/08 - 1996/08:	driver's licenses for cars, motorbikes and trucks up to 7.5 tons

Interests:

traveling, sports (running, mountainbiking, scuba diving, snowboarding, skiing, hiking, windsurfing, kitesurfing, wakeboarding), engine rebuilding, boating, motorcycling, beer brewing, cooking, fishing

Languages:

German:	native tongue
English:	fluent (written and spoken)
Dutch:	fluent (written and spoken)
French:	good command
Italian:	basic command
Latin	
Spanish	

Yerseke, April 10, 2009 

(Additional information on my personal page: http://www.nioo.knaw.nl/ppages/ahofmann/)

C. The cover: Markus-Lyapunov fractal "Zircon Zity"

Thesis covers are as variable as theses themselves. Some people go for a plainly coloured background, while others prefer photographs of their favourite sample locations or fancy, colourful designs. Although a seemingly unimportant detail, I always wanted the cover of my thesis to mean something, and that is, more than just depicting the ecosystem I applied my models to. However, finding a cover for my thesis that means something while not being a photograph of the Scheldt estuary, was not straightforward. Visualizing pH and pH modelling also seemed not to be very promising, especially since I exhaustively explored ways of cumulative plotting of influences of kinetic processes on pH for various of my papers. I wanted my thesis cover to look stunning - and those cumulative plots definitively were not. Fortunately, while surfing the internet not long ago, I came across this website: http://en.wikipedia.org/wiki/Lyapunov_fractal. I was always a fan of fractals, in secondary school I even wrote several programs in Pascal to explore the Mandelbrot and Julia sets. It is just amazing what beauty, precision and detail there is in fractals - all generated by a simple algorithm, not man-made, already there, just discovered, the hidden beauty of nature. A hint of something more than our small physical world maybe? When I then saw those Markus-Lyapunov fractals I was instantly in love. And the best thing: they are derived from the logistic growth function which is also used in ecological modelling! The Lyapunov-exponent can there describe the degree of chaotic behaviour in the population size of organisms that grow with two different growth rates at different times. It is a fractal flowing forth from not exactly what I did for my thesis, but from something close to it! That highly intrigued me! Of course I could have downloaded "Zircon Zity", the already "discovered" picture that I liked the most from Wikipedia, but that seemed too easy to me. So I embarked on another challenge. A lot of the work for my thesis was done in the interpreted, open-source, statistical programming language R. While R has great capabilities for statistical analysis of data, visualization of the results of those analyses, as well as plotting capabilities of all kinds, it is not very well suited for extensive and lengthy calculations and the creation of pixel images as needed for fractal generation. Nevertheless, I wanted to recalculate a slightly extended "Zircon Zity" with R, so I translated the algorithm to generate Markus-Lyapunov fractals

define a sequence s of A, B and concatenate it N times to form sequence s', where N needs to be sufficiently large.

define intervals a, b $\subset$ [0,4]

sample the space a $\times$ b with sufficient resolution: calculate $\forall$ (a',b') $\in$ a $\times$ b

- let $x_0 = 0.5$
- calculate $\forall$ $s_i \in$ s'
  - r_i = a' if s_i == A and r_i = b' if s_i == B
  - $x_{i+1} = r_i\ x_i\ (1 - x_i)$
- $\lambda = (\sum_i (\log |r_i\ (1 - 2\ x_i)|)) /$ length of s'
- choose color c(a',b') for the point (a',b') according to the value of λ

into the R script

```
s <- c(2,2,2,2,2,2,1,1,1,1,1,1)

a <- seq(3.3, 4.0, 0.00025); lena <- length(a)
b <- seq(2.4, 3.5, 0.00025); lenb <- length(b)

n <- 125

lambda <- matrix(nrow=lenb, ncol=lena)
for (v in 1:lenb)
  {
    print(paste(v, "of", lenb))
    for (w in 1:lena)
      {
        x <- 0.5
        sld <- 0
        for (i in 1:n)
          {
            expsld <- 1
            for (st in s)
              {
                r <- c(a[[w]],b[[v]])[[st]]
                if (i>1) {expsld <- expsld*r*(1-2*x)}
                x <- r*x*(1-x)
              }
            sld <- sld + log(abs(expsld))
          }
        lambda[v,w] <- sld/(n*length(s))
      }
    }

write(lambda)
jpeg(filename="ZirconZity.jpg", width=lenb, height=lena, quality=100)
par(mar=c(0,0,0,0), oma=c(0,0,0,0))
image(z=lambda, col=rainbow(100000, start=1/6, end=4/6))
dev.off()
```

which ran for about four days on the computer in my office and resulted in this thesis's cover.

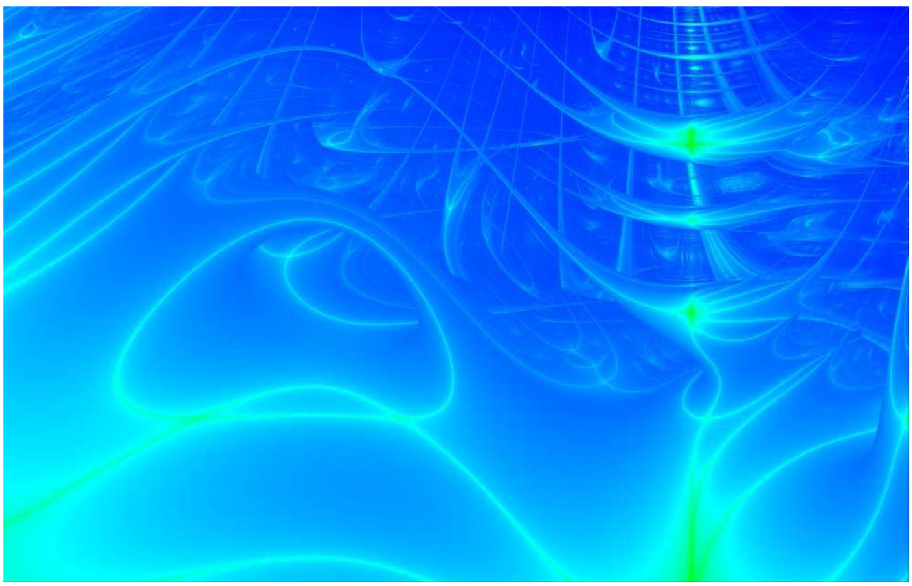

Tom and Johan, thanks for bearing the fan noise while I was on vacation ☺.

D. List of Figures

E. List of Tables

F. References

Abril, G., Etcheber, H., Borges, A. V., and Frankignoulle, M.: Excess atmospheric carbon dioxide transported by rivers into the Scheldt estuary, Comptes Rendus De L Academie Des Sciences Serie Ii Fascicule a-Sciences De La Terre Et Des Planetes, 330, 761–768, 2000. 2.4.4.2

Alley, R., Berntsen, T., Bindoff, N. L., and al., e.: Climate Change 2007: The Physical Science Basis - Summary for Policymakers (WGI contribution), Tech. rep., Geneva, 2007. 3.1

Aloisi, G.: The calcium carbonate saturation state in cyanobacterial mats throughout Earth's history, Geochimica et Cosmochimica Acta, 72, 6037–6060, 2008. 6.1

Anderson, L. G., Turner, D. R., Wedborg, M., and Dyrssen, D.: Determination of total alkalinity and total dissolved inorganic carbon, in: Methods of Seawater Analysis, edited by Grasshoff, K., Gremling, K., and Ehrhardt, M., Wiley-VCH, 1999. 3, 6.1, 6.4.3, 1, 3

Andersson, M. G. I.: Nitrogen cycling in a turbid, tidal estuary, Ph.D. thesis, Universiteit Utrecht, 2007. 2.4.1.1

Andersson, M. G. I., Brion, N., and Middelburg, J. J.: Comparison of nitrifier activity versus growth in the Scheldt estuary - a turbid, tidal estuary in northern Europe, Aquatic Microbial Ecology, 42, 149–158, 2006. 2.2.2.1, 2.2.2.9, 2.3.2, 2.5, 2.4.1, 3.1, 3.3.1, 3.14, D, E

Archer, D.: Upper Ocean Physics as Relevant to Ecosystem Dynamics - a Tutorial, Ecological Applications, 5, 724–739, 1995. 5.5

Archer, D.: Modeling CO_2 in the Ocean: a review, in: Scaling of Trace Gas Fluxes between Terrestrial and Aquatic Ecosystems and the Atmosphere, edited by Bouwman, A. F., vol. 24, pp. 169–184, Elsevier Sciences, Amsterdam, 1999. 5.5

Archer, D., Kheshgi, H., and Maier-Reimer, E.: Dynamics of fossil fuel CO_2 neutralization by marine $CaCO_3$, Global Biogeochemical Cycles, 12, 259–276, 1998. 5.5

Aris, R. and Mah, R. H. S.: Independence of Chemical Reactions, Industrial & Engineering Chemistry Fundamentals, 2, 90–&, 1963. 3.2.5, 3.2.7, 3.4.2, 5.7.1

Arndt, S., Vanderborght, J. P., and Regnier, P.: Diatom growth response to physical forcing in a macrotidal estuary: Coupling hydrodynamics, sediment transport, and biogeochemistry, Journal of Geophysical Research-Oceans, 112, –, 2007. 2.4.1

Atkins, P. W.: Physikalische Chemie, VCH Weinheim, 2nd edn., 1996. 2.2.2.4, 2.6.1, 6.2, 6.6.3.1.1, 6.6.3.7.1

Banks, R. B. and Herrera, F. F.: Effect of Wind and Rain on Surface Reaeration, Journal of the Environmental Engineering Division-Asce, 103, 489–503, 1977. 2.2.2.4

Ben-Yaakov, S.: A Method for Calculating the in Situ pH of Seawater, Limnology and Oceanography, 15, 326–328, 1970. 1.2, 3.2.9, 4.2.3, 5.2.2, 5.6

Ben-Yaakov, S.: Ph Buffering of Pore Water of Recent Anoxic Marine Sediments, Limnology and Oceanography, 18, 86–94, 1973. 4.1

Biello, D.: Climate Change Science moves from Proof to Prevention, Scientific American, February 1, 2007. 1.1

Billen, G., Somville, M., Debecker, E., and Servais, P.: A Nitrogen Budget of the Scheldt Hydrographical Basin, Netherlands Journal of Sea Research, 19, 223–230, 1985. 2.1, 2.4.4.1, 2.4.4.1

Bjerknes, V. and Tjomsland, T.: Flow and pH modelling to study the effects of liming in regulated, acid salmon rivers, Water Air and Soil Pollution, 130, 1409–1414, 2001. 3.1

Blackford, J. C. and Gilbert, F. J.: pH variability and CO_2 induced acidification in the North Sea, Journal of Marine Systems, 64, 229–241, 2007. 1.1, 4.1, 4.4.1, 5.5, 5.6, 6.1

Borges, A. V., Vanderborght, J. P., Schiettecatte, L. S., Gazeau, F., Ferron-Smith, S., Delille, B., and Frankignoulle, M.: Variability of the gas transfer velocity of CO_2 in a macrotidal estuary (the Scheldt), Estuaries, 27, 593–603, 2004. 2.2.2.4, 3.3.1, 3.14, 6.6.3.1.2, E

Borges, A. V., Schiettecatte, L. S., Abril, G., Delille, B., and Gazeau, E.: Carbon dioxide in European coastal waters, Estuarine Coastal and Shelf Science, 70, 375–387, 2006. 1.3, 2.1, 2.4.4.2, 2

Boudreau, B. P.: A Steady-State Diagenetic Model for Dissolved Carbonate Species and Ph in the Porewaters of Oxic and Suboxic Sediments, Geochimica Et Cosmochimica Acta, 51, 1985–1996, 1987. 3.2.8, 3.4.2, 3.4.3

Boudreau, B. P.: Modelling the sulfide-oxygen reaction and associated pH gradients in porewaters, Geochimica et Cosmochimica Acta, 55, 145–159, 1991. 3.2.8, 3.4.2, 3.4.3

Boudreau, B. P.: Diagenetic Models and Their Implementation, Springer, 1996a. 1.2, 3.2.4, 5.1, 5.7.3, 6.2, 6.6.3.1.1, 6.8

Boudreau, B. P.: A method-of-lines code for carbon and nutrient diagenesis in aquatic sediments, Computers & Geosciences, 22, 479–496, 1996b. 3.4.2, 3.4.3

Boudreau, B. P. and Canfield, D. E.: A Provisional Diagenetic Model for Ph in Anoxic Porewaters - Application to the Foam Site, Journal of Marine Research, 46, 429–455, 1988. 3.2.8, 3.4.2, 3.4.3, 4.1

Boudreau, B. P. and Canfield, D. E.: A Comparison of Closed-System and Open-System Models for Porewater Ph and Calcite-Saturation State, Geochimica Et Cosmochimica Acta, 57, 317–334, 1993. 3.2.8, 3.4.2, 3.4.3

Brewer, P. G. and Barry, J.: Rising Acidity in the Ocean: The Other CO_2 problem, Scientific American Earth 3.0, October 2008, 2008. 1.1

Caldeira, K. and Wickett, M. E.: Anthropogenic carbon and ocean pH, Nature, 425, 365–365, 2003. 1.1, 5.5, 5.6, 6.1

Caldeira, K. and Wickett, M. E.: Ocean model predictions of chemistry changes from carbon dioxide emissions to the atmosphere and ocean, Journal of Geophysical Research-Oceans, 110, –, 2005. 1.1, 5.5, 5.6, 6.1

Canfield, D., Thamdrup, B., and Kristensen, E.: Aquatic Geomicrobiology, Elsevier Academic Press, Advances in Marine Biology, Volume 48, 2005. 2.2.2.1, 2.2.2.1

Chilakapati, A., Ginn, T., and Szecsody, J.: An analysis of complex reaction networks in groundwater modeling, Water Resources Research, 34, 1767–1780, 1998. 3.2.4, 3.2.7, 3.4.2

Clark, J. F., Schlosser, P., Simpson, H. J., Stute, M., Wanninkhof, R., and Ho, D. T.: Relationship between Gas Transfer Velocities and Wind Speeds in The Tidal Hudson River Determined by the Dual Tracer Technique, in: Air-Water Gas Transfer, edited by Jaehne, B. and Monahan, E., pp. 785–800, AEON Verlag, 1995. 2.2.2.4

Cloern, J. E.: Our evolving conceptual model of the coastal eutrophication problem, Marine Ecology-Progress Series, 210, 223–253, 2001. 2.1

Culberson, C. H.: Calculation of the Insitu Ph of Seawater, Limnology and Oceanography, 25, 150–152, 1980. 1.2, 3.2.9, 4.2.3, 5.2.2, 5.6

Davis, C.: Ocean Acidification, The Other Threat of Rising CO_2 Emissions, World Resources Institute: Earth Trends - Environmental Information, September 2007 Monthly Update, http://earthtrends.wri.org/updates/node/245, 2007. 1.1

de Bie, M. J. M., Speksnijder, A. G. C. L., Kowalchuk, G. A., Schuurman, T., Zwart, G., Stephen, J. R., Diekmann, O. E., and Laanbroek, H. J.: Shifts in the dominant populations of ammonia-oxidizing beta-subclass Proteobacteria along the eutrophic Schelde estuary, Aquatic Microbial Ecology, 23, 225–236, 2001. 2.2.2.1

Dickson, A. G.: An Exact Definition of Total Alkalinity and a Procedure for the Estimation of Alkalinity and Total Inorganic Carbon from Titration Data, Deep-Sea Research Part a-Oceanographic Research Papers, 28, 609–623, 1981. 2.2.2.10, 3.2.8, 3.4.2, 3.4.3, 3.6.2, 4.2.4, 5.1, 5.2.2, 3, 5.4.2, 6.1, 6.3.3, 6.4.3, 2, 2a, 2a, 2c, 2c, 3, E

Dickson, A. G.: pH Scales and Proton-Transfer Reactions in Saline Media Such as Sea-Water, Geochimica Et Cosmochimica Acta, 48, 2299–2308, 1984. 2.2.2.7, 3.2.3, 4.2.2, 4.2.5, 4.6.1.2, 6.3.3, 6.2, 6.6.3.10

Dickson, A. G.: Thermodynamics of the Dissociation of Boric-Acid in Synthetic Seawater from 273.15-K to 318.15-K, Deep-Sea Research Part a-Oceanographic Research Papers, 37, 755–766, 1990a. 2.3, 6.2, 6.6, E

Dickson, A. G.: Standard Potential of the Reaction - AgCl(S)+1/2h-2(G)=Ag(S)+HCl(Aq) and the Standard Acidity Constant of the Ion HSO_4^- in Synthetic Sea-Water from 273.15-K to 318.15-K, Journal of Chemical Thermodynamics, 22, 113–127, 1990b. 2.3, 6.2, 6.4, E

Dickson, A. G. and Millero, F. J.: A Comparison of the Equilibrium-Constants for the Dissociation of Carbonic-Acid in Seawater Media, Deep-Sea Research Part a-Oceanographic Research Papers, 34, 1733–1743, 1987. 6.2, 6.4

Dickson, A. G. and Riley, J. P.: Estimation of Acid Dissociation-Constants in Seawater Media from Potentiometric Titrations with Strong Base .1. Ionic Product of Water - Kw, Marine Chemistry, 7, 89–99, 1979a. 2.3, 6.2, 6.4, 6.6.3.10, E

Dickson, A. G. and Riley, J. P.: Estimation of Acid Dissociation-Constants in Seawater Media from Potentiometric Titrations with Strong Base .2. Dissociation of Phosphoric-Acid, Marine Chemistry, 7, 101–109, 1979b. 6.2, 6.6, 6.7

Dickson, A. G., Sabine, C., and Christian, J. R.: Guide to best practices for ocean CO_2 measurements, PICES special publications, pp. 1–191, 2007. 3, 5.4, 6.1, 6.3.2, 6.1, 6.4.3, 1, 6.6.3.1.1, 6.6.3.1.3, 6.6.3.1.4, 6.6.3.3, 6.6.3.5, 6.3, 6.4, 6.5, 6.6, 6.7, 3, D, E

DiToro, D. M.: Combining Chemical Equilibrium and Phytoplankton Models - A General Methodology, in: Modelling Biochemical Processes on Aquatic Ecosystems, edited by Canale, R. P., pp. 233–255, Ann Arbor Science, 1976. 3.2.5, 3.2.7, 3.2.8, 3.4.2, 3.4.3, 5.7.1

DOE: Handbook of Methods for the Analysis of the Various Parameters of the Carbon Dioxide System in Sea Water, ORNL/CDIAC-74, 1994. 2.2.2.10, 2.6.2, 3.2.2, 3.2, 3, 5.2.2, 5.4, 6.1, 6.3.2, 6.4.3, 6.2, 6.6.3.1.3, 6.6.3.1.4, 6.6.3.2, 6.6.3.3, 6.6.3.4, 6.6.3.6, 6.3, 6.4, 6.5, 6.6, 6.7, 6.6.3.10, 3, E

Doney, S. C.: The Dangers of Ocean Acidification, Scientic American, March 2006, 58–65, 2006. 1.1

Doney, S. C., Mahowald, N., Lima, I., Feely, R. A., Mackenzie, F. T., Lamarque, J.-F., and Rasch, P. J.: Impact of anthropogenic atmospheric nitrogen and sulfur deposition on ocean acidification and the inorganic carbon system 10.1073/pnas.0702218104, Proceedings of the National Academy of Sciences, 104, 14 580–14 585, 2007. 1.1, 5.5, 5.6, 6.1

Doney, S. C., Fabry, V. J., Feely, R. A., and Kleypas, J. A.: Ocean Acidification: The Other CO_2 Problem, Annual Review of Marine Science, 1, 169 LP – 192, 2009. 1.1, 6.1

Duce, R. A., LaRoche, J., Altieri, K., Arrigo, K. R., Baker, A. R., Capone, D. G., Cornell, S., Dentener, F., Galloway, J., Ganeshram, R. S., Geider, R. J., Jickells, T., Kuypers, M. M., Langlois, R., Liss, P. S., Liu, S. M., Middelburg, J. J., Moore, C. M., Nickovic, S., Oschlies, A., Pedersen, T., Prospero, J., Schlitzer, R., Seitzinger, S., Sorensen, L. L., Uematsu, M., Ulloa, O., Voss, M., Ward, B., and Zamora, L.: Impacts of atmospheric anthropogenic nitrogen on the open ocean, Science, 320, 893–897, 2008. 5.5, 5.6

Durst, R.: Standard Reference Materials: Standardisation of pH Measurements, NBS Special Publications, 260-53, 1975. 2.2.2.7, 6.3.3, 6.2, 6.6.3.10

Dyrssen, D. and Sillen, L. G.: Alkalinity and Total Carbonate in Sea Water . A Plea for P-T-Independent Data, Tellus, 19, 113–, 1967. 2c

Elzhov, T. V. and Mullen, K. M.: minpack.lm: R interface to the Levenberg-Marquardt nonlinear least-squares algorithm found in the MINPACK Fortran library, `http://cran.r-project.org/web/packages/minpack.lm/index.html`, r package version 1.1-1, 2008. 6.4.3, 3

EUR-OCEANS: Ocean Acidification - the other half of the CO_2 problem, EUR-OCEANS Knowledge Transfer Unit Fact Sheet 7 (May 2007), 2007. 1.1

Fabian, G., Van Beek, D. A., and Rooda, J. E.: Index Reduction and Discontinuity Handling Using Substitute Equations, Mathematical and Computer Modelling of Dynamical Systems, 7, 173–187, 2001. 3.2.4, 3.2.6

Feistel, R.: A Gibbs function for seawater thermodynamics for-6 to 80 degrees C and salinity up to 120 g kg(-1), Deep-Sea Research Part I-Oceanographic Research Papers, 55, 1639–1671, 2008. 6.3.1, 6.1, 6.2, 6.6.3.5, 6.6.3.9

Fofonoff, N. P. and Millard, R. C. J.: Algorithms for computation of fundamental properties of seawater, Unesco technical papers in marine science, 44, 55 pp, 1983. 6.2, 6.6.3.5, 6.6.3.5

Follows, M. J., Williams, R. G., and Marshall, J. C.: The solubility pump of carbon in the subtropical gyre of the North Atlantic, Journal of Marine Research, 54, 605–630, 1996. 3.4.2, 3.4.3

Follows, M. J., Ito, T., and Dutkiewicz, S.: On the solution of the carbonate chemistry system in ocean biogeochemistry models, Ocean Modelling, 12, 290–301, 2006. 2.2.2.7, 3.2.9, 3.2.9, 3.2.10, 3.4.2, 3.4.3, 4.2.3, 5.1, 5.2.2, 5.6, 6.3.4, 6.4.1

Frankignoulle, M.: A Complete Set of Buffer Factors for Acid-Base Co2 System in Seawater, Journal of Marine Systems, 5, 111–118, 1994. 1.2, 3.2.10, 5.4.2, 5.6, 6.3.5, 7

Frankignoulle, M., Abril, G., Borges, A., Bourge, I., Canon, C., DeLille, B., Libert, E., and Theate, J. M.: Carbon dioxide emission from European estuaries, Science, 282, 434–436, 1998. 1.3, 2.1, 2.1, 2.4.4.1, 2.4.4.2, 2.4.4.2

Froelich, P. N., Klinkhammer, G. P., Bender, M. L., Luedtke, N. A., Heath, G. R., Cullen, D., Dauphin, P., Hammond, D., Hartman, B., and Maynard, V.: Early Oxidation of Organic-Matter in Pelagic Sediments of the Eastern Equatorial Atlantic - Suboxic Diagenesis, Geochimica Et Cosmochimica Acta, 43, 1075–1090, 1979. 2.2.2.1, 2.2.2.1

Garcia, H. E. and Gordon, L. I.: Oxygen Solubility in Seawater - Better Fitting Equations, Limnology and Oceanography, 37, 1307–1312, 1992. 3.3.1

Gazeau, F., Gattuso, J. P., Middelburg, J. J., Brion, N., Schiettecatte, L. S., Frankignoulle, M., and Borges, A. V.: Planktonic and whole system metabolism in a nutrient-rich estuary (the Scheldt estuary), Estuaries, 28, 868–883, 2005. 2.1, 2.2.2.1, 2.2.2.9, 2.4, 2.4.3, 2.4.4.1, D

Gazeau, F., Quiblier, C., Jansen, J. M., Gattuso, J. P., Middelburg, J. J., and Heip, C. H. R.: Impact of elevated CO_2 on shellfish calcification, Geophysical Research Letters, 34, 2007. 1.1, 4.1, 5.1, 5.6, 6.1

Gehlen, M., Mucci, A., and Boudreau, B.: Modelling the distribution of stable carbon isotopes in porewaters of deep-sea sediments, Geochimica Et Cosmochimica Acta, 63, 2763–2773, 1999. 3.4.2, 5.1

Gran, G.: Determination of the Equivalence Point in Potentiometric Titrations .2., Analyst, 77, 661–671, 1952. 3, 2a

Guinotte, J. M. and Fabry, V. J.: Ocean acidification and its potential effects on marine ecosystems, Year in Ecology and Conservation Biology 2008, 1134, 320–342, 2008. 1.1, 4.1, 5.1, 5.2.2, 5.5, 5.4, 5.6, 6.1, 6.6.3.1.2, D

Gurney, W. S. C. and Nisbet, R. M.: Ecological Dynamics, Oxford University Press, 1998. 2.2.2.1

Hansson, I. and Jagner, D.: Evaluation of Accuracy of Gran Plots by Means of Computer Calculations - Application to Potentiometric Titration of Total Alkalinity and Carbonate Content in Sea-Water, Analytica Chimica Acta, 65, 363–373, 1973. 3, 2, 2b

Haraldsson, C., Anderson, L. G., Hassellov, M., Hulth, S., and Olsson, K.: Rapid, high-precision potentiometric titration of alkalinity in ocean and sediment pore waters, Deep-Sea Research Part I-Oceanographic Research Papers, 44, 2031–2044, 1997. 2a

Harned, H. S. and Davis, R.: The Ionization Constant of Carbonic Acid in Water and the Solubility of Carbon Dioxide in Water and Aqueous Salt Solutions from 0 to 50 deg C, Journal of the American Chemical Society, 65, 2030–2037, 1943. 6.2, 6.5

Harned, H. S. and Scholes, S. R.: The Ionization Constant of HCO_3^- from 0 to 50 deg C, Journal of the American Chemical Society, 63, 1706–1709, 1941. 6.2, 6.5

Heip, C.: Biota and Abiotic Environment in the Westerschelde Estuary, Hydrobiological Bulletin, 22, 31–34, 1988. 1.3, 2.2.1, 3.3.1, 4.2.1

Helder, W. and Devries, R. T. P.: Estuarine Nitrite Maxima and Nitrifying Bacteria (Ems-Dollard Estuary), Netherlands Journal of Sea Research, 17, 1–18, 1983. 2.2.2.1

Hellings, L., Dehairs, F., Van Damme, S., and Baeyens, W.: Dissolved inorganic carbon in a highly polluted estuary (the Scheldt), Limnology and Oceanography, 46, 1406–1414, 2001. 2.1, 2.4.4.1, 2.4.4.2, 3.3.1, 3.14, E

Henderson, C.: Ocean acidification: the other CO_2 problem, New Scientist, 2563, 05 August 2006, 2006. 1.1

Hester, K. C., Peltzer, E. T., Kirkwood, W. J., and Brewer, P. G.: Unanticipated consequences of ocean acidification: A noisier ocean at lower pH, Geophysical Research Letters, 35, –, 2008. 1.1, 7

Hofmann, A., Meysman, F., Soetaert, K., and Middelburg, J.: Factors governing the pH in a heterotrophic, turbid, tidal estuary, Biogeosciences Discussion, 6, 197–240, 2009a. 5.2.3, 5.7.3, 6.1, 6.1, 6.3.5, 6.3.5, 6.3.5, 6.3.5, 6.2, 6.6.3.13

Hofmann, A. F., Meysman, F. J. R., Soetaert, K., and Middelburg, J. J.: A step-by-step procedure for pH model construction in aquatic systems, Biogeosciences J1 - BG, 5, 227–251, 2008a. 2.2.2.2, 2.2.2.6, 2.2.2.7, 2.3.4, 4.1, 1, 4.2.2, 4.2.3, 4.2.4, 4.2.4, 4.2.5, 5.1, 5.2.2, 5.2, 5.2.2, 5.2.3, 5.7.3, 5.7.4, 6.1, 6.1, 6.3.5, 6.3.5, 6.4.1, 6.2, 6.6.3.13, E

Hofmann, A. F., Soetaert, K., and Meysman, F. J. R.: AquaEnv - Aquatic modelling Environment in R,
http://r-forge.r-project.org/projects/aquaenv/, 2008b. 4

Hofmann, A. F., Soetaert, K., and Middelburg, J. J.: Present nitrogen and carbon dynamics in the Scheldt estuary using a novel 1-D model, Biogeosciences J1 - BG, 5, 981–1006, 2008c. 4.1, 4.1, 4.2.2, 4.2.2, 4.2.3, 4.2.4, 4.2, 4.2.7.1, 4.2.7.2, 4.3, 4.4.1, 4.4.2, D, E

Hofmann, A. F., Middelburg, J., Soetaert, K., Wolf-Gladrow, D. A., and Meysman, F.: Buffering, stoichiometry and the sensitivity of pH to biogeochemical and physical processes: a proton-based model perspective, submitted to Geochimica et Cosmochimica Acta, 2009b. 6.1, 6.3.5, 6.3.5, 6.4.1, 6.4.1, 6.4.1, 6.2

Holland, A.: The waste loads on the Scheldt estuary (1980 - 1988), Tidal Waters Division, Middelburg, The Netherlands, 1991. 2.2.2.11

IPCC: Emission Scenarios, Summary for Policymakers, A Special Report of IPCC Working Group III, 2000. 7.1, D

IPCC: Climate Change 2007: Synthesis Report. Contributions of Working Groups I, II, and III to the Fourth Assessment Report of the Intergovernmental Panel on Climate Change, Tech. rep., Geneva, Switzerland, 2007. 1.1, 5.1, 5.5, 5.4, 6.1, D

Johansson, O. and Wedborg, M.: On the Evaluation of Potentiometric Titrations of Sea-Water with Hydrochloric-Acid, Oceanologica Acta, 5, 209–218, 1982. 6.4.3, 3

Jorgensen, B. B.: Processes at the Sediment - Water Interface, in: The Major Biogeochemical Cycles and Their Interactions, edited by Bolin, B. and Cook, R. B., pp. 477–509, SCOPE, 1983. 2.2.2.1

Jourabchi, P., Van Cappellen, P., and Regnier, P.: Quantitative interpretation of pH distributions in aquatic sediments: A reaction-transport modeling approach, American Journal of Science, 305, 919–956, 2005. 3.1, 3.2.3, 3.2.8, 3.2.10, 3.4.2, 3.4.4, 4.1, 5.1, 6.1

Kleypas, J. A., Feely, R. A., Fabry, V. J., Langdon, C., Sabine, C. L., and Robbins, L. L.: Impacts of Ocean Acidification on Coral Reefs and Other Marine Calcifiers: A Guide for Future Research, report of a workshop held 18-20 April 2005, St. Petersburg, FL, sponsored by NSF, NOAA, and the U.S. Geological Survey, Tech. rep., 2006. 1.1, 5.1, 5.6

Kremer, J. N., Reischauer, A., and D'Avanzo, C.: Estuary-specific variation in the air-water gas exchange coefficient for oxygen, Estuaries, 26, 829–836, 2003. 2.2.2.4

Kremling, K.: Determination of the major constituents, in: Methods of Seawater Analysis, edited by Grasshoff, K., Gremling, K., and Ehrhardt, M., Wiley-VCH, 1999. 2

Kuss, J., Nagel, K., and Schneider, B.: Evidence from the Baltic Sea for an enhanced CO_2 air-sea transfer velocity, Tellus Series B-Chemical and Physical Meteorology, 56, 175–182, 2004. 2.2.2.4

Lavigne, H., Proye, A., Gattuso, J.-P., Epitalon, J.-M., Gentili, B., Orr, J., and Soetaert2, K.: seacarb: Calculates parameters of the seawater carbonate system, `http://www.obs-vlfr.fr/~gattuso/seacarb.php`, R package version 2.0.3, 2008. 6.1, 6.5

Levitus, S., Boyer, T. P., Conkright, M. E., O'Brien, T., Antonov, J., Stephens, C., Stathoplos, L., Johnson, D., and Gelfeld, R.: World Ocean Database 1998, vol.1: Introduction, NOAA NESDIS, Washington, DC., 1998. 5.4, E

Lewis, E. L. and Wallace, D. W. R.: Program Developed for CO_2 System Calculations, 1998. 6.1, 6.1, 6.5, 6.2, 6.6.2, 6.6, 6.6.3.9, 6.6.3.9, 5

Lichtner, P. C.: Continuum formulation of multicomponent-multiphase reactive transport, Reactive Transport in Porous Media, 34, 1–81, 1996. 3.2.7, 3.4.2, 5.2.2

Liss, P. S. and Merlivat, L.: Air-Sea Gas Exchange Rates: Introduction and Synthesis, in: The Role of Air-Sea Exchange in Geochemical Cycling, edited by Buat-Menard, P., pp. 113–127, D. Reidel Publishing Company, 1986. 2.2.2.4

Lueker, T. J., Dickson, A. G., and Keeling, C. D.: Ocean pCO_2 calculated from dissolved inorganic carbon, alkalinity, and equations for K_1 and K_2: validation based on laboratory measurements of CO_2 in gas and seawater at equilibrium, Marine Chemistry, 70, 105–119, 2000. 6.1, 6.2, 6.5, D

Luff, R., Haeckel, M., and Wallmann, K.: Robust and fast FORTRAN and MATLAB (R) libraries to calculate pH distributions in marine systems, Computers & Geosciences, 27, 157–169, 2001. 1.2, 2.2.2.7, 3.1, 3.2.3, 3.2.8, 3.2.9, 3.4.2, 3.4.3, 4.2.3, 5.1, 5.2.2, 5.6, 6.1, 6.4.1

MacIntyre, F.: Toward a minimal model of the world CO2 system. I. Carbonate-alkalinity version, Thalassia Jugoslavica, 14, 63–98, 1978. 5.5

Marinelli, R. L. and Boudreau, B. P.: An experimental and modeling study of pH and related solutes in an irrigated anoxic coastal sediment, Journal of Marine Research, 54, 939–966, 1996. 3.4.2, 5.1

Marshall, T.: Ocean acidification - the other CO_2 problem, Natural Environment Research Council: Planet Earth online - Environmental Research News, 5 January 2009, http://planetearth.nerc.ac.uk/features/story.aspx?id=265, 2009. 1.1

McGillis, W. R., Edson, J. B., Hare, J. E., and Fairall, C. W.: Direct covariance air-sea CO_2 fluxes, Journal of Geophysical Research-Oceans, 106, 16 729–16 745, 2001. 2.2.2.4

Meehl, G. A., Stocker, T. F., Collins, W. D., Friedlingstein, P., Gaye, A. T., Gregory, J. M., Kitoh, A., Knutti, R., Murphy, J. M., Noda, A., Raper, S. C. B., Watterson, I. G., Weaver, A. J., and Zhao, Z.-C.: Global Climate Projections, in: Climate Change 2007: The Physical Science Basis. Contribution of Working Group I to the Fourth Assessment Report of the Intergovernmental Panel on Climate Change, edited by Solomon, S., Qin, D., Manning, M., Chen, Z., Marquis, M., Averyt, K. B., Tignor, M., and Miller, H. L., Cambridge University Press, Cambridge, UK and New York, NY, USA, 2007. 1.1, 7.1, D

Meire, P., Ysebaert, T., Van Damme, S., Van den Bergh, E., Maris, T., and Struyf, E.: The Scheldt estuary: A description of a changing ecosystem, Hydrobiologia, 540, 1–11, 2005. 1.3, 2.2.1, 2.2, 2.2.2.1, 2.3.4, E

Meysman, F.: Modelling the influence of ecological interactions on reactive transport processes in sediments, Ph.D. thesis, Netherlands Institute of Ecology, 2001. 3.2.4, 3.2.7, 3.2.9, 3.2.10, 3.4.2, 5.2.2

Meysman, F. J. R., Middelburg, J. J., Herman, P. M. J., and Heip, C. H. R.: Reactive transport in surface sediments. II. Media: an object-oriented problem-solving environment for early diagenesis, Computers & Geosciences, 29, 301–318, 2003. 3.4.2

Middelburg, J. J. and Nieuwenhuize, J.: Uptake of dissolved inorganic nitrogen in turbid, tidal estuaries, Marine Ecology-Progress Series, 192, 79–88, 2000. 2.4.1

Middelburg, J. J., Klaver, G., Nieuwenhuize, J., Wielemaker, A., deHaas, W., Vlug, T., and vanderNat, J. F. W. A.: Organic matter mineralization in intertidal sediments along an estuarine gradient, Marine Ecology-Progress Series, 132, 157–168, 1996. 3.1, E

Middelburg, J. J., Nieuwenhuize, J., Iversen, N., Hogh, N., De Wilde, H., Helder, W., Seifert, R., and Christof, O.: Methane distribution in European tidal estuaries, Biogeochemistry, 59, 95–119, 2002. 2.2.2.1

Millero, F. J.: Thermodynamics of the Carbonate System in Seawater, Geochimica Et Cosmochimica Acta, 43, 1651–1661, 1979. 6.2, 6.5, 6.6.3.9

Millero, F. J.: The Thermodynamics of Seawater, Part 1. The PVT Properties, Ocean Science and Engineering, 7, 403–460, 1982. 6.2, 6.6.3.4

Millero, F. J.: Thermodynamics of the Carbon-Dioxide System in the Oceans, Geochimica Et Cosmochimica Acta, 59, 661–677, 1995. 2.3, 3.3.1, 6.1, 6.2, 6.6.2, 6.3, 6.4, 6.5, 6.6, 6.7, 6.6.3.9, 6.6.3.9, 4, D, E

Millero, F. J. and Pierrot, D.: A chemical equilibrium model for natural waters, Aquatic Geochemistry, 4, 153–199, 1998. 6.3.3, 6.6.3.11

Millero, F. J. and Poisson, A.: International One-Atmosphere Equation of State of Seawater, Deep-Sea Research Part a-Oceanographic Research Papers, 28, 625–629, 1981. 2.3, 2.2.2.4, 6.2, 6.6.3.6, E

Millero, F. J., Plese, T., and Fernandez, M.: The Dissociation of Hydrogen-Sulfide in Seawater, Limnology and Oceanography, 33, 269–274, 1988. 6.2, 6.6, 6.7

Millero, F. J., Yao, W. S., and Aicher, J.: The Speciation of Fe(II) and Fe(III) in Natural-Waters, Marine Chemistry, 50, 21–39, 1995. 6.2, 6.6

Millero, F. J., Feistel, R., Wright, D. G., and McDougall, T. J.: The composition of Standard Seawater and the definition of the Reference-Composition Salinity Scale, Deep-Sea Research Part I-Oceanographic Research Papers, 55, 50–72, 2008. 6.3.1

Moatar, F., Fessant, F., and Poirel, A.: pH modelling by neural networks. Application of control and validation data series in the Middle Loire river, Ecological Modelling, 120, 141–156, 1999. 3.1

Monismith, S. G., Kimmerer, W., Burau, J. R., and Stacey, M. T.: Structure and flow-induced variability of the subtidal salinity field in northern San Francisco Bay, Journal of Physical Oceanography, 32, 3003–3019, 2002. 2.2.2.5, 2.3.1

Mook, W. G. and Koene, B. K. S.: Chemistry of Dissolved Inorganic Carbon in Estuarine and Coastal Brackish Waters, Estuarine and Coastal Marine Science, 3, 325–336, 1975. 4.1, 4.1, D

Morel, F. M. and Hering, J. G.: Principles and Applications of Aquatic Chemistry, John Wiley & sons, 1993. 1.2, 1.2, 1.2, 3.2.2, 3.2.4, 3.2.4, 3.5, 3.2.6, 3.2.8, 3.11, 3.4.3, 4.1, 5.1, 5.4.2, 5.6, 6.3.5, 7, E

Mucci, A.: The Solubility of Calcite and Aragonite in Seawater at Various Salinities, Temperatures, and One Atmosphere Total Pressure, American Journal of Science, 283, 780–799, 1983. 5.2.2, 6.2, 6.8

Murray, C. N., Riley, J. P., and Wilson, T. R. S.: Solubility of Gases in Distilled Water and Sea Water .I. Nitrogen, Deep-Sea Research, 16, 297–&, 1969. 6.3

MVG: Ministerie van de Vlaamse Gemeenschap - Afdeling Maritieme toegang. 2.2.2.11

Nightingale, P. D., Liss, P. S., and Schlosser, P.: Measurements of air-sea gas transfer during an open ocean algal bloom., Geophysical Research Letters, 27, 2117–2120, 2000. 2.2.2.4

Olander, D. R.: Simultaneous Mass Transfer and Equilibrium Chemical Reaction, Aiche Journal, 6, 233–239, 1960. 3.2.5, 5.7.1

Orr, J. C., Aumont, O., Yool, A., Plattner, G. K., Joos, F., Maier-Reimer, E., Weirig, M. F., Schlitzer, R., Caldeira, K., Wickett, M. E., and Matear, R.: Ocean CO_2 sequestration efficiency from 3-D ocean model comparison, in: Greenhouse Gas Control Technologies, edited by Durie, B., McMullan, P., Paulson, C., and Smith, A., pp. 469–474, 2001a. 5.5

Orr, J. C., Maier-Reimer, E., Mikolajewicz, U., Monfray, P., Sarmiento, J. L., Toggweiler, J. R., Taylor, N. K., Palmer, J., Gruber, N., Sabine, C. L., Le Quere, C., Key, R. M., and Boutin, J.: Estimates of anthropogenic carbon uptake from four three-dimensional global ocean models, Global Biogeochemical Cycles, 15, 43–60, 2001b. 5.5

Orr, J. C., Fabry, V. J., Aumont, O., Bopp, L., Doney, S. C., Feely, R. A., Gnanadesikan, A., Gruber, N., Ishida, A., Joos, F., Key, R. M., Lindsay, K., Maier-Reimer, E., Matear, R., Monfray, P., Mouchet, A., Najjar, R. G., Plattner, G. K., Rodgers, K. B., Sabine, C. L., Sarmiento, J. L., Schlitzer, R., Slater, R. D., Totterdell, I. J., Weirig, M. F., Yamanaka, Y., and Yool, A.: Anthropogenic ocean acidification over the twenty-first century and its impact on calcifying organisms, Nature, 437, 681–686, 2005. 1.1, 3.1, 4.1, 5.1, 5.6

Otto, N. C. and Quinn, J. A.: Facilitated Transport of Carbon Dioxide through Bicarbonate Solutions, Chemical Engineering Science, 26, 949–&, 1971. 3.2.5

Ouboter, M. R. L., Van Eck, B. T. M., Van Gils, J. A. G., Sweerts, J. P., and Villars, M. T.: Water quality modelling of the western Scheldt estuary, Hydrobiologia, 366, 129–142, 1998. 2.2.2.5, 2.4.3, 2.4.4.1

Perez, F. F. and Fraga, F.: Association Constant of Fluoride and Hydrogen-Ions in Seawater, Marine Chemistry, 21, 161–168, 1987. 6.2, 6.4

Peters, J. and Sterling, A.: L Estuaire de l Escaut, Project Mer. Rapport final., vol. 10, chap. Hydrodynamique et transports de sediments de l estuaire de l Escaut, pp. 1–65, Service de Premier Ministre, Bruxelles, 1976. 1.3, 2.2.1

Petzold, L. R.: A Description of DASSL: A Differential/Algebraic System Solver, in: IMACS World Congress, Sandia National Laboratories, Montreal, Canada, 1982. 3.2.6, 3.2.7, 3.4.2

Pierrot, D., E., L., and R., W. D. W.: MS Excel Program Developed for CO_2 System Calculations, ORNL/CDIAC-105. Carbon Dioxide Information Analysis Center, Oak Ridge National Laboratory, U.S. Department of Energy, Oak Ridge, Tennessee., 2006. 6.1, 6.1, 6.5

Prentice, C., Farquhar, G. D., Fasham, M. J. R., Goulden, M. L., Heimann, M., and Jaramillo, V. J.: The carbon cycle and atmospheric carbon dioxide, in: Climate Change 2001: The Scientific Basis, edited by Houghton, J. and al., e., pp. 185–237, Cambridge University Press, New York, 2001. 1.1, 3.1, 5.5

Press, W., Teukolsky, S., and Vetterling, W.: Numerical recipes in FORTRAN : the art of scientific computing, Cambridge University Press, Cambridge, 2nd ed. edn., 1992. 3.2.4, 3.2.9

R Development Core Team: R: A language and environment for statistical computing, R Foundation for Statistical Computing, Vienna, Austria, http://www.r-project.org, ISBN 3-900051-07-0, 2005. 2.2.3, 4.2.6, 4, 6.1

Raymond, P. A. and Cole, J. J.: Gas exchange in rivers and estuaries: Choosing a gas transfer velocity, Estuaries, 24, 312–317, 2001. 2.2.2.4, 3, 3.5, E

Regnier, P., Wollast, R., and Steefel, C. I.: Long-term fluxes of reactive species in macrotidal estuaries: Estimates from a fully transient, multicomponent reaction-transport model, Marine Chemistry, 58, 127–145, 1997. 2.1, 2.2.2.1, 2.2.2.1, 2.4.2, 2.4.3, 2.4.4.1, 3.2.8, 3.3.2, 3.4.2, 4.1, 4.1, 4.2.3, 4.4.1

Riordan, E., Minogue, N., Healy, D., O'Driscoll, P., and Sodeau, J. R.: Spectroscopic and optimization modeling study of nitrous acid in aqueous solution, Journal of Physical Chemistry A, 109, 779–786, 2005. 6.2, 6.6.3.1.1

Roche, M. P. and Millero, F. J.: Measurement of total alkalinity of surface waters using a continuous flowing spectrophotometric technique, Marine Chemistry, 60, 85–94, 1998. A

Roy, R. N., Roy, L. N., Lawson, M., Vogel, K. M., Moore, C. P., Davis, W., and Millero, F. J.: Thermodynamics of the Dissociation of Boric-Acid in Seawater at S=35 from 0-Degrees-C to 55-Degrees-C, Marine Chemistry, 44, 243–248, 1993a. 3.3.1, 6.6

Roy, R. N., Roy, L. N., Vogel, K. M., PorterMoore, C., Pearson, T., Good, C. E., Millero, F. J., and Campbell, D. M.: The dissociation constants of carbonic acid in seawater at salinities 5 to 45 and temperatures O to 45 degrees C (vol 44, pg 249, 1996), Marine Chemistry, 52, 183–183, 1993b. 2.3, 4.6.1.2, 5.2.2, 6.1, 6.2, 6.6.2, 6.6.3.4, 6.4, 6.5, 6.6.3.10, D, E

Royal Society: Ocean Acidification Due to Increasing Atmospheric Carbon Doxide. Policy Document 12/05, The Royal Society, London, UK, 2005. 1.1, 6.1

Saaltink, M. W., Ayora, C., and Carrera, J.: A mathematical formulation for reactive transport that eliminates mineral concentrations, Water Resources Research, 34, 1649–1656, 1998. 3.2.5, 3.2.7, 3.2.10, 3.4.2, 5.7.1

Salisbury, J., Green, M., Hunt, C., and Campbell, J.: Coastal Acidification by Rivers: A Threat to Shellfish?, EOS, Transactions American Geophysical Union, 89, 2008. 1.1

Sarmiento, J. L. and Gruber, N.: Ocean Biogeochemical Dynamics, Princeton University Press, Princeton, 2006. 3.1, 5.5, 5.4, E

Skoog, D. A. and West, D. M.: Fundamentals of Analytical Chemistry, Holt-Saunders International Editions, Holt-Saunders, 1982. 1.2, 5.2.3, 5.6, 6.4.1, 6.2, 2c

Soetaert, K.: rootSolve: Nonlinear root finding, equilibrium and steady-state analysis of ordinary differential equations, http://cran.r-project.org/web/packages/rootSolve/index.html, R package version 1.2, 2008. 6.1

Soetaert, K. and Herman, P.: MOSES Model of the Scheldt Estuary - Ecosystem Development under SENECA, Tech. rep., Netherlands Institute of Ecology, 1994a. 3.3.1

Soetaert, K. and Herman, P. M. J.: One Foot in the Grave - Zooplankton Drift into the Westerschelde Estuary (the Netherlands), Marine Ecology-Progress Series, 105, 19–29, 1994b. 2.1

Soetaert, K. and Herman, P. M. J.: Nitrogen Dynamics in the Westerschelde Estuary (Sw Netherlands) Estimated by Means of the Ecosystem Model Moses, Hydrobiologia, 311, 225–246, 1995a. 2.1, 2.2.2.1, 2.2.2.1, 2.2.2.1, 2.2.2.10, 2.4.2, 2.4.4.1, 2.4.4.1, 3.1, 3.3.1, 3.14, 3.3.2, E

Soetaert, K. and Herman, P. M. J.: Estimating Estuarine Residence Times in the Westerschelde (the Netherlands) Using a Box Model with Fixed Dispersion Coefficients, Hydrobiologia, 311, 215–224, 1995b. 1.3, 2.1, 2.2.1, 2.2.2.5, 2.2.2.11, 2.3.1, 4.2.1

Soetaert, K. and Herman, P. M. J.: Carbon Flows in the Westerschelde Estuary (the Netherlands) Evaluated by Means of an Ecosystem Model (Moses), Hydrobiologia, 311, 247–266, 1995c. 2.1, 2.2.2.1, 2.2.2.1, 2.2.3, 2.4.1, 2.4.2, 2.4.4.1, 3.1, E

Soetaert, K. and Herman, P. M. J.: A Practical Guide to Ecological Modelling, Springer, 2009. 1.2, 6.1

Soetaert, K., Herman, P. M. J., and Middelburg, J. J.: A model of early diagenetic processes from the shelf to abyssal depths, Geochimica Et Cosmochimica Acta, 60, 1019–1040, 1996. 2.2.2.1, 2.2.2.1

Soetaert, K., deClippele, V., and Herman, P.: FEMME, a flexible environment for mathematically modelling the environment, Ecological Modelling, 151, 177–193, 2002. 2.2.3, 3.3.1, 4.2.6

Soetaert, K., Middelburg, J. J., Heip, C., Meire, P., Van Damme, S., and Maris, T.: Long-term change in dissolved inorganic nutrients in the heterotropic Scheldt estuary (Belgium, The Netherlands), Limnology and Oceanography, 51, 409–423, 2006. 1.3, 2.1, 2.1, 2.2.1, 2.2.2.6, 2.2.2.11, 2.4.4.1, 2.4.4.1, 2.4.4.1, 3.2.2, 4.1, 4.2.1

Soetaert, K., Hofmann, A. F., Middelburg, J. J., Meysman, F. J., and Greenwood, J.: The effect of biogeochemical processes on pH, Marine Chemistry, 105, 30–51, 2007. 2.2.2.7, 3.2.8, 3.2.10, 3.2.10, 3.4.2, 5, 3.4.4, 3.6.2, 4.1, 4.1, 5.1, 5.4.2, 5.4, 6.2, 6.6.3.1.1, E

Soetaert, K., Petzold, T., and Setzer, R. W.: deSolve: General solvers for (ordinary) differential (algebraic) equations, http://cran.at.r-project.org/web/packages/deSolve/, R package version 1.1, 2008. 4, 6.1

Soetaert, K., Petzoldt, T., and Meysman, F.: marelac: Constants, conversion factors, utilities for the MArine, Riverine, Estuarine, LAcustrine and Coastal sciences, http://r-forge.r-project.org/projects/marelac/, R package version 1.4, 2009. 6.6.3.5, 6.6.3.5

Sommer, U.: Biologische Meereskunde, Springer Verlag, Berlin Heidelberg, 1998. 7

Spiteri, C., Van Cappellen, P., and Regnier, P.: Surface complexation effects on phosphate adsorption to ferric iron oxyhydroxides along pH and salinity gradients in estuaries and coastal aquifers, Geochimica Et Cosmochimica Acta, 72, 3431–3445, 2008. 4.1

Steefel, C. I. and MacQuarrie, K. T. B.: Approaches to modeling of reactive transport in porous media, Reactive Transport in Porous Media, 34, 83–129, 1996. 3.2.4, 3.2.4, 3.2.7, 3.4.2

Stumm, W. and Morgan, J. J.: Aquatic Chemistry: Chemical Equilibria and Rates in natural Waters, Wiley Interscience, New York, 1996. 1.1, 1.2, 1.2, 1.2, 2.2.2.2, 2.2.2.7, 3.1, 3.2, 4.1, 5.1, 5.2.3, 5.4.2, 5.6, 6.3.5, 6.4.1, 6.2, 7, E

Thomann, R. V. and Mueller, J. A.: Principles of Surface Water Quality Modeling and Control, Harper & Row, New York, 1987. 2.2.2.4, 2.2.2.5, 2.2.2.5, 3.2.5

Van Damme, S., Struyf, E., Maris, T., Ysebaert, T., Dehairs, F., Tackx, M., Heip, C., and Meire, P.: Spatial and temporal patterns of water quality along the estuarine salinity gradient of the Scheldt estuary (Belgium and The Netherlands): results of an integrated monitoring approach, Hydrobiologia, 540, 29–45, 2005. 1.3, 2.2.1, 2.3.4, 2.4.4.1

van Eck, B.: De Scheldeatlas: een beeld van een estuarium, Schelde Informatie Centrum / Rijksinstituut voor Kust en Zee, Middelburg, 1999. 2.2.2.11, 2.3.4

van Gils, J. A. G., Ouboter, M. R. L., and De Roij, N. M.: Modelling of Water and Sediment Quality in the Scheldt Estuary, Netherlands Journal of Aquatic Ecology, 27, 257–265, 1993. 2.2.2.11

Vanderborght, J. P., Wollast, R., Loijens, M., and Regnier, P.: Application of a transport-reaction model to the estimation of biogas fluxes in the Scheldt estuary, Biogeochemistry, 59, 207–237, 2002. 2.1, 4, 2.1, 2.2.2.1, 2.3.3.2, 2.4.4.1, 2.4.4.2, 4.1, 4.1, 4.2.3, 4.4.1

Vanderborght, J.-P., Folmer, I. M., Aguilera, D. R., Uhrenholdt, T., and Regnier, P.: Reactive-transport modelling of C, N, and O_2 in a river-estuarine-coastal zone system: Application to the Scheldt estuary, Marine Chemistry Special issue: Dedicated to the memory of Professor Roland Wollast, 106, 92–110, 2007. 1.3, 2.1, 4, 2.1, 2.2.1, 2.3.1, 2.4.2, 2.4.4.1, 4.2.1, 4.4.1, 6.1

Wang, Y. F. and VanCappellen, P.: A multicomponent reactive transport model of early diagenesis: Application to redox cycling in coastal marine sediments, Geochimica Et Cosmochimica Acta, 60, 2993–3014, 1996. 3.4.2

Wanninkhof, R.: Relationship between Wind-Speed and Gas-Exchange over the Ocean, Journal of Geophysical Research-Oceans, 97, 7373–7382, 1992. 2.2.2.4, 3.3.1, 3.14, E

Weiss, R. F.: Solubility of Nitrogen, Oxygen and Argon in Water and Seawater, Deep-Sea Research, 17, 721–&, 1970. 2.2.2.4, 2.6.1, 6.2, 6.3, 6.6.3.7.1

Weiss, R. F.: Carbon dioxide in water and seawater: the solubility of a non-ideal gas, Marine Chemistry, 2, 203–215, 1974. 2.2.2.4, 2.6.1, 3.3.1, 3.14, 5.2.2, 6.2, 6.3, E

Whitfield, M. and Turner, D. R.: The Carbon-Dioxide System in Estuaries - an Inorganic Perspective, Science of the Total Environment, 49, 235–255, 1986. 4.1, 4.1, D

Williams, D. R.: NASA Earth Fact Sheet, http://nssdc.gsfc.nasa.gov/planetary/factsheet/earthfact.html, 2004. 2.2.2.4, 2.6.1, 6.2, 6.6.3.1.2, 6.6.3.7.1

Wischmeyer, A. G., Del Amo, Y., Brzezinski, M., and Wolf-Gladrow, D. A.: Theoretical constraints on the uptake of silicic acid species by marine diatoms, Marine Chemistry, 82, 13–29, 2003. 6.2, 6.7

Wolf-Gladrow, D. A., Bijma, J., and Zeebe, R. E.: Model simulation of the carbonate chemistry in the microenvironment of symbiont bearing foraminifera, Marine Chemistry, 64, 181–198, 1999. 5.7.1

Wolf-Gladrow, D. A., Zeebe, R. E., Klaas, C., Koertzinger, A., and Dickson, A. G.: Total alkalinity: the explicit conservative expression and its application to biogeochemical processes, Marine Chemistry, 2007. 3.2.8, 3.4.3, 5.1, 5.2.2, 2a

Wong, G. T. F.: Alkalinity and Ph in the Southern Chesapeake Bay and the James River Estuary, Limnology and Oceanography, 24, 970–977, 1979. 4.1

Zachos, J. C., Dickens, G. R., and Zeebe, R. E.: An early Cenozoic perspective on greenhouse warming and carbon-cycle dynamics, Nature, 451, 279–283, 2008. 5.5, 5.6

Zeebe, R. E.: Modeling CO2 chemistry, [delta]13C, and oxidation of organic carbon and methane in sediment porewater: Implications for paleo-proxies in benthic foraminifera, Geochimica et Cosmochimica Acta, 71, 3238–3256, 2007. 3.4.2, 5.7.1

Zeebe, R. E. and Wolf-Gladrow, D.: CO_2 in Seawater: Equilibrium, Kinetics, Isotopes, no. 65 in Elsevier Oceanography Series, Elsevier, first edn., 2001. 1.1, 1.2, 1.2, 2.2.2.6, 2.2.2.7, 3.2.3, 3.2.4, 3.5, 3.8, 4.2.5, 4.6.1.2, 5.1, 5.1, 5.2.1, 5.2, 5.7.1, 6.3.3, 6.3.5, 6.3.7, 6.4.1, 6.4.2, 6.4.3, 6.2, 6.6.3.1.1, 6.6.3.2, 6.6.3.4, 6.3, 6.4, 6.5, 6.6, 6.6.3.10, 6.6.3.11, 6.6.3.12, 2a, 3, E

Zeebe, R. E., Zachos, J. C., Caldeira, K., and Tyrrell, T.: Oceans - Carbon emissions and acidification, Science, 321, 51–52, 2008. 1.1, 5.1, 5.5, 5.6, 6.1, 6.3.3

G. Acknowledgements

This thesis was supported by the EU (Carbo-Ocean, 511176-2) and the Netherlands Organisation for Scientific Research (833.02.2002).

Chapter 2: Present nitrogen and carbon dynamics in the Scheldt estuary:

We thank two anonymous reviewers for constructive critical comments. The publication based in this chapter is publication number 4331 of the NIOO-CEME and was edited by M. Dai

Chapter 3: A step-by-step procedure for pH model construction in aquatic systems:

We thank D. Wolf-Gladrow for sharing his knowledge and expertise on seawater carbonate chemistry and pH modeling at various occasions. We thank B. P. Boudreau and an anonymous reviewer for their constructive criticism on an earlier version of this manuscript. The publiction based on this chapter is publication 4230 of the NIOO-CEME and was edited by Y. Prairie

Chapter 4: Factors governing the pH in a heterotrophic, turbid, tidal estuary:

The publiction based on this chapter is edited by: A. Borges

Chapter 6: AquaEnv - an Aquatic acid-base modelling Environment in R

The first author would like to thank Jan Peene, Anna de Kluiver, Ilse Kamerling, and Sarah Fiorini, for support in obtaining laboratory data for an earlier version of AquaEnv as well as beta testing the package. Filip Meysman is supported by an Odysseus reseach grant from F.W.O. (Research Foundation Flanders).

Personal Acknowledgements

Along the course of my life which, so far, culminated in the completion of this thesis, there was many a valuable person who influenced me, helped me, or simply believed in me. It is impossible to mention them all individually. Thank you very much for everything.

However, there are a some people which definitely deserve to be mentioned by name. First, there is Carlo Heip whose group at Ghent University I found on the internet and sent my open job application to in 2004. Carlo, thanks for bringing first my CV and then myself to the NIOO-CEME, without you I would not be where I am today. Then there are Karline Soetaert, Jack Middelburg, and Adri Knuit who believed in my potential during my job interview and gave me the chance to spend four years in Yerseke and complete this thesis - thank you very much for that! Of course, Karline and Jack have done much more than just believe in me over the last four years. Karline, thank you for helping me getting started in the world of ecological modelling, endlessly correcting early versions of my manuscript, being a real whiz at programming, and - most importantly - having such a refreshing attitude and a thundering laugh: it really is a pleasure working with you! Jack, thank you for always having an open door, for your to-the-point corrections and suggestions for manuscripts that can settle disputes amongst co-authors, for sharing your incredible knowledge about everything, and for opening many doors for me via sending me to various conferences and courses, even as far away as China. Very importantly, there is Filip Meysman. Originally, nobody had in mind that I would work together with Filip, but thanks to the open and communicative atmosphere of the NIOO-CEME we found out along the way that we have similar interests and we commenced a fruitful collaboration that hopefully will continue for a long time. Filip, thank you for putting up with me being stubborn and thank you for being stubborn yourself: you urged me to do round after round of rewriting manuscripts until the - as you put it - raw diamonds where crafted into shimmering brilliants. I am glad you did so, thank you very much for that. I also would like to thank Dieter Wolf-Gladrow whom I met at a conference in 2005. Dieter, I have to admit that I was a bit scared at first since I only knew you as one of the authors of the "CO_2 bible", but you turned out to be very down-to-earth, kind, and helpful - you even agreed to write a letter of recommendation for me. I enjoyed every one of our discussions that took place all over Europe during the last four years. Also, your written input to various versions of my manuscripts helped me a lot. Finally, you agreed to be on my thesis committee. Dieter, vielen Dank für Alles! Of course I would also like to thank the rest of my thesis committee: Bernie Boudreau, Philippe Van Cappellen, Gert de Lange, and Frank Millero. Many thanks also to Tetsuro Miyatake and my brother Stephan Hofmann for giving me moral support during my defense by being my "paranimfen".

Work is not everything, friends and a personal life are at least as important, and there are many people who made my life in Yerseke as enjoyable as it can be. We met as strangers and we will part as close friends! Hopefully, we will see each other again many times, you are all invited to visit me and Silke wherever we will live in the future. Tetsuro, over the last four years you became one of my closest friends. Thank you very much for endlessly listen to my stories about cars and engines, accompanying me on various scuba dives - at least if it was not too cold ☺. And, of course, arigato for all the mutually hosted culinary adventures with you and Sayuri! Tom, je bent een geweldige kamergenoot, en een heel goede vriend! Samen gaan duiken, boot varen of eraan rommelen, of gewoon ergens een weekendje doorbrengen samen

met jou en Els - ik zal het zeker erg missen. En Tom, als je op bezoek gaat komen, beloof ik, niet in een koperen pot te koken! Karel, bedankt ervoor dat je een zo goede vriend bent, ik kan met je echt over alles praten. Ook hebben we veel gezamenlijke interesses, of het nu samen-in-een-kamer-werken, hardlopen, fietsen, duiken, wind- en kitesurfen, berg beklimmen, skiën, snowboarden, zuipen en naar hair-rock luisteren of gewoon levendig discussiëren is, met jou is alles leuk! Jeroen, je bent echt een bron van inspiratie, het is gewoon zalig jouw enthoesiasme te voelen als het over je werk of onderwater-exploratie plannen gaat. Je was de expeditieleider van ons Schaar van Colijnsplaat actie, je wilde bij elk weer gaan duiken en je had altijd zin in een boot de Oosterschelde op te gaan, of het nu zeven uur in een badkuip naar de Zeelandbrug was of zonder vaarbewijs in mijn Zodiac - Jeroen, bedankt voor alles. Dank ook aan jou en Brenda voor het delen van informatie over bevalling en kinderopvoeding. Henrik, unfortunately we did not have too much time together here, but during the time we did see each other, it was great working in the same room together with you, going mountain biking and skiing together, enjoying Ikea shrimps together with you and Maria, or being shown around Stockholm by the two of you. Tack så mycket for everything! Francesc, bedankt voor het altijd hulpvaardig zijn, ons in jullie huis laten slapen en het extra voor mijn verjaardag naar Workum rijden! Arnon, thanks for your great hot-and-sour salad and for all the ICC's you organized in the Keete. Fred, thanks for letting me help with your experiments on the Luctor, and it has been great sharing rooms (and beds ☺) with you at various conferences and skiing holidays. Merçi pour tout. Sandra, Stephane and Victor, thanks for making me feel at home right away in Yerseke and the Keete. And to all the other people at the NIOO-CEME, the Keete, or elsewhere, which I met during the last four years and which made my life interesting and worthwhile: thank you very much!

Mama und Papa, vielen Dank dafür daß Ihr mir ein liebevolles zu Hause, eine traumhafte Kindheit und eine wertvolle Ausbildung zu Teil werden habt lassen. Ihr habt mir alles ermöglicht, mich nie zu etwas gezwungen und mich schon als Kind ernst genommen, was meine Persönlichkeit wachsen ließ. Ich bin Euch unendlich dankbar für alles was Ihr für mich getan habt, Ihr seid einfach Klasse, ich könnte mir keine besseren Eltern vorstellen!

Nicht zuletzt gilt mein Dank meiner Verlobten und bald Mutter-unseres-ersten-Kindes Silke. Silke, vielen Dank daß Du offen für alles bist, immer für mich da bist, immer zu mir stehst, daß Du mit mir in die Niederlande gezogen bist und daß Du nun mit mir nach Kalifornien ziehst. Ich bin Dir von Herzen dankbar daß ich mich nicht zwischen Dir und meinen Träumen entscheiden muss, sondern daß wir uns gemeinsam entfalten können. Ein Leben und eine Familie zusammen mit Dir ist mein Traum, ich liebe Dich von ganzem Herzen!

Cover layout in collaboration with Silke Donner (www.donnergraphics.com).
Printed by Royal Wöhrmann Print Service, Zutphen (www.wps.nl).